

This work is protected by copyright and other intellectual property rights and duplication or sale of all or part is not permitted, except that material may be duplicated by you for research, private study, criticism/review or educational purposes. Electronic or print copies are for your own personal, non-commercial use and shall not be passed to any other individual. No quotation may be published without proper acknowledgement. For any other use, or to quote extensively from the work, permission must be obtained from the copyright holder/s.

**Understanding the chemistry of hydroxyaluminosilicates :
from the mechanism of formation to the determination of an
equilibrium constant.**

by

Céline SCHNEIDER

Thesis submitted in partial fulfilment of the requirements of

Keele University

for the degree of Doctor of Philosophy

January 2003

Keele University (United Kingdom)

Abstract

The proposition in recent years that silicic acid ($\text{Si}(\text{OH})_4$) acts as an environmental control of the biological availability of aluminium (Al) has presented inorganic chemistry with an intriguing scientific challenge. $\text{Si}(\text{OH})_4$ reacts with Al to form hydroxyaluminosilicates (HAS) and thereby ameliorates the toxic effects of Al. However, in spite of the recent progress made in the identification and characterisation of these materials, very little is known about the kinetics underlying the formation of HAS. In particular, the rate at which HAS are formed and achieve stability with respect to their environment will be critical to their role in defining the biological availability of aluminium.

This research project investigated different aspects of the chemistry of the formation and precipitation of HAS. The interaction between Al and methyl-substituted analogues of $\text{Si}(\text{OH})_4$ using solution and solid state NMR as well as SEM-EDX revealed that the substituents prevented any reaction with Al, suggesting a significant degree of specificity in the formation of HAS. Atomic force microscopy (AFM) was used in solution to follow the phenomenon of growth and agglomeration of HAS particles with time and provided new insight into the deposition of HAS on a silica substrate, in particular helping to discriminate two forms of HAS, HAS_A and HAS_B , by their charge and rate of agglomeration. X-ray photoemission spectroscopy (XPS) was used to characterise precipitates of HAS_A and HAS_B and provided new information on their structure from the observed shift in their binding energies. Fluorimetry was used to study the reaction of $\text{Si}(\text{OH})_4$ with Al. The formation of the aluminium-morin complex was used as an estimate of the free Al concentration. The establishment of a reliable experimental protocol enabled an indirect measurement of the formation of HAS and how both the concentrations of Al and $\text{Si}(\text{OH})_4$ influenced the reaction.

Most importantly, the quantification of the fluorimetric results when coupled with speciation calculations using the SolGasWater Al speciation model resulted in the first significant attempt to determine an equilibrium constant for the formation of HAS. This constant ($\text{Log } K_{\text{HASB}} = -10.94$ at 20°C) has enabled significant advances in bringing together experimental and theoretical data concerning HAS in the environment and the control of the bioavailability of Al.

Acknowledgements

I would not have complete this research without the help and support of many colleagues and friends. I first would like to express my sincere gratitude to my supervisor Dr Chris Exley for being present and available at all time, for offering me his experience in the subject and sound advice, and for his encouragement and support throughout the all project. It was a great privilege to work with him and to benefit from his supervision.

I also wish to thank Dow Corning Ltd (Barry, Wales) for providing financial and technical support. I am particularly grateful to Dr. Ian Moss for helpful discussions, Drs A. Kretschmer and S. Bones for their advice and supervision of solution state NMR experiments, L.A. O'Hare for her invaluable help on AFM and XPS experiments, R. Taylor for helping me to synthesise DMSD and TMDS, and D. Tapscott for his contribution to the SEM-EDX analyses.

My gratitude is extended to Prof. S. Sjoberg for giving me the opportunity to visit him at the department of Inorganic Chemistry at Umeå University (Sweden) and to have access to the SGW software. Without his support and suggestions, the *determination of the equilibrium constant* would not have been possible.

My thanks are also due to Dr. P. Tekely from the University of Nancy I (France) for giving me access to solid state NMR, as well as to the rest of the methodology research group for making me feel at home on each of my visits.

Many thanks also to my colleagues, H. Taylor and F. Doucet, for their help advice and support.

And last but not least, I would like to express my gratitude to my family and friends. To my mum, my dad, mamie and Chantal: thank you for your love and support; I would not be the person I am without you. Thanks to Fiona for being the most marvellous friend, Rémy for listening and keeping me focused, Frédérique for her hospitality and her

most helpful ideas, Stéphane, Carl, Mouk and all the others who put a smile on my face. I could not have done it without all of you. And Léo, I can't wait to read yours!

*“...c’est avec la logique que nous prouvons
et avec l’intuition que nous trouvons.”*

Henri Poincaré

TABLE OF CONTENTS

CHAPTER 1 : INTRODUCTION. THE FORMATION OF HYDROXYALUMINOSILICATES (HAS) AS A CONTROL OF THE BIOAVAILABILITY OF ALUMINIUM.	5
1.1. The chemistry of aluminium and silicon in the natural environment	5
1.1.1. The toxicity of Al	5
1.1.2. The formation of monomeric $\text{Si}(\text{OH})_4$	6
1.1.3. The chemistry of natural waters	7
1.2. The chemistry of hydroxyaluminosilicates (HAS)	11
1.2.1. Structure of HAS	11
1.2.2. Mechanism and kinetics of formation of HAS	12
1.2.3. Agglomeration	16
1.3. Aims of this study	16
CHAPTER 2 : MATERIALS AND METHODS	18
2.1. Molecular spectroscopy	18
2.1.1. General principles	18
2.1.2. UV-Visible spectroscopy	20
2.1.3. Fluorimetry	26
2.2. Graphite Furnace Atomic Spectroscopy (GFAAS)	32
2.2.1. General principles	32
2.2.2. The influence of $\text{Si}(\text{OH})_4$ on the measurement of Al by GFAAS.	36
2.3. NMR	52
2.3.1. General principles	52
2.3.2. Instrumentation	56

2.3.3. Solution NMR	57
2.3.4. Solid state NMR (Engelhardt, 1987)	58
2.4. AFM	60
2.4.1. General principles	60
2.4.2. Tapping mode AFM in solution	61
2.5. XPS	63
2.5.1. Principles.	63
2.5.2. Instrumentation	63
2.5.3. Qualitative and quantitative analysis	66
2.6. SEM-EDX (Chescoe, 1990)	67
2.7. SolGasWater software	68

CHAPTER 3 : THE INTERACTION OF ALUMINIUM WITH SUBSTITUTED FORMS OF SILICIC ACID. **69**

3.1. Aim	69
3.2. Experimental	71
3.2.1. Preparation of TMDS (tetramethyldisilane-diol)	71
3.2.2. Preparation of DMSD (dimethylsilane-diol)	71
3.2.3. Preparation of samples	73
3.2.4. Instrumentation	74
3.3. Study by NMR	75
3.3.1. Solution state NMR	75
3.3.2. Solid-state NMR	81
3.4. Analysis by SEM-EDX	83
3.5. Conclusions.	89

CHAPTER 4 : THE DIRECT OBSERVATION OF HYDROXYALUMINOSILICATES

FORMATION BY ATOMIC FORCE MICROSCOPY. **92**

4.1. Aim	92
4.2. Experimental	93
4.2.1. Preparation of the samples	93
4.2.2. Tapping-mode AFM in solution	93
4.2.3. XPS	94
4.3. Results	95
4.3.1. The growth of HAS observed by AFM	95
4.3.2. Analysis of the material by XPS	107
4.4. Conclusion	119

CHAPTER 5 : THE STUDY OF HYDROXYALUMINOSILICATES (HAS) FORMATION

USING MORIN-BASED FLUORIMETRY **122**

5.1. Introduction	122
5.2. The establishment of a reliable protocol: evolution of the different experimental protocols	125
5.2.1. Experimental	125
5.2.2. Results	132
5.2.3. Discussion	148
5.3. The measurement of the influence of Si(OH)_4 on the AIM formation	151
5.3.1. Experimental	151
5.3.2. Results	152
5.3.3. Discussion	157
5.4. Conclusions	158

CHAPTER 6 : THE DETERMINATION OF AN EQUILIBRIUM CONSTANT FOR THE

FORMATION OF A HYDROXYALUMINOSILICATE. **160**

6.1. Introduction	160
6.2. Description of the different systems	160
6.2.1. The Al system	160
6.2.2. The Al/Morin system	162
6.2.3. The Al/Si(OH) ₄ /Morin system	166
6.2.4. Equilibrium constants	168
6.3. Calculations using the fluorimetry data and SGW	169
6.3.1. Calibration	170
6.3.2. Calculation of K _{HAS}	174
6.4. The use of K_{HASB} to describe Al/Si(OH)₄ systems	180
6.4.1. The limits of formation of HAS _B	180
6.4.2. Comparison between calculations and previous experimental results	183
6.5. Conclusions	186

<u>CHAPTER 7 : GENERAL DISCUSSION. HYDROXYALUMINOSILICATES AS A CONTROL OF THE TOXICITY OF ALUMINIUM.</u>	187
--	------------

<u>APPENDIX A: "SILICIC ACID (SI(OH)(4)) IS A SIGNIFICANT INFLUENCE UPON THE ATOMIC ABSORPTION SIGNAL OF ALUMINIUM MEASURED BY GRAPHITE FURNACE ATOMIC ABSORPTION SPECTROMETRY (GFAAS)."</u>	202
---	------------

<u>APPENDIX B: "THE REACTION OF ALUMINIUM WITH SILICIC ACID IN ACIDIC SOLUTION: AN IMPORTANT MECHANISM IN CONTROLLING THE BIOLOGICAL AVAILABILITY OF ALUMINIUM?"</u>	209
---	------------

<u>REFERENCES</u>	219
--------------------------	------------

Chapter 1 : Introduction. The formation of hydroxy aluminosilicates

(HAS) as a control of the bioavailability of aluminium.

1.1.The chemistry of aluminium and silicon in the natural environment

Silicon (Si) and aluminium (Al) are respectively the second and third most abundant elements in the lithosphere and when combined together form the largest group of minerals present in the earth's crust, i.e. aluminosilicates. Despite the fact that aluminosilicates are believed to be of low solubility, in the pH range for typical surface and ground waters, aqueous forms of Al and Si(OH)_4 present in natural water may react together to form dissolved aluminosilicate complexes (Swaddle 2001). Acid rain is responsible for the release of Al from soils into fresh waters (Bache 1986a; Schecher and Driscoll 1988), raising the problem of the control of the bioavailability of this element (Martin 1994).

1.1.1.The toxicity of Al

Over the years, Al was shown to be highly toxic to all forms of life (Research in Aluminium toxicity 1996; Chadwick and Whelan 1992; Exley and Birchall 1992a; Ganrot 1986) through the bounding of Al^{3+} to the functional groups on target ligands. It was shown that the presence of Al in acidic soils limited plant productivity, thus causing severe damage to forests and plants in general (Campbell et al. 1983; Plochmann 1984; Postel 1984; Wood and Cooper 1984; Wood et al. 1984). Al toxicity has also been implicated in fish loss in lakes and streams of acidic pH through damage to gill epithelia and loss of osmoregulatory capacity (Bache 1986b; Campbell et al. 1983; Exley 1996; Exley et al. 1991; Exley and Struthers 1992; Exley et al. 1994; Exley et al. 1996). In humans, Al is likely to be responsible for neuropathological diseases such as bone diseases (Abreo 2001),

presenile dementia, dialysis dementia (Altmann 2001) and Alzheimer's disease (Exley 2001).

1.1.2. The formation of monomeric $\text{Si}(\text{OH})_4$

Monosilicic acid ($\text{Si}(\text{OH})_4$) is the predominant aqueous form of Si in natural water at $\text{pH} < 9$ and $[\text{Si}] < 2 \text{ mmol} \cdot \text{dm}^{-3}$ (McKeague and Cline 1963; Sjöberg 1996). It is a weak acid of neutral charge in aqueous solution with $\text{pK}_1 = 9.84$ and $\text{pK}_2 = 13.43$ at infinite dilution and 25°C . Consequently, the formation of monosilicates ($\text{SiO}(\text{OH})_3^-$ and $\text{SiO}_2(\text{OH})_2^{2-}$) through the dissociation of monomeric $\text{Si}(\text{OH})_4$ in natural waters, where the pH rarely exceeds 8, is very unlikely (Aston 1983). Moreover, there is little evidence of the polymerisation of $\text{Si}(\text{OH})_4$ in natural waters. This last observation contrasts with the essentiality of $\text{Si}(\text{OH})_4$ in regards to living organisms, such as diatoms, which has been thoroughly reported (Carlisle 1972; Carlisle 1974; Epstein 1994; Epstein 1999; Rafi et al. 1997; Schwartz and Milne 1972). Most importantly, it was shown that $\text{Si}(\text{OH})_4$ interacts with Al to reduce the bioavailability of Al. Birchall et al (1989) showed that the presence of an excess of $\text{Si}(\text{OH})_4$ at **pH 5** eliminates the acute toxicity of Al to fish through they suggested the formation of HAS. In conifers, Al was shown to co-deposit with Si suggesting that a mechanism of sequestration occurred in defence against the damage caused by Al toxicity (Hodson and Sangster 1999). Birchall et al (1989) suggested that a similar interaction might reduce the absorption of Al by humans. Several studies confirmed this hypothesis as $\text{Si}(\text{OH})_4$ seems to both reduce the gastrointestinal absorption of Al and increase its renal clearance (Belia et al. 1996; Edwardson et al. 1993; King et al. 1997; Popplewell et al. 1998). Thus, the reaction between $\text{Si}(\text{OH})_4$ and Al may be of unique importance to life on earth (Exley 1998).

1.1.3. The chemistry of natural waters

The water quality of rivers and lakes is defined by a combination of hydrogeochemical processes (Neal et al. 1997). For example:

1. The soil zone is important in generating acidic waters due to the release of humic substances.
2. The bedrock is important in neutralizing acidic waters in the soil and in generating pH buffered waters with the generation of base cations (calcium and magnesium, mainly).
3. The climate is important in regulating the type of soils present and the extent of chemical weathering due to both hydrological and temperature based controls.
4. The pollution climate is important in that the input of acidic oxides from car and industrial sources can lead to soil and stream acidification.
5. The hydrology is important in that this determines the proportion of acidic soil and less acidic groundwater inputs entering the stream and lake.

In the United Kingdom, the major areas of acidification problems are in the “hard rock” regions with low base cation status and low acid buffering capacity. These regions are essentially the upland areas where rainfall and high acidic deposition occur.

With regards to the variability in water chemistry, for the acidic waters of particular concern in this thesis, there are two types of system, one of low pH and low aluminium concentration, the other of low pH and high aluminium concentration. In the former case, the waters have a high acidity due to the presence of humic acids with or without acidifying pollutants. Where the humic acids are high, then the aluminium is mainly in an

organically complexed form. In the latter case, the high aluminium is generated by the reaction of the acid waters with aluminium hydroxide in the matrix of the soil: in this case the aluminium is often in an inorganic form.

In terms of the variation in water chemistry in these acidic areas, this is largely controlled by the hydrology and the varying proportions of soil and groundwater inputs. In the case of the rivers, pH, aluminium and silica concentrations fluctuate. Under base flow conditions, the waters are enriched in base cations and silica from weathering sources (shallow groundwater) and the pH is relatively high. Under storm flow conditions, the soil water dominates in the stream and hence the waters are acidic, aluminium bearing and depleted in silica (the major source of silicon is from within the catchment – rainfall inputs of silicon are low). In the case of lakes as opposed to streams, the fluctuations in chemistry are damped out due to the high water storage.

To illustrate the range in pH, aluminium and silica levels in UK surface waters for acidic and acid sensitive systems, the resources of the United Kingdom Acid Waters Monitoring programme can be consulted.

(UKAWM: www.geo.ucl.ac.uk/ukawmn/report/AWMNannualReport2001-02.pdf).

Table 1.1-1 provides a summary of the chemistry of river and lake waters across the United Kingdom with sites in England, Wales, Scotland and Northern Ireland. This summary is based on several years of weekly to quarterly monitoring. Information on temperature is also provided as within the thesis thermodynamic data is provided which will be temperature dependent.

The UKAWMN results show the following key features.

- Silicon concentrations average around $41.11 \mu\text{mol.dm}^{-3}$ within a range of 1.79 to $192.86 \mu\text{mol.dm}^{-3}$.
- Aluminium concentrations vary in their proportions of organic and inorganic forms. On average 55.2 % is as inorganic aluminium and the ranges for inorganic and organic forms are 0.09 to $20.24 \mu\text{mol.dm}^{-3}$ and 0.09 to $11.48 \mu\text{mol.dm}^{-3}$.
- pH varies between 3.79 and 7.44 with a mean of 5.6.
- Temperature averages at 8.7°C with a range of 0 to 21.6°C . This is much cooler than the fixed temperature used in the laboratory. Experiments in this work were carried out at room temperature and the determination of the constant of formation of HAS_B was determined at 20°C . The lower temperature measured in field could affect the formation of HAS and further experiments would be needed to investigate the effect of temperature on the formation of HAS.

Table 1.1-1: Hydrochemistry of UK surface waters (from the UKAWMN database).

<http://www.geog.ucl.ac.uk/ukawmn/report/AWMNAnnualReport2001-02.pdf>

	site	pH			temp °C		labile Al inorganic $\mu\text{mol.dm}^{-3}$		
		min	max	mean	min	max	mean	min	max
1	Loch Coire nan Arr	5.75	6.96	8.53	1.80	19.30	0.11	0.09	0.30
2	Allt a Mharcaidh	5.12	7.08	6.19	0.20	13.80	0.21	0.09	1.70
3	Allt na Coire nan Con	4.94	6.70	8.17	0.40	18.00	0.57	0.09	3.63
4	Lochnagar	4.95	5.81	5.49	0.00	14.10	0.79	0.09	5.07
5	Loch Chon	4.99	6.47	9.62	3.00	18.40	0.62	0.09	2.56
6	Loch Tinker	5.42	6.75	8.16	0.90	20.60	0.11	0.09	0.52
7	Round Loch of Glenhead	4.72	5.49	9.35	1.90	20.10	1.93	0.30	4.11
8	Loch Grannoch	4.27	5.04	9.68	2.30	19.00	8.07	2.19	20.44
9	Dargall Lane	4.28	6.51	8.52	0.00	19.50	0.99	0.09	4.93
10	Scoat Tarn	4.90	5.57	7.84	1.50	15.50	3.50	0.09	10.88
11	Burnmoor Tarn	4.38	7.01	10.10	1.50	21.40	0.11	0.09	0.52
12	River Etherow	3.79	7.22	8.75	0.80	17.80	1.99	0.09	14.59
13	Old Lodge	4.10	5.30	10.06	0.00	19.00	6.06	0.83	19.65
14	Narrator Brook	4.93	6.45	9.67	4.60	12.80	1.05	0.09	6.15
15	Llyn Llaji	4.78	6.30	8.00	2.00	15.00	1.25	0.09	5.89
16	Llyn Cmm Mynach	4.70	6.30	10.42	4.50	16.40	2.09	0.09	10.78
17	Afon Hafren	4.31	6.60	7.74	1.00	20.00	3.56	0.09	13.78
18	Afon Gwy	4.50	6.40	9.74	0.50	20.30	1.87	0.09	9.22
19	Beaghs Burn	4.31	7.18	8.43	0.50	18.00	0.36	0.09	2.22
20	Bencrom River	4.38	6.27	9.19	0.70	18.00	4.21	0.09	11.41
21	Blue Loch	4.51	5.11	9.16	1.00	20.20	10.22	4.33	17.41
22	Coneyglen Burn	4.60	7.44	9.45	0.30	21.60	0.26	0.09	7.81

	non labile Al organic/poly $\mu\text{mol.dm}^{-3}$			Si $\mu\text{mol.dm}^{-3}$			DOC mg-C/l		
	mean	min	max	mean	min	max	mean	min	max
1	0.53	0.09	1.26	17.25	1.79	28.57	2.46	0.10	5.90
2	1.09	0.09	5.56	87.33	25.00	142.86	2.43	0.10	12.10
3	1.84	0.37	4.41	35.71	10.71	75.00	4.29	0.10	11.00
4	0.61	0.09	1.52	36.31	10.71	53.57	1.20	0.20	3.40
5	1.46	0.26	2.96	15.55	1.79	25.00	3.61	1.70	7.00
6	0.69	0.09	1.63	12.95	1.79	57.14	5.07	1.90	9.90
7	1.36	0.59	2.59	12.10	1.79	21.43	3.28	1.60	5.20
8	3.01	0.81	6.04	28.15	1.79	67.86	4.64	2.70	12.80
9	0.63	0.09	2.41	32.47	7.14	67.86	1.76	0.30	5.90
10	0.40	0.09	1.07	20.37	7.14	32.14	0.99	0.10	2.70
11	0.25	0.09	1.30	25.52	3.57	50.00	2.24	0.94	4.70
12	3.02	0.09	8.81	113.89	1.79	164.29	6.46	0.30	34.00
13	2.12	0.09	11.48	64.26	21.43	114.29	5.63	0.20	26.00
14	1.42	0.09	5.78	76.59	39.29	103.57	1.61	0.30	5.80
15	1.51	0.09	3.48	12.04	1.79	146.43	2.63	0.10	5.50
16	2.14	0.09	5.85	22.48	1.79	164.29	2.68	0.10	10.70
17	2.98	0.09	9.07	52.68	17.86	132.14	2.11	0.10	8.10
18	2.28	0.09	7.44	31.81	10.71	117.86	2.34	0.10	11.00
19	1.72	0.09	3.93	30.85	1.79	160.71	12.06	3.10	37.00
20	2.81	0.09	8.78	99.48	32.14	175.00	4.49	1.20	16.00
21	2.73	0.67	5.04	33.81	1.79	192.86	3.83	1.40	6.80
22	1.29	0.09	3.04	42.81	3.57	85.71	9.73	1.70	26.90

1.2.The chemistry of hydroxyaluminosilicates (HAS)

The reaction of Al with Si(OH)_4 to form HAS may be the key mechanism in controlling the biological availability of Al and a comprehensive review of the interaction of Al with monomeric Si(OH)_4 has been published recently (Exley et al. 2002). The precipitation of HAS has previously been observed in several studies on solutions containing Si(OH)_4 and Al at different concentrations and pH. Their characterisation either indirectly, using filtration, or directly, using solid-state NMR, led to some important information on their structure. The mechanism of formation of HAS, however, remained mostly hypothetical and the determination of parameters such as stability, size and rate of formation, are essential to fully comprehend the subject.

1.2.1.Structure of HAS

HAS are amorphous solid materials (Luciuk and Huang 1974) with a structure which is highly dependent upon the concentration of the species in the parent solution (Doucet et al. 2001a; Luciuk and Huang 1974). The molar ratios of Si:Al in the precipitates of HAS can vary from 0.5 to 1 depending on the molar ratio of the parent solution, indicating the formation of at least two form of HAS. Indeed, when Al is in excess to Si(OH)_4 in the parent solution, HAS_A precipitates with an ideal Si:Al ratio of 0.5. Its structure is constituted of octahedral Al onto which Si is co-ordinated through 3 Si-O-Al bounds ($\text{Q}^3(3\text{Al})$) (Figure 1.2-1 a). When the amount of Si(OH)_4 in the parent solution increases to exceed $[\text{Al}]$, the ideal Si:Al ratio in the material is 1 and, although some of the original HAS_A structure remains, it now includes a framework of tetrahedral Al and $\text{Q}^3(1-2\text{Al})$ and $\text{Q}^4(1-2\text{Al})$ Si. This form is referred to as HAS_B (Figure 1.2-1 b).

However, more information about the structure such as internuclear distances, motions and dynamics could be retrieved using more advanced solid-state NMR techniques to complete the characterisation of these materials.

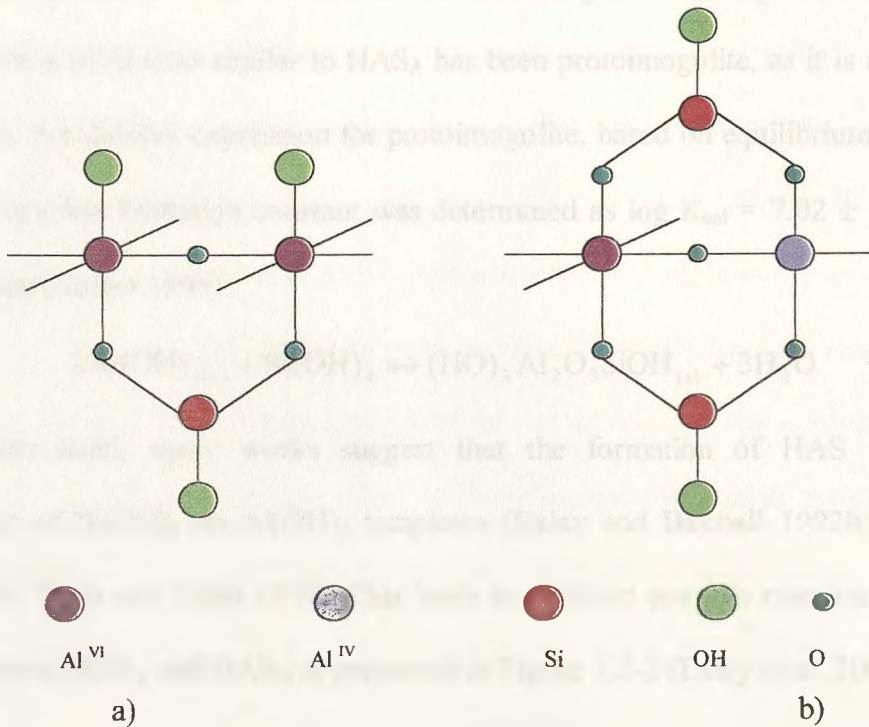
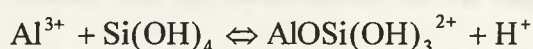


Figure 1.2-1: Structural unit of a) HAS_A and b) HAS_B as proposed by Doucet (2001a).

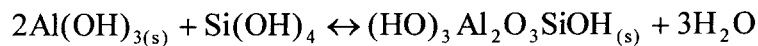
1.2.2. Mechanism and kinetics of formation of HAS

Several mechanisms of formation of HAS have been proposed through the years without however being fully elucidated. This problem is mainly related to the form of Al involved in the reaction with Si(OH)₄.

On the one hand, the formation of soluble aluminosilicates species through the substitution of H₂O in the coordination sphere of Al³⁺ by Si(OH)₄ was suggested in several studies (Browne and Driscoll 1992; Farmer and Lumsdon 1994; Gout et al. 1999; Pokrovski et al. 1996):



and a constant of formation based on this reaction scheme was determined using potentiometry at $pK_{110} = 2.50 \pm 0.05$ at 25°C (Farmer and Lumsdon 1994). However, there is little evidence to support this mechanism as $\text{AlH}_3\text{SiO}_4^{2+}$ has never been directly characterised and if it formed, it would not be stable at $\text{pH} > 4$ (Exley and Birchall 1995). An HAS with a Si:Al ratio similar to HAS_A has been protoimogolite, as it is the precursor of imogolite. A solubility expression for protoimogolite, based on equilibrium dialysis and the aforementioned formation constant was determined as $\log K_{\text{sol}} = 7.02 \pm 0.05$ at 25°C (Lumsdon and Farmer 1995):

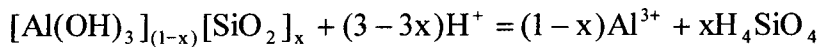


On the other hand, many works suggest that the formation of HAS involves the condensation of $\text{Si}(\text{OH})_4$ on $\text{Al}(\text{OH})_3$ templates (Exley and Birchall 1992b; Luciuk and Huang 1974; Wada and Kubo 1975). This leads to different possible reaction schemes for the formation of HAS_A and HAS_B as presented in Figure 1.2-2 (Exley et al. 2002).

The study of the reaction of substituted forms of $\text{Si}(\text{OH})_4$, such as where OH groups are replaced with other non-reactive groups such as methyl, with Al should reveal some important information on the mechanism of formation of HAS. If one or more of the OH groups of $\text{Si}(\text{OH})_4$ is replaced by an other functional group (CH_3 , C_2H_5 ,...), the approach of the $\text{Si}(\text{OH})_4$ analogue towards the $\text{Al}(\text{OH})_3$ template may be altered and the reaction itself might be jeopardised by the steric factors.

The determination of a constant of formation should also bring a new light on the mechanism itself and most importantly should help to understand how Al may be transported between the abiotic and the biotic cycles of the biogeochemical cycle of Al. The speciation and the geochemical control of Al in natural water is highly dependant upon

its interaction with $\text{Si}(\text{OH})_4$ to form HAS. The lack of kinetic information on this reaction may lead to a misinterpretation of modelling systems, in which results differ from experimental measurements. In most studies, the speciation of Al is considered to be controlled by the solubility of gibbsite, despite the lack of evidence that such an equilibrium exists. Gibbsite equilibrium is often assumed at moderate to high pHs, but it is not observed in most temporal zonal soils and there is a strong argument that the thermodynamic methods of evaluation may be misleading (Neal 1995; Neal et al. 1987). The explanation for the gibbsite undersaturation observed at low pH may lie in the presence of other Al-bearing materials such as Al-sulfate minerals or aluminosilicates which depict disequilibrium conditions (Brezonik et al. 2003). When investigating the origin of such a phenomenon, the effect of SiO_2 is described using Paces' model on solubility controls for aluminosilicates of variable composition (Paces 1978):



$$\text{with } x = 1.24 - 0.135 \text{ pH}$$

which led to the conclusion that aluminosilicate minerals did not control dissolved Al. However, the reliability of this model has been discussed by Neal and Williams when they reported the lack of a linear relationship between x and pH on experimental results (Neal and Williams 1988). They pointed out that the presence of aluminosilicate phases may be responsible for the kinetic controls of water quality instead of the simple solubility of gibbsite and that the nature and chemistry of such solid phases should be taken in account. This emphasises the crucial necessity of the determination of an equilibrium constant of formation for HAS, as they are most likely to be present in acidic natural water. Knowing this constant would permit a more reliable modelling of natural water systems.

1.2.3. Agglomeration

One of the main parameters in the control of the toxicity of Al by the formation of HAS is the stability of this material. Exley et al stressed this point in their study of the effect of Si(OH)_4 on aluminium toxicity in fish (Exley et al. 1997). They demonstrated that a minimum amount of Si(OH)_4 was required ($>100 \mu\text{mol.dm}^{-3}$) to form HAS at pH 5. Moreover, for $[\text{Si(OH)}_4] = 200 \mu\text{mol.dm}^{-3}$, the formation of HAS resulted in an increase in the toxicity of Al, suggesting that HAS were not stable enough towards dissolution to reduce toxicity. The excess of Si(OH)_4 in solution after formation of HAS might operate as a shield by surrounding the individual HAS particles and preventing them to aggregate. As a result, the size of the HAS particles remains very small (smaller than Al(OH)_3) and they are therefore more likely to release Al^{3+} , incidentally increasing the toxicity. However, they showed that by increasing either the pH or $[\text{Si(OH)}_4]$, HAS gained in stability and were therefore efficient in the elimination of the acute Al toxicity in fish (Birchall et al. 1989; Exley et al. 1997). These observations emphasise the necessity to understand the phenomenon of agglomeration of HAS, i.e. the way individual particles grow and aggregate together to form a stable species, as well as to define the minimum and optimal parameters, such as pH, $[\text{Al}]$, $[\text{Si(OH)}_4]$, under which HAS will form.

1.3. Aims of this study

The purpose of this work was to elucidate further the detailed inorganic chemistry of the reaction of Al with Si(OH)_4 . First, in order to better understand the mechanism behind the reaction between Si(OH)_4 and Al, I studied the interaction between Al and two analogue forms of Si(OH)_4 , dimethylsiloxane-diol (DMSD) and its dimer tetramethyldisiloxane-diol (TMDS), by both solution and solid state NMR and SEM-EDX. I also investigated the phenomenon of agglomeration of HAS_A and HAS_B with time by tapping-mode AFM in

solution and I characterised some of these samples using XPS. This last technique was used for the first time on this kind of material and revealed new information on the structure of HAS. The main aim of this research was then to study the influence of $\text{Si}(\text{OH})_4$ on the formation of the Al-morin complex (AlM) by fluorimetry in order to observe indirectly the formation of HAS in very dilute solutions. The quantification of the fluorimetric results coupled with calculations using a speciation software (SGW) enabled the determination of an equilibrium constant for the formation of HAS at 20°C.

Chapter 2 : Materials and methods

2.1.Molecular spectroscopy

This section is based on two books (Fifield and Kealey 2000; Skog et al. 1998).

2.1.1.General principles

Molecular spectroscopy may be defined as the study of the interaction of electromagnetic waves and matter. The concept of the particle-like description of electromagnetic radiation combined with the wave-like description leads to a direct relationship between the energy (E) of a photon and the frequency (ν) of the radiation:

$$E = h\nu = \frac{hc}{\lambda}$$

where h is Planck's constant.

When a molecule absorbs or emits radiation, the energy of the radiation emitted or absorbed ($h\nu$) must be equal to the energy difference (ΔE) between the initial and final states of the molecule, according to the principle of energy conservation. As energy levels are specific to each molecule, the analysis of the emitted or absorbed radiation is a direct characterisation of the molecular constitution.

The nature of molecular energy is complex and has contributions from (i) translational, rotational and vibrational motions, (ii) electrons occupying molecular orbitals and (iii) nuclear spins. A representation of the different energy levels is shown in Figure 2.1-1. The separation between each of the quantized levels varies for each type of molecular energy and has the following order:

$$\Delta E_{\text{electronic}} > \Delta E_{\text{vibrational}} > \Delta E_{\text{rotational}} > \Delta E_{\text{nuclear spin}}$$

Most of the time, only the absorption spectra are studied. Three techniques are important for analytical purpose: UV-visible spectrometry (electronic), infrared spectrometry (vibrational) and nuclear magnetic resonance spectrometry (nuclear spin).

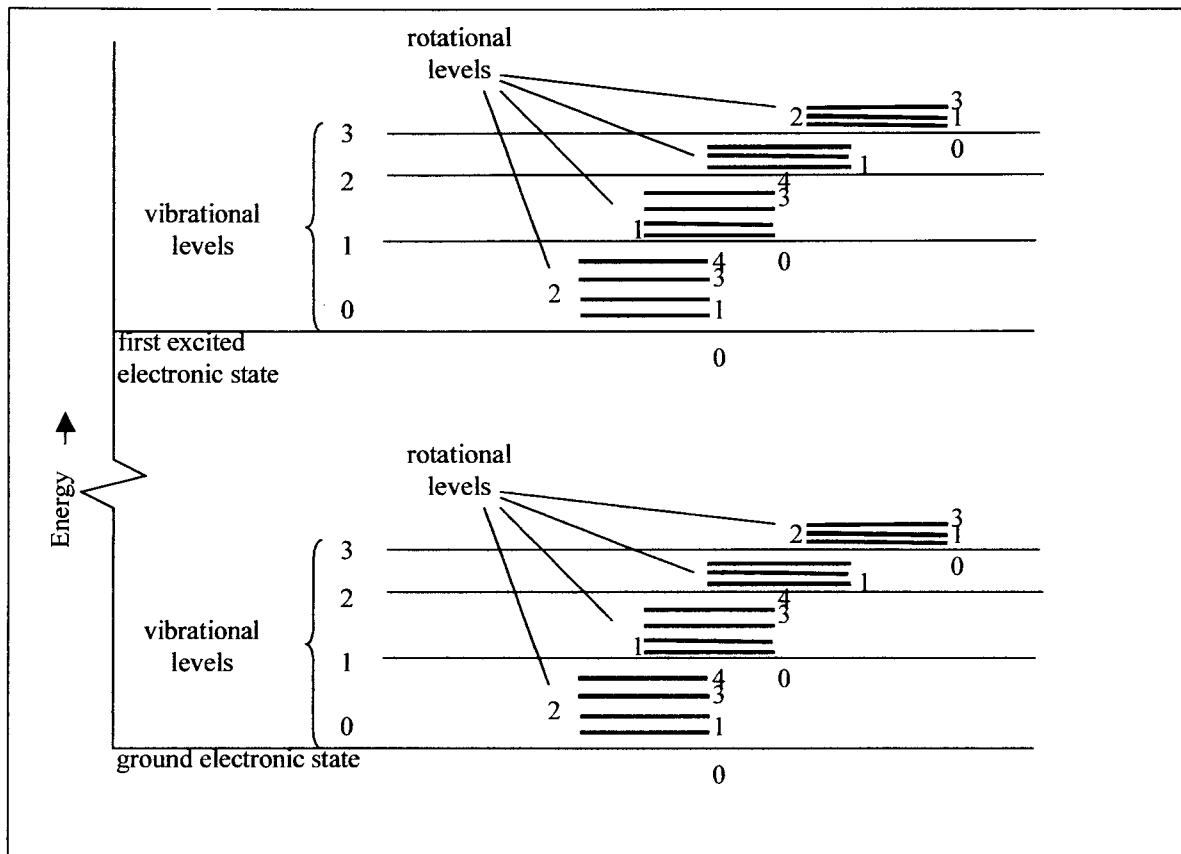


Figure 2.1-1: Schematic representation of the different energy levels in a molecule.

When electromagnetic radiation interacts with matter, the energy of the incident photons is transferred to the molecules raising them from the ground state to an excited state. This phenomenon is known as absorption. It results in an attenuation of the incident radiation. The absorbed energy is rapidly lost by collisions allowing the system to relax to the ground state. However, it happens sometimes that the energy is re-emitted a few milliseconds later – this phenomenon, known as fluorescence, generally occurs in a number of complex organic molecules. The measurement of fluorescence radiation is known as fluorimetry.

2.1.2.UV-Visible spectroscopy

• Principles

UV-visible spectrometry consists of the absorption of electromagnetic radiation in the visible and ultraviolet regions of the spectrum resulting in changes in the electronic structure of ions and molecules. In UV-visible spectroscopy, the wavelengths of the radiation involved cover a range from 200 to 800 nm. When a beam of intensity I_0 passes through a solution, a part of its energy is absorbed as a result of its interaction with the analyte present in solution (Figure 2.1-2). Consequently, the emergent beam has a lower intensity I . Molecular absorption spectroscopy is based on the measurement of this effect, generally translated as transmittance or absorbance.

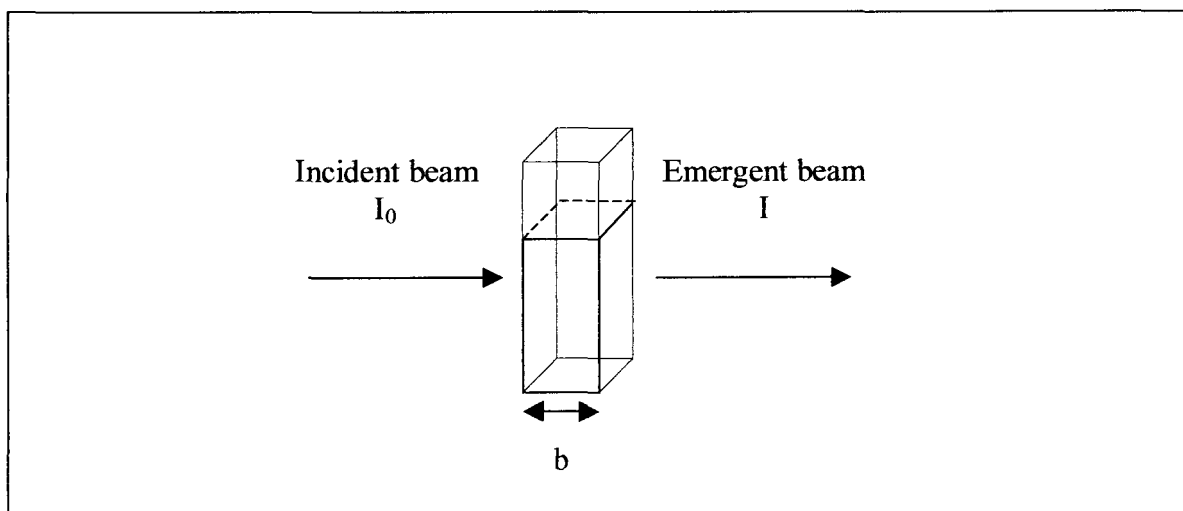


Figure 2.1-2: Attenuation of radiation by interaction with analyte.

Transmittance (T) is the ratio of emergent intensity to incident intensity. A more useful measure of the amount of radiation absorbed by a solution is the absorbance (A).

$$T = \frac{I}{I_0}$$

$$A = -\log T = \log \frac{I_0}{I}$$

As the amount of radiation absorbed by an analyte in solution is affected by the concentration of the solution, UV-visible spectroscopy is a method of choice for

quantitative analysis. The relationship between absorbance and concentration is described by the Beer-Lambert law as follow:

$$A = abc$$

where a is a proportionality constant, known as the absorptivity, c the analyte concentration and b the pathlength. In order to apply this simple law to the measurement of unknown concentrations of analyte, it is necessary to run a calibration using standard solutions.

There are few exceptions to the generalisation of the linearity between absorbance and pathlength in the Beer-Lambert law, but deviations from direct proportionality between absorbance and concentrations are frequently encountered. These deviations result in calibration graphs which are not linear, with the departure from non-linearity being particularly severe at high concentrations. Some of these deviations are fundamental and represent *real deviations* of the law. Others are related to the instrument or to chemical changes.

Real limitations of the Beer-Lambert law:

At high concentration (usually above 0.01 mol.dm^{-3}), the average distance between the molecules responsible for absorption is diminished to the point that each molecule interacts with its neighbours, altering in return the ability of the molecules to absorb a given wavelength of radiation. This can also happen in less concentrated solutions containing high concentrations of electrolytes, by mean of electrostatic interactions.

Instrumental deviations

The Beer-Lambert law can only be observed with truly monochromatic radiation. This is another limitation to the law. Unfortunately, the use of a continuum source has taken over

from the use of single wavelength radiation. The use of a polychromatic beam results in a non-linear relationship between the measured absorbance and the concentration when the molar absorptivities differ. However, it is shown that the departure from the law is not significant if the effective bandwidth of the monochromator is less than 1/10 of the half width of the absorption peak at half height.

Another possible deviation from the law comes from the contamination of the exiting radiation by a small amount of scattered or stray radiation. This results from scattering and reflections from various internal surfaces. When measurements are made in the presence of stray radiation, serious deviations from the linear relationship between absorbance and concentration as well as between absorbance and pathlength can be observed (Sharpe 1984).

Chemical deviations

Departures from the law can also be observed when the analyte undergoes dissociation, association or reaction with a solvent to produce a product of different absorption spectrum.

•*Instrumentation*

Figure 2.1-3 shows the optical system of the spectrometer. Radiation is emitted from either the deuterium lamp (UV range: 100 nm - 360 nm) or the halogen lamp (visible range: 360 nm – 750 nm), depending on the positioning of the mirror M1. The beam is then directed onto the mirror M2 which reflects it through an optical filter on the filter wheel assembly. The radiation passes then through the entrance slit of the monochromator and is dispersed at the grating to produce a spectrum. An appropriate rotation of the grating allows the selection of a segment of the spectrum, reflecting it through the exit slit to mirror M3.

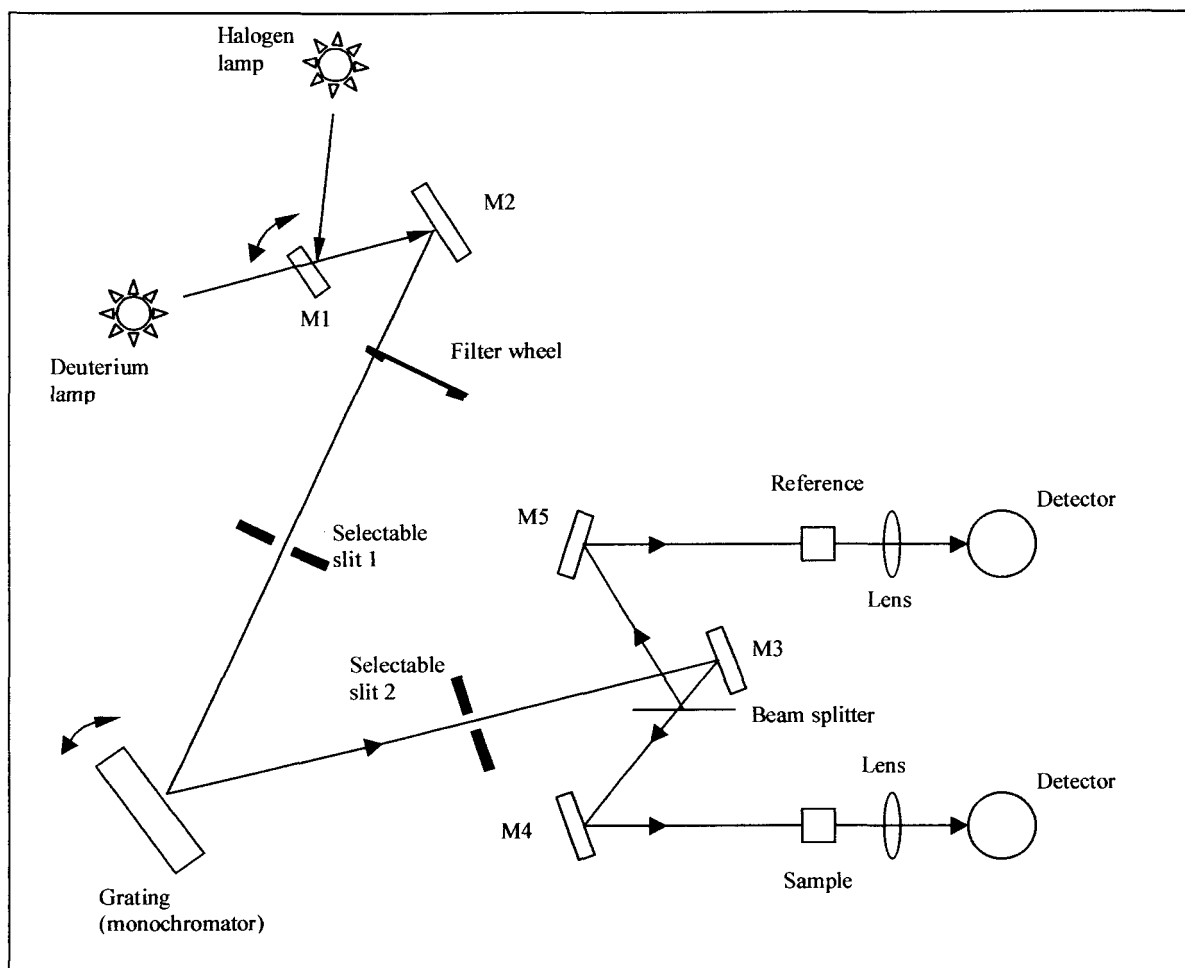


Figure 2.1-3: Optical path for a UV-Visible Spectrometer Lambda 14 (Perkin Elmer).

The exit slit restricts the spectrum segment to a near-monochromatic radiation beam. From M3, the radiation is reflected onto a beam splitter which allows 50% of the radiation to pass onto mirror M4 and reflects 50% onto mirror M5. The two beams are then transmitted through the sample cell and the reference cell respectively and they are focused on to the photodiode collector.

•*The Molybdenum blue assay*

Throughout my research, I used UV-Visible spectrometry to measure $[\text{Si}(\text{OH})_4]$ using the molybdenum blue assay method. I followed the procedure described in 1980 by Imperial Chemical Industries Ltd to measure monomeric and dimeric silicic acids in solution (Industries 1980). The basis of this method is the reaction of ammonium molybdate under

controlled acid conditions with Si(OH)_4 to form the yellow molybdosilicic acid followed by its reduction in situ with ascorbic acid to yield a silicomolybdenum blue complex which is measured spectrophotometrically. This method allows a large range of silicon concentrations (up to 10 mg.L^{-1}) to be measured. Some pre-treatment may be required for the measurement of the total silicon concentration. The spectrophotometric measurement is made at 700 nm in a 10 mm cell. It is also necessary to perform a calibration curve prior to any analysis. The calibration curve is linear up to 10 mg.L^{-1} and is made using different dilutions of a standard solution. In order to obtain reliable results, it is preferable to carry out a series of blank determinations before analysing the samples. A blank made with good quality reagents should not exceed $10 \mu\text{g.L}^{-1}$.

The general protocol is described in Figure 2.1-4.

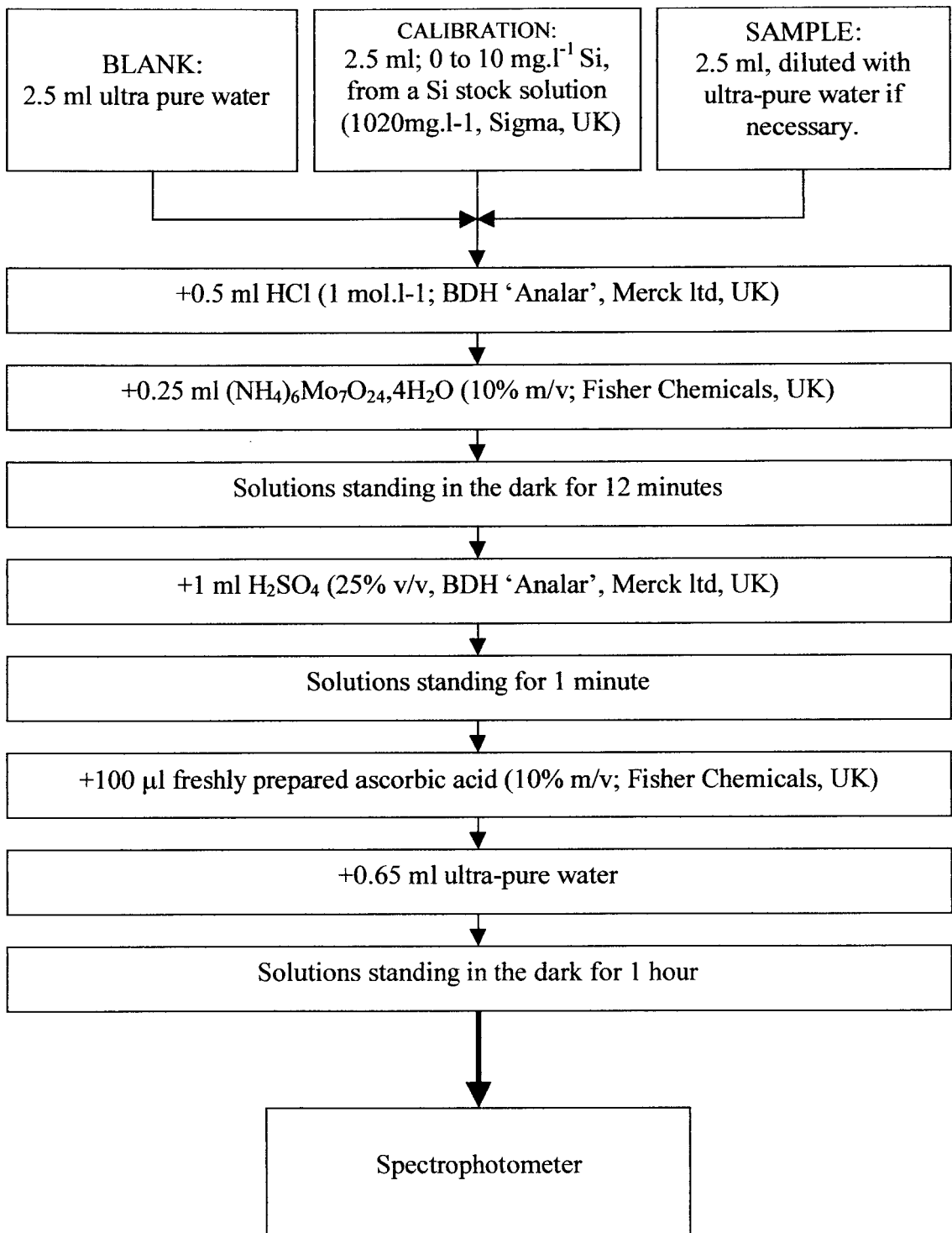


Figure 2.1-4: Protocol for the determination of molybdate-reactive silicon concentration.

2.1.3. Fluorimetry

- Principles

A fluorescence emission spectrum arises from transitions between the lowest vibrational level of the first excited electronic state and different vibrational levels of the ground state.

Figure 2.1-5 summarises the different relaxation mechanisms.

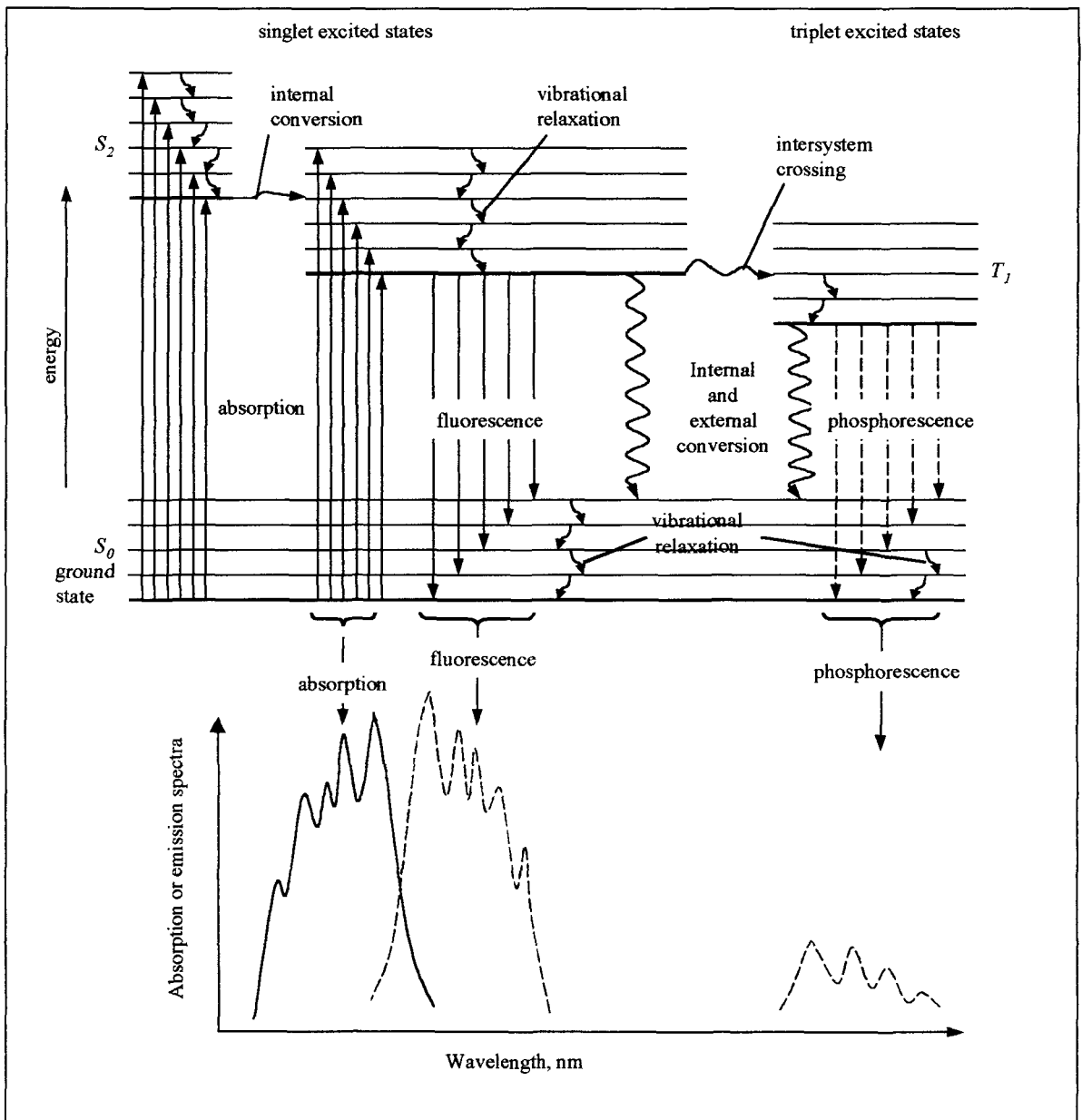


Figure 2.1-5: Schematic of the different relaxation phenomenon.

The determination of inorganic species involves the formation of a fluorescing chelate and the measurement of its emission. The most successful fluorimetric reagents for cation analyses have aromatic structures with two or more donor functional groups that permit chelate formation with the metal ion.

The intensity of fluorescent emission is dependent on a quantum efficiency factor Φ_F which can vary from 0 (no fluorescence) to 1 (all excited molecules relax by fluorescence). This factor is dependent upon a number of structural characteristics such as the presence of heteroatoms, the degree of rigidity, the number of conjugation.

- *Instrumentation*

The components of instruments used in fluorimetry are very similar to those found in UV-visible photometers or spectrophotometers and are shown Figure 2.1-6. Double-beam optics are used in order to compensate for fluctuations in the power of the source. The sample beam first passes through an excitation filter or monochromator, which transmits radiation that will excite fluorescence. The sample scatters the fluorescence radiation in all directions, but it is preferable to observe it at right angle to the excitation beam to reduce errors in measurement. The emitted radiation reaches a phototransducer after passing through a second monochromator that isolates the fluorescence. The reference beam passes through an attenuator that reduces its power to that of the fluorescence radiation and the two signals are sent to a difference amplifier before undergoing data processing.

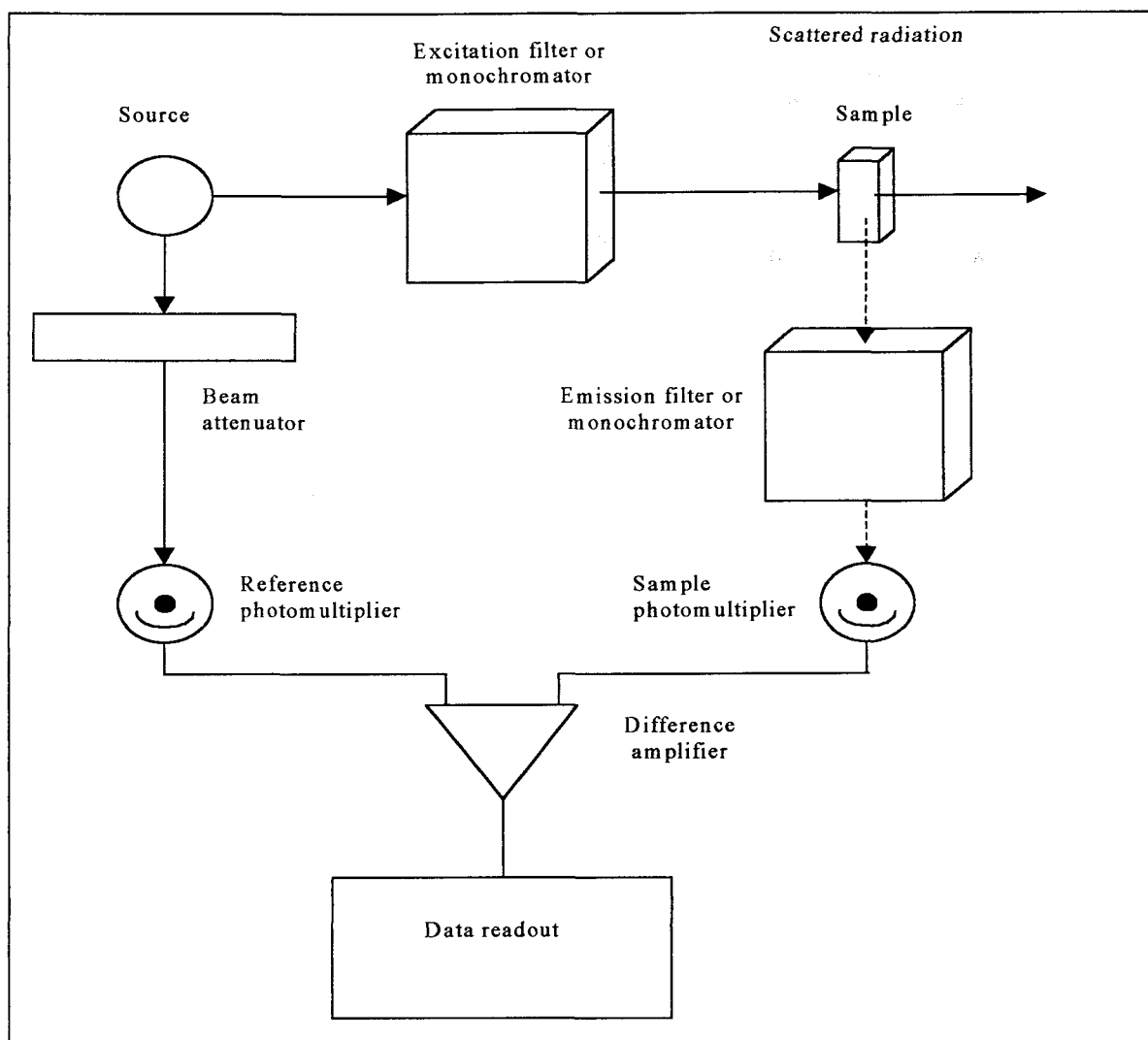


Figure 2.1-6: Components of a fluorometer or a spectrofluorometer.

•*The morin reactive complex*

In my research, I used fluorimetry to measure the amount of Al available to morin in solution. As mentioned earlier in this chapter, the measurement of inorganic species by fluorimetry involves the reaction with a fluorescing chelating agent. In 1990, Browne et al proposed a procedure based upon the complexation of Al^{3+} with morin (2,3,4,5,7-pentahydroxy-flavone) to measure aqueous Al in acidic pH (Browne et al. 1990b).

Morin is a pentaprotic acid with five weakly acidic functional groups. In the acidic pH range, only the first proton dissociation ($pK_a = 5.04$) is found to be relevant and one can

use a simple monoprotic model to describe the distribution of morin species before its complexation with Al. Al reacts with morin to form complexes of 1:1, 1:2 and/or 1:3 Al/morin stoichiometry. However, at low morin concentration (near $1 \mu\text{mol.l}^{-1}$), only 1:1 species are prevalent. The mechanisms involved in (i) the first proton dissociation and (ii) the formation of the Al-morin (AlM) complex are described Figure 2.1-7. The first proton dissociation occurs on the 3-hydroxy group due to the proximity of the electronegative 4-keto oxygen which confers a greater acidity to this group.

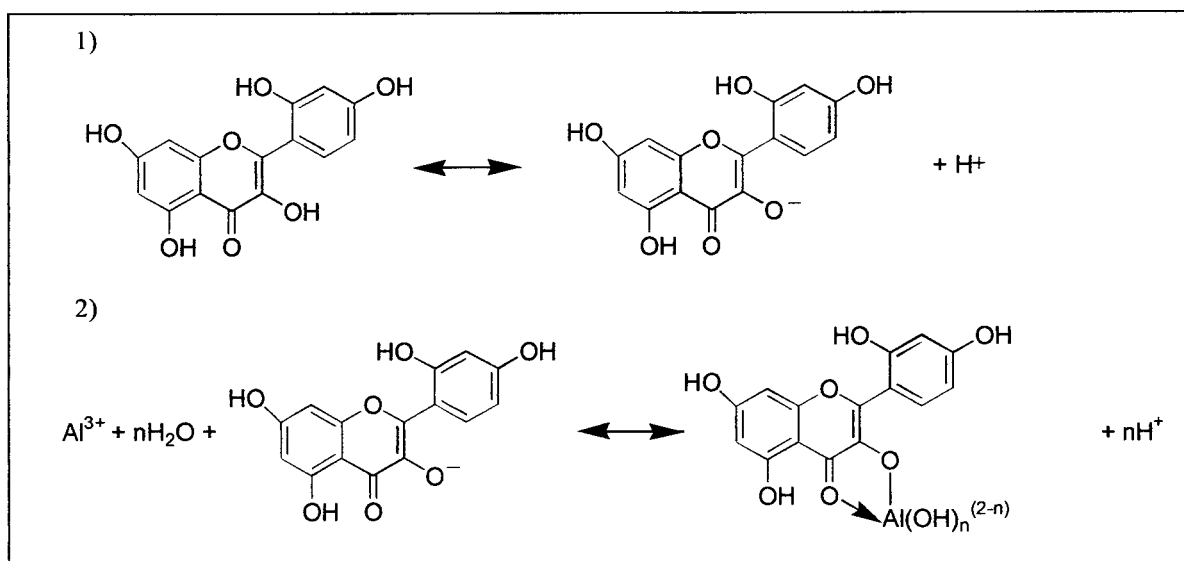


Figure 2.1-7: 1) Mechanism of the first proton dissociation of morin. 2) Mechanism of Al complexation with morin.

The absorbance spectrum of morin is strongly dependant upon pH and the deprotonation can easily be observed by UV-Vis. The spectra of $125 \mu\text{mol.dm}^{-3}$ morin solution recorded for different pH are presented in Figure 2.1-8. It shows a first absorbance maximum at 368 nm attributed to H_5MOR and a second maximum at 405 nm attributed to H_4MOR^- . The peak at 320 nm was due to the presence of KNO_3 in solution. The presence of an isoabsorptive point at 360 nm confirmed the presence of only two species.

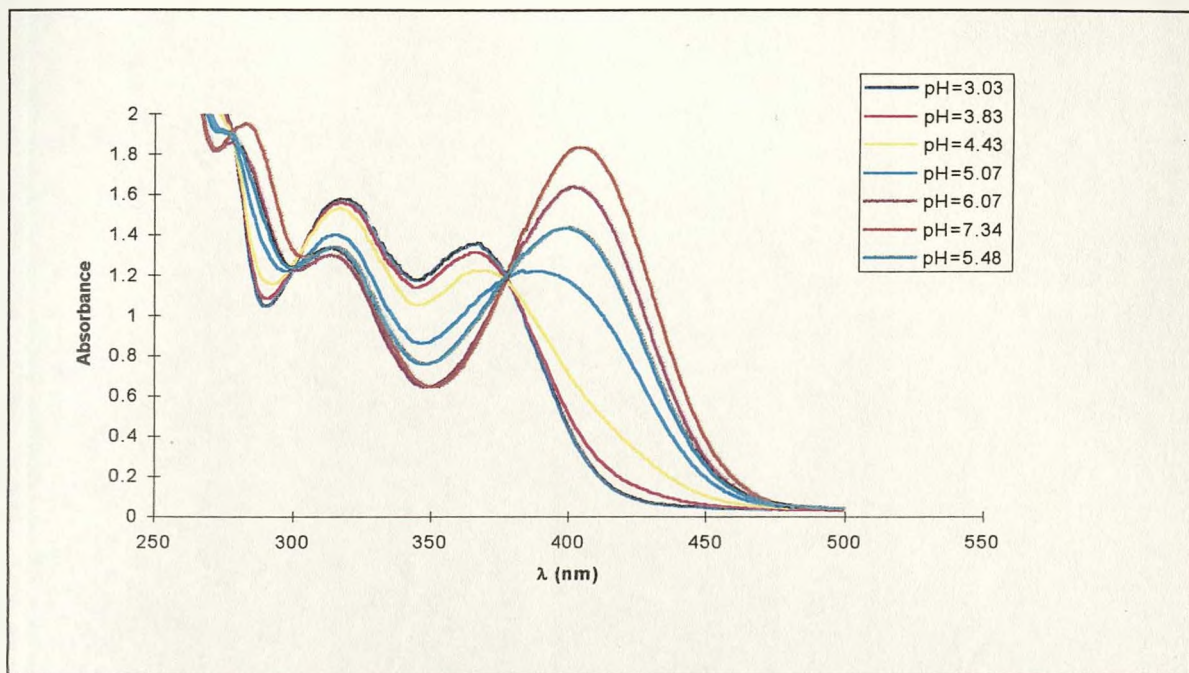


Figure 2.1-8: Influence of pH on the UV-Visible absorbance spectra of [morin] = 125 $\mu\text{mol}\cdot\text{dm}^{-3}$. 1: KNO_3 ; 2: H_5MOR ; 3: H_4MOR^- . Isoabsorptive point.

To prevent any misleading interpretation of the measurement of AIM, it was absolutely required that only H_5MOR and H_4MOR^- were present during the preparation of the samples. A pre-study on the influence of morin concentration on the species distribution led to the determination of the maximum concentration to be used in the experiments. The results are shown in Figure 2.1-9. Hence, it was shown that a concentration above 125 $\mu\text{mol}\cdot\text{dm}^{-3}$ is unsuitable for the purpose of this study, even after dilution.

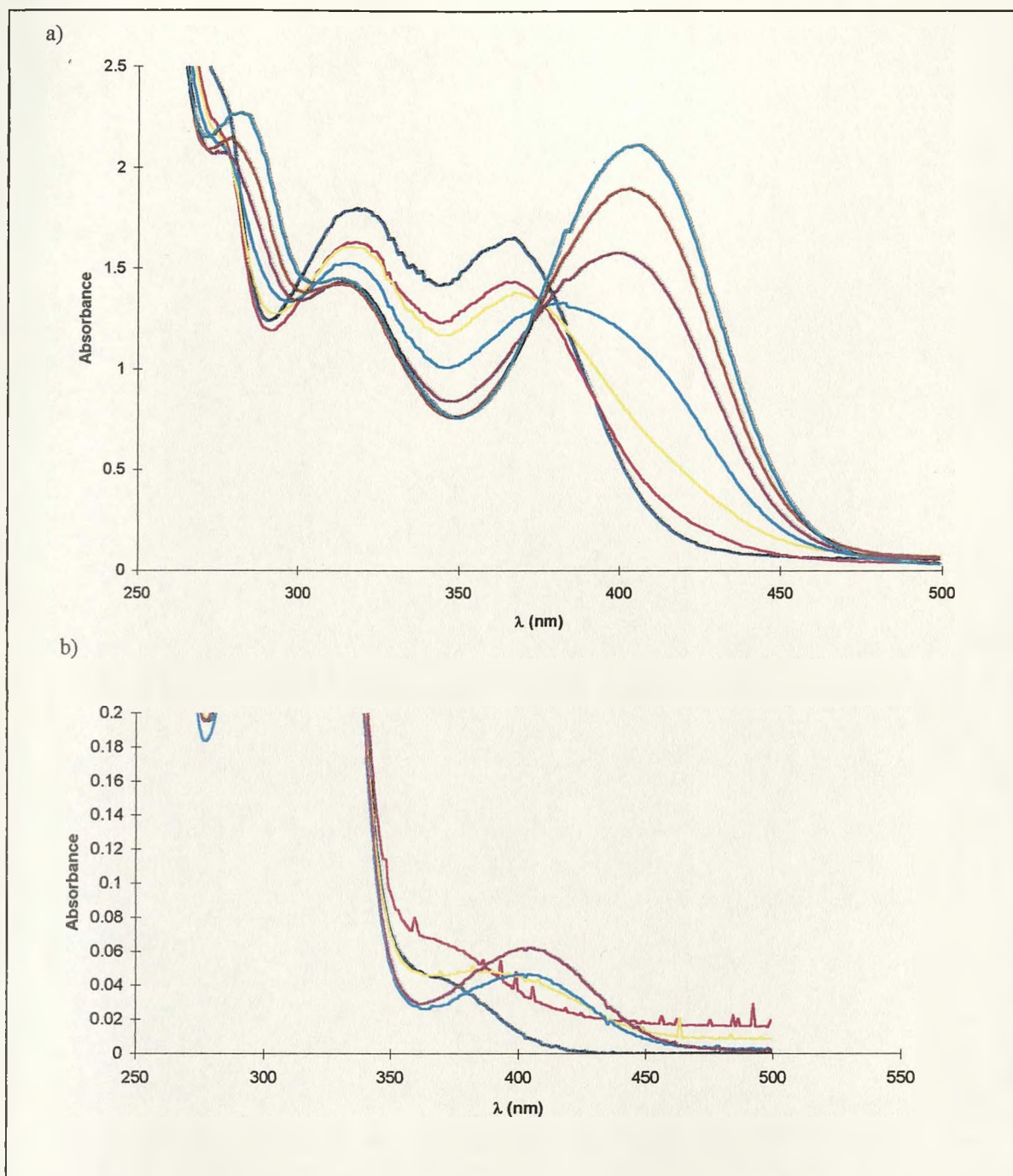


Figure 2.1-9: Influence of pH on UV-visible spectra of a) $[morin] = 150 \mu mol \cdot dm^{-3}$; b) $[morin] = 5 \mu mol \cdot dm^{-3}$, after dilution of a $[morin] = 150 \mu mol \cdot dm^{-3}$. There is no isoabsorptive point.

2.2. Graphite Furnace Atomic Spectroscopy (GFAAS)

2.2.1. General principles

• *Definition*

Spectrometry might be defined as the application of the interaction of light with matter to the quantitative determination of that matter. Light is electromagnetic radiation and combines both the properties of wave and particles. The relationship between the frequency and the energy of the photon is:

$$E = h\nu = \frac{hc}{\lambda}$$

In GFAAS, the interaction of light of a specific wavelength with gaseous atoms is measured. The graphite furnace acts as an atom cell and converts the sample into gaseous atoms. *Absorption* is described as the promotion of a valence electron from the ground to the excited state by transfer of the energy of a photon (Figure 2.2-1). Consequently, the energy of the photon must be equal to the difference in energy between the ground and the excited states.

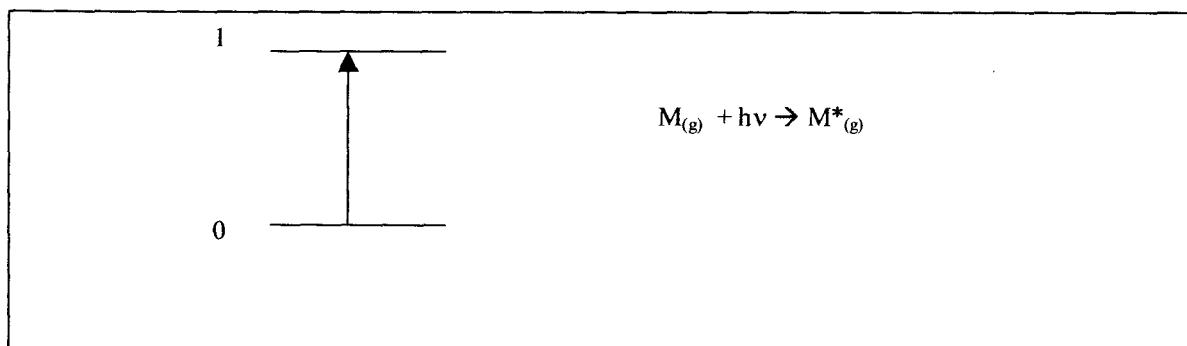


Figure 2.2-1: Atomic absorption transition between ground state 0 and the excited state 1. The gaseous atom M is promoted to its excited state M*.

•Signal

A quantitative atomic absorption measurement is illustrated in Figure 2.2-2. A light beam of intensity I_0 passes through a cell and the transmitted beam of intensity I is detected. If the cell is empty, the transmitted intensity is equal to I_0 . If the cell contains analyte, the transmitted intensity is then lower than I_0 as a part of the intensity is absorbed in the excitation of analyte electrons.

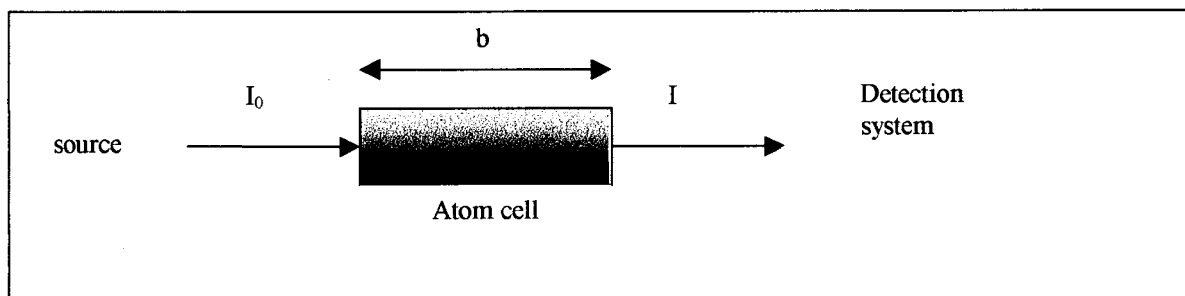


Figure 2.2-2: Schematic diagram of atomic absorption process.

The transmittance T is defined as the ratio of the transmitted intensity to the incident intensity and is unitless:

$$T = \frac{I}{I_0}$$

This represents the fraction of light transmitted through the cell. Generally, absorption measurements are made using absorbance A (unitless):

$$A = -\log T = -\log \frac{I}{I_0} = \log \frac{I_0}{I}$$

It should be noted that when the concentration of analyte in the cell (the number of atoms) is increased, the absorbance A is also increased. There is a direct relationship between absorbance (A) and concentration (c , g/L). The Beer-Lambert law describes this quantitative relationship:

$$A = abc$$

where a is the absorptivity (L/g cm) and b is the pathlength of the cell (cm). Because of the direct proportionality between absorbance and pathlength, GFAAS usually employs a relatively long illuminated volume.

•*Instrumentation*

A schematic diagram of the GFAAS is shown in Figure 2.2-3. The sample is introduced into the tube through a dosing hole. A power supply sends a control current to heat the tube at different temperatures for specified period of times. This process is called the atomisation cycle and is described in Figure 2.2-4. The tube is surrounded by argon to prevent combustion in air at elevated temperatures. It is preferable to use a pyrolytically coated graphite tube to reduce diffusion of analytes into the graphite and chemical reactivity. It is therefore specifically used to reduce any carbide formation. A light source is then sent through the tube to excite analyte atoms. To ensure that only the analyte atoms absorbs this light, the emission from the source is caused by excited atoms of the designated analyte. The detection system records the quantity of light absorbed in the tube and deduces the amount of analyte present in the sample.

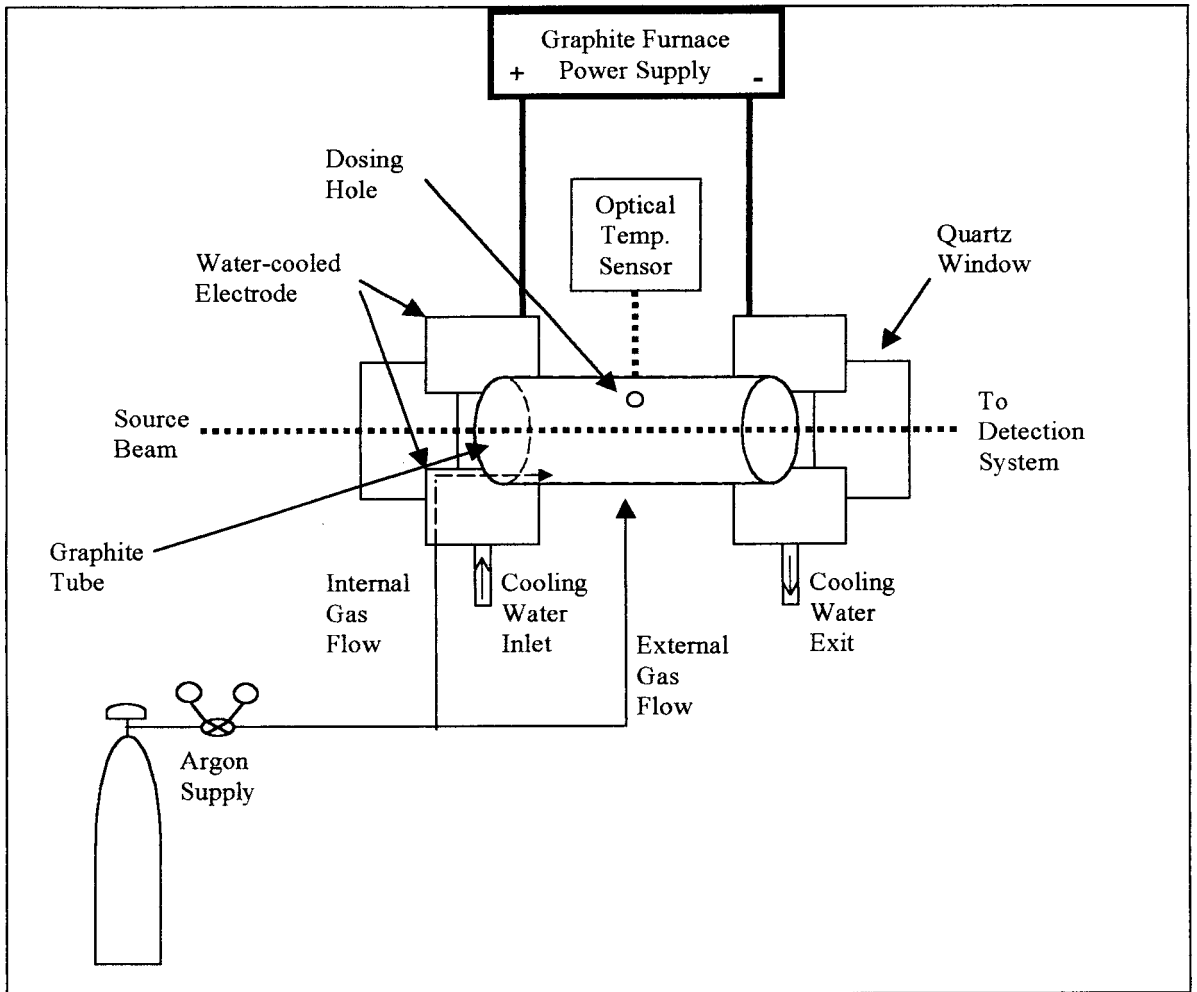


Figure 2.2-3: Schematic diagram of a GFAAS instrument.

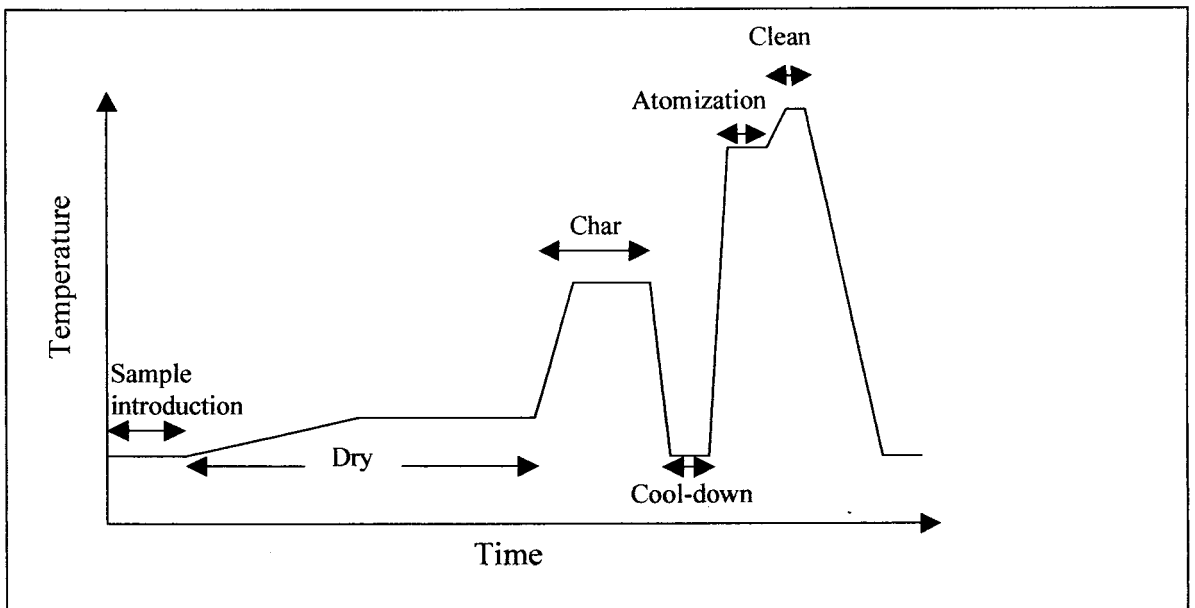


Figure 2.2-4: Schematic diagram of the atomisation cycle.

2.2.2. The influence of Si(OH)₄ on the measurement of Al by GFAAS.

• *Introduction*

GFAAS is a widely used technique to analyse $\mu\text{g.L}^{-1}$ concentrations of elements, and, in particular, metals such as Al (Berube and Brule 1999; Gardiner et al. 1981; Lajunen et al. 1990; Manning and Slavin 1983; Ranau et al. 1999; Xu et al. 1992). L'vov (1978) has described the theory which governs the determination of species by GFAAS, as well as the possible chemical effects which can arise from the interaction between analytes and (i) furnace walls, (ii) gaseous atmosphere and (iii) analytical matrices. More specifically, the determination of Al by GFAAS presents a number of difficulties, for example (i) the formation of an AlH spike in the graphite atomiser (Ohlsson et al. 1992a), (ii) the reduction of Al oxides by carbon to form aluminium carbide which can be responsible for the formation of a spike (Lvov et al. 1991), (iii) the redistribution of Al in the sample due to spike formation (Ohlsson et al. 1992b). Wilhelm et al (1990) have also indicated the importance of storage conditions on Al determination by GFAAS. In order to optimise the detection of Al, i.e. to reduce the number of interferences during the atomisation process to obtain more reliable results, several studies have been carried out on the possible enhancement of the absorbance signal of Al by adding different species, for example orthophosphoric acid (Craney et al. 1986; Woolfson and Gracey 1987), $\text{Cu}(\text{NO}_3)_2$, $\text{Ca}(\text{NO}_3)_2$, Na_2SO_4 , NaH_2PO_4 , K_2HPO_4 , NaCl , MgCl_2 , CaCl_2 , CuCl_2 , HClO_4 , $\text{Mg}(\text{NO}_3)_2$ (Manning et al. 1982). However, it would seem that the most efficient modifier described to date is $\text{Mg}(\text{NO}_3)_2$ (Katskov et al. 1999; Manning and Slavin 1983; Slavin et al. 1981). Styris et al (1987) have described the mechanisms that govern the atomisation process as the thermal dissociation of condensed-phase Al_2O_3 . They also showed that $\text{Mg}(\text{NO}_3)_2$ stabilised Al in a two step process: (i) the formation of magnesium hydroxide which

inhibits the formation of aluminium hydroxide and thus, the loss of aluminium during the pre-treatment; (ii) the reduction of magnesium oxide which allows the retention of aluminium oxide before atomisation. The possibility that Si might interfere with the determination of Al by GFAAS was, coincident with my study, briefly examined by Nukatsuka et al (2000).

•*Experimental*

Instrumentation and reagents

The total [Al] was determined by graphite furnace atomic absorption spectrometry (GFAAS), using a Perkin Elmer atomic absorption spectrometer 3300 under argon furnace (HGA 600) atmosphere, with an auto-sampler (AS40). The wavelength used was 309.3 nm. The pre-treatment temperature was 1450°C and the atomisation temperature was 2650°C. The temperature programme is presented in Table 2.2-1 . The volume of injection was 30 µL.

Table 2.2-1: Temperature programme.

Step number	Temp (°C)	Time (s)		Int. Flow (mL/min)
		Ramp	Hold	
1	80	5	5	300
2	120	10	30	300
3	500	10	10	300
4	1450	10	15	300
5	2650	0	5	0
6	2700	1	5	300

Al standards were prepared from a certified Al stock (37 mmol.dm^{-3} in 2% HNO_3 , Perkin Elmer Instruments) in ultra-pure water (conductivity $< 0.5 \text{ }\mu\text{S.cm}^{-1}$). Si(OH)_4 was prepared by cation-exchange of a 2 mmol.dm^{-3} Na_4SiO_4 solution (Industries 1980). Magnesium was added as $\text{Mg(NO}_3)_2 \cdot 6\text{H}_2\text{O}$ (Aldrich).

Preparation of normal calibration standard

The blank correction was done with 1% HNO_3 . 10 ppm Al in 1% HNO_3 was used to prepare the highest standard by hand. Lower calibration standards were prepared by the AS40 using 1% HNO_3 as the diluent.

Preparation of calibration standards containing Si(OH)_4

The blank corrections were prepared with $[\text{Si(OH)}_4] = 0.1, 0.2, 0.4, 0.8, 1 \text{ mmol.dm}^{-3}$ in 1% HNO_3 . 10 ppm Al in the corresponding $[\text{Si(OH)}_4]$, 1% HNO_3 was used to prepare the highest standard by hand. Lower calibration standards were prepared by the AS40 using $[\text{Si(OH)}_4]$, 1% HNO_3 as the diluent.

Influence of Si(OH)_4 on the Al absorbance

A 10 ppm Al in 1% HNO_3 stock solution was used to prepare samples with $[\text{Al}] = 1.11, 2.22, 3.33, 4.44, 4.81, 5.55, 6.66, 7.77, 8.88 \text{ }\mu\text{mol.dm}^{-3}$. The influence of the $[\text{Si(OH)}_4]$ was observed also, as $[\text{Si(OH)}_4] = 0, 100, 500, 1000, 2000 \text{ }\mu\text{mol.dm}^{-3}$. Because $[\text{Al}]$ vs. absorbance was not a linear relationship over a wide range of absorbance, it was necessary to ensure that all comparisons of absorbance signal were made within linear portions of the curve (i.e. similar absorbance signal). To achieve this, the volume of injection was changed as a function of the Al concentration studied. Two ranges of absorbance were necessary,

depending on the Al concentration studied, in order to keep a useful volume of injection.

The parameters are given in the Table 2.2-2.

Table 2.2-2: Volume of injection, integration time and average absorption of Al only samples for a range of [Al]. Light grey: 1st range of absorbance. Dark grey: 2nd range of absorbance.

[Al] ($\mu\text{mol.dm}^{-3}$)	1.11	2.22	3.33	4.44	4.81		5.55	6.66	7.77	8.88
Volume (μl)	40	20	15	11	10	22	20	15	12	10
Integrated Time (min)	1.5	1.5	1.5	1.5	1.5	1.8	1.8	1.8	1.8	1.8
Absorption (Al alone)	0.33	0.34	0.35	0.34	0.33	0.57	0.6	0.59	0.60	0.58

Comparative effect of $\text{Mg}(\text{NO}_3)_2$ on the Al absorbance.

A 10 ppm Al in 1% HNO_3 solution was used to prepare samples with $[\text{Al}] = 2.22, 4.81, 7.77 \mu\text{mol.dm}^{-3}$ containing either (i) no further addition, (ii) $10 \text{ mmol.dm}^{-3} \text{Mg}(\text{NO}_3)_2$, (iii) $2 \text{ mmol.dm}^{-3} \text{Si}(\text{OH})_4$ or (iv) $10 \text{ mmol.dm}^{-3} \text{Mg}(\text{NO}_3)_2 + 2 \text{ mmol.dm}^{-3} \text{Si}(\text{OH})_4$. The volumes of injection were adjusted as described above and each sample was replicated 5 times.

Application to real samples.

33 samples from a previous study (Doucet et al. 2001b), containing known $[\text{Si}(\text{OH})_4] = 0.05\text{-}2 \text{ mmol.dm}^{-3}$ and unknown $[\text{Al}]$ were analysed by GFAAS using either a normal calibration or a matrix-matched calibration using the requisite $[\text{Si}(\text{OH})_4]$. A further two unknown samples taken from hot springs in southern Iceland (Fairchild et al. 1999) were

analysed for $[\text{Si}(\text{OH})_4]$, using the molybdenum-blue assay, before being analysed for $[\text{Al}]$ by GFAAS.

Finally, certified samples containing $[\text{Al}] = 1, 1.5, 2 \text{ mmol.dm}^{-3}$ were prepared in 1% HNO_3 in the presence of either 0, 0.05, 0.1, 0.5 or 2 mmol.dm^{-3} $\text{Si}(\text{OH})_4$. Their $[\text{Al}]$ was then measured using Al calibration curves prepared either in the presence or the absence of the appropriate $[\text{Si}(\text{OH})_4]$.

•Results

During measurement of $[\text{Al}]$ of samples containing both $\text{Si}(\text{OH})_4$ and morin, a discrepancy between the theoretical amount and the measured amount of Al was observed. These results are presented in Table 2.2-3. To begin with, the measured $[\text{Al}]$ in Al only solution of $\text{pH} > 5$ was always substantially lower than the added amount. This loss was probably due to the precipitation of $\text{Al}(\text{OH})_3$ which will adsorb to the surface of the bottle. This effect was observed despite (i) the use of Teflon bottles to reduce the interaction of added Al with the bottle surface and (ii) a vigorous shaking of the solutions prior to sampling.

Secondly, the measured $[\text{Al}]$ in solutions containing both Al and $\text{Si}(\text{OH})_4$ was always greater than the added amount, regardless of the pH of the solution. It follows from this second observation that the phenomenon described was not only due to the aforementioned surface-Al effect.

In order to clarify this point, several experiments on $[\text{Al}]$ determination by GFAAS in presence of $\text{Si}(\text{OH})_4$ were performed. They included the preparation of calibration curves, the study of the influence of $\text{Si}(\text{OH})_4$ on the Al absorption and finally the comparison of this effect with the one obtained when $\text{Mg}(\text{NO}_3)_2$ was used as matrix modifier.

Table 2.2-3: GFAAS results at different pH and different Al concentration, in presence of morin and

Si(OH)₄.

	pH	[Al] _{nominal} μmol.dm ⁻³	[Al] _{measured} μmol.dm ⁻³
[KNO ₃] = 0.1 mol.dm ⁻³	3.99	10	9.63
	4.43		9.81
	5.09		8.70
	5.33		6.67
[KNO ₃] = 0.1 mol.dm ⁻³	3.94	5	6.29
	4.33		5.96
	4.67		5.37
	5.49		2.96
[KNO ₃] = 0.1 mol.dm ⁻³ , [Si(OH) ₄] = 2 mmol.dm ⁻³	3.77	10	12.78
	4.31		12.04
	5.06		9.07
	5.42		11.11
[KNO ₃] = 0.1 mol.dm ⁻³ , [Si(OH) ₄] = 2 mmol.dm ⁻³	3.88	5	7.04
	4.41		6.29
	5.29		6.67
	5.13		5.96

Calibration curves

The purpose of this part was to look at the effect on the calibration curve when Si(OH)_4 was added into both the blank and the Al standards. The results are presented in Figure 2.2-5.

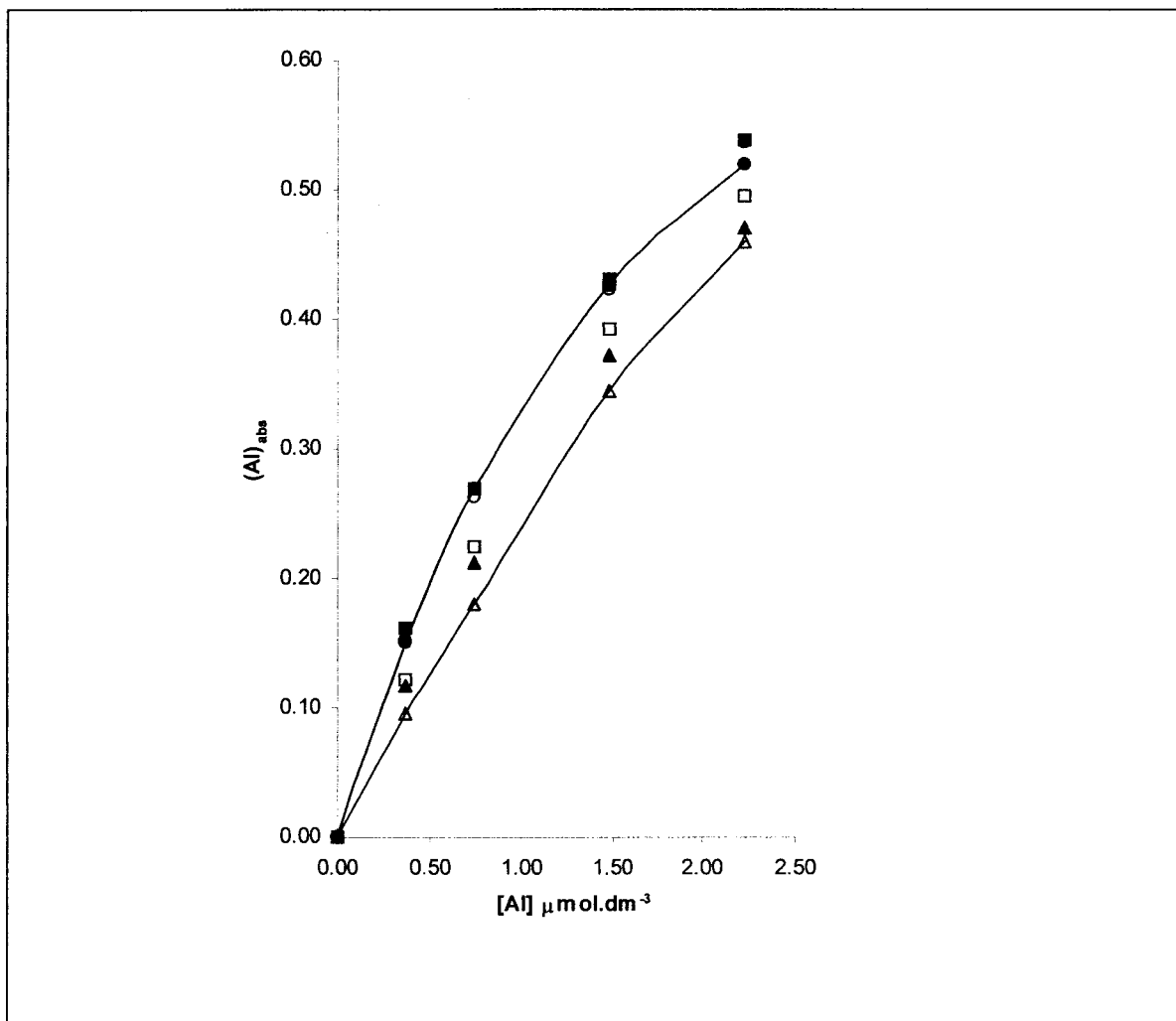


Figure 2.2-5: GFAAS calibration curves. Influence of $[\text{Si(OH)}_4]$. $N=5$. Δ : $0\text{mmol.dm}^{-3} \text{Si(OH)}_4$; \blacktriangle : $0.1\text{mmol.dm}^{-3} \text{Si(OH)}_4$; \square : $0.2\text{mmol.dm}^{-3} \text{Si(OH)}_4$; \blacksquare : $0.4\text{mmol.dm}^{-3} \text{Si(OH)}_4$; \circ : $0.8\text{mmol.dm}^{-3} \text{Si(OH)}_4$; \bullet : $1\text{mmol.dm}^{-3} \text{Si(OH)}_4$.

The influence of Si(OH)_4 was noticeable. It was also determined that the effect of Si(OH)_4 on the calibration curve was dependant upon the $[\text{Si(OH)}_4]$. However, the influence of $[\text{Si(OH)}_4]$ appeared to be saturated at $[\text{Si(OH)}_4] > 0.4 \text{ mmol.dm}^{-3}$. The observed influence of Si(OH)_4 may have helped to explain previous discrepancies in the measurement of Al by

GFAAS. When Al was measured with Si(OH)₄ present in the calibration the measured amount was similar to the normal [Al]. The amount of Al was rectified and the recovery in this case was good. Table 2.2-4 shows the results obtained when an adapted calibration was performed prior to any measurements.

Table 2.2-4: GFAAS results with and without Si(OH)₄ in the calibration. Recovery =

$$[\text{Al}]_{\text{measured}}/[\text{Al}]_{\text{nominal}} \times 100$$

Samples	[Al] measured (μmol.dm ⁻³)	Recovery (%)
2 μmol.dm ⁻³ Al	1.92	96
	1.96	98
2 μmol.dm ⁻³ Al + 0.4 mmol.dm ⁻³ Si(OH) ₄	2.56	128
	2.41	120
2 μmol.dm ⁻³ Al + 0.4 mmol.dm ⁻³ Si(OH) ₄ with Si(OH) ₄ calibration	1.85	93
	1.71	85

Influence of Si(OH)₄ on the Al absorbance.

In order to better understand the influence of Si(OH)₄ on Al measurement by GFAAS, the absorbance was measured at different [Al] in the presence or not of Si(OH)₄. A typical absorbance profile is shown Figure 2.2-6. It was shown that the absorbance resulting from the Si(OH)₄ only sample was extremely small and could not explain the increase in absorbance observed in the Si(OH)₄ plus Al sample compared to the absorbance in the Al only sample.

The results, presented in Figure 2.2-7, are given as a ratio:

$$\text{Absorbance (Si(OH)}_4 + \text{Al) / Absorbance (Al).$$

In order to compare the results, the absorbance of Al only samples was maintained approximately constant whatever the Si(OH)₄ concentration was. By maintaining the

absorbance constant, the linearity of the graphs was ensured and the absorbance was measured in respect of the Beer-Lambert law. Two ranges of absorbance were used, dependent on the Al concentration: (i) $[Al] = 1.11-4.81 \mu\text{mol}\cdot\text{dm}^{-3}$ and (ii) $[Al] = 4.81-8.88 \mu\text{mol}\cdot\text{dm}^{-3}$. A $\text{Si}(\text{OH})_4$ concentration above $100 \mu\text{mol}\cdot\text{dm}^{-3}$ significantly enhanced GFAAS measurements of Al for $[Al]$ below $4.44 \mu\text{mol}\cdot\text{dm}^{-3}$. For higher Al concentrations, $\text{Si}(\text{OH})_4$ still tended to increase Al absorption but this effect was marginal and did not depend upon the $\text{Si}(\text{OH})_4$ concentration.

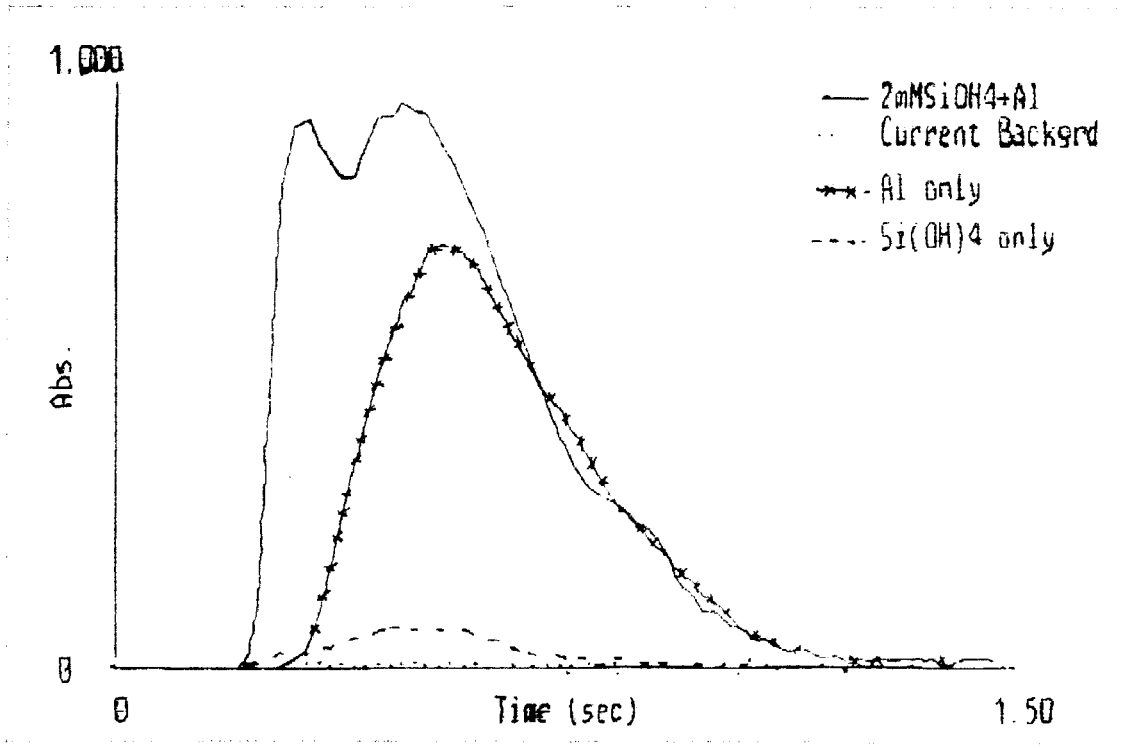


Figure 2.2-6: Al absorbance profiles.

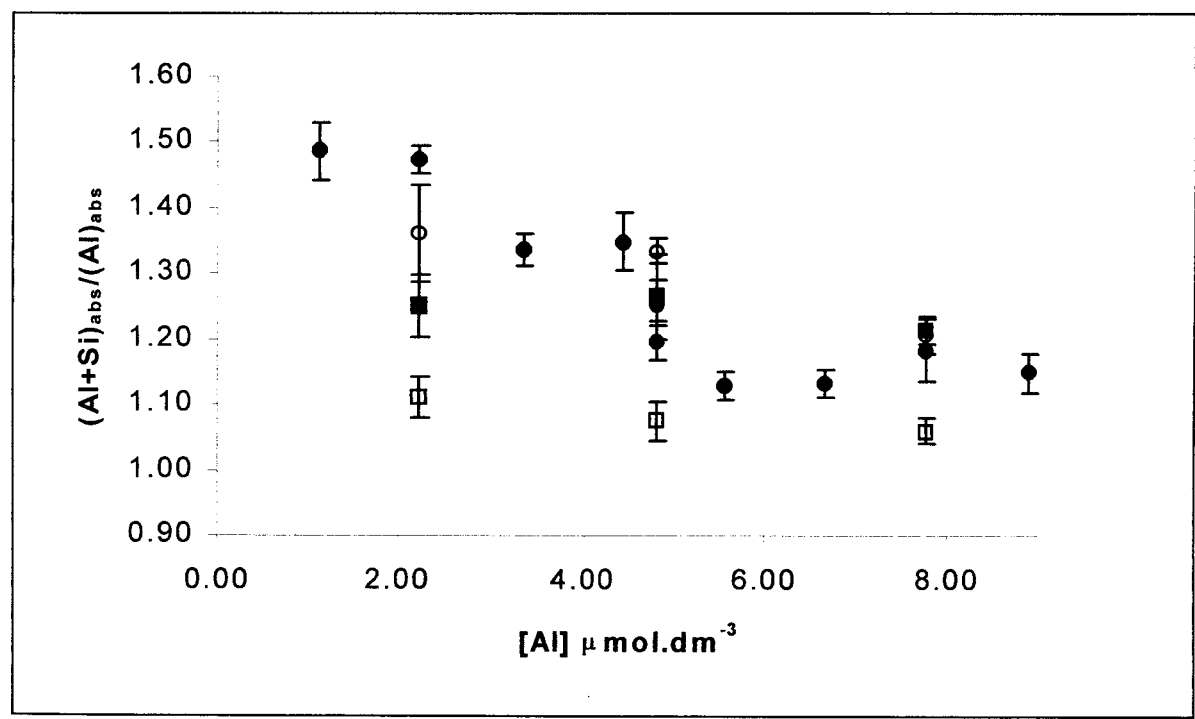


Figure 2.2-7: Effect of Si(OH)₄ on the Al absorbance towards [Al]. N = 25. □: 100 μmol.dm⁻³ Si(OH)₄; ■: 500 μmol.dm⁻³ Si(OH)₄; ○: 1000 μmol.dm⁻³ Si(OH)₄; ●: 2000 μmol.dm⁻³ Si(OH)₄.

Comparative effect of $\text{Mg}(\text{NO}_3)_2$ as a matrix modifier

$\text{Mg}(\text{NO}_3)_2$ is routinely used in Al measurement by GFAAS to modify the Al absorbance signal. The aim at this point of the study was to look at the influence of $\text{Mg}(\text{NO}_3)_2$ on the Al only signal and also on the signal in presence of $\text{Si}(\text{OH})_4$. The results in Figure 2.2-8 are presented as a ratio of absorbance against Al concentration. The presence of $10 \text{ mmol}\cdot\text{dm}^{-3}$ $\text{Mg}(\text{NO}_3)_2$ improved significantly the determination of Al in Al only samples. This depended upon the Al concentration, and for high amounts of Al the effect was only marginal. Nevertheless, if an increase of 8 to 25 % is observed in presence of $\text{Mg}(\text{NO}_3)_2$, it was still not as high as the increase of 20 to 50% observed in presence of $2 \text{ mmol}\cdot\text{dm}^{-3}$ $\text{Si}(\text{OH})_4$. Furthermore, the presence of $\text{Mg}(\text{NO}_3)_2$ in samples with $\text{Si}(\text{OH})_4$ and Al completely removed the enhancement due to $\text{Si}(\text{OH})_4$ and even resulted in a decrease when compared to the $\text{Mg}(\text{NO}_3)_2$ samples.

Finally, calibration curves were performed in presence of $\text{Si}(\text{OH})_4$ and $\text{Mg}(\text{NO}_3)_2$, separately and together. The results are shown in Figure 2.2-9. For concentrations above $20 \mu\text{g}\cdot\text{L}^{-1}$ Al, the influence of $\text{Mg}(\text{NO}_3)_2$ was less significant than that of $\text{Si}(\text{OH})_4$. In contrast, the influence of $\text{Si}(\text{OH})_4$ on the Al absorbance signal occurred over all of the Al concentrations studied. In fact, $\text{Mg}(\text{NO}_3)_2$ inhibited the $\text{Si}(\text{OH})_4$ enhancement on Al calibration curves.

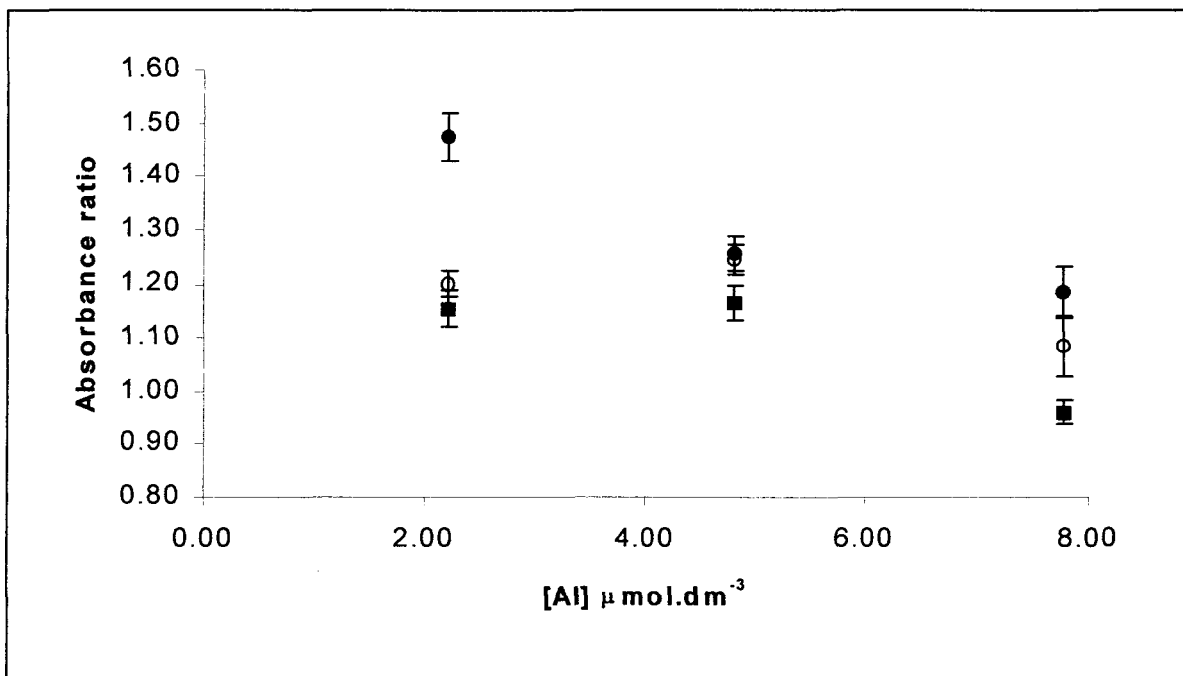


Figure 2.2-8: Effect of $10\text{ mmol}\cdot\text{dm}^{-3}\text{ Mg}(\text{NO}_3)_2$ on the enhancement of the Al absorbance signal in the presence and absence of $2\text{ mmol}\cdot\text{dm}^{-3}\text{ Si}(\text{OH})_4$. ● (Al+Si)_{abs}/(Al)_{abs}, ○ (Al+Mg)_{abs}/(Al)_{abs}, ■ (Al+Si+Mg)_{abs}/(Al)_{abs}

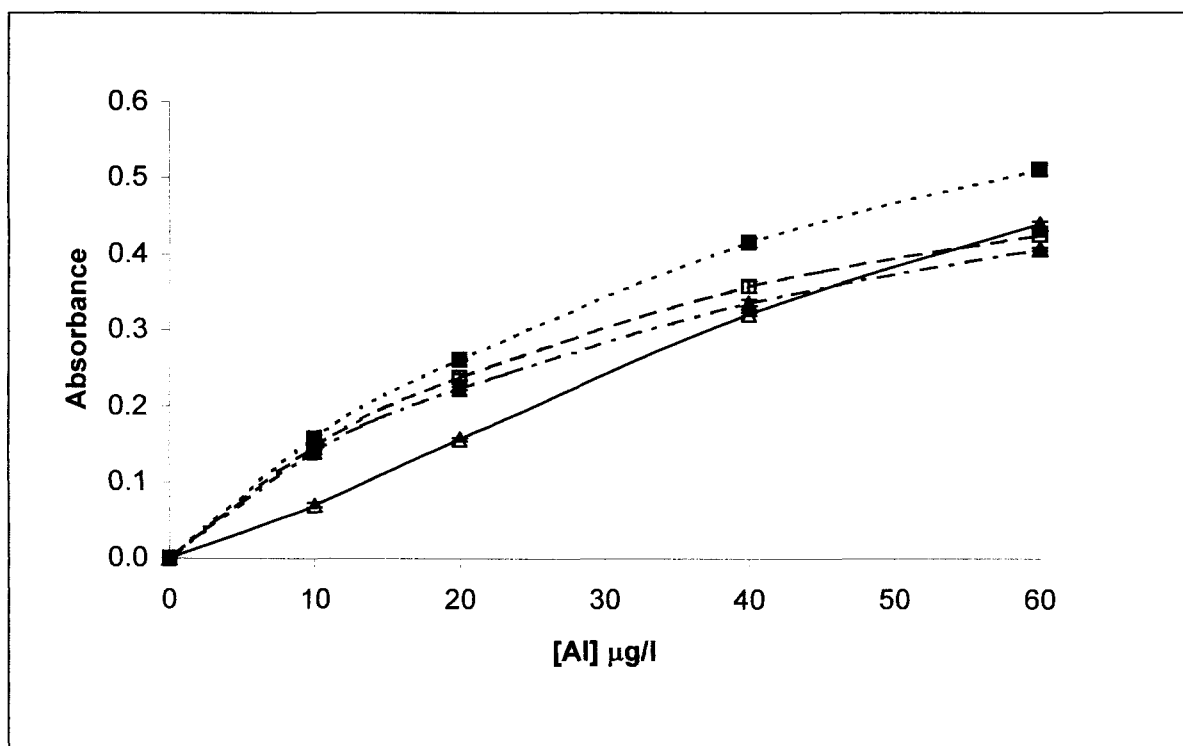


Figure 2.2-9: Calibration curves. Influence of $2\text{ mmol}\cdot\text{dm}^{-3}\text{ Si}(\text{OH})_4$ and $10\text{ mmol}\cdot\text{dm}^{-3}\text{ Mg}(\text{NO}_3)_2$. Δ: Al only; ▲: $10\text{ mmol}\cdot\text{dm}^{-3}\text{ Mg}(\text{NO}_3)_2$; □: $2\text{ mmol}\cdot\text{dm}^{-3}\text{ Si}(\text{OH})_4 + 10\text{ mmol}\cdot\text{dm}^{-3}\text{ Mg}(\text{NO}_3)_2$; ■: $2\text{ mmol}\cdot\text{dm}^{-3}\text{ Si}(\text{OH})_4$.

Application to real samples

Some samples of known $[\text{Si}(\text{OH})_4]$ (range 50 to 2000 $\mu\text{mol}\cdot\text{dm}^{-3}$) and unknown $[\text{Al}]$ were analysed by GFAAS using Al standards either with or without $\text{Si}(\text{OH})_4$ at the respective concentration. The results are plotted as $[\text{Al}]_{-\text{Si}}$ against $[\text{Al}]_{+\text{Si}}$ and are shown Figure 2.2-10.

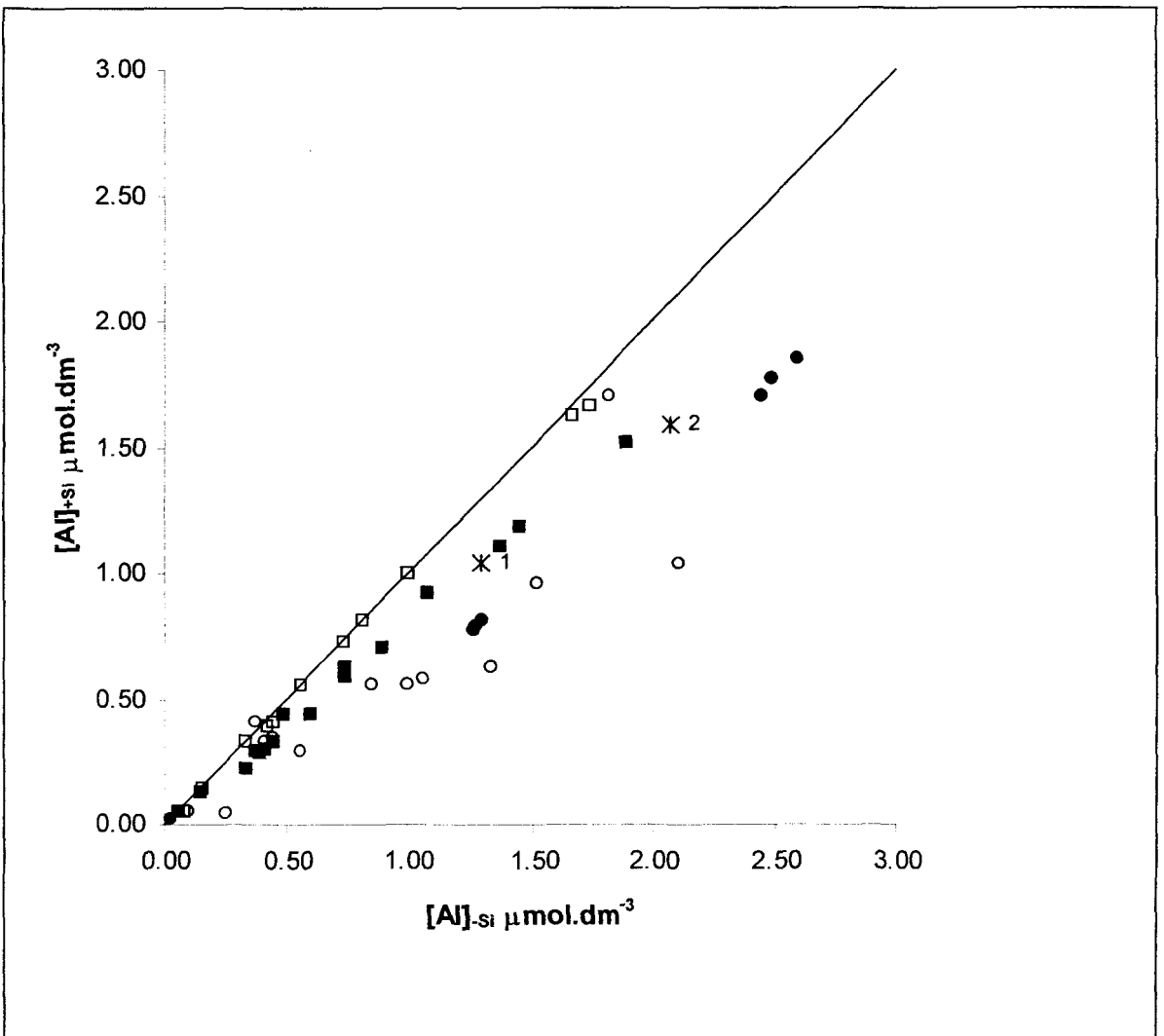


Figure 2.2-10: Al measurement in either the presence $[\text{Al}]_{+\text{Si}}$ or absence $[\text{Al}]_{-\text{Si}}$ of the sample concentration of $\text{Si}(\text{OH})_4$. ● 2 $\text{mmol}\cdot\text{dm}^{-3}$ $\text{Si}(\text{OH})_4$, ○ 0.5 $\text{mmol}\cdot\text{dm}^{-3}$ $\text{Si}(\text{OH})_4$, ■ 0.1 $\text{mmol}\cdot\text{dm}^{-3}$ $\text{Si}(\text{OH})_4$, □ 0.05 $\text{mmol}\cdot\text{dm}^{-3}$ $\text{Si}(\text{OH})_4$. * denotes the two Icelandic samples. The straight line indicates when the measurement of Al was not affected by the presence of $\text{Si}(\text{OH})_4$.

The deviation from the straight line shown on the figure was the result of the influence of the presence of Si(OH)_4 . When the same experiment was repeated on samples of known Al and Si(OH)_4 concentration, the measurement by GFAAS of Al in sample containing $[\text{Si(OH)}_4] > 0.5 \text{ mmol.dm}^{-3}$ was overestimated unless matrix-matched standards are used to prepared calibration curves. These last results are presented in Figure 2.2-11.

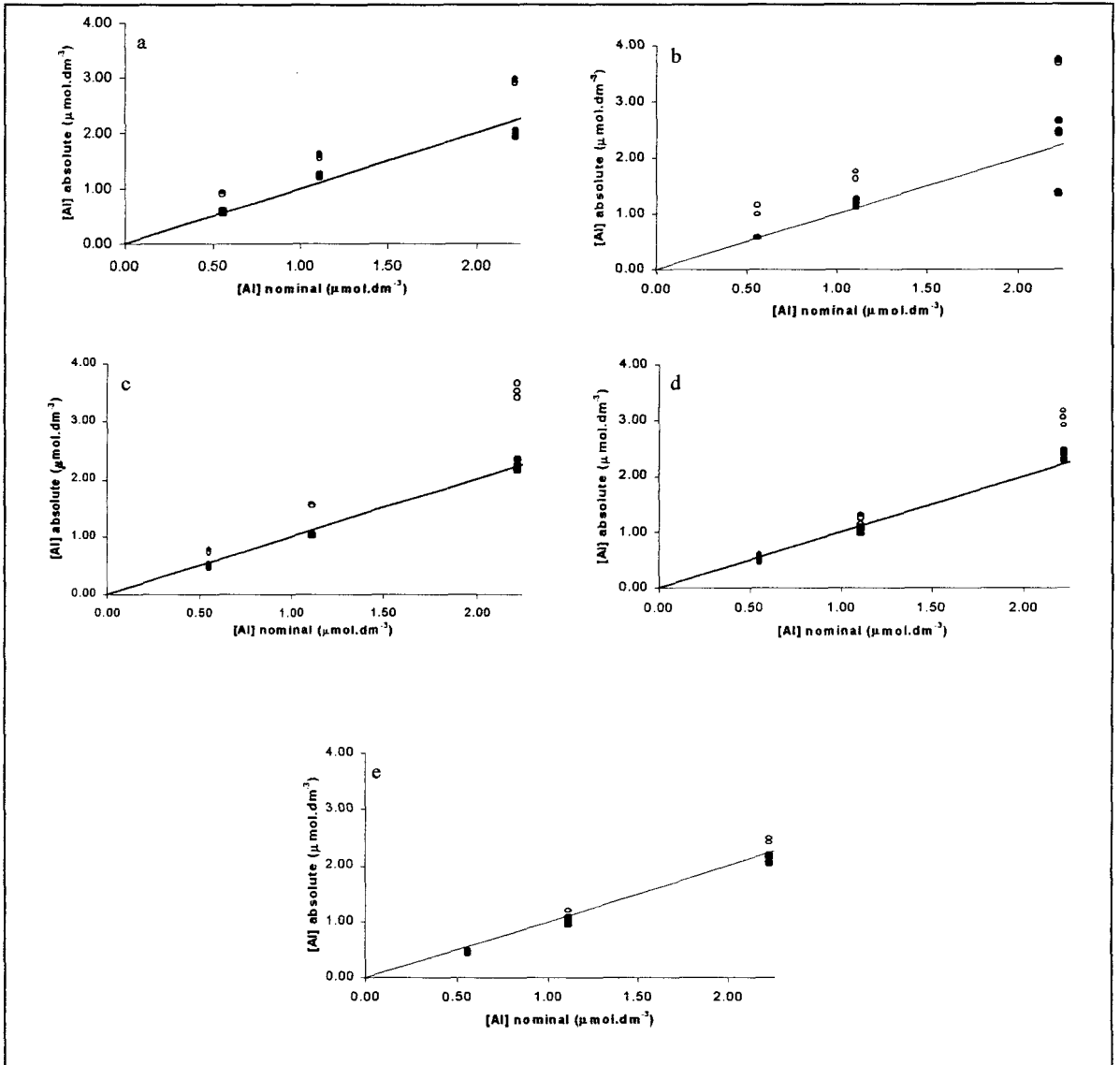


Figure 2.2-11: Plot of measured [Al] of samples of known concentration using either matrix-matched (●) or non-matrix matched (○) calibration standards. $[\text{Si(OH)}_4]$ = a) 2 mmol.dm^{-3} , b) 1 mmol.dm^{-3} , c) 0.5 mmol.dm^{-3} , d) 0.1 mmol.dm^{-3} , e) 0.05 mmol.dm^{-3} . N = 3.

Optimisation of the temperature programme

In order to optimise the absorbance signal in the presence of $\text{Si}(\text{OH})_4$, the temperature of both pre-treatment and atomisation were studied for a $2 \text{ mmol}\cdot\text{dm}^{-3} \text{ Si}(\text{OH})_4 + 2.22 \text{ }\mu\text{mol}\cdot\text{dm}^{-3} \text{ Al}$ sample. The results are shown in Figure 2.2-12. Both maximum intensity and good replication were important in defining the optimal conditions.

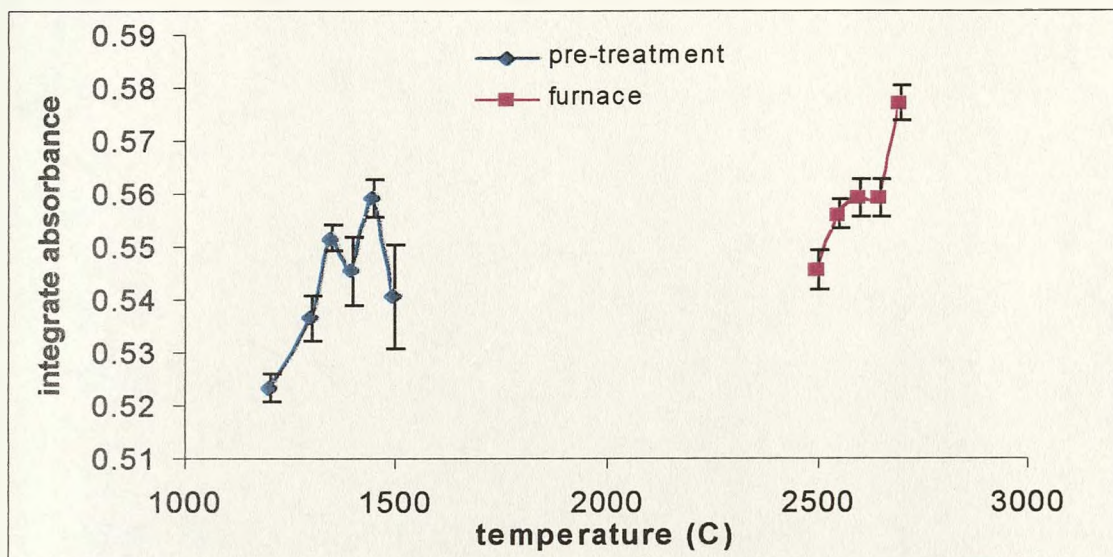


Figure 2.2-12: Influence of temperature on the Al absorbance in presence of $2 \text{ mmol}\cdot\text{dm}^{-3} \text{ Si}(\text{OH})_4$.

$\text{Si}(\text{OH})_4$ had no influence upon the optimal parameters. Therefore, the measurement of $[\text{Al}]$ in samples containing $\text{Si}(\text{OH})_4$ can be performed using the furnace programme outlined in Table 2.2-1.

•Discussion

It was shown that the presence of $\text{Si}(\text{OH})_4$ in samples containing Al resulted in an overestimation of the total amount of Al in those samples by up to 50%. This effect can be corrected by including the requisite amount of $\text{Si}(\text{OH})_4$ in the preparation of the calibration standards. Thus, the application of a matrix-matched calibration ensured an accurate determination of the total amount of Al. It was also shown that this effect was dependant

upon both [Al] and [Si(OH)₄]. A [Si(OH)₄] ≥ 0.5 mmol.dm⁻³ significantly increased the Al absorbance signal for [Al] ≤ 4.44 μmol.dm⁻³. The enhancement of the Al absorbance by Si(OH)₄ was compared to the effect of the use of a matrix modifier Mg(NO₃)₂. It was shown that Si(OH)₄ had a more pronounced effect than Mg(NO₃)₂ on the absorbance signal and **that** the co-inclusion of both these modifiers inhibited the effect of Si(OH)₄. The mechanism behind the enhancement of the Al absorbance by Si(OH)₄ was not investigated. However, in view of other studies investigating the interference during the determination of Al by GFAAS (Lvov et al. 1991; Styris and Redfield 1987) it was possible to speculate **that the presence of Si(OH)₄ prevented the loss of Al during the pre-treatment process.** The thermal dissociation of Al₂O₃ is believed to be the precursor of the Al_(g) measured by GFAAS (Frech et al. 1985; Sturgeon et al. 1976). However, gas-phases intermediates are formed during the vaporisation and the atomisation process, such as lower oxides, **adsorbed Al and carbides, cyanides and hydroxides.** During the pre-treatment process, losses of Al are observed in form of aluminium dihydroxides. One can then make the **assumption that Si(OH)₄ reacts with the latter, thus preventing analyte loss.** But this has still to be proved.

This **study** confirmed the observation made in a previous paper (Nukatsuka et al. 2000) on the effect of Si(OH)₄ on the Al absorbance and it investigated the experimental conditions under which it occurred. It revealed the importance of the use of a matrix matched calibration in the Al determination in samples containing both Al and Si(OH)₄. To ignore **this effect** would lead to an overestimation of the [Al], as was shown in the measurement of [Al] in real samples. It also suggested that Si(OH)₄ can be used as more efficient **modifier than Mg(NO₃)₂ for the determination of low [Al].**

Finally, it should be pointed out that matrix-matched calibration would be applied for the **rest of this PhD project.**

2.3.NMR

2.3.1.General principles

Nuclear Magnetic Resonance (NMR) spectroscopy is based upon the existence of nuclear spin and the possibility to influence this property through magnetisation. Nuclei with an odd mass number A have a nuclear spin I of half-integral value. This is the case for ^1H , ^{13}C , ^{29}Si , ^{27}Al . The characteristics of these nuclei are summarised in Table 2.3-1.

Table 2.3-1: characteristics of different elements.

Element	Abundance	Spin I	Frequency (MHz) at 2.348T
^1H	100%	1/2	100
^{13}C	1.108%	1/2	25.15
^{27}Al	100%	5/2	26.08
^{29}Si	4.70%	1/2	19.87

A nuclear spin can be described as a microscopic magnetised needle. The magnetic momentum μ associated with the kinetic momentum of spin I is:

$$\vec{\mu} = \gamma \hbar \vec{I}$$

where γ is the magnetogyric ratio and $\hbar = h/2\pi$, with h the Plank constant.

When there is no external magnetic field, spins are orientated randomly and are, therefore, indistinguishable. However, when placed in an external magnetic field, they will position themselves either parallel (α) or anti-parallel (β) to the direction of the field. The application of a strong external magnetic field B_0 on nuclei of spin I will split the energy level into $2I+1$ levels. Figure 2.3-1 illustrates this phenomenon.

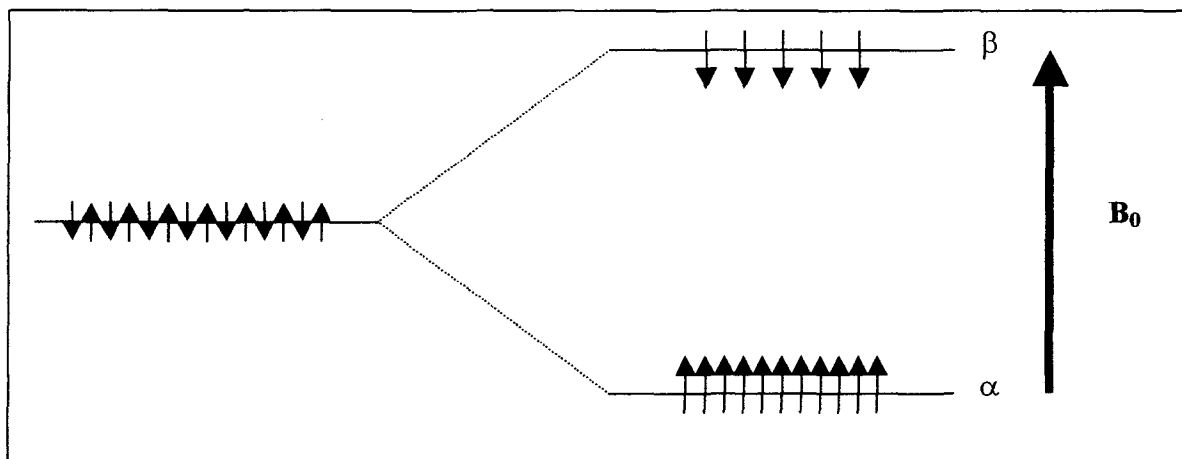


Figure 2.3-1: Splitting of energy levels under the application a magnetic field B_0 . Spin $I=1/2$.

Each level has an energy of:

$$E = -\gamma\hbar m_z B_z$$

Hence, the α level is more stable and thus more populated. It is then possible to induce a transition between these levels by applying a wave of energy:

$$\Delta E = \gamma\hbar B_0$$

A resonance will occur if :

$$\Delta E = h\nu_0$$

where ν_0 is the resonance frequency or Larmor frequency.

Consequently,

$$\nu_0 = \frac{\gamma B_0}{2\pi}$$

However, the electronic environment of the nucleus disturbs the interaction between B_0 and the nucleus itself. It is the specificity of the electronic charge distribution around the nuclei that leads to the discrimination of a nucleus and of its chemical environment. It is thus necessary to introduce a correction factor in the previous equation to translate the effect of the electronic environment. This factor is σ_i , the screen coefficient:

$$\nu_{0i} = \frac{\gamma B_0}{2\pi} (1 - \sigma_i)$$

A more commonly used expression of this effect is the chemical shift, which characterises the electronic charge distribution around a nucleus related to a reference:

$$\delta_i = \frac{\nu_{0i} - \nu_{0ref}}{\nu_{0ref}} 10^6 = \frac{\sigma_{ref} - \sigma_i}{1 - \sigma_{ref}} 10^6$$

To summarise, in the first step of the NMR experiment, a macroscopic magnetisation M_0 resulting from the difference of population of the energy levels α and β is generated under the influence of an external constant magnetic field B_0 . M_0 follows the direction of B_0 (z).

In a second step, an alternating magnetic field B_1 , perpendicular to B_0 , induces a transition between the levels α and β . B_1 is a rotating field of frequency ν which is able to put M_0 out of its equilibrium position. When the magnetisation is rotated to the xOy plane (90° pulse), it is placed in the measuring plane. M_0 then returns to its equilibrium position along the z axis by a relaxation process. The evolution of M_0 with time is therefore measurable and gives rise to a signal called Free Induction Decay (FID). This signal is modified by a Fourier transformation to obtain a conventional NMR spectrum.

In order to fully understand the principles of NMR, it is necessary to consider two aspects of the phenomena describing a NMR experiment: the kinetics of the system, which relies on a classical description, and a short description of the quantum mechanics.

•*Classical description:*

In a constant external field \mathbf{B}_0 (0, 0, B_0) which defines the z direction of the laboratory frame, the magnetisation M_0 is set aside from its equilibrium position by an angle α and will precess around \mathbf{B}_0 with a constant angular velocity (Larmor frequency):

$$\omega_0 = 2\pi\nu_0$$

This phenomenon is described into Figure 2.3-2.

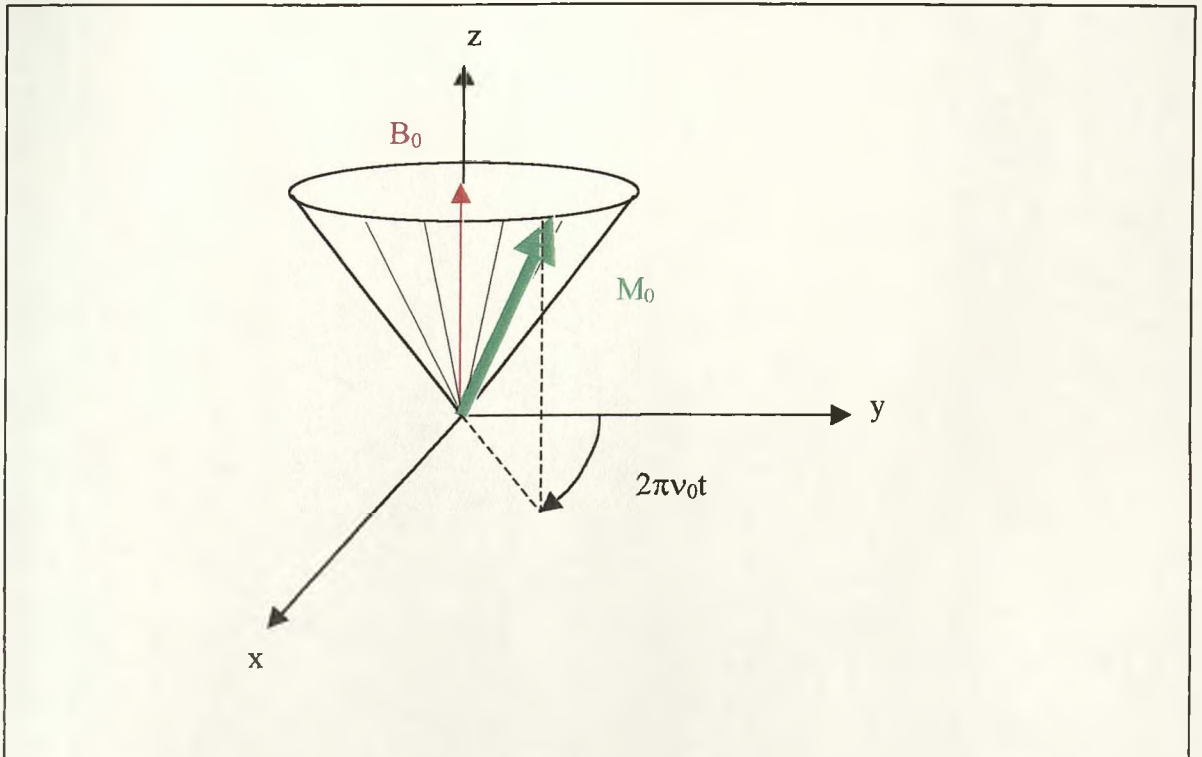


Figure 2.3-2: Precession of the magnetisation M_0 in a constant magnetic field with induction B_0 .

In the second step of the experiment, a rotating field B_1 , perpendicular to B_0 , is applied with a frequency ν . If $\nu \neq \nu_0$, there is no interaction between B_1 and μ and M_0 still precesses around z . But if $\nu = \nu_0$, a transition arises between the two energy levels and the angle α between M and the z axis is changed. A resonance has been created.

The rotating angle α is defined as:

$$\alpha = \gamma B_1 t_p$$

where t_p is the pulse time. By changing t_p , α can be modified and the magnetisation can be placed in an interesting plane. A commonly used angle is $\alpha = 90^\circ$; the magnetisation is then in the xOy plane and it reaches its maximum intensity.

• *Quantum mechanics:*

Any quantum system is described by Hamiltonian \mathcal{H} and is characterised by a wave function Ψ in order to satisfy the Schrödinger equation:

$$i \frac{d\Psi}{dt} = \mathcal{H}\Psi$$

This Hamiltonian can be divided into 4 Hamiltonians, each describing one of the possible interactions in a diamagnetic sample:

$$\mathcal{H} = \mathcal{H}_z + \mathcal{H}_{CS} + \mathcal{H}_D + \mathcal{H}_Q$$

\mathcal{H}_z is the Zeeman Hamiltonian which accounts for the interaction between B_0 and the nuclear spin:

$$\mathcal{H}_z = -\gamma\hbar I B_0$$

As mentioned earlier, the chemical shift is due to the screening of B_0 by the surrounding electrons. It is therefore necessary to include a Hamiltonian which transcribes this effect:

$$\mathcal{H}_{CS} = +\gamma\hbar I \sigma B_0$$

\mathcal{H}_D describes the magnetic dipole-dipole interactions between nuclear moments $\gamma_i \hbar I_i$ and $\gamma_k \hbar I_k$ being separated by a distance r_{ik} :

$$\hbar \mathcal{H}_D = \gamma_i \gamma_k \hbar^2 \left[I^i \cdot I^k - 3 \left(I^i \cdot r_{ik} \right) \left(I^k \cdot r_{ik} \right) \right] / r_{ik}^3$$

\mathcal{H}_Q takes into account the quadrupolar interactions for nuclear magnetic moments with spin $I > 1/2$, such as Al.

2.3.2. Instrumentation

Figure 2.3-3 shows a diagrammatic representation of a Fourier transform spectrometer. The sample is placed into a strong, highly stable magnet (B_0), generally a superconducting solenoid. To compensate the non-homogeneity of the magnetic field throughout the sample, a set of two coils, known as shim coils, are placed around the sample (not shown on the figure). The remaining inhomogeneities are minimised by spinning the sample tube about its long axis so that the sample molecules experience average fields.

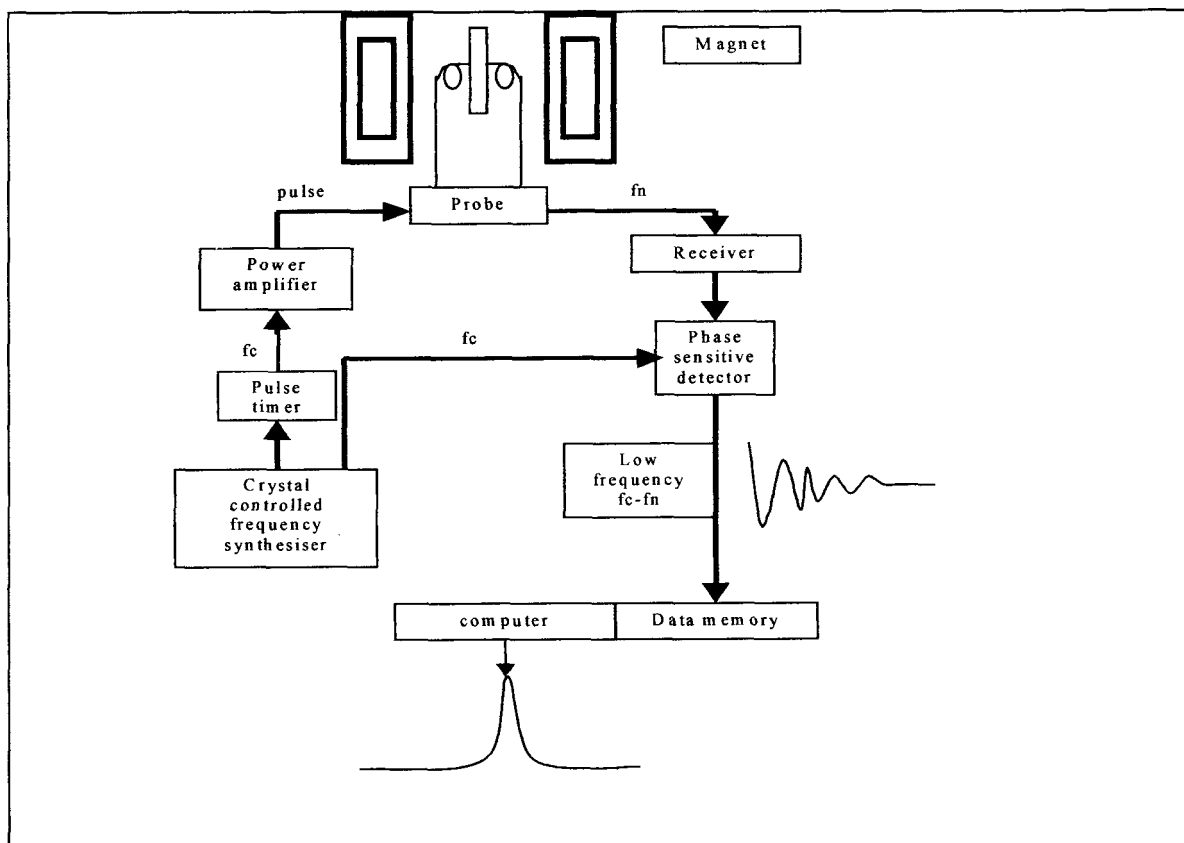


Figure 2.3-3: A basic Fourier transform spectrometer.

The B_1 field is produced by a gated (switched input) power amplifier driven by a stable, crystal-controlled continuous oscillator. The length of the pulse is controlled by the pulse timer. The nuclear signals following the B_1 pulse (f_n) are then amplified and compared to the original signal (f_c). The difference is a low-frequency, time dependant signal which contains frequency, phase and amplitude information (FID). This signal is finally transformed using a Fourier transform programme to obtain a spectrum.

2.3.3. Solution NMR

Solution NMR was used in ^{29}Si and ^{13}C for the characterisation of tetramethyldisilane-diol (TMDS) / dimethylsilandiol (DMSD) samples in the presence or not of Al, before and after filtration. Experiments were performed using a DEPT pulse sequence (Blinka 1983). This polarisation transfer technique is a multinuclear pulse sequence in which proton and/or

silicon/carbon pulses are separated by free precession periods. The main advantage of this technique is a great enhancement of the transfer of polarisation and its relatively non-selectivity.

2.3.4. Solid state NMR (Engelhardt, 1987)

Solid-state NMR was used in ^{27}Al and ^{29}Si for the characterisation of the materials obtained by filtration. Contrary to the liquid-state, the local magnetic interactions in the solid-state are not averaged by the rapid, random internal motions. These fundamental spin interactions, each described by a Hamiltonian (see section 2.3.1), lead to broad resonance lines in solid-state NMR and need to be artificially manipulated in order to obtain a high-resolution spectrum. Generally, manipulation of spin variables can be attained by application of multiple-pulse sequences and by high-power dipolar decoupling, whereas spatial variables are affected by magic-angle spinning. The signal-to-noise ratio can also be improved by combining these techniques with cross-polarisation between abundant and rare spins.

• *High-power dipolar decoupling*

To suppress the influence of the heteronuclear dipolar Hamiltonian $\mathcal{H}_{D,IS}^{\circ}$ for an ensemble of rare spins (S), the heteronuclear dipolar coupling with the system of abundant spins (I) has to be eliminated (Mehring 1983). This is achieved by applying a strong continuous or pulsed radio-frequency field $B_{II}(t)$ with a resonance frequency $\omega_I/2\pi$.

•Magic-angle spinning (MAS) NMR

To average spin interactions due to both chemical shift anisotropy and dipolar interactions, the sample can be rapidly spun around a specific axis. The angular dependent part of the dipolar interaction is proportional to $3\cos^2\theta - 1$, where θ is the angle between the sample and the magnetic field B_0 (Andrew et al. 1958; Kessemeier and Norberg 1967; Lowe 1959). This expression is nulled for $\theta = 54.73^\circ$, known as the magic angle. The magic-angle spinning (MAS) technique consists of producing a rotation of frequency ν around an axis R inclined by $\theta = 54.73^\circ$ from B_0 as described in Figure 2.3-4. Hence, magic angle spinning yields the same isotropic chemical shifts as does the random motion in liquids.

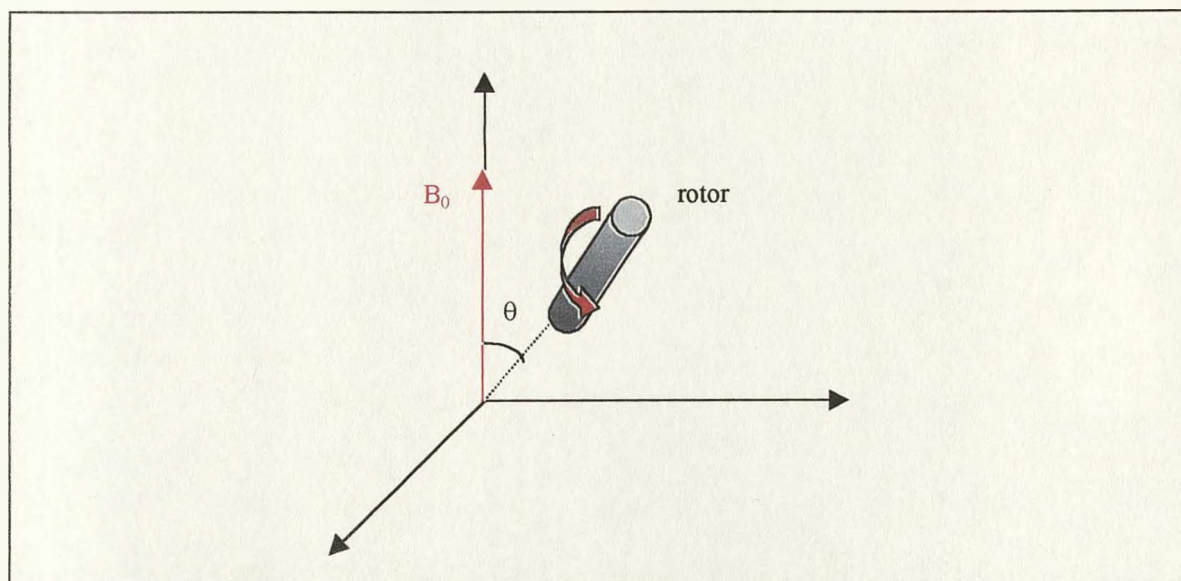


Figure 2.3-4: Schematic of MAS technique.

•Cross-polarisation

The cross-polarisation method consists of the transfer of polarisation from the abundant spins I to the rare spins S (Pines et al. 1973), such as $^1\text{H} \rightarrow ^{29}\text{Si}$ or $^1\text{H} \rightarrow ^{27}\text{Al}$. This is achieved if the Hartmann-Hahn conditions is fulfilled:

$$\gamma_S \tilde{B}_{IS} = \gamma_I \tilde{B}_{II}$$

This ensures that the split between the energy levels is the same for both nuclei.

A typical cross-polarisation sequence is shown in Figure 2.3-5. As the delay time between each acquisition is now dependant on the generally shorter relaxation time of the proton, the time of the experiment is generally a lot improved. Moreover, the efficiency of the transfer is dependant upon the dipolar coupling. Information on the proton-silicon or proton-aluminium distances can then be retrieved.

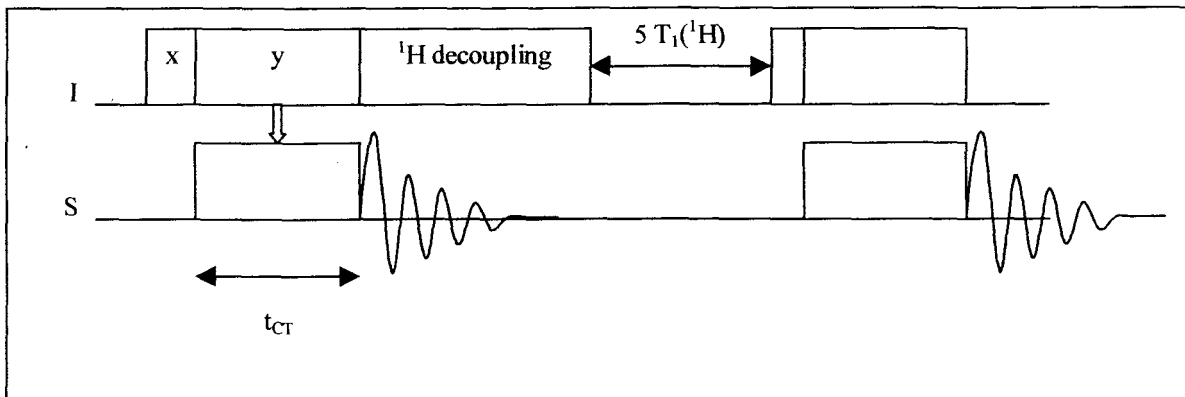


Figure 2.3-5: I→S cross polarisation sequence. I: abundant spin. S: rare spin. T_1 is the relaxation time.

t_{CT} is the transfer time.

2.4.AFM

2.4.1.General principles

Atomic Force Microscopy (AFM) is one of the application of Scanning Probe Microscopy (SPM) which consists of measuring the properties of a surface. Measurements in SPM are performed using a sharp probe scanning over the surface while maintaining a very close spacing to the surface. This technique allows measurements on surface as small as $5 \mu\text{m}$. More specifically, AFM uses a very sharp tip to probe and map the morphology of the surface. The tip is at the end of a long cantilever with a low spring constant. The deflection of the cantilever resulting from the interaction between the tip and the surface gives a measurement of the tip-sample forces which can be then transformed into a map of the surface topography.

AFM has a lot of different modes of operation (contact, lateral force, tapping, phase imaging) and can also be used in solution. For the purpose of my study, I used the tapping-mode in wet cell. The main advantage of tapping mode over contact mode is described in Figure 2.4-1.

Tapping mode allows high resolution topographic imaging of sample surfaces that are easily damaged or loosely attached to their substrate. In contact mode, the tip can easily drag off the surface, damaging the sample's deposition. In tapping mode, problems associated with friction, adhesion and electrostatic force are overcome, providing better conservation of the sample.

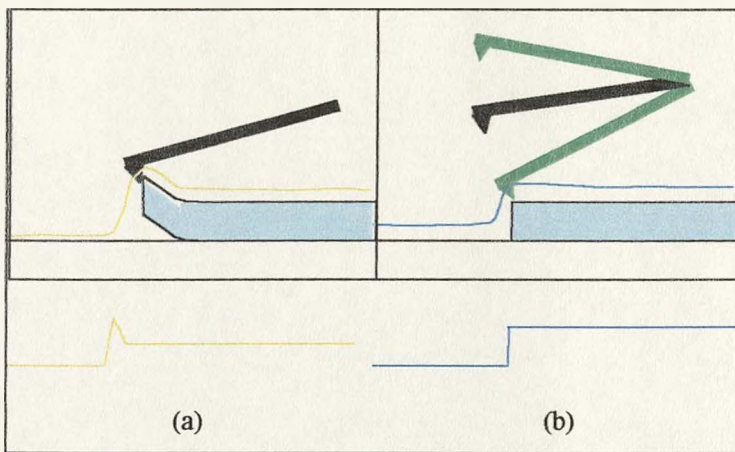


Figure 2.4-1: Interaction tip-sample in (a) contact mode (b) tapping mode

2.4.2. Tapping mode AFM in solution

In the tapping-mode, a piezo stack excites the cantilever's substrate vertically, causing the tip to bounce up and down. Consequently, the reflected laser beam is deflected in a regular pattern over a photodiode array, generating a sinusoidal, electronic signal. When the cantilever encounters the sample surface, the reflected laser beam reveals information

about the vertical height of the sample surface and some characteristics of the sample material itself, such as elasticity, magnetic and/or electric forces present. Figure 2.4-2 shows the interaction of the cantilever with the surface.

To work in solution one needs to take some precautions on the material used. A special device exists to prevent any interactions between the solution and the electrical components. The fluid tip holder consists of a small glass assembly with a wire clip for holding the cantilever substrate. The glass surface provides a flat interface so that the AFM laser beam may pass into the fluid without being distorted by an unstable fluid surface. The fluid tip holder also has four sockets on the top side that are used to attach the tip holder to the 4 pins at the end of the SPM head's tube.

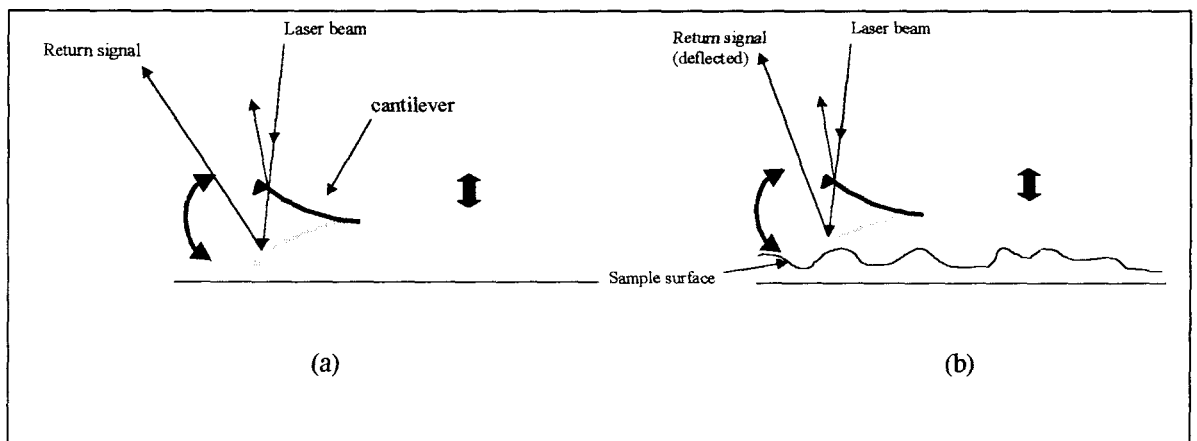


Figure 2.4-2: (a) tapping cantilever in free air. (b) Tapping cantilever on sample surface. Note the deflection of cantilever and return signal (exaggerated).

2.5.XPS

2.5.1.Principles.

X-ray Photoemission Spectroscopy (XPS), also called Electron Spectroscopy for Chemical Analysis (ESCA) consists of the measurement of the kinetic energy of ejected photoelectrons resulting from the interaction of an X-ray photon with a sample as described in Figure 2.5-1. The kinetic energy, E_k , is related to the photon energy by the equation:

$$E_k = h\nu - E_B - W$$

where $h\nu$ is the X-ray photon energy, E_B is the binding energy of the photoelectron, and W is the work function of the instrument. The binding energy is the parameter which identifies the electron specifically and it can be easily calculated as E_k , $h\nu$ and W are known or measurable.

The photoelectron spectrum will reproduce the electronic structure of an element quite accurately as long as the binding energy is less than the photon energy. The chemical specificity is the major strength of the XPS technique as it is not only possible to identify the elements present in the sample but also their chemical state. Moreover a change in the chemical environment of the element induces a slight variation in the binding energy known as the chemical shift.

2.5.2.Instrumentation

The spectrometer design generally requires a vacuum system, a sample, a source of the primary beam, an electron energy analyser and detection system and a data-system. A schematic representation is shown Figure 2.5-2.

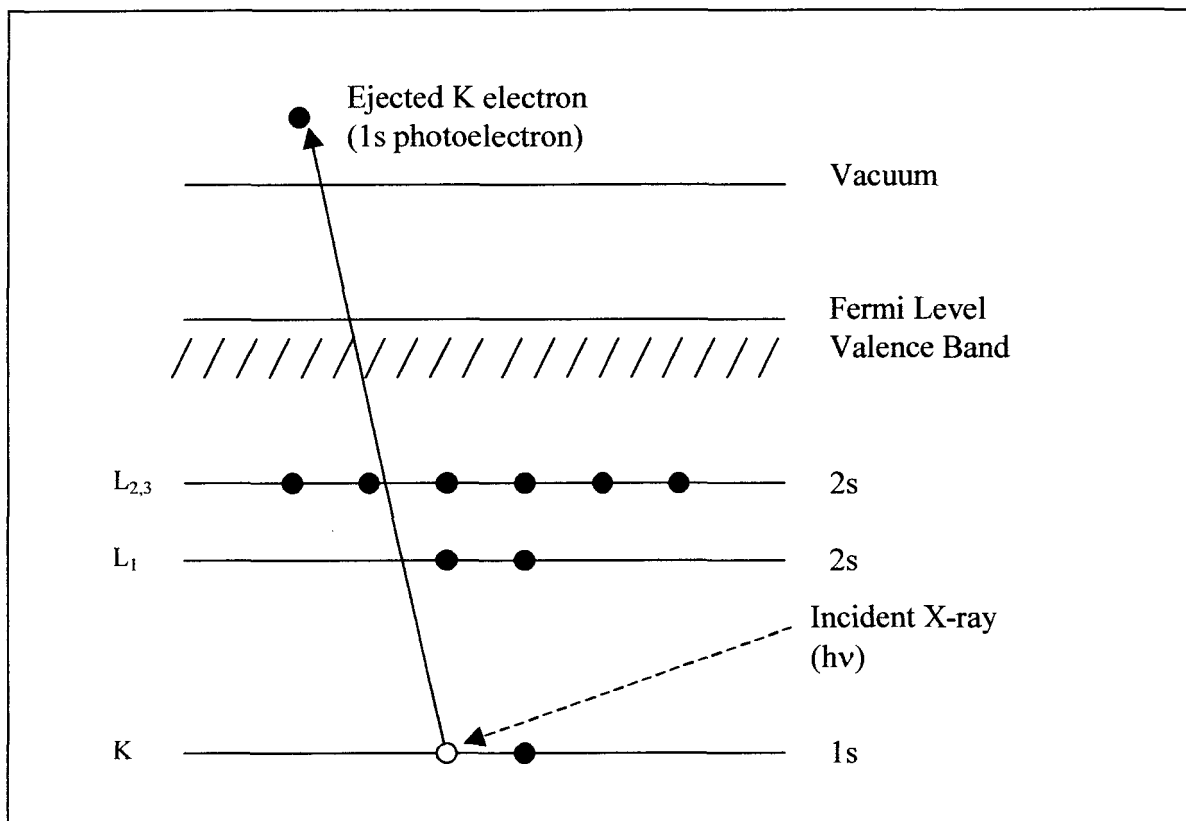


Figure 2.5-1: Schematic of the XPS process, showing the photoionization of an atom by the ejection of a K shell electron.

•*The vacuum system*

All XPS experiments must be carried out in the ultra-high vacuum (UHV) range of 10^{-8} to 10^{-10} mbar for two reasons. First, UHV reduces the concentration of residual gas molecules, thus the scattering of low energy electron, and consequently decreases the level of noise present within the spectrum. Secondly, it prevents the adsorption of a monolayer of gas onto the surface reducing the sensitivity of the technique.

•*The sample.*

XPS can be carried out on any kind of sample: gases, liquids and solids. Yet, this technique is more appropriate to obtain surface chemical information on solid samples. Solid samples

must be stable within the UHV chamber of the spectrometer. The two types of materials which can pose problems are very porous materials and those with low vapour pressure.

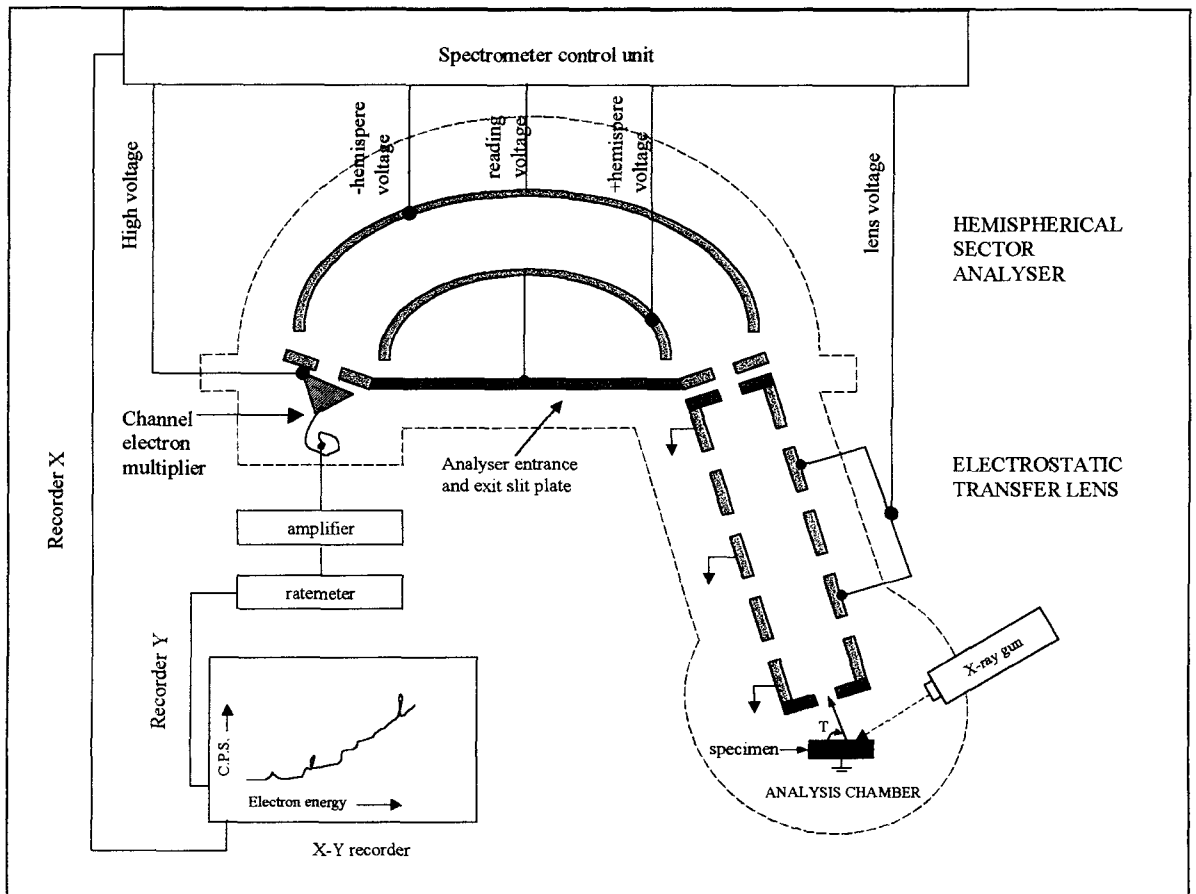


Figure 2.5-2: Schematic diagram of the analysis chamber and analyser of the XPS spectrometer.

•The X-ray source.

It must fulfil two requirements:

- it must generate photons of high enough energy to excite an intense photoelectron peak from all elements of the periodic table with the exception of H and He (too light);
- the natural X-ray line width should not limit the spectrum resolution.

The most popular anode materials are aluminium (Al $K\alpha$, 1486.6 eV) and magnesium (Mg $K\alpha$, 1253.6 eV). The most popular source is a twin anode (Mg/Al) which provides both kinds of photon.

- The analyser*

The most common type is the Hemispherical Sector Analyser (HSA) due to its good resolution. It consists of two hemispheres with a potential difference applied to their surfaces and with an equipotential between them. It is generally combined with an electron transfer lens and a detection system.

2.5.3. Qualitative and quantitative analysis

The first step in the analysis of a surface is to undertake the identification of the elements present. This is achieved by recording a survey or wide spectrum over a region that will provide fairly strong peaks for all elements in the periodic table. A range of 0-1000 eV on a binding energy scale is sufficient. The individual peaks can be indexed thanks to a data library. The electron background is relatively small and increases in a step-like manner after each spectral feature. It results from the scattering of photoelectrons by the matrix. This kind of analysis relies on the ability to determine a peak position with good accuracy, at least 0.1 eV. That is why accurate calibration of the spectrometer is absolutely necessary. Once the peaks have been attributed, it is possible to determine the atomic percentage of the elements concerned by dividing the peak area by the sensitivity factor and expressing the result as a fraction of the summation of all normalised intensities:

$$[A]_{\text{atomic}\%} = \left\{ (I_A / F_A) / \sum (I / F) \right\} \times 100\%$$

2.6.SEM-EDX (Chescoe, 1990)

SEM-EDX combines the imaging by Scanning Electron Microscope with Energy Dispersive X-ray analysis. The principle of operation of SEM is described in Figure 2.6-1.

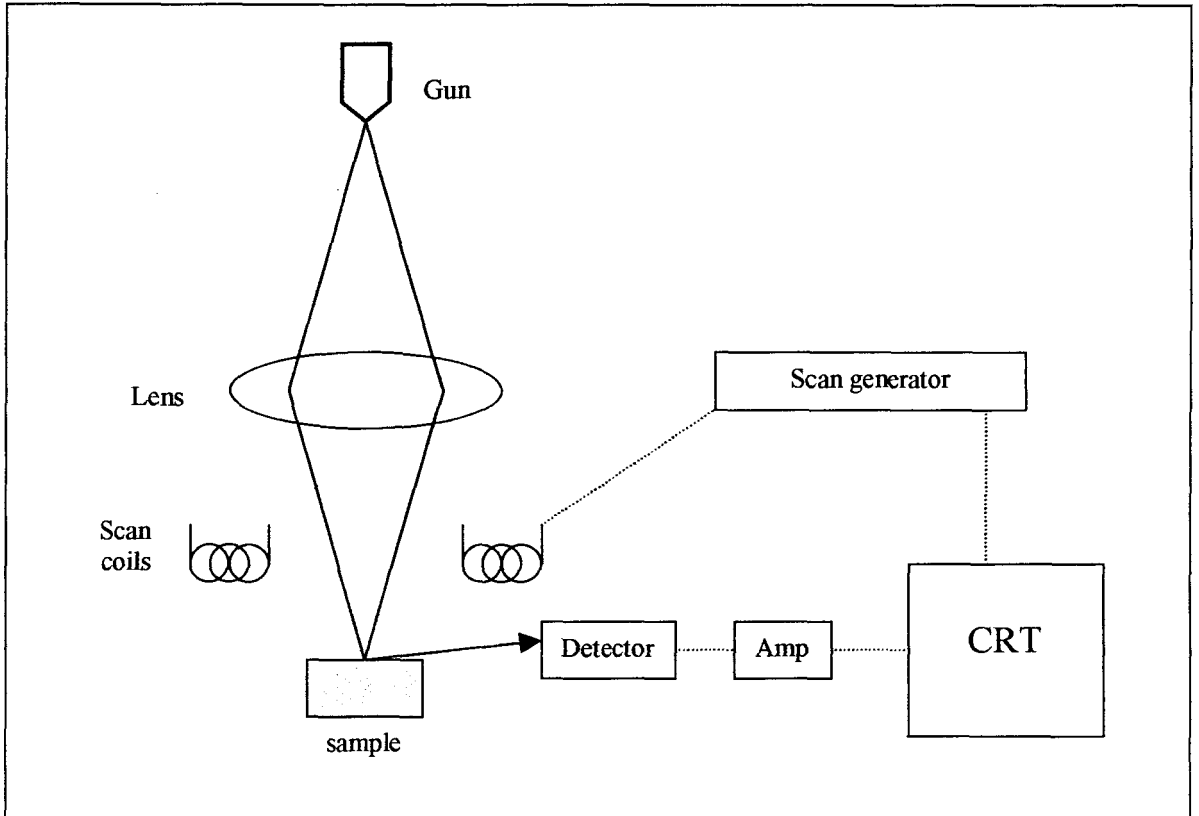


Figure 2.6-1: Components of a SEM. CRT: cathode ray tube display.

A fine beam of electrons, generated by the electron gun, is scanned across the sample surface in synchronism with the spot of the display cathode ray tube (CRT). A detector monitors the intensity of a chosen secondary signal from the specimen (for example secondary electrons). If the intensity of the emitted secondary signal changes across the specimen, the contrast will be seen in the image on the CRT.

EDX uses characteristic X-rays excited from the small volume of specimen irradiated by the beam and is generally fitted to the side of the microscope.

2.7.SolGasWater software

WinSGW has been developed at the department of Inorganic Chemistry, Umeå University to perform chemical equilibrium calculations in a fast and easy way. I used it to calculate the species present at equilibrium in different systems: Al, Al/morin, Al/morin/Si(OH)₄. The reactive species and the reactions occurring in the system are entered into a matrix as well as their equilibrium constants. SGW gives then the possibility to calculate the distribution of the species depending on the pH, the initial concentration of one or more species, etc...

Chapter 3 : The interaction of aluminium with substituted forms of silicic acid.

3.1.Aim

In a previous study (Doucet et al. 2001b), the precipitation of HAS of different Al:Si ratios and their characterisation by solid-state NMR and SEM-EDX brought a new light on the understanding of HAS formation. This was not only a significant breakthrough from the structural point of view, it also showed that two distinct forms of HAS could be observed depending upon the initial solution composition. That information stressed the importance of the initial solution composition on the mechanism of formation of HAS.

In order to better understand the mechanism of formation of HAS, different substituted forms of $\text{Si}(\text{OH})_4$ were used to look at: (i) the influence of the substituent size on the reaction scheme, (ii) the preferential Al attack site and (iii) the effect of the substituent on the formation of HAS. Dimethylsilane-diol (DMSD) and its dimer tetramethyldisilane-diol (TMDS), shown in Figure 3.1-1, were chosen for the study of their interaction with Al essentially because of their structure and also their presence in soils.

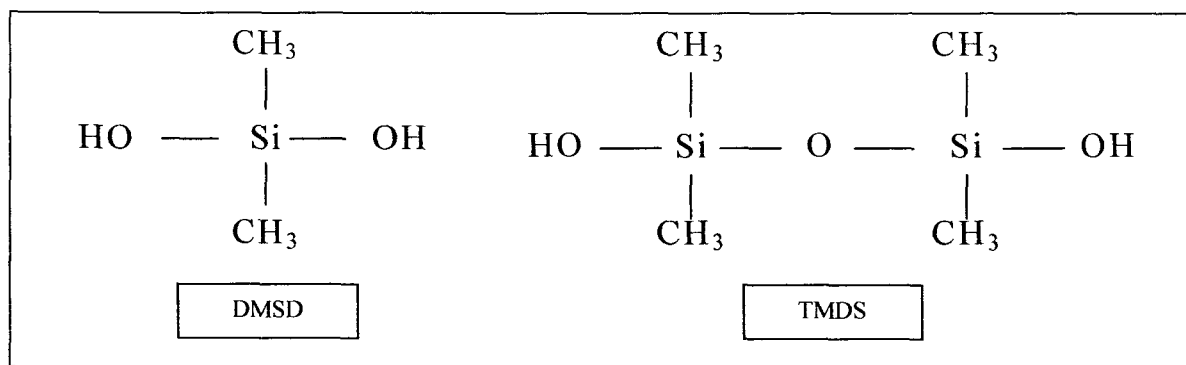


Figure 3.1-1: Composition of DMSD and TMDS.

The presence of methyl groups in both species changes the size and shape of the Si(OH)_4 analogue and should therefore make the approach of the Al(OH)_3 template more difficult. This should give some information on the way Si(OH)_4 reacts with Al to form HAS.

Polydimethylsiloxanes (PDMS) are widely used in industry and consumer products (Tomanek 1991). They enter the environment via the waste water from industrial and domestic applications where they end up in the sewage sludge. When the disposal of this sludge is made by soil amendment, PDMS enter the soil compartment. The fate of this polymer in the soil has been the subject of intensive studies over the years (Lehmann et al. 2000; Lehmann et al. 2002; Lehmann et al. 1995). It was shown that clays are the catalytic soil component responsible for the oligomerisation and hydrolysis of PDMS into silanols. The main product in soil was identified as the monomeric silanol DMSD (Carpenter et al. 1995; Lehmann et al. 1998). DMSD can then (i) volatilise and be oxidised (Lehmann and Miller 1996), (ii) undergo biodegradation (Lehmann et al. 1998), or (iii) be bound to soil humus (Griessbach and Lehmann 1999).

By its nature, DMSD is in contact with Al in the environment and is consequently a perfect candidate for this study. The dimer TMDS is only an intermediate in the degradation process of PDMS into DMSD, but the importance of the reversible condensation of the silanols has been emphasised previously (Spivack et al. 1997) and therefore the study of TMDS should not be neglected.

3.2.Experimental

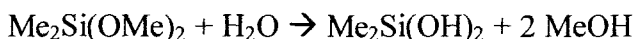
3.2.1.Preparation of TMDS (tetramethyldisilane-diol)

This preparation was made using an internal Dow Corning reference.

A buffer solution was prepared by mixing 0.33 g NaH₂PO₄ and 19.9 g of 0.1 mol.dm⁻³ NaOH in 500 mL of water. 5.4 g of this solution was measured out and added to the reaction. 25 mL of acetone was added as well as 0.32 g of palladium on carbon (10% with 50% by wt water). Tetramethyldisiloxane was then added slowly so as to keep the temperature below 25°C. Gas evolution occurred rapidly on addition of the siloxane. The reaction was continued until gas evolution had stopped. The mixture was filtered and the solvent was removed under vacuum at 25°C. The residue was extracted with hexane (100 mL), the aqueous layer removed and the hexane layer dried over magnesium sulphate followed by filtration and removal of hexane under vacuum giving a colourless liquid.

3.2.2.Preparation of DMSD (dimethylsilane-diol)

The following reaction was performed as described in the literature (Hyde 1953; Varaprath and Lehmann 1997):



Dimethyldimethoxysilane (30g) was added to distilled water (80g) in a plastic bottle and the solution was stirred until a homogeneous mixture was obtained. Contrary to the literature, this took between 15 mins and 30 mins instead of the 2h-24h stated in the literature!

However, after the removal of water on the rotovap under vacuum, a viscous oil dispersed in water was obtained which, when analysed by ²⁹Si NMR, showed a mixture of Me₂Si(OH)₂, HOSiMe₂OMe₂SiOH and cyclic siloxanes. The reaction was repeated 4

times, changing the order of addition and type of equipment used (glass, plastic). No diol was obtained as a pure solid in any of these reactions.

It was thought that the silane must be contaminated with acid and that this acid was causing the condensation to occur. A sample of the silane (5g) was placed in a glass bottle and calcium carbonate (1g) added to it. The mixture was shaken occasionally for 5 minutes. A sample of the silane (3g) was removed with a syringe filter, added to water (8g) in a 50 mL flask and stirred until homogeneous for 15-20 minutes. The mixture was then placed on the rotovap and the water removed at 45-60°C until a white solid appeared. The mixture was removed from the rotovap and pentane (20 mL) was added to the flask and shaken. The mixture was filtered through a Buckner funnel and the filtrate placed back on the rotovap. The solvent was removed to dryness at 45°C giving more white solid. This was washed with pentane (20 mL) and filtered. The resulting white solid from both filtrations was dried under vacuum at room temperature for 2h.

The ^{29}Si NMR showed only one peak at -0.25 ppm for $\text{Me}_2\text{Si}(\text{OH})_2$. The solid was stable at -10°C for over 72 hours. The ^{29}Si NMR spectrum presented in Figure 3.2-1 was recorded over night and showed a shift of -2.28 ppm for the $\text{Me}_2\text{Si}(\text{OH})_2$ possibly due to concentration or no lock solvent.

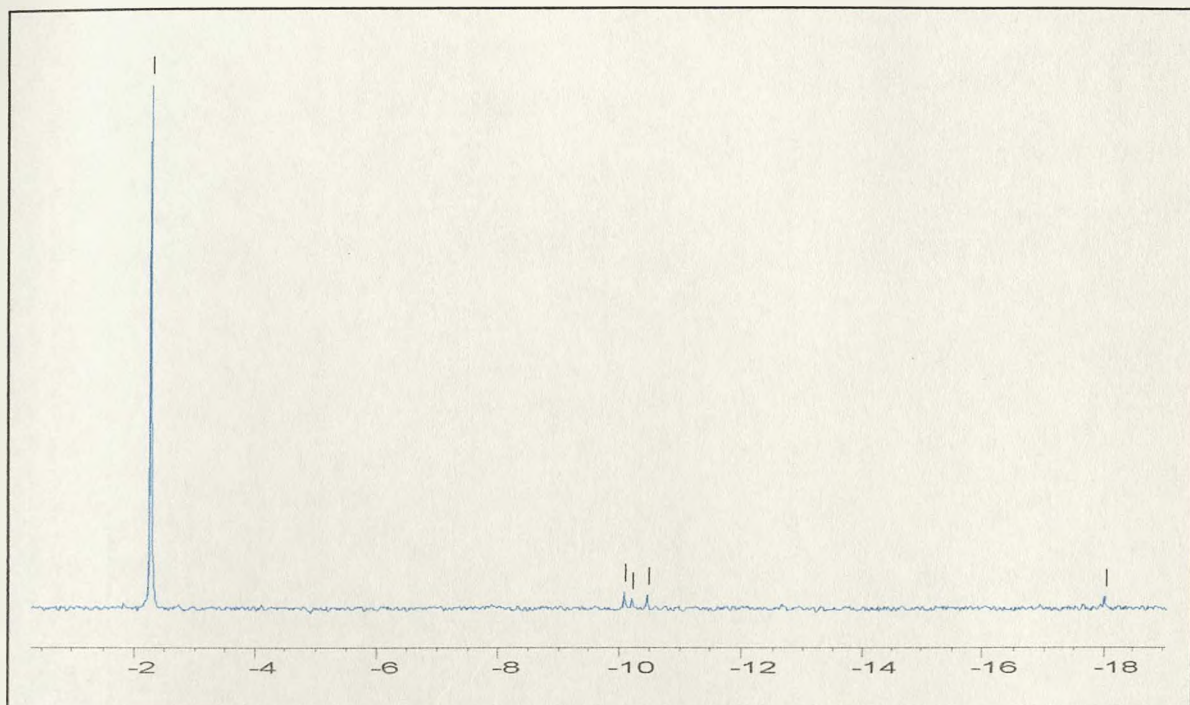


Figure 3.2-1: ^{29}Si NMR spectrum of DMSD, recorded after 24h.

3.2.3. Preparation of samples

The protocol followed for the preparation of the samples was the same as used by F. Doucet to prepare HAS (2001b). 5 L of a $0.1 \text{ mol}\cdot\text{dm}^{-3}$ KNO_3 stock solution was prepared. TMDS or DMSD was added in order to get $[\text{TMDS}]$ or $[\text{DMSD}] = 1 \text{ mmol}\cdot\text{dm}^{-3}$. The pH was then adjusted below 3 using HNO_3 . $\text{Al}(\text{NO}_3)_3\cdot 9\text{H}_2\text{O}$ was dried in a desiccator for several days before being added into the solution. The pH was then adjusted to 6.2 with NaOH and the solutions were left to stand in the dark for 6 months before filtration.

The samples were analysed by ^{29}Si and ^{13}C solution-state NMR before and after filtration. A $0.2 \mu\text{m}$ polycarbonate membrane was used to filter the sample. The precipitates collected by filtration were analysed by ^{29}Si and ^{27}Al NMR and by SEM-EDX. Samples were replicated twice and control solutions were also prepared. A summary of the nomenclature of the samples is presented in Table 3.2-1.

Table 3.2-1: nomenclature of the samples.

Name	[Al] mol.dm ⁻³	[TMDS] mol.dm ⁻³	[DMSD] mol.dm ⁻³
1 and 2	2	1	-
3 and 4	2	-	1
CT1	-	1	-
CT2	-	-	1
CT3	2	-	-

3.2.4. Instrumentation

•Solution-state NMR

All measurement were carried out on a Jeol Lambda 400 MHz, using a 5 mm probe. Spectra were recorded at room temperature using a DEPT pulse sequence. The parameters used for ²⁹Si and ¹³C are summarised in Table 3.2-2. The number of scans was 10 000.

Table 3.2-2: NMR parameters for DEPT pulse sequence.

I	90° (I) pulse	45° (¹ H) pulse	90° (¹ H) pulse	J(I- ¹ H)	Acquisition time
²⁹ Si	10.9 μs	5.6 μs	11.2 μs	7 Hz	3.3 s
¹³ C	8.5 μs	6 μs	12 μs	145 Hz	2.7 s

•Solid-state NMR

²⁷Al measurements were carried out on a Bruker DSX300 spectrometer in a magnetic field of 7.0 T (proton frequency of 300.13 MHz), with a MAS probe for a 4 mm rotor. Spectra were recorded using a single pulse proton decoupling sequence (decoupling frequency = 2709.8 Hz) with a $\pi/12$ pulse of 0.7 μs. The spinning frequency ν_r was 8 kHz. The

acquisition time was 20 ms and the number of scans was 1000. Chemical shifts were measured relative to the signal of $0.5 \text{ mol.dm}^{-3} \text{ AlCl}_3$.

•SEM-EDX

The analytical composition of the samples was measured by SEM-EDX using a 'JEOL 5600 LV' Scanning Electron Microscope coupled with 'Princeton Gamma-Tech (PGT) PRISM' Digital Energy Dispersive X-Ray Spectrometer (EDS). The experimental parameters were as follows:

- Electron gun HV = 15 kV
- Take off angle from sample to X-Ray detector = 35 degrees
- Acquisition time = 200 seconds
- Specimen working distance = 25 mm
- Specimen tilt angle = 0 degrees

Generally, system generated standards were used for the calibration; i.e. the software creates theoretical standards related to the specified analysis parameters. Matrix effects including particle size variation were minimised by using a take off angle greater than 30 degrees and correction algorithms.

The analysis of each sample was replicated three times.

3.3.Study by NMR

3.3.1.Solution state NMR

Spectra of the samples were recorded before and after filtration for ^{29}Si and ^{13}C . They are presented in Figure 3.3-1 and Figure 3.3-2. The chemical shifts observed are summarised in Table 3.3-1.

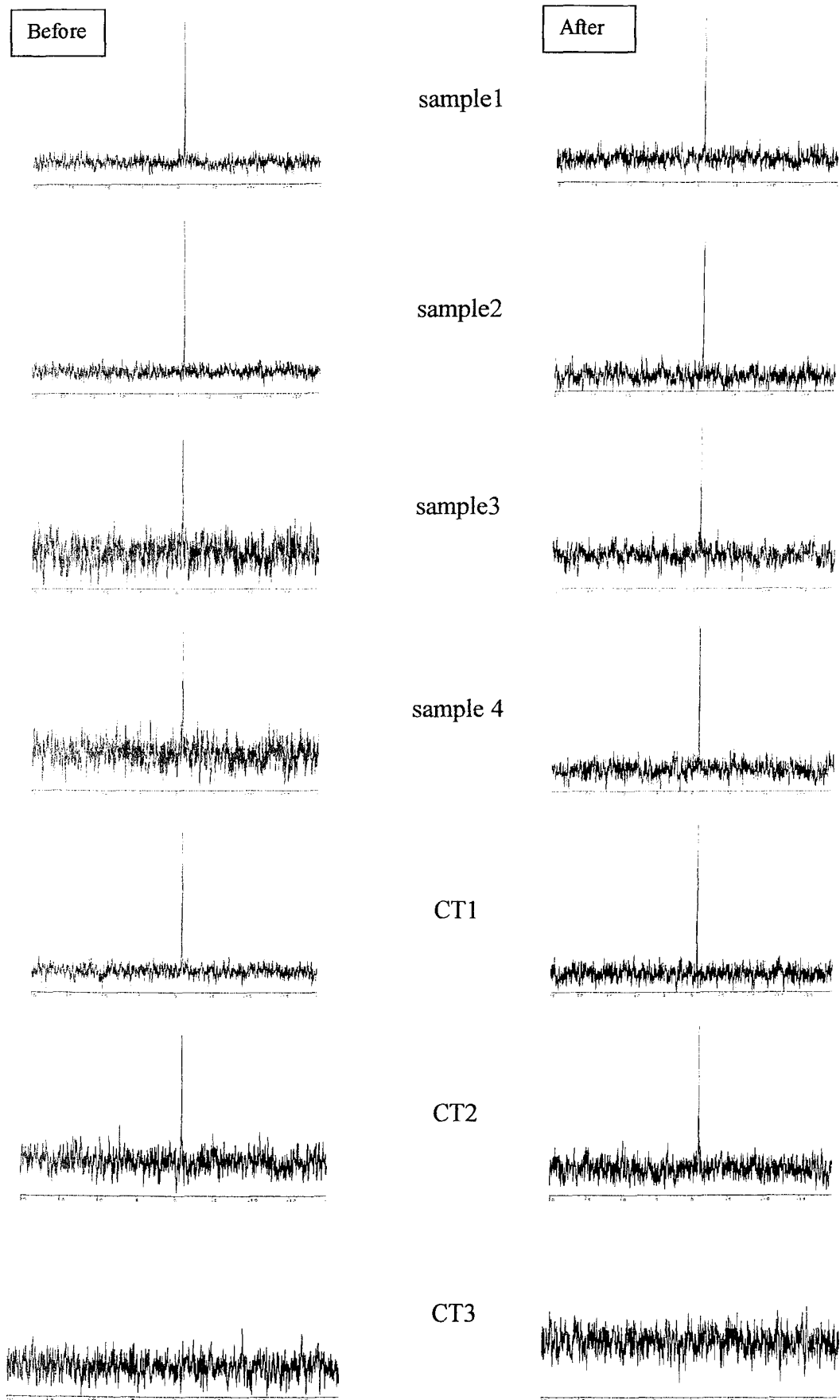


Figure 3.3-1: ^{29}Si DEPT spectra before and after filtration.

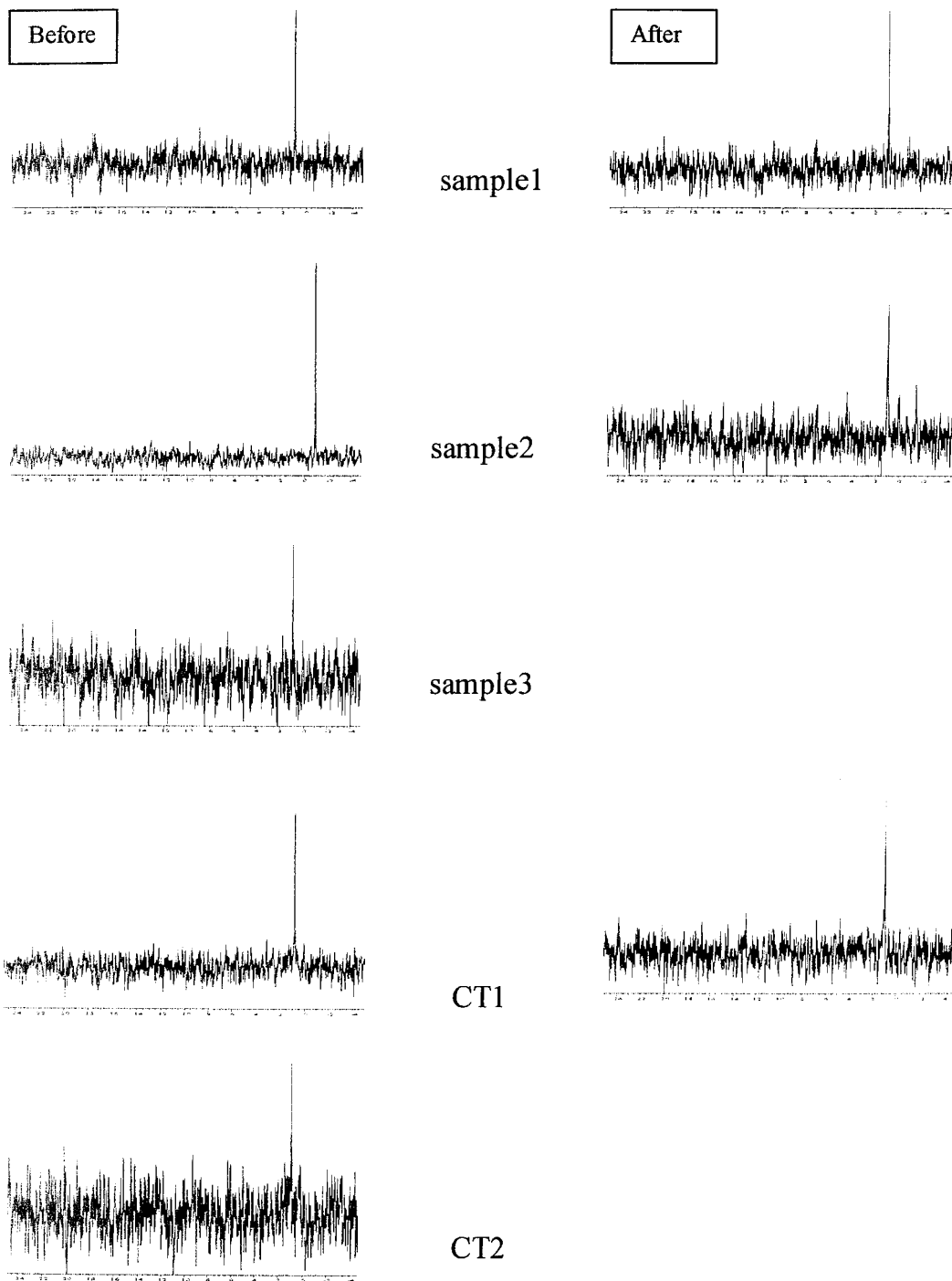


Figure 3.3-2: ^{13}C DEPT spectra recorded before and after filtration.

Table 3.3-1: Chemical shifts before and after filtration.

Sample	^{29}Si δ ppm		^{13}C δ ppm	
	Before filtration	After filtration	Before filtration	After filtration
1	-0.94	-0.94	0.94	0.86
2	-0.98	-0.94	0.86	0.87
3	-0.93	-0.96	0.87	N/A
4	-0.95	-0.94	N/A	N/A
CT1	-0.99	-0.95	0.88	0.87
CT2	-0.94	-0.94	0.80	N/A
CT3	Not detected	Not detected	Not detected	Not detected

The first point to be noted was that the chemical shifts both in ^{29}Si and ^{13}C were not significantly affected by the presence of Al. CT1 and samples 1 and 2 were comparable as well as CT2 and samples 3 and 4. The filtration process did not have any effect on the chemical shifts neither. This observation implied that the compound detected in solution in the different samples was the same and that it was still present in solution after filtration. However, it was also remarkable that the ^{29}Si chemical shifts of the TMDS only solution (CT1) after 6 months were in the range of the ^{29}Si chemical shift expected for DMSD (CT2). This result prompted for more experiments on the stability of TMDS in solution. It was obvious that TMDS was not present in the sample anymore after 6 months and that this had nothing to do with the presence of Al as it was observed in the control solution as well. ^{29}Si and ^{13}C NMR measurements were carried out on freshly prepared TMDS samples of high concentration (450 mmol.dm^{-3}). These measurements were repeated as the sample was ageing. The evolution of the ^{29}Si and ^{13}C spectra with time are shown in Figure 3.3-3 and Figure 3.3-4 respectively.

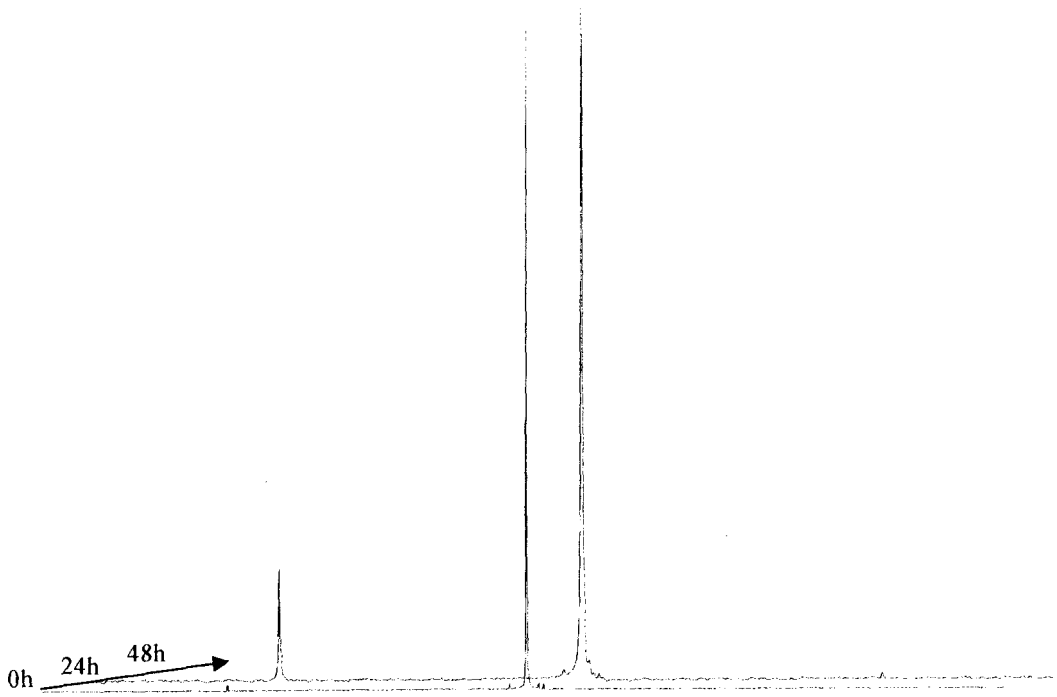


Figure 3.3-3: Evolution with time of ^{29}Si DEPT spectra of 450 mmol.dm⁻³ TMDS solution in water.

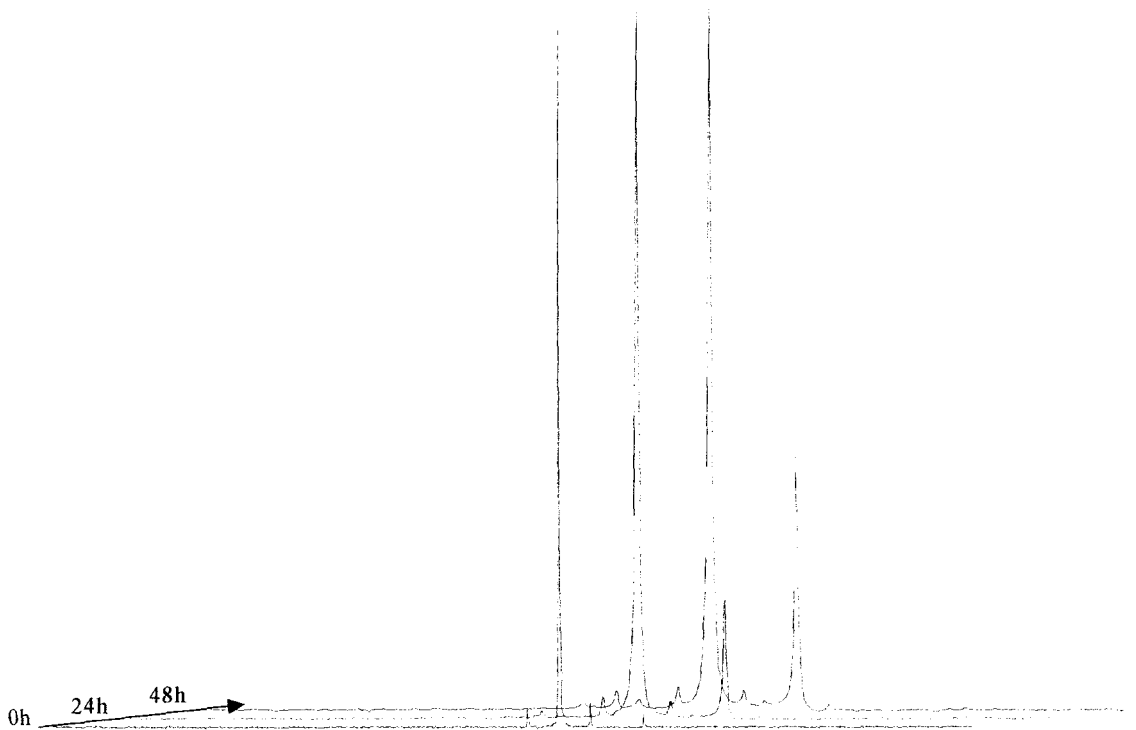


Figure 3.3-4: Evolution with time of ^{13}C DEPT spectra of 450 mmol.dm⁻³ TMDS solution in water.

After just 1 day, a new species appeared on both ^{29}Si and ^{13}C spectra and after 2 days a third species was noticeable on the ^{29}Si spectrum. A closer look at the chemical shifts as well as at the possible reactions involved in this system led to the attribution of the peaks. Figure 3.3-5 summarises the reaction scheme of both the polymerisation of TMDS and the hydrolysis of TMDS and the NMR peak attribution.

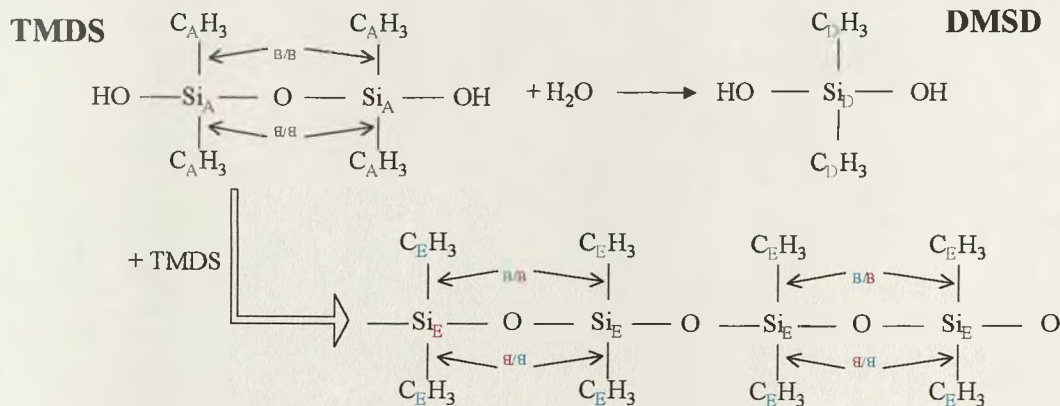
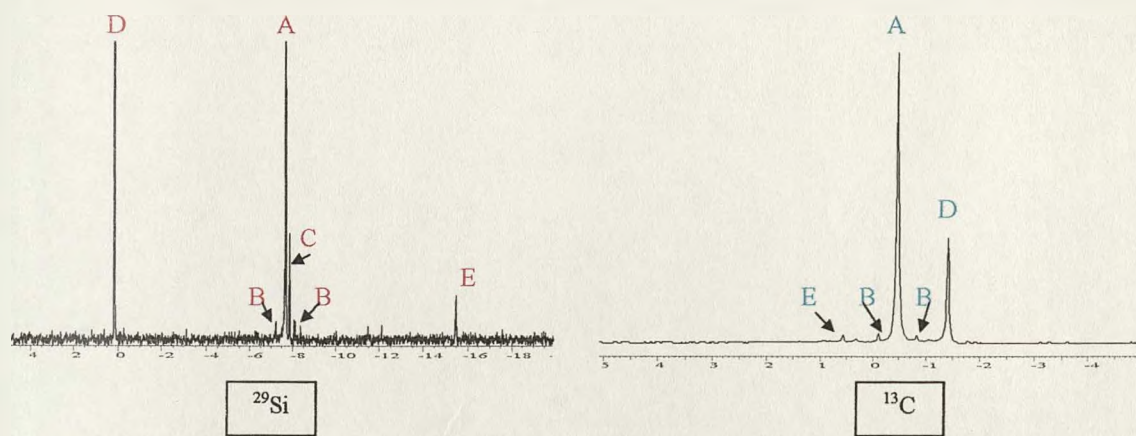


Figure 3.3-5: Peak attribution for ^{29}Si and ^{13}C NMR spectra. Spectra were recorded after 3 days.

This experiment showed that TMDS was not stable in water with time. TMDS would very rapidly hydrolyse to form DMSD and even polymerise. At high concentration ($450 \text{ mmol}\cdot\text{dm}^{-3}$), 50% of TMDS was transformed into DMSD after just a week. It was easy to assume that the less concentrated the solution, the quicker TMDS would hydrolyse into DMSD.

The solutions prepared with Al were left to settle down for 6 months. Almost all the TMDS should be hydrolysed into DMSD by this time. It was unlikely for Al to react with TMDS because of its dimeric form. The structure of DMSD could be in favour of a reaction with Al. However, by the time DMSD was formed and stable in solution, it was most likely for Al to have reacted with itself to form $\text{Al}(\text{OH})_3$.

3.3.2. Solid-state NMR

The material collected after filtration was analysed by ^{27}Al solid-state NMR. Only samples containing Al in their initial composition, i.e. samples 1, 2, 3, 4 and CT3, formed a solid material. The filtration process was easier for samples 3 and 4 and even more for CT3. This seemed to imply that the material collected might be of a different nature. Figure 3.3-6 shows the spectra obtained by solid-state NMR. The shape of the peaks is due to the quadrupolar nature of the Al nucleus. All spectra indicated the presence of only one form of Al. The position of the peak around 0 ppm indicated that the material collected by filtration was constituted of octahedral Al. A signal at 60.5 ppm indicated the presence of tetrahedral Al in samples 1, 2, 4 and CT3. It was not detected in sample 3. Its presence in the Al only control solution suggested that it was not due to the interaction with Si. Moreover, ^{29}Si CP-MAS NMR and ^{13}C MAS NMR gave no signal which suggests that neither of those nuclei were present in the material. A recent study (Furrer et al. 2002) reported the presence of a similar signal in ^{27}Al MAS NMR spectra of natural and synthetic aluminium hydroxide gels and the peak was attributed to the tetrahedral Al fraction of Al_{13} . However, the intensity of the tetrahedral signal in my samples did not exceed 1 to 2 % as compared to the ratio $\text{Al}_{(\text{IV})} / \text{Al}_{(\text{VI})} = 1/13$ representative of the Al_{13} stoichiometry.

These results revealed that $\text{Al}(\text{OH})_3$ was formed and precipitated in all the samples, independently of the initial composition of the solution. There was no incorporation of silicon or carbon into the structure. However, the difference observed in the rate of filtration might suggest that the materials collected are different forms of $\text{Al}(\text{OH})_3$.

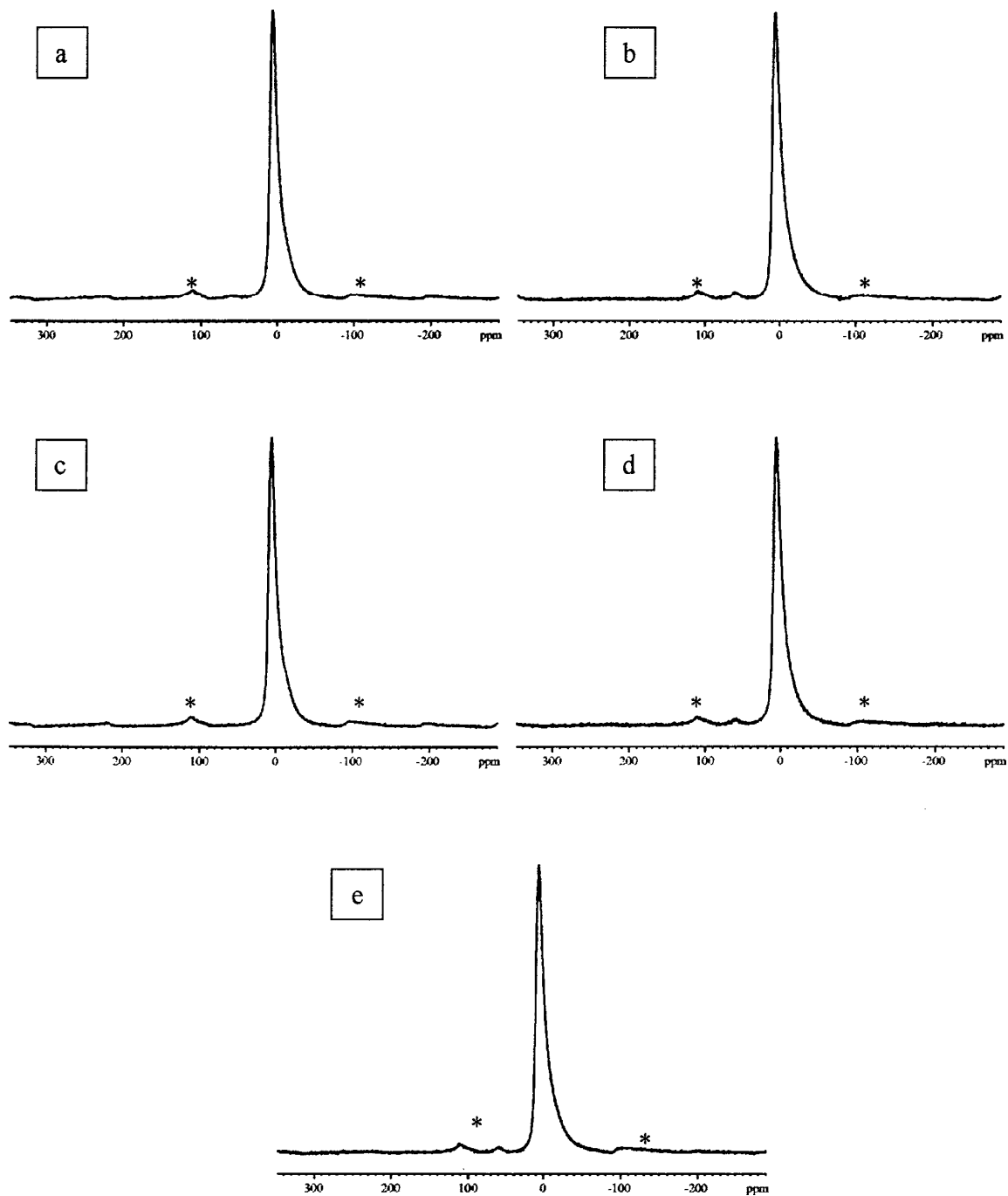


Figure 3.3-6: ^{27}Al MAS spectra. a: sample 1; b: sample 2; c: sample 3; d: sample 4; e: CT3. * : spinning band.

3.4. Analysis by SEM-EDX

The elemental composition of the material collected by filtration of each sample was analysed by EDX and images of the structures were taken by SEM. An X-ray spectrum is shown in Figure 3.4-1. No Si was detected in any of the samples.

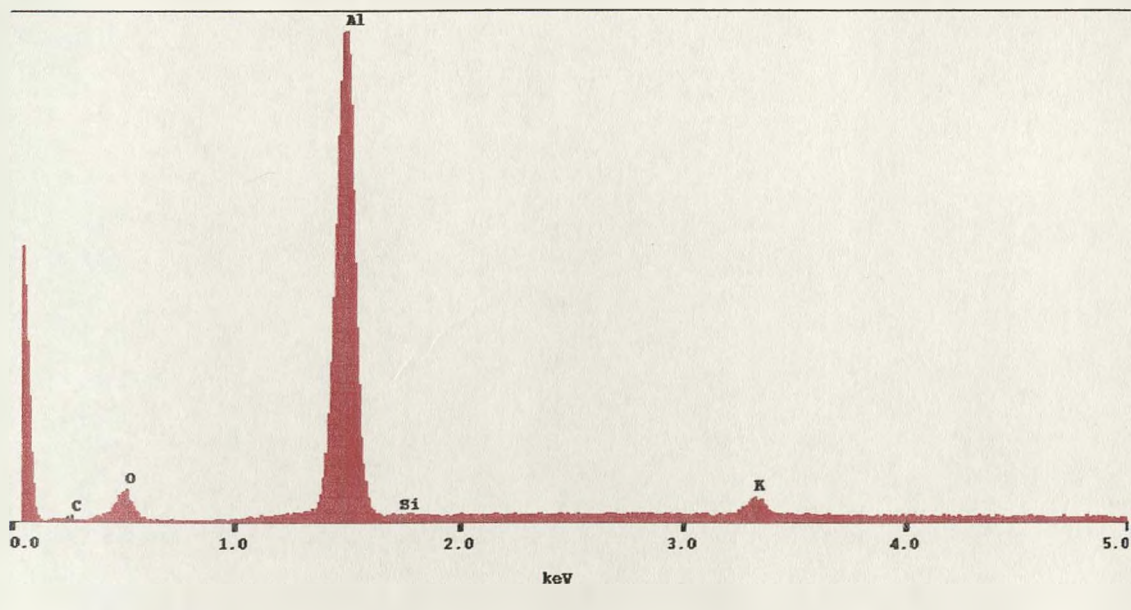


Figure 3.4-1: X-ray spectrum for sample 1.

SEM images at low and high magnification of the collected samples 1, 2, 3, 4 and CT3 are presented in Figures 3.4-2, 3.4-3, 3.4-4, 3.4-5 and 3.4-6 respectively. The low magnification images (a) of the ground material all showed the same morphology, dense and compact. Close-up views of the materials (b: $\times 3000$, c: $\times 10\ 000$ and d: $\times 20\ 000$) indicated a fluffy morphology, arranged in layers with deposition of small particles ($< 1\ \mu\text{m}$) on the surface. There was no noticeable difference of structure between the samples, indicating that the presence of either TMDS or DMDS did not obviously influence the formation and the precipitation of $\text{Al}(\text{OH})_3$.

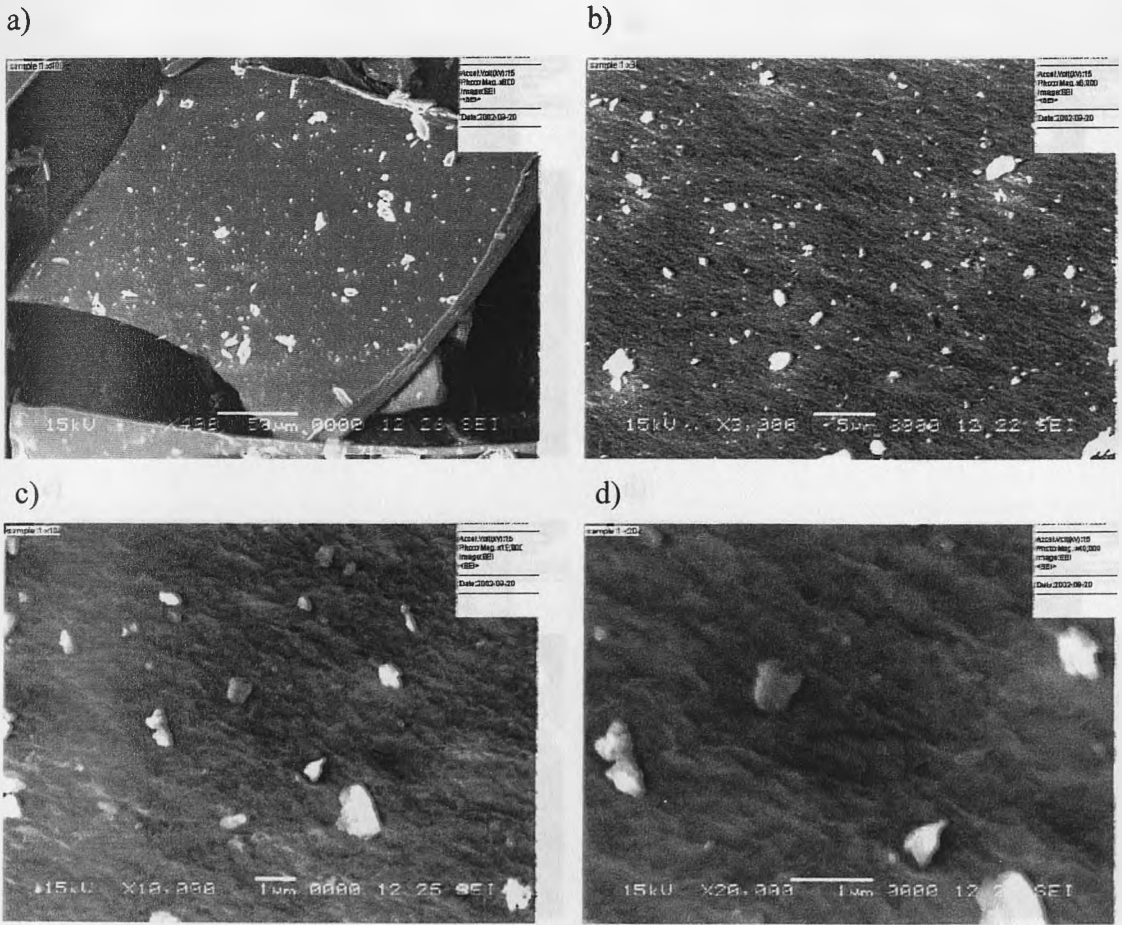


Figure 3.4-2: SEM images of material collected from parent solution 1 $[Al] = 2 \text{ mmol.d}^{-3}$ and $[(TMDS)] = 1 \text{ mmol.dm}^{-3}$. a) Low magnification. b, c, d) High magnification.

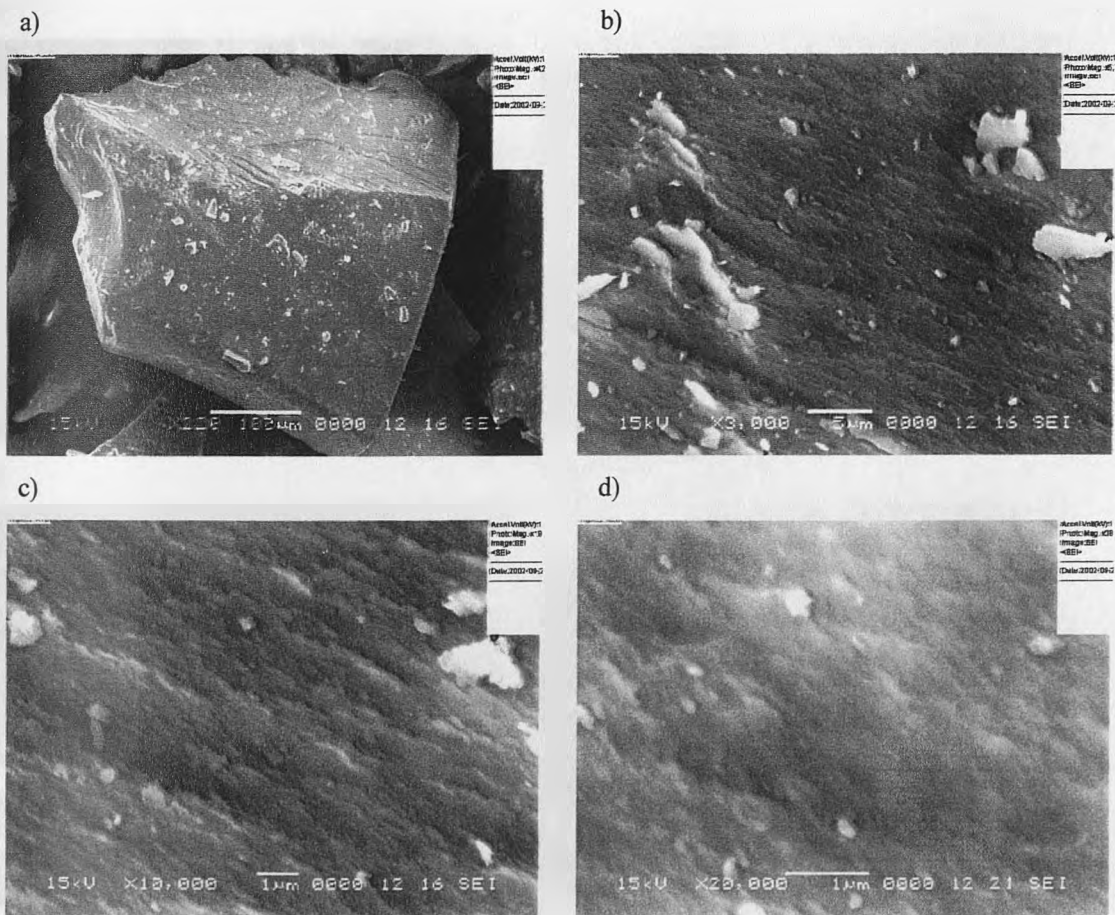


Figure 3.4-3: SEM images of material collected from parent solution 2 $[Al] = 2 \text{ mmol.dm}^{-3}$ and $[(TMSD)] = 1 \text{ mmol.dm}^{-3}$. a) Low magnification. b, c, d) High magnification.

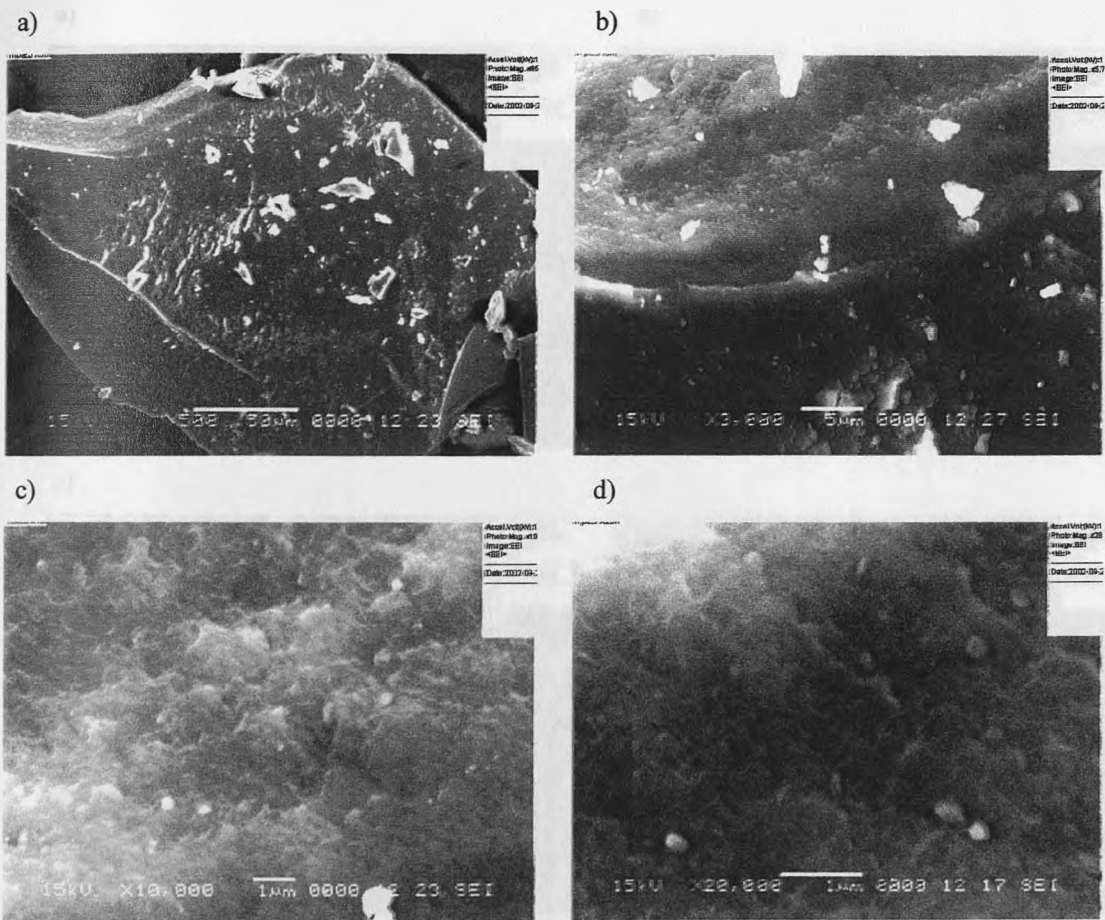


Figure 3.4-4: SEM images of material collected from parent solution 3 $[Al] = 2 \text{ mmol}\cdot\text{d}^{-3}$ and $[DMDS] = 1 \text{ mmol}\cdot\text{dm}^{-3}$. a) Low magnification. b, c, d) High magnification.

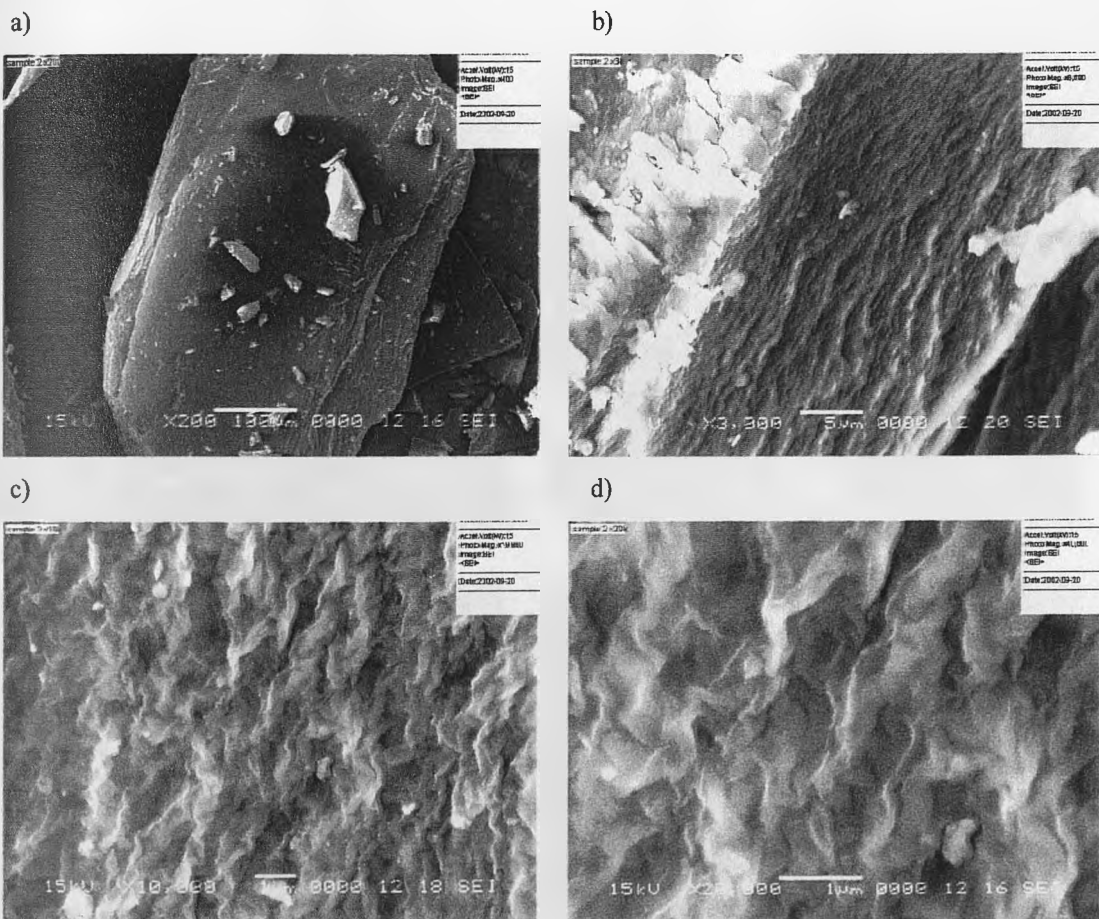


Figure 3.4-5: SEM images of material collected from parent solution $[Al] = 2 \text{ mmol} \cdot \text{dm}^{-3}$ and $[DMDS] = 1 \text{ mmol} \cdot \text{dm}^{-3}$. a) Low magnification. b, c, d) High magnification.

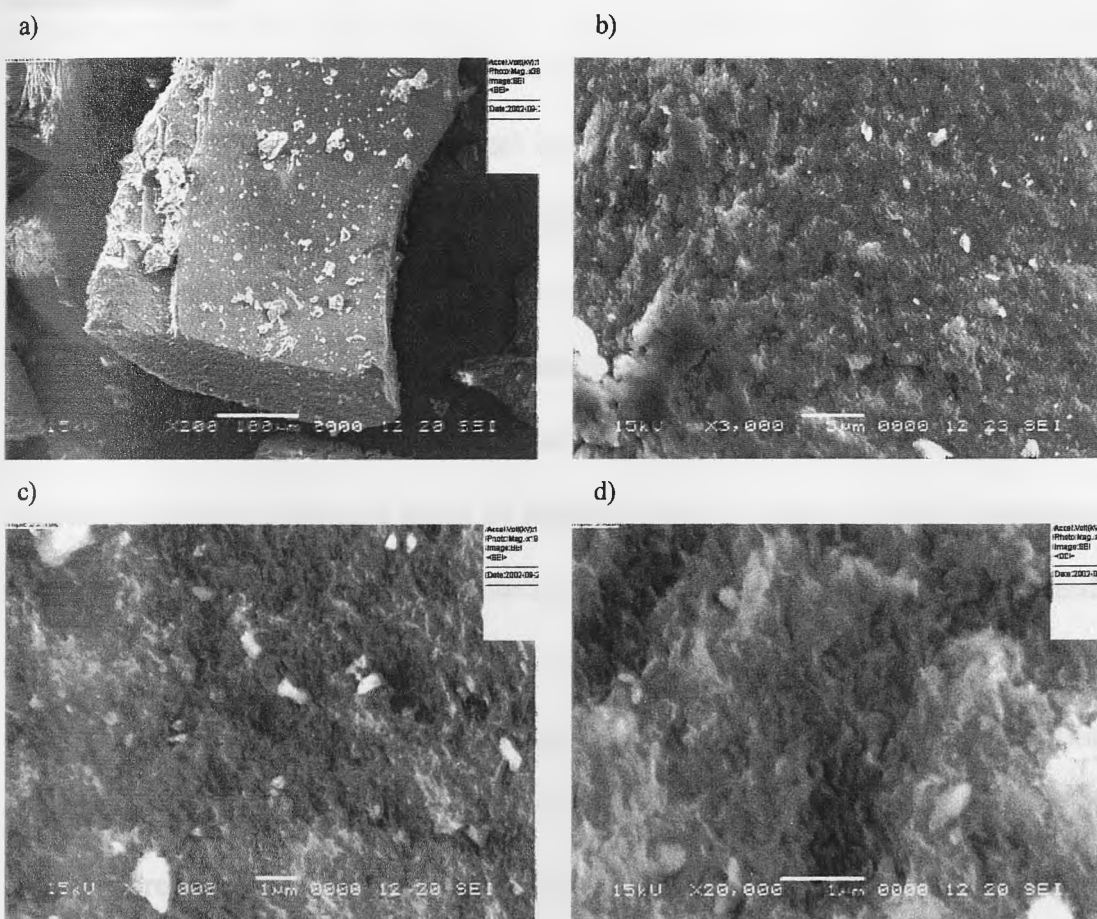


Figure 3.4-6: SEM images of material collected from parent solution CT3 $[Al] = 2 \text{ mmol} \cdot \text{d}^{-3}$. a) Low magnification. b, c, d) High magnification.

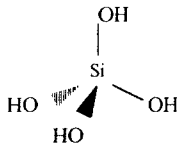
3.5. Conclusions.

Al was mixed with substituted forms of $\text{Si}(\text{OH})_4$ potentially available in soils, namely DMSD and TMDS. The experimental conditions were those under which the reaction between $\text{Si}(\text{OH})_4$ and Al is the more likely to occur to form HAS. The analysis of the samples before filtration by ^{29}Si and ^{13}C solution-state NMR showed no difference from the control solutions, implying that no interaction occurred between DMSD/TMDS and Al. The ^{29}Si spectra obtained after filtration of the samples indicated no change either, which suggested that the substituted forms of $\text{Si}(\text{OH})_4$ were not affected by the formation of the precipitate collected. Only the degradation of TMDS into DMSD was noticed and it did not seem to be affected by the presence of Al. The ^{27}Al solid-state NMR spectra of the materials collected by filtration indicated that the precipitates were all constituted of octahedral Al and that the samples collected from the solutions containing TMDS or DMSD were identical to the Al only control solution. No ^{29}Si signal was observed. The analysis of the elemental composition of the samples by EDX confirmed that no Si was present in the materials collected. All these observations led to the following conclusions:

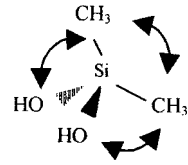
- there was no interaction between Al and DMSD or TMDS;
- the material collected from all the samples was $\text{Al}(\text{OH})_3$ and its precipitation was not altered by the presence of either of the PDMS.

The difference of rate observed in the filtration process of the samples of different initial composition might have been due to a difference of structure of the material collected. The images obtained by SEM showed that all the materials collected had similar aspect and morphology.

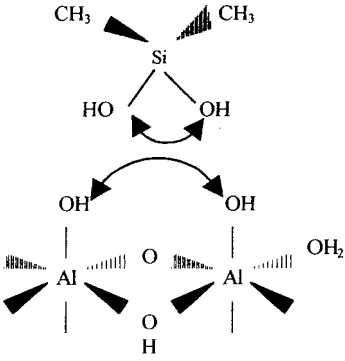
PDMS were the ideal candidates to study the potential reaction of Al with other Si-based compounds. However, the results proved that this reaction did not occur even under optimal conditions. This might suggest that (i) the size of the substituted $\text{Si}(\text{OH})_4$ was an obstacle to the reaction or (ii) the reaction between Al and $\text{Si}(\text{OH})_4$ to form HAS is specific. At pH 6.2, it was found that $\text{Al}(\text{OH})_3$ precipitated independently of the presence of either DMSD or TMDS but that a phenomenon of degradation occurred for TMDS into DMSD. The lack of interaction between Al and both polydimethylsilanols suggested that the size of the substituted groups prevented the approach of the Si compound onto the $\text{Al}(\text{OH})_3$ templates. This also reinforced the hypothesis of the formation of a template as a prerequisite to the reaction of formation of HAS. If one considers the reaction of $\text{Al}(\text{OH})_3$ with DMSD, there is no structural obstacle for the formation of an Al-Si complex. However, if a $\text{Al}(\text{OH})_3$ template is involved as proposed in the different schemes in Figure 1.2-2 (Chapter 1), the presence of the two methyl groups on the Si by changing the size of the molecule as well as the OSiO angle cannot bridge over the two Al-OH groups (schemes 3 and 4). This is summarised in Figure 3.5-1. The dimer (TMDS) structure is even less flexible due to the Si-O-Si bond and the OH groups are still less likely to approach the $\text{Al}(\text{OH})_3$ templates in order to react.



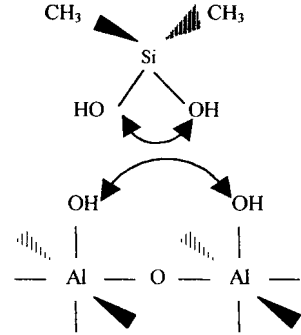
Si(OH)_4



DMSD



Scheme 3



Scheme 4

Figure 3.5-1: Influence of the methyl groups on the mechanism of formation of HAS.

Chapter 4 : The direct observation of hydroxyaluminosilicates formation by Atomic Force Microscopy.

4.1. Aim

Atomic Force Microscopy (AFM) has been used previously (Doucet et al. 2001a) to study and characterise 3 month old HAS of different parent solution Al/Si ratio. The use of such a technique does not only allow one to visualise HAS for the first time but it also permits a direct observation of the particles in their parent solution. F. Doucet's study using contact mode AFM was the first to show evidence of two different forms of HAS particles in solution: HAS_A and HAS_B. He demonstrated that depending on the Al/Si ratio in the parent solution, the particles found in solution are either of a rectangular (up to 170 nm in length, HAS_A, Al in excess) or discoid (up to 43 nm in length, HAS_B, Si(OH)₄ in excess) shape.

The next step of the characterisation of HAS in situ was to follow the formation of particles by AFM at different stages of the reaction.

The aim of this study was to analyse HAS using tapping mode AFM on different aged solutions in order to get information on the process of growth of such a system. The questions to be answered were the following:

- Can particles be observed at an early stage?
- How quickly does the reaction occur?
- Can HAS_A be observed as a precursor of HAS_B formation?
- How do the particles aggregate?

4.2.Experimental

4.2.1.Preparation of the samples

2 control solutions and 2 relevant Al/Si ratios were prepared:

A: Al/Si=2/0

B: Al/Si=0.5/2

C: Al/Si=2/0.5

D: Al/Si=0/2

- 50 mL 0.1M KNO₃ +/- Si(OH)₄ was prepared
- 0.025g Na azide was added to prevent growth of organisms.
- The pH was adjusted below 3.
- Al(NO₃)₃.9H₂O was added to the required concentration
- PIPES was added as a buffer (50 mmol.dm⁻³)
- The pH was then adjusted to 6 with NaOH pellets.

The solutions were then left to age for different lengths of time: 1 day, 1 week, 2 weeks, 1 month, 2 months, 3 months and 4 months.

4.2.2.Tapping-mode AFM in solution

AFM was carried out on a Digital Instruments Dimension 3100, in the TappingMode® under water using a silicon tip.

Silicon wafers were used as substrates for surface deposition. Prior to any experiments, they were carefully washed following the piranha cleaning method.

- The wafers were first cleaned in a solution of organic solvent (propanol, followed by acetone) for 15 mins in an ultra-sonic bath.

- After being rinsed with ultra-pure water, the substrates were oxidised in a mixed solution of H₂O₂:H₂SO₄ (3:7 vol.) for a minimum of 30 minutes.
- Finally they were thoroughly rinsed with ultra pure water before being transferred into the sample for 24h.

To prevent any phenomenon of dissolution, each substrate was put into a liquid cell containing the original sample solution. This precaution ensured that the particles were in equilibrium with their parent solution and were not affected by the external medium. The surface was then imaging using tapping mode AFM.

4.2.3.XPS

Some of the samples were characterised after filtration using XPS (see section 3.5). X-ray photoelectron spectroscopy (XPS) involves irradiation of a sample with soft X-rays, and the energy analysis of photo-emitted electrons that are generated close to the sample surface. XPS has the ability to detect all elements (with the exception of Hydrogen) in a quantitative manner from an analysis depth of 10 nm (or less). As well as elemental information, XPS can probe the chemical state of elements through the concept of binding energy shift.

Instrument:	Kratos Analytical Axis Ultra
Sampling:	Monochromated Al K α X-rays
Spectra Acquired:	Survey, Na 1s, O 1s, N 1s, C 1s, Si 2s, Si 2p, Al 2p

All samples were analysed using a nominal power of 300 W, with a survey spectrum being captured using a pass energy of 160 eV and high resolution scans being captured using a pass energy of 20 eV. A survey spectrum of each sample was carried out initially to identify which elements were present on the surface. High resolution scans for each element were then carried out in order to obtain quantitative information, and elemental environment information. Elemental information is reported as the mean of three positions on one sample, with the standard deviation being reported at 95% confidence limits.

4.3.Results

4.3.1.The growth of HAS observed by AFM

Tapping mode AFM gives pictures of a good resolution on this kind of sample and seems to not disturb the surface deposition as much as contact mode. Aggregates and particles, when present, can be observed very clearly.

Figure 4.3-1 shows images of the control solutions after 1 day and 4 months. In Al only solution, the images show precipitation of $\text{Al}(\text{OH})_3$ as expected at this pH even after one day. Nothing was observed for $0.1 \text{ mol.dm}^{-3} \text{ KNO}_3$ or $2 \text{ mmol.dm}^{-3} \text{ Si}(\text{OH})_4$. Figures 4.3-2; 4.3-3; 4.3-4; 4.3-5; 4.3-6; 4.3-7 and 4.3-8 present the images for solutions of ratio Al/Si = 0.5/2 and Al/Si = 2/0.5 after 1 day, 1 week, 2 weeks, 1 month, 2 months, 3 months and 4 months respectively. Ten by 10 μm surfaces images are shown as well as close ups (0.164 by 0.164 μm) on individual particles. All images were recorded in the height mode. After just a day (Figure 4.3-2), some deposition can be noticed on the surface for Al:Si = 2/0.5 (b and d) . The particles observed for this ratio at this stage were rectangular. However, when $\text{Si}(\text{OH})_4$ was in excess in the parent solution (a and c), there was no formation of particles

observed. After 1 week (Figure 4.3-3), particles were present in both solution. There was a lot of deposition on the surface of the Al:Si = 0.5/2 solution (a) and the shape of the particles observed for this ratio was rectangular (c). The surface of the Al:Si = 2/0.5 (b) was smoother and some aggregates started to form. Both discoid and rectangular particles were observable (d). AFM images of 2 week old solution (Figure 4.3-4) showed the formation of aggregates for both Al:Si ratio. Individual particles were present as well and their shape was rectangular for Al:Si = 0.5/2 (c) and mostly discoid for Al:Si = 2/0.5 (d). It also seemed that rectangular particles were formed by the merging of two discoids as shown on Figure 4.3-4 (d). After 1 month, very little was noticeable. The surface of Al:Si = 0.5/2 (Figure 4.3-5 (a) and (c)) was very smooth and no individual particles were observed. This could be explain either by (i) the constitution of the smooth layer of material on the wafer by aggregation of the particles or (ii) the instability of HAS in solution and the phenomenon of formation/dissolution prior to equilibrium. The images of Al:Si =2/0.5 (Figure 4.3-5 (b) and (d)) showed the presence of a lot of particles merging together to almost constitute a uniform layer. After 2 months, images of Al:Si = 0.5/2 (Figure 4.3-6 (a) and (c)) showed the presence of larger aggregates and individual particles were bigger and mostly discoid. Discoid particles were also observed for Al:Si = 2/0.5 (d).The number and the size of aggregates increased after 3 and 4 months (Figures 4.3-7 and 4.3-8). It seemed that they formed a smooth layer on the top of which new particles were growing and aggregating. This was particularly noticeable for Al:Si = 2/0.5 after 4 months (Figure 4.3-8 (b)). Table 4.3-1 summarises the shape and the size of the particles observed for both Al:Si ratios with time. The majority of the particles observed in Al:Si = 0.5/2 solution were rectangular whilst they were mostly discoid for Al:Si = 2/0.5. The size of the particles increased with time to form agglomerates. The size of the discoid particles was generally smaller than the size of the rectangular ones. Images tend to show that rectangular particles

were the result of the merging of discoids. This reinforced the idea that HAS_A exists prior to HAS_B. The particles then agglomerated to constitute a smooth layer on which new particles were depositing.

The images taken by AFM showed that HAS were formed very quickly. Even after one day, some particles were visible. The same observation could be made just by watching the samples. All samples presented a stable but cloudy suspension except for the Si(OH)₄ only ones. If the sample was shaken, the agglomerates are broken down proving that the particles were not strongly bound. This observation has never been made before at such an early stage, implying that the presence of a buffer, preventing the pH to change according to the species present in solution, could accelerate the growth of HAS. As a consequence, the suspensions had to be analysed further.

Table 4.3-1: Size of the particles observed by tapping-mode AFM. id: the length was similar to the width of the particle.

Sample	Age	Height (nm)	Length (nm)	Width (nm)	
Al:Si = 0.5/2	1 day	n.d.	n.d.	n.d.	
	1 week	1.3	39.1	32	
		1.4	30.1	26.9	
		1.1	32	28.8	
		3	55	24.3	
		5.2	52.5	26.3	
		4.9	58.9	21.8	
		2.9	85.2	16	
		2 weeks	2.45	47.6	16.5
			1.15	32.9	14
			0.73	28.2	14.1
	1.05		36.5	19.8	
	0.67		42.3	11.2	
	0.69		16.5	10.6	
	0.57		18.2	10.6	
	2 months	0.37	8.9	id	
		0.18	6.8	id	
		2.08	33.3	13.4	
		4.86	115.6	46.7	
		5.6	97.4	90.3	
	3 months	1.4	49.5	14.7	
		1.3	38.4	12.1	
		1.2	39.7	16.6	
4 months	1.12	30.7	17.9		
Al:Si = 2/0.5	1 day	2.95	162.5	85.5	
	1 week	2.07	38.4	21.8	
		2.8	30.12	19.8	
		2.7	35.2	23.7	
		1.04	33.3	15.3	
		3.4	62.16	51.3	
		4.9	42.9	40.3	
		1.8	24.4	21.7	
		3.1	33.3	35.8	
		2 weeks	4	38.5	id
			4	29.5	id
	3.4		30.1	id	
	4.3		35.9	id	
	2.1		33.9	id	
	5.8		54.5	id	
	1.25		25.0	id	
	1.49		26.2	id	
	1 month	1.3	46.9	13.4	
		1.5	51.8	17.1	
		1.6	46.9	16.4	
	2 months	2.6	95.5	65.4	
		0.57	26.3	14.7	
		2.15	73.7	56.4	
	3 months	1.5	47.3	id	
		1.3	38.9	id	
	4 months	1.6	31.8	id	
		1.03	10.9	id	

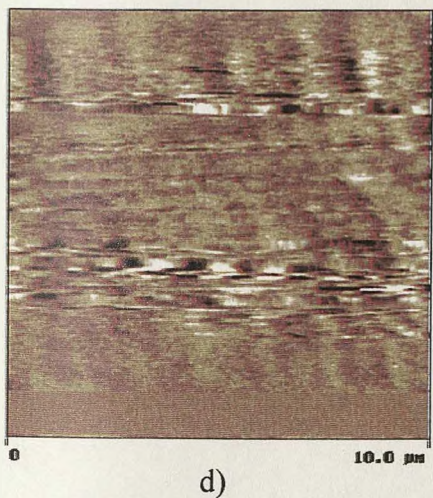
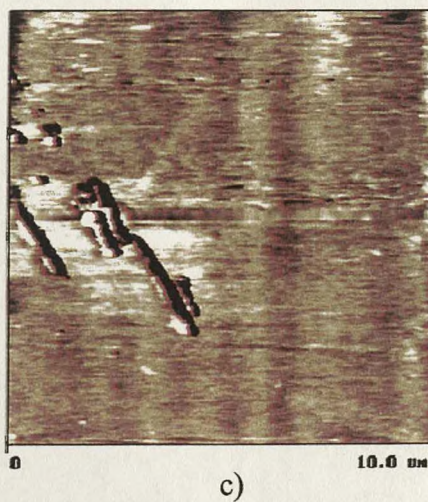
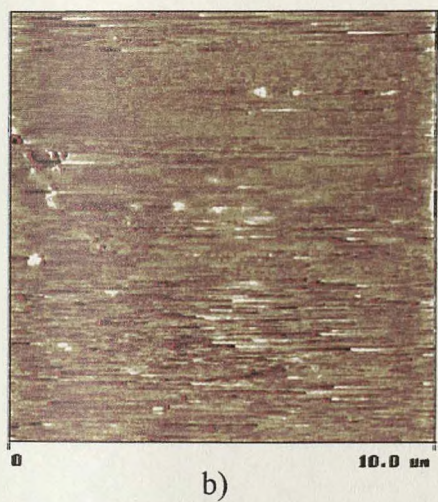
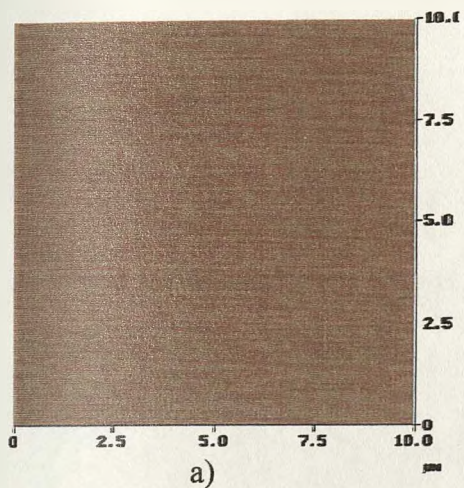


Figure 4.3-1: Tapping mode AFM images, $10 \times 10 \mu\text{m}$, height scale: $z = 10 \text{ nm}$. a) $0.1 \text{ mol.dm}^{-3} \text{ KNO}_3$; b) $2 \text{ mmol.dm}^{-3} \text{ Al}$, 1 day old; c) $2 \text{ mmol.dm}^{-3} \text{ Al}$, 4 months old; d) $2 \text{ mmol.dm}^{-3} \text{ Si(OH)}_4$, 1 day old; e) $2 \text{ mmol.dm}^{-3} \text{ Si(OH)}_4$, 4 months old.

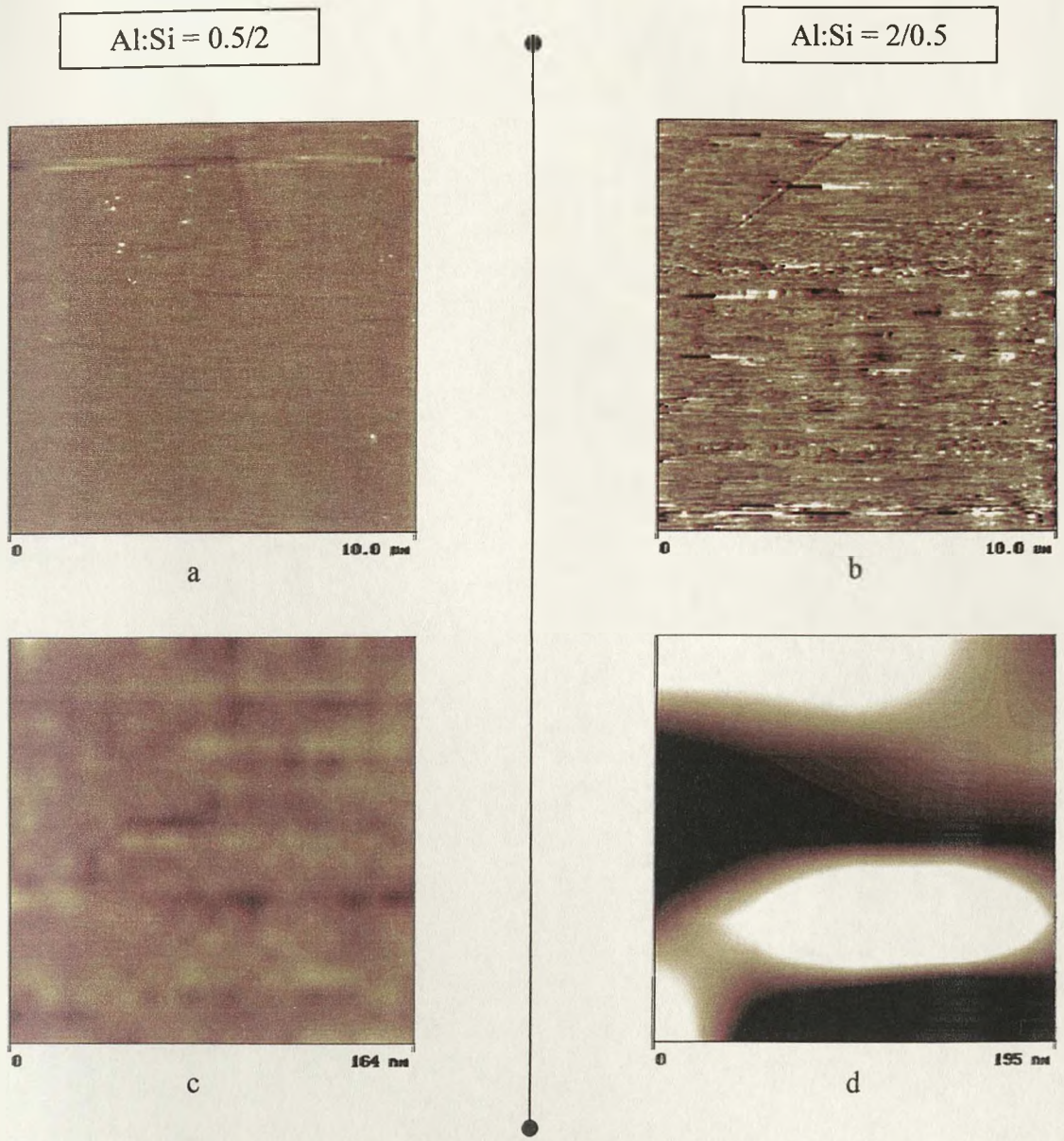


Figure 4.3-2: Tapping mode AFM images of 1 day old solutions. a) and b) 10×10 μm, height scale: z= 10 nm. c) and d) close up: z = 2 nm.

Al:Si = 0.5/2

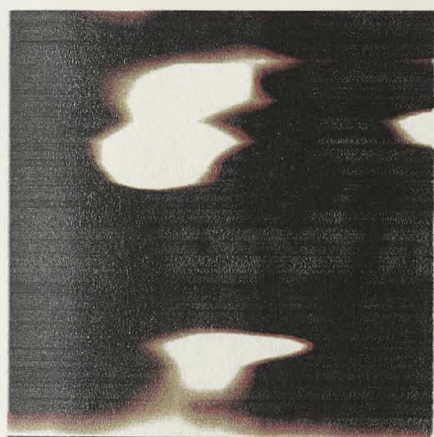
Al:Si = 2/05



a



b



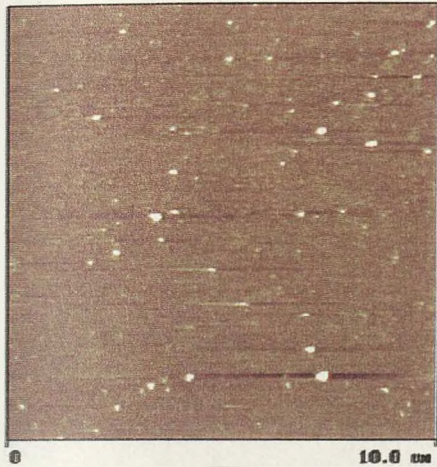
c



d

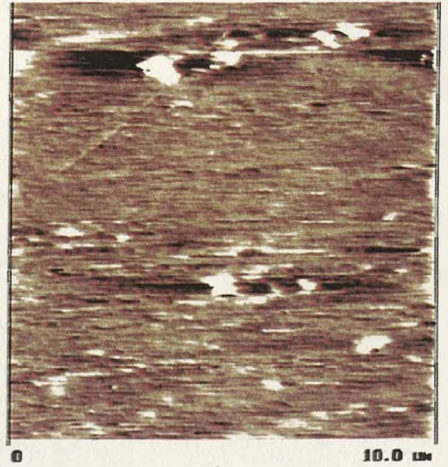
Figure 4.3-3: Tapping mode AFM images of 1 week old solutions. a) and b) $10 \times 10 \mu\text{m}$, height scale: $z = 10 \text{ nm}$. c) and d) close up: $z = 2 \text{ nm}$.

Al:Si = 0.5/2

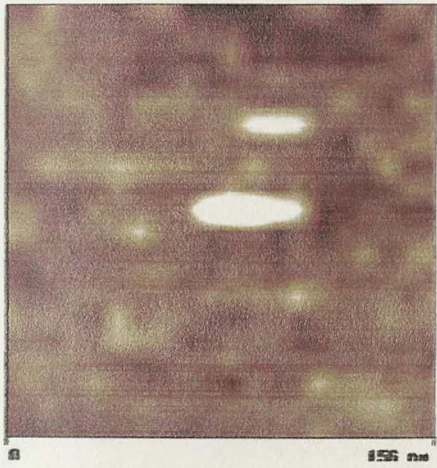


a

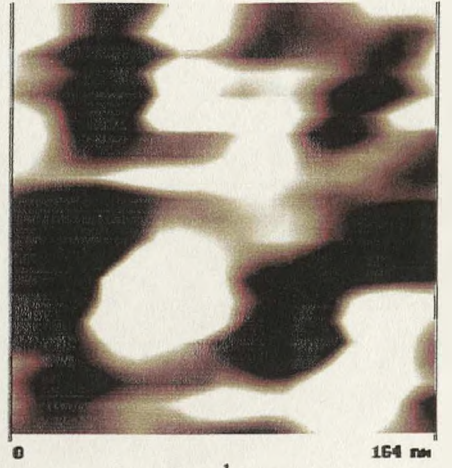
Al:Si = 2/0.5



b



c



d

Figure 4.3-4: Tapping mode AFM images of 2 weeks old solutions. a) and b) $10 \times 10 \mu\text{m}$, height scale: $z = 10 \text{ nm}$. c) and d) close up: $z = 2 \text{ nm}$.

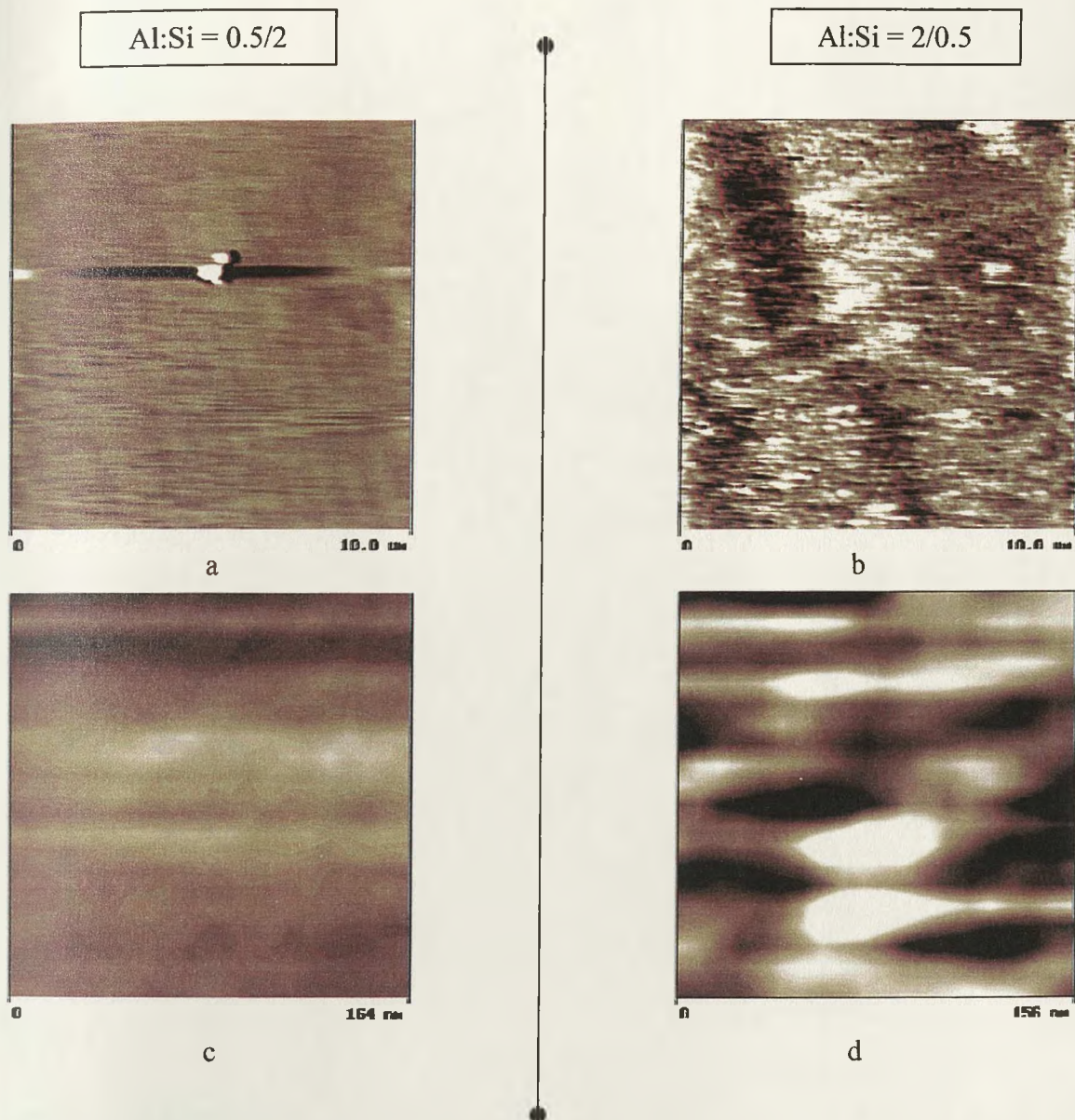
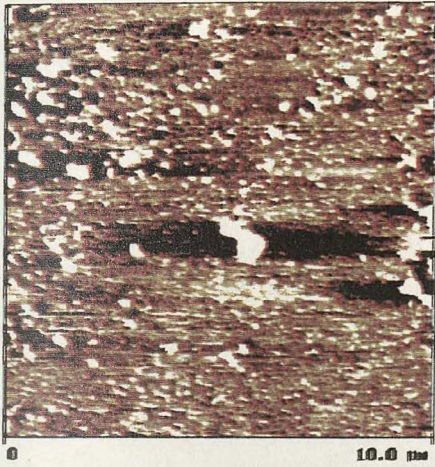
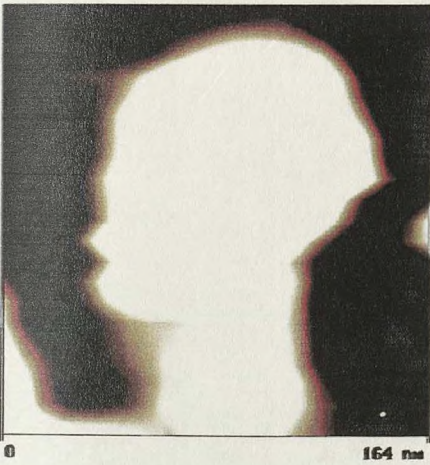


Figure 4.3-5: Tapping mode AFM images of 1 month old solutions. a) and b) $10 \times 10 \mu\text{m}$, height scale: $z = 10 \text{ nm}$. c) and d) close up: $z = 2 \text{ nm}$.

Al:Si = 0.5/2



a



c

Al:Si = 2/0.5



b



d

Figure 4.3-6: Tapping mode AFM images of 2 months old solutions. a) and b) $10 \times 10 \mu\text{m}$, height scale: $z = 10 \text{ nm}$. c) and d) close up: $z = 2 \text{ nm}$.

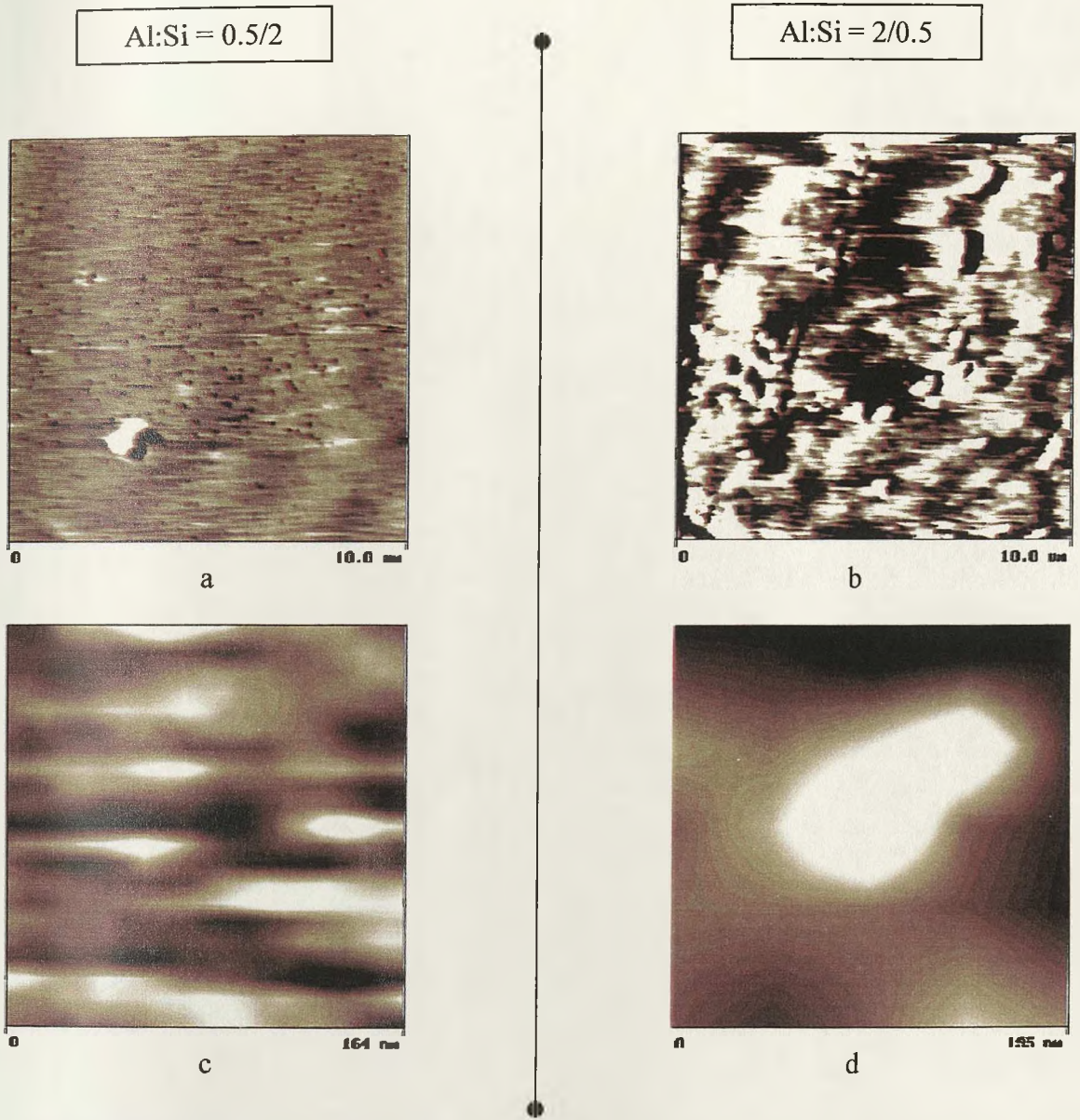


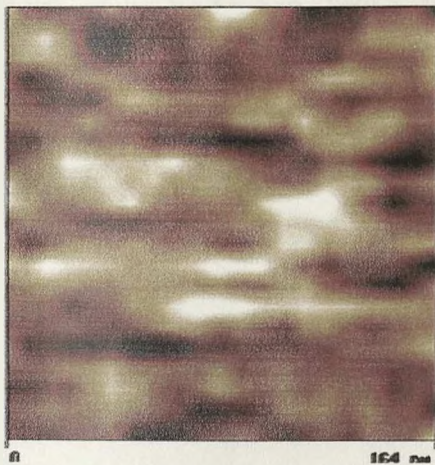
Figure 4.3-7: Tapping mode AFM images of 3 months old solutions. a) and b) 10×10 μm, height scale: z= 10 nm. c) and d) close up: z = 2 nm.

Al:Si = 0.5/2

Al:Si = 2/0.5



a



c



b



d

Figure 4.3-8: Tapping mode AFM images of 4 months old solutions. a) and b) $10 \times 10 \mu\text{m}$, height scale: $z = 10 \text{ nm}$. c) and d) close up: $z = 2 \text{ nm}$.

4.3.2. Analysis of the material by XPS

Two month old samples were filtered using a 0.05 μm pore size polycarbonate (PC) membrane. [Al] in solution was measured by GFAAS before and after filtration. The material collected by filtration was dried and then analysed by XPS and was referred to as PC film. For the sake of comparison, powder samples previously collected (Doucet et al. 2001b) were also analysed by XPS. The composition of these samples has been identified as HAS_A and HAS_B respectively using ²⁹Si and ²⁷Al solid-state NMR. They had the same initial Al:Si ratio in solution as the samples prepared for this study and they were referred to as powders. The elemental analysis of the samples is presented in Table 4.3-2.

Table 4.3-2: Elemental composition of the samples determined by XPS. The results are expressed in atomic %. N = 3 (relative S.D). * %O expressed in this table is corrected by the %O present in the PC film.

Description	%Na	%N	%K	%C	%Si	%Al	%O*	Si/Al	(Si+Al)/O
Al:Si = 0.5/2 on PC film	0.81 (0.00)	2.44 (0.03)	3.21 (0.07)	47.86 (2.75)	5.56 (0.05)	5.35 (0.05)	25.50 (0.73)	1.04 (0.02)	0.43 (0.01)
Al:Si = 0.5/2 powder	0.32 (0.00)	1.71 (0.02)	n.d.	8.69 (0.31)	14.41 (0.18)	14.73 (0.24)	60.14 (1.78)	0.98 (0.06)	0.48 (0.01)
Al:Si = 2/0.5 on PC film	0.00 (0.00)	3.14 (0.02)	0.00 (0.00)	61.87 (5.18)	1.59 (0.01)	6.02 (0.11)	15.63 (1.10)	0.26 (0.01)	0.49 (0.04)
Al:Si = 2/0.5 powder	0.00 (0.00)	2.31 (0.03)	1.15 (0.02)	25.78 (0.35)	5.18 (0.04)	13.46 (0.17)	52.12 (1.13)	0.39 (0.05)	0.36 (0.01)
Al:Si = 2/0 on PC film	0.00 (0.00)	3.34 (0.02)	0.56 (0.00)	16.13 (0.15)	0.00 (0.00)	17.67 (0.05)	59.24 (1.10)	0.00 (0.00)	0.30 (0.01)

C was a highly detected element in these samples. Its presence could be explained in all samples as CO₂. However the higher amount of C present in the elemental analysis of samples collected on PC film was due to the PC film itself. The deposit on the membrane was thin and non-homogeneous and the PC film was consequently exposed to the X-ray. Consequently, a part of the O detected was due to the PC film and not to the sample itself. The percentage of O shown in this table has been corrected in order to represent only the O present in the sample. It has been calculated as the difference between the total %O detected and the %O linked to C in the PC film (known from the elemental analysis of a blank PC film). This was only applied for the samples collected on PC film but not on the powders. For Al:Si = 0.5/2, the Si/Al ratio in the material was around 1 (1.04 for PC film and 0.98 for powder). This indicated that, in samples where Si(OH)₄ was in excess in the parent solution, HAS contained as much Al as Si. This was in agreement with the description of HAS_B. For a parent solution with a ratio Al:Si = 2/0.5, the Si/Al ratio in the material collected was of 0.29 and 0.39 in PC film and powder respectively. There was more Al than Si in the material. HAS_A was expected to form for this initial conditions and it has been described with a ratio Si/Al below 0.5.

The elemental composition of Al:Si = 2/0 suggested that Al(OH)₃ was formed and precipitated with a Al/O ratio of 0.3. The (Si+Al)/O ratio in the other samples increased to (i) 0.49 and 0.36 for Al:Si = 2/0.5 and (ii) 0.43 for Al:Si = 0.5/2. This indicated that there was less O present in HAS than in Al(OH)₃. This supported the idea of the substitution of OH group in Al(OH)₃ templates by Si(OH)₄ in the formation of HAS. The difference between samples collected on PC film and powders could be explained by the non-correction of the %O in powder samples.

Figure 4.3-9 presents the survey spectrum obtained for Al:Si = 0.5/2 collected on a PC film. Figures 4.3-10 and 4.3-11 show the Si 2p and Al 2p spectra for Al:Si = 0.5/2 residue on PC film and powder respectively. Figures 4.3-12 and 4.3-13 show the Si 2p and Al 2p spectra for Al:Si = 2/0.5 residue on PC film and powder respectively. A summary of the binding energies is shown in Table 4.3-3.

Survey

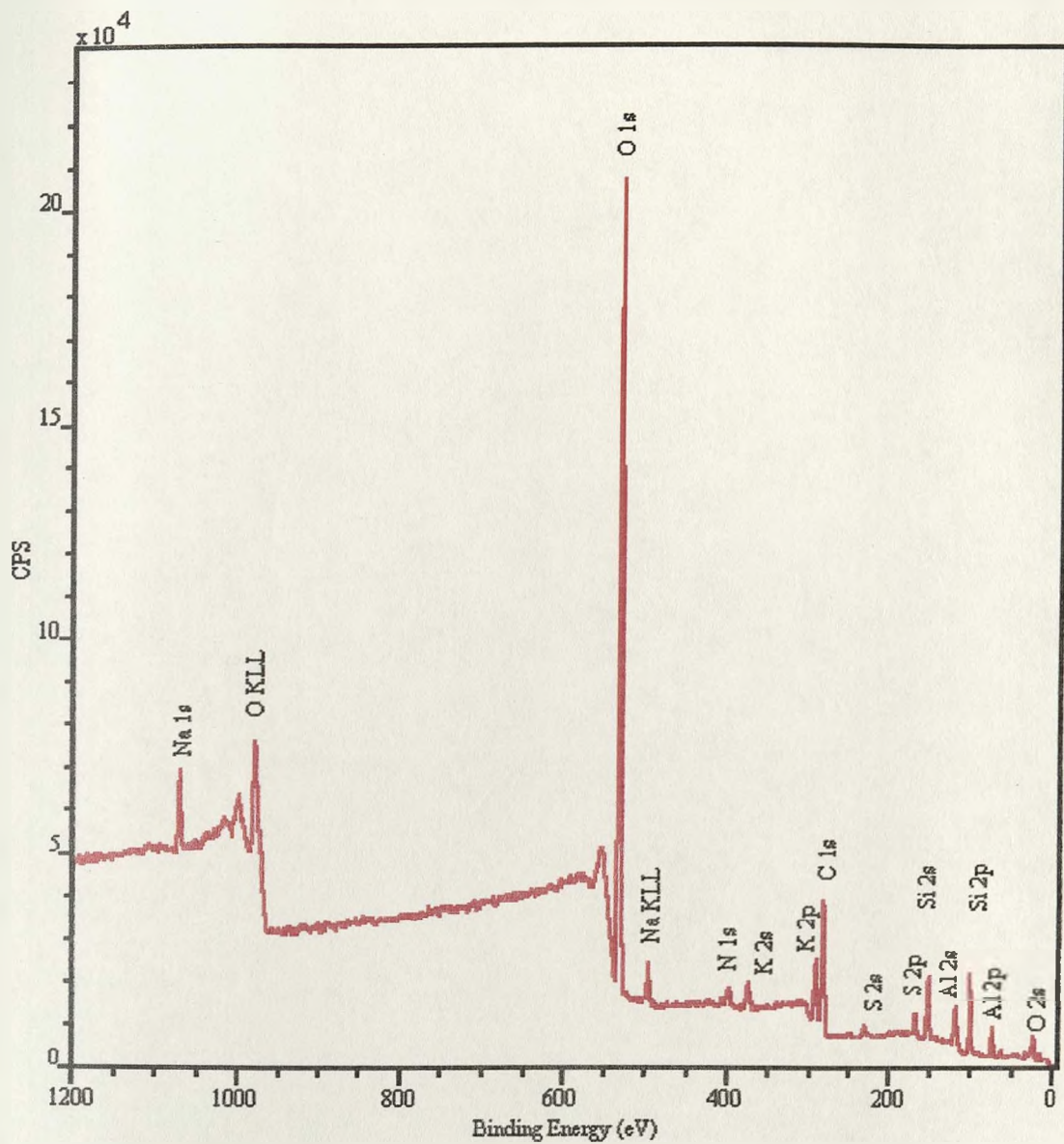
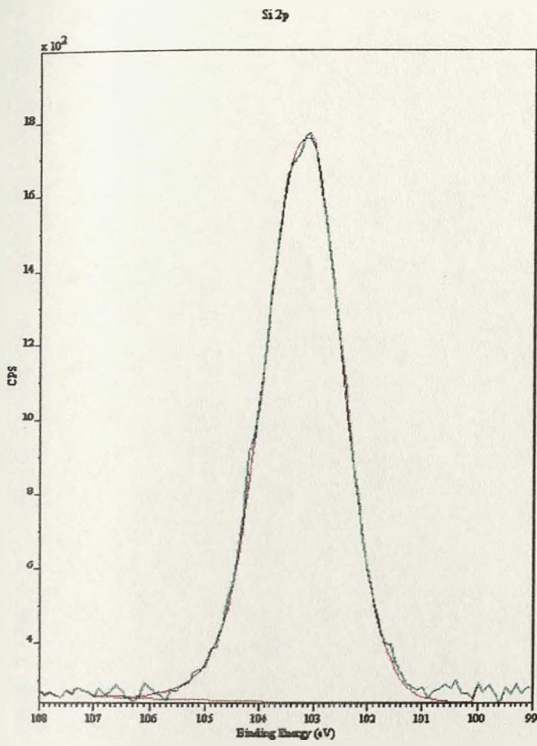
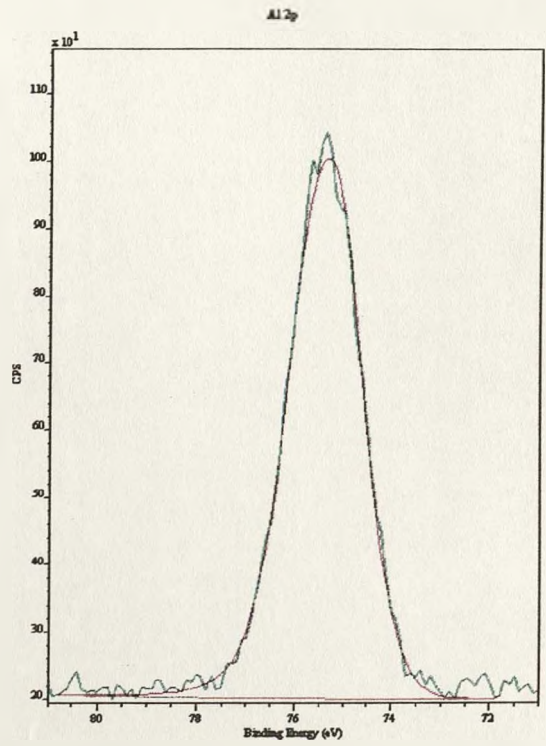


Figure 4.3-9: Survey spectra for Al:Si = 0.5/2 on PC film.

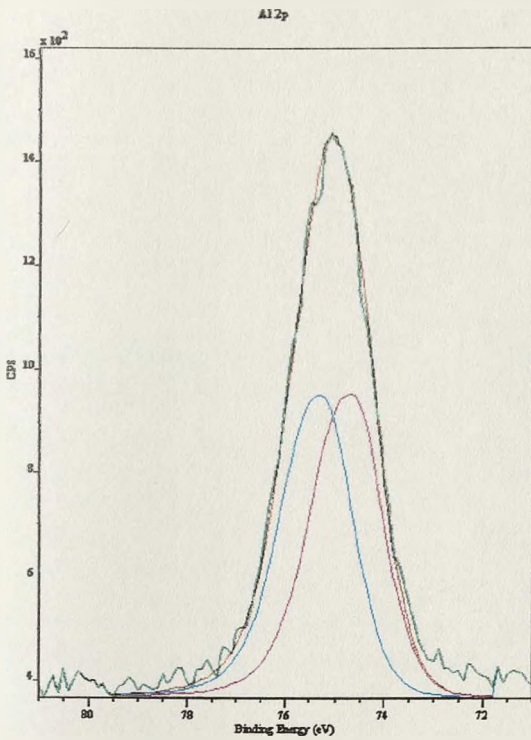
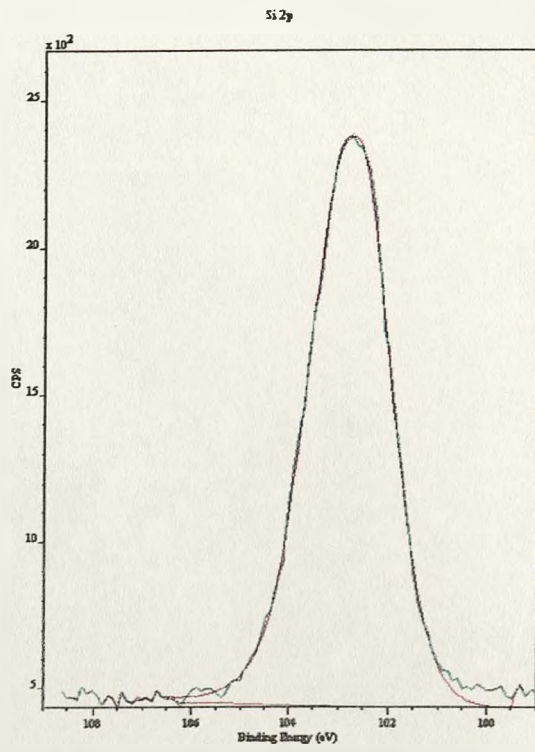


a)

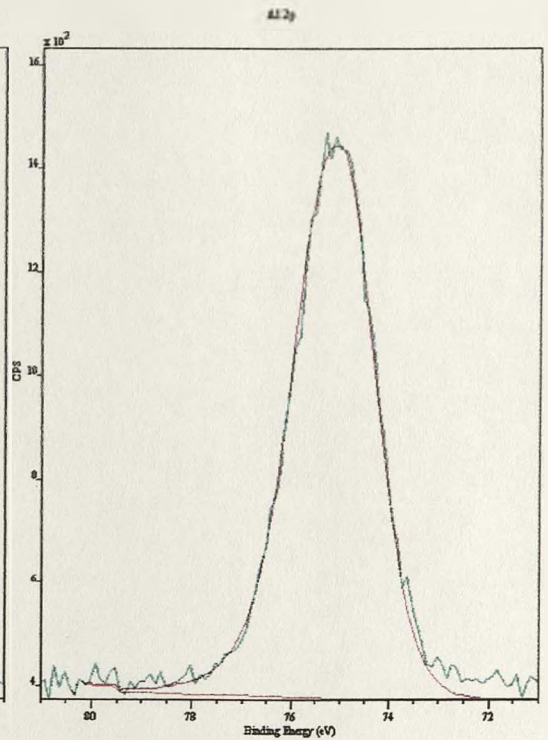


b)

Figure 4.3-10: a) Si 2p and b) Al 2p curve-fitted spectra for Al:Si = 0.5/2 on PC film.



b)



c)

Figure 4.3-11: a) Si 2p and b) Al 2p (two Al environment) c) Al 2p (one Al environment) curve-fitted spectra for Al:Si = 0.5/2 powder.

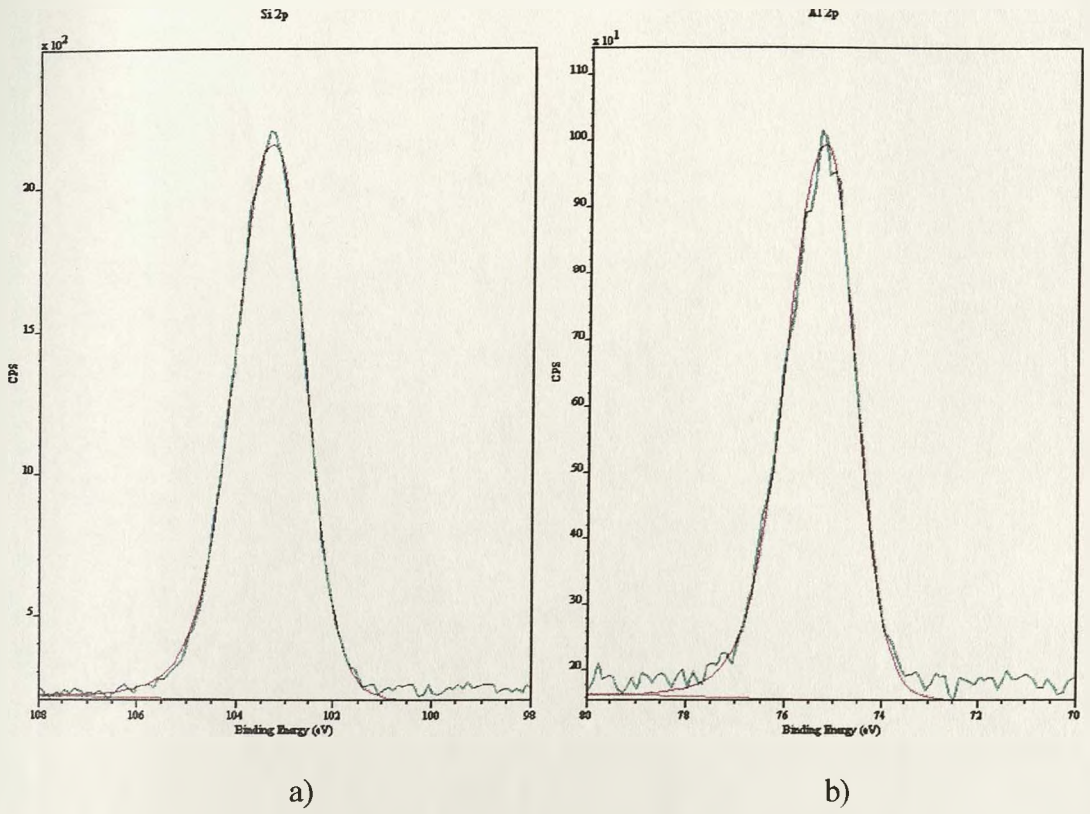


Figure 4.3-12: a) Si 2p and b) Al 2p curve-fitted spectra for Al:Si = 2/0.5 on PC film.

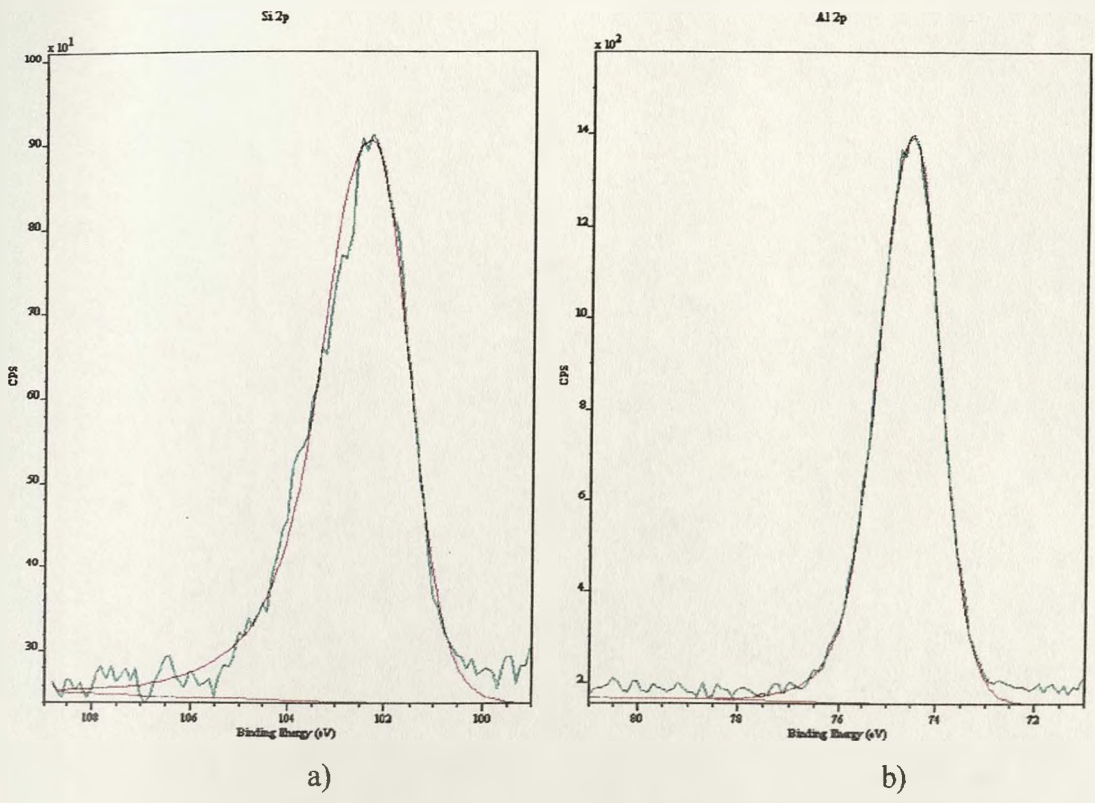


Figure 4.3-13: a) Si 2p and b) Al 2p curve-fitted spectra for Al:Si = 2/0.5 powder.

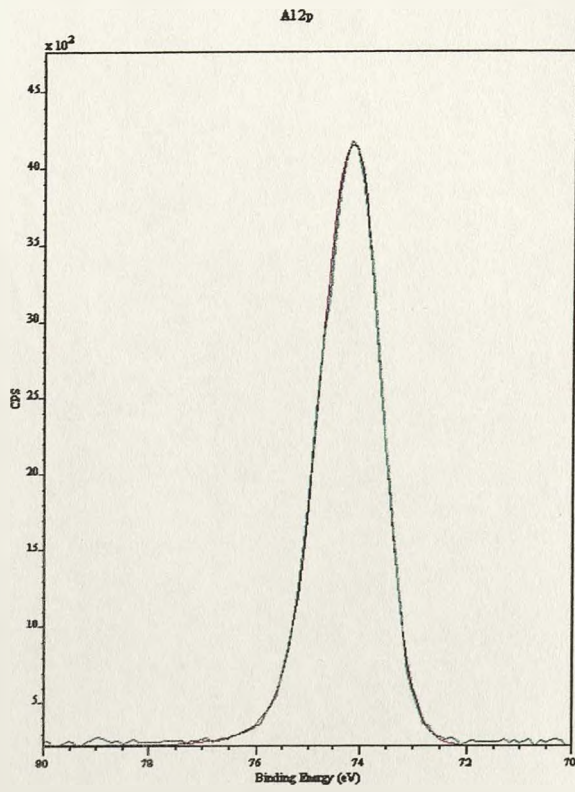


Figure 4.3-14: Al 2p curve-fitted spectra for Al:Si = 2/0 on PC film.

Table 4.3-3: Binding energies and full width at half maximum found by XPS. The NMR results are from (Doucet et al. 2001b). (1) results based on one Al environment curve-fitting. (2) results based on two Al environment curve-fitting.

Description	Si 2p		Al 2p		NMR		Proposed structure
	BE (eV)	fwhm	BE (eV)	fwhm	% Al tetra	% Al octa	
Al:Si = 2/0 on PC film	N/A	N/A	74.13	1.22	N/A	N/A	
Al:Si = 0.5/2 on PC film	103.1	1.55	75.3	1.5	N/A	N/A	
Al:Si = 0.5/2 powder ⁽¹⁾	102.7	1.72	75	1.75	47.1	52.9	HAS _B +
Al:Si = 0.5/2 powder ⁽²⁾	102.7	1.72	74.6 / 75.3	1.5	47.1	52.9	HAS _A
Al:Si = 2/0.5 on PC film	103.2	1.53	75.2	1.5	N/A	N/A	
Al:Si = 2/0.5 powder	103.2	1.75	74.5	1.35	2.9	97.1	HAS _A

Aluminium

The Al 2p binding energy found for Al:Si = 2/0 was similar to the value referenced for Al(OH)₃ (Barr et al. 1997; Briggs and Seah) and was therefore associated to octahedral Al. When Al:Si = 2/0.5, the Al 2p binding energy increased slightly to 74.5 for the powder material and 75.2 for the material on PC film. This was still in the range of octahedral Al and this was confirmed by the NMR results which presented 97% of octahedral Al in the powder. The fwhm was the same for the two samples but was broader than the one observed for Al(OH)₃. The increase of fwhm indicated a interaction between Al and Si. The results by XPS confirmed the formation of HAS_A. For Al:Si = 0.5/2 on PC film the binding energy increased to 75.3, with a broad peak (fwhm = 1.5). The results for the powder of equivalent Al:Si ratio could be obtained in two way: (i) the peak could be analysed as one broad peak with a binding energy of 75 eV and fwhm = 1.75 or (ii) it could be decomposed as the fitting of two curves of binding energies 74.6 eV and 75.3 eV, each curve representing 50% of the total experimental envelope. The use of a two curves fitting introduced the presence of two Al environments – tetrahedral Al and octahedral Al - as

shown by the NMR experiments. As the binding energies of octahedral Al are always higher than those of tetrahedral Al (Barr et al. 1997), I could easily associate tetrahedral Al to 74.6 eV and octahedral Al to 75.3 eV. This was in full accord with the description of HAS_B.

A shift was observed in the binding energy of Al 2p for octahedral Al depending of the presence of Si. Figure 4.3-15 shows the influence of Si on both the binding energy and the fwhm of Al 2p. The more Si was present in the material, the higher the binding energy and the broader the peak.

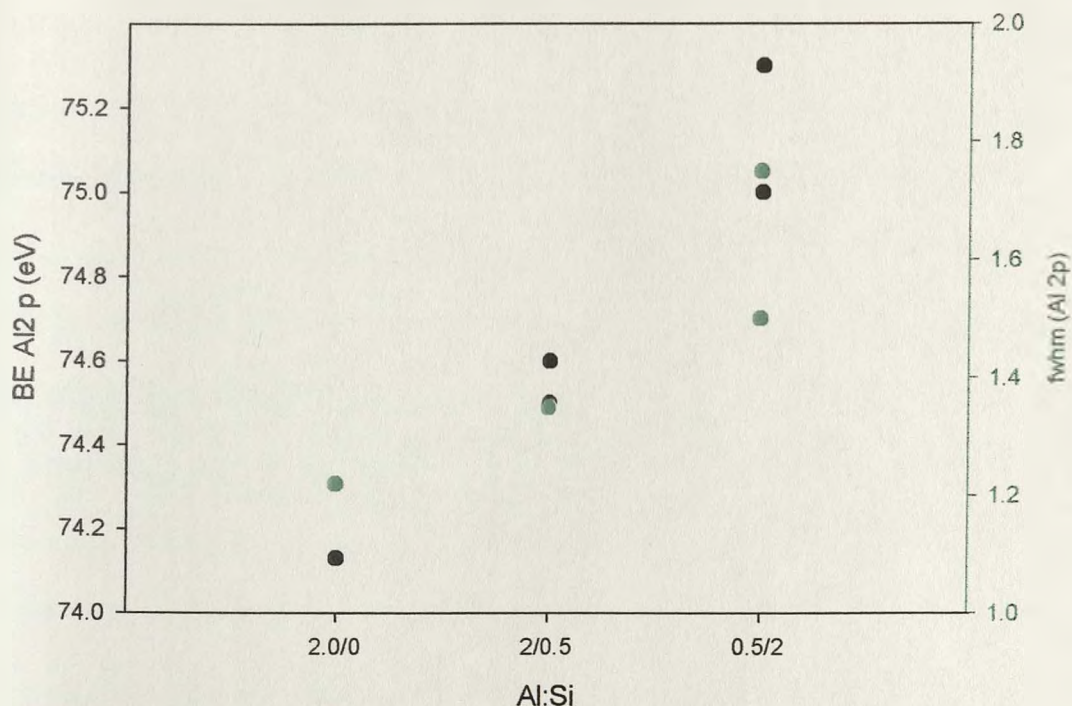


Figure 4.3-15: Influence of the presence of Si on the binding energy and fwhm of Al 2p.

Silicon

The Si 2p binding energies were not much affected by the nature of the samples. The biggest difference can be observed between Al:Si = 0.5/2 on PC film at 103.1 eV and the powder at 102.7 eV. The overall value of Si 2p was ca. 103 eV, in the range of SiO₂ (Briggs and Seah). However, a noticeable difference can be observed in the fwhm values obtained for PC film and those obtained for powders with broader peaks for the powder samples indicating the nature of the samples.

Discussion

The change in the peak position relates to the change of the chemical state of the atom (Klinowski and Barr 1999). More specifically, an increase in the binding energy of a metal M results from a more ionic M-O bond (Barr et al. 1994). In this study, the binding energy of Al 2p increased with the amount of Si present in the sample as well as the fwhm. The increase observed in the value of the fwhm shows the interaction between Al and Si. Several studies also described the increase of the binding energy with the Si content as the result of the increased population of Si-O units forcing the Al-O bond to be more ionic (Barr 1983; Barr 1990; Barr 1995; Barr et al. 1995; Barr et al. 1997). This phenomenon can be observed on both tetrahedral and octahedral Al but some problems can arise for low Al:Si ratio when the binding energy of tetrahedral Al is shifted over 74 eV (Barr and Lishka 1986). The high values obtained for Si 2p in all samples can be explained by a lower degree of Si polymerisation, implying the presence of more Al-O-Si and less Si-O-Si bonds (Childs et al. 1997) in the structure. For the sake of comparison, Table 4.3-4 presents the binding energies of other aluminosilicate compounds. Whilst HAS_A presents the same characteristics as kaolinite, HAS_B is much more difficult to interpret. The similarities between HAS_B and albite for both Si 2p and the tetrahedral Al 2p give a idea of

the nature of the Si-O and ^(iv)Al-O bonds, i.e. the ^(vi)Al-O bonds become even more ionic. The decrease of the value of Si 2p binding energy between HAS_A and HAS_B can be interpreted as a more covalent Si-O bond.

Table 4.3-4: Binding energies of HAS_A and HAS_B together with other aluminosilicates values. * value from Barr *et al.* (1997), ** values from Seyama and Soma (1988), * values from He *et al* (1995), **** value from Childs *et al* (1997)**

Sample	Si 2p (eV)	Al 2p (eV)	
		Octahedral	Tetrahedral
HAS _A	103.2	74.5	
HAS _B	102.7	75.3	74.6
Al(OH) ₃ (gibbsite) *	-	74.1	
Kaolinite **	103.0	74.7	
Allophane ***	102.3	74.3	
Silica springs allophane ****	102.6	75.0	
Albite**	102.8		74.6

4.4. Conclusion

Tapping-mode AFM in solution gave the opportunity to observe the shape and growth of HAS in situ. Particles were formed just after one day in a parent solution of Al:Si = 2/0.5, a phenomenon which was not observed for Al:Si = 0.5/2. This suggested that the formation of HAS_A was quicker than that of HAS_B. However, particles were observed in both solutions after a week, emphasising the rapidity at which the reaction occurred under the present experimental conditions. The shape of the particles was found to be mostly discoid for solutions of ratio Al:Si = 2/0.5 and rectangular for solutions with Al:Si = 0.5/2, a very surprising result as the exact opposite has been described in the previous study made by

Doucet. The discoid particle was generally of smaller dimension than the rectangular particle and discoids were found to merge in order to form a rectangle. This observation tends to support the hypothesis of HAS_A being the precursor in the formation of HAS_B. The particles aggregated then to a greater system, the growth being essentially plan-orientated. A smooth layer was then formed, on the top of which new particles precipitated. At a larger scale, HAS_A and HAS_B should therefore have a layered morphology. A general scheme of the growth of the HAS particles is presented in Figure 4.4-1.

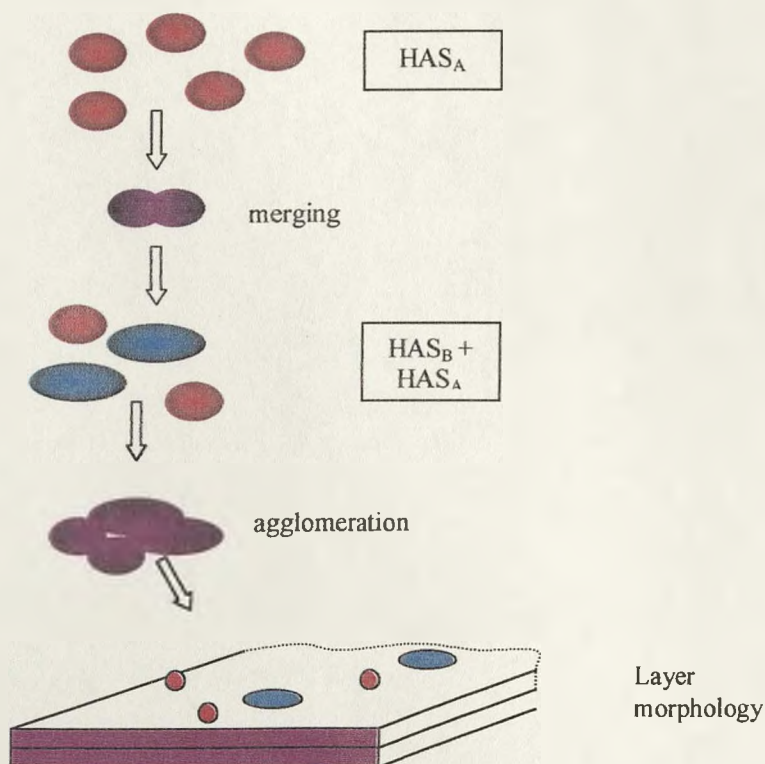


Figure 4.4-1: Schematic representation of the growth of HAS particles.

Although AFM enabled the direct visualisation of HAS particles in solution, the technique proved to be relatively deceptive as the phenomenon of surface deposition took over the phenomenon of particles aggregation. Thus, the results obtained were difficult to analyse

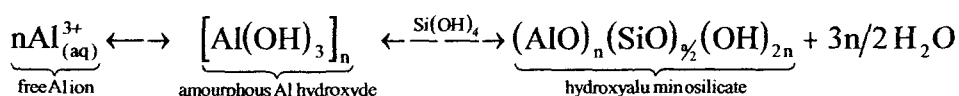
and the difference of shape observed between the two sets of samples relied on the analyst's subjectivity.

The XPS technique proved to be a reliable and useful instrument for the characterisation of the structure of the different HAS. Not only the different environments of Al were discriminated as octahedral and tetrahedral, in accordance with the previous NMR studies, but it also gave access to the chemical nature of the bonds. The results showed that the ionicity of the Al-O bond increased in the presence of Si whereas the Si-O bond became more covalent. The high binding energy for Si 2p suggests that there was little Si polymerisation, i.e. few Si-O-Si bonds. On the downside, XPS didn't give as much information on Si environment as ^{29}Si NMR, as it was impossible to distinguish the different Si(nAl). The elemental analysis also confirmed that the Al:Si ratios in the material were of 1 for HAS_B and below 0.5 for HAS_A. It also showed that the Al+Si/O ratio increased with the Si amount, implying the substitution of OH groups by Si(OH)₄ in the structure.

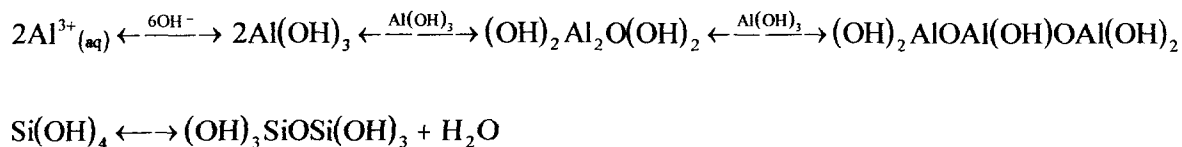
Chapter 5 : The study of hydroxyaluminosilicates (HAS) formation using morin-based fluorimetry

5.1. Introduction

The major aim of my research was to understand both the quantitative and kinetic aspects of the formation of HAS. This implied the definition of the optimal parameters under which the reaction would occur such as pH, [Al], [Si(OH)₄]. Many studies, which had been carried out previously to identify the formation of HAS, led to some useful information concerning the reaction conditions. An excess of Si(OH)₄ and pH = 5 reduced the acute toxicity of Al in fish through the formation of HAS (Birchall et al. 1989). The minimum concentrations of species required in solution for HAS to be stable as identified by microfiltration were shown to be as little as [Si(OH)₄] = 100 μmol.dm⁻³ (Exley et al. 1991) and [Al] < 10 μmol.dm⁻³ (Exley and Birchall 1992b; Exley and Birchall 1993). HAS precipitation was observed in the pH range 5.5 to 7.5 with a maximum effect at 6 (Exley and Birchall 1992b), i.e. when the degree of hydrolysis of Al increased (Luciuk and Huang 1974). It was also shown that the presence of Si(OH)₄ reduced the number of hydroxyl bridges per Al, suggesting that a condensation reaction occurred between Si(OH)₄ and hydroxy-Al ions (Luciuk and Huang 1974). These are strong evidences of the importance of the form of Al involved in the reaction. A mechanism describing this reaction has been proposed as a condensation reaction (Exley et al. 1997):

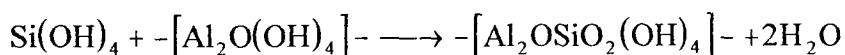


This theory implied the formation of $\text{Al}(\text{OH})_3$ as a prerequisite to the formation of HAS, emphasising the importance of pH and $[\text{Al}]$. It also stressed the possibility for $\text{Si}(\text{OH})_4$ to react in competition with both aluminium hydroxide and itself:

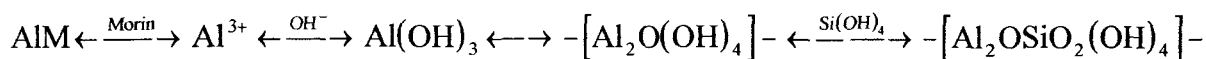


This suggested that three simultaneous competitive condensation reactions needed to be considered in solution.

In order to prevent silicic acid auto-condensation, it was necessary to work with $[\text{Si}(\text{OH})_4] \leq 2 \text{ mmol.dm}^{-3}$. $\text{Si}(\text{OH})_4$ reacted with Al at $\text{pH} > 4$, the pH under which the auto-condensation of $\text{Al}(\text{OH})_3$ will occur to form polymers and aggregates. It has been shown that the simplest form of condensation product, a dimeric unit, will condense with $\text{Si}(\text{OH})_4$ to form HAS with Si:Al stoichiometry ratio above 0.5:



In this study, I used the fluorescent agent morin to make indirect measurements of HAS formation. More precisely, I looked at the effect of $\text{Si}(\text{OH})_4$ on the formation of the Al-morin complex (AIM). Morin reacts with the portion of Al which remains available after the distribution of Al species in solution, i.e. Al^{3+} , $\text{Al}(\text{OH})^{2+}$, $\text{Al}(\text{OH})_2^+$, $\text{Al}(\text{OH})_3$ and $\text{Al}(\text{OH})_4^-$. When $\text{Si}(\text{OH})_4$ is present in solution, a competitive reaction occurs with the formation of HAS. This can be described as following:



In the Al/Morin system, the intensity measured by fluorimetry (If) is directly proportional to [AlM]. When Si(OH)₄ is present in solution, this should affect the [Al] available to morin and therefore If should reflect this effect. The influence of species concentrations and pH on the different equilibria were studied and the reaction of formation of HAS followed by fluorimetry.

The first section of this chapter is dedicated to the establishment of a reliable experimental protocol. It emphasises the problems encountered due to external problems such as solution pH, concentrations of each species and sample stabilisation and shows the experimental steps that were followed towards gaining a better understanding of the chemistry involved in the different systems Al/Morin and Al/Si(OH)₄/Morin.

The second part shows the affect of Si(OH)₄ on the formation of AlM. The results obtained lead to the determination of the parameters influencing the formation of HAS and to the indirect observation of the kinetics of the reaction.

5.2. The establishment of a reliable protocol: evolution of the different experimental protocols

5.2.1. Experimental

•Instrumentation

Fluorimetry

The fluorimeter used was a Perkin Elmer luminescence spectrometer LS50B. Two different methods were used:

- Time-Drive (TD): the change in AIM fluorescence was recorded over time using the time-drive application. The evolution of the intensity was followed during time for a fixed emission wavelength (500 nm) and a fixed excitation wavelength (420 nm). This method gave information on the change of fluorescence over time and therefore the kinetics of the formation of AIM. The experiments were recorded for 900 s.
- Scans: the scan application enabled fluorescence measurements to be made using an emission spectrum (from 475 nm to 535 nm) and a fixed excitation wavelength (420 nm). A background of the fluorescence of morin only was subtracted.

All experiments were conducted under a constant temperature of 20°C. A quartz cell (path length = 1 cm) was used.

pH-metry

pH was measured using a pH-meter HannaH Instruments (HI 931402 Microprocessor pH meter).

When mentioned, pH was recorded in situ by a microprocessor pH-meter (Hanna Instruments). Thus, pH was followed in the same experimental conditions (stirring, temperature) as fluorimetry occurs.

UV-Visible

UV-visible spectrometry was used to check any formation of aluminium aggregate with increasing pH. The spectrum was recorded with a Perkin Elmer UV-Vis Spectrometer Lambda 14 between 900 nm and 250 nm.

GFAAS

The concentration of total Al was determined by GFAAS with a Perkin Elmer atomic absorption spectrometer 3300 under argon furnace (HGA 600) atmosphere, using an auto-sampler (AS40). The wavelength used was 309.3 nm. The pre-treatment temperature was 1450°C and the atomisation temperature was 2650°C. The volume of injection was 30 µL. The blank correction was done with 1% HNO₃. 10 ppm Al in 1% HNO₃ was used to prepare the highest standard by hand. Lower calibration standards were prepared by the AS40 using 1% HNO₃ as the diluent. When mentioned, the blank correction and the calibration standard were prepared using a matrix-matched solution of the known [Si(OH)₄] for the reasons explained in Chapter 2.2.

•Stock solutions

Preparation of Si(OH)₄ solution

Si(OH)₄ was prepared by cation exchange of sodium orthosilicate Na₄SiO₄ (Alfa) using the Na⁺ form of a sulphonated cation exchange resin (Amberlite 200). The resin was washed with ultra pure water (conductivity below 0.5 µS.cm⁻¹) and HNO₃ (1% v/v) for 15 minutes to be converted from Na⁺ to H⁺. Then it was rinsed 3 times with ultra pure water, filtered and dried before being added to a 2 mmol.dm⁻³ Na₄SiO₄ solution. Na⁺ in Na₄SiO₄ solution were removed by cation exchange to form 2 mmol.dm⁻³ Si(OH)₄. The reaction was followed by pH: the pH will drop from 12 to 4 as a result of the completion of the cation exchange. When mentioned, the solution was diluted using ultra pure water.

Preparation of Morin solution

Morin (Sigma, MW = 302.2g.mol⁻¹) was dissolved in ultra-pure water under boiling for 5 minutes. The solution was cooled at room temperature and the volume was adjusted to 250 mL. Morin was prepared before each experiment and was used fresh. The pH was adjusted by adding 0.1 mol.dm⁻³ NaOH or 1.4 mol.dm⁻³ HNO₃. When mentioned, the solution was diluted using ultra pure water.

Preparation of Al solution

There were two modes of preparing Al stock solutions.

- Mode A used aluminium nitrate Al(NO₃)₃.9H₂O (AnalaR, MW = 375.13 g.mol⁻¹) dissolved in ultra pure water. pH was adjusted to below 2.5 by adding HNO₃ in order to avoid aluminium complex formation.
- Mode B used an Al standard solution (Perkin Elmer Pure, 1000 µg.mL⁻¹, 2% HNO₃) **diluted** to a suitable concentration using 2% HNO₃ in ultra pure water.

•Protocols

All samples were prepared in a medium of 0.1 mol.dm⁻³ KNO₃ (AnalaR, MW = 101.1 g.mol⁻¹) in order to maintain the ionic strength of the solution constant when other electrolytes are added. All materials were pre-washed in an acid bath and rinsed several times with ultra pure water. Table 5.2-1 summarises the techniques applied for each protocol. The concentration and type of stock solutions used are shown in Table 5.2-2. The samples' concentrations and pH are displayed in Table 5.2-3.

Table 5.2-1: Techniques used for each protocol.

Protocol	Fluorimetry	pH-metry	UV-visible	GFAAS
2	TD / 900 s	In situ		
4	TD / 900 s	Before and after experiment	Yes	Not matrix-matched
6	TD / 900s Scans / N=10	Measured for 7 days		Matrix-matched calibration
10-11	Scans	measured during preparation of samples		

Table 5.2-2: Concentration of stock solutions

Protocol	[Si(OH) ₄] mmol.dm ⁻³	[Mor] mmol.dm ⁻³	[Al] mode A mmol.dm ⁻³	[Al] mode B mmol.dm ⁻³
2	2	0.10	500	
4	2	0.10		37
6	2	0.01		37
10-11	2	0.01, 0.02, 0.03, 0.04, 0.05, 0.06, 0.07, 0.08, 0.09, 0.10, 0.11, 0.12, 0.125		0.25, 0.5, 1, 2, 3

Table 5.2-3: Concentrations of species and pH of samples.

Protocol	[KNO ₃] mol.dm ⁻³	[Si(OH) ₄] μmol.dm ⁻³	[Morin] μmol.dm ⁻³	[Al] μmol.dm ⁻³	pH
2	0.1	0 & 2000	1	1	3, 4, 5, 6, 7
4	0.1	0 & 2000	1	1	3, 4, 4.5, 5, 5.5, 6, 7
6	0.1	0 & 2000	0.1	1, 5, 10, 50	4, 4.5, 5, 5.5
10 + Buffer	0.1	0 & 2000	1, 2, 3, 4, 5, 6, 7, 8, 9, 10, 11, 12, 12.5	0.5, 1, 2, 4, 6	6.5
11 + Buffer	0.1	0 & 2000	1, 2, 3, 4, 5, 6, 7, 8, 9, 10, 11, 12, 12.5	0.5, 1, 2, 4, 6	6

The modus operandi of the protocols are described as follows.

Protocol 2

- pH was adjusted in KNO₃/Si(OH)₄ stock solutions by adding 0.1 mol.dm⁻³ NaOH or 1.4 mol.dm⁻³ HNO₃.
- 3.5 mL of the stock solution was put into a fluorimetry cell.
- 35 μL morin stock solution was added into the cell.
- The cell was placed into the fluorimeter and the TD measurement was started. The solution was continually stirred during the measurement of fluorescence.
- After 100 s, 7 μL of Al stock solution was added with a micro-pipette in situ. The event was marked on the continuous measurement.

Protocol 4

- 6.75 μL of Al stock solution was added to 250 mL KNO_3 / Si(OH)_4 stock solutions.
- After pH stabilisation, pH was adjusted by adding 0.1 $\text{mol}\cdot\text{dm}^{-3}$ NaOH or 1.4 $\text{mol}\cdot\text{dm}^{-3}$ HNO_3 .
- 3.5 mL of this solution was studied by UV-Visible absorbance and compared to the reference, i.e. Al stock solution.
- 3.5 mL of this same solution was put into a fluorimetry cell, previously rinsed with detergent and ultra pure water to be sure that all Al was desorbed.
- TD measurement was started.
- After few seconds, 35 mL morin stock solution was added to the cell. Solution was stirred during all the experiment. The event was marked.

Protocol 6

Teflon bottles were used for all the steps of this protocol to reduce any phenomena of surface adsorption.

- A pre-determined volume of Al stock solution was added to 250 mL of KNO_3 +/- Si(OH)_4 stock solution with a pH below 3 to obtain the required [Al] in solution.
- The solution was stirred until pH stabilised.
- The pH was then adjusted with 0.1 $\text{mol}\cdot\text{dm}^{-3}$ NaOH or 1.4 $\text{mol}\cdot\text{dm}^{-3}$ HNO_3 .
- For each pH, 50 mL of the solution was stored in a 60 mL Teflon bottle.

The same operation was repeated for each [Al]. A total of 32 samples were prepared with the nomenclature X_n found in Table 5.2-4. For example A_1 : $[\text{Si(OH)}_4] = 0$, $[\text{Al}] = 1 \mu\text{mol}\cdot\text{dm}^{-3}$, pH = 4 and A_3 : $[\text{Si(OH)}_4] = 0$, $[\text{Al}] = 1 \mu\text{mol}\cdot\text{dm}^{-3}$, pH = 5.

Table 5.2-4: Nomenclature of Protocol 6 samples.

X	A	B	C	D	E	F	G	H
[Si(OH) ₄] μmol.dm ⁻³	0	0	0	0	2000	2000	2000	2000
[Al] μmol.dm ⁻³	1	5	10	50	1	5	10	50
n	1	2	3	4				
pH	4	4.5	5	5.5				

The pH was recorded over 7 days, until it had completely stabilised (± 0.05). After 7 days, a pre-study was performed using TD experiments to determine the delay time (dt) after which the fluorescence intensity reached a plateau. I made the assumption that the reaction between morin and Al was complete when a plateau was observed. On the eighth day, morin was added to samples and the mixtures were allowed to stabilise for dt. To simplify the protocol, the same dt had to be applied for each of the samples, which in practice meant that the longest dt observed was used for all samples. The scans were then performed with a number of replicates (N=10). After the fluorimetry was achieved, the sample was acidified in the cell with HNO₃ to release all Al present in the cell. The total amount of Al was then determined by GFAAS, with matrix-matched calibration.

Protocols 10 & 11

A buffer was used in these protocols to maintain the pH absolutely constant throughout the preparation and the running of the experiments. PIPES (1,4-piperazinebis-(ethanesulfonic acid)) (Aldrich, MW=302.37 g.mol⁻¹) has been chosen for its non-interaction with any of the compounds in solution as well as for its pH-range.

- 250 mL of KNO_3 +/- $\text{Si}(\text{OH})_4$ was prepared with 50 mmol.dm^{-3} PIPES.
- pH was adjusted with NaOH pellets. The presence of the buffer enabled a very accurate pH (+/- 0.01).
- 13 bijou bottles were filled with 5 mL of the prepared solution.
- Every 2 mins, $10 \mu\text{L}$ of the required Al stock solution was added subsequently into each bottle.
- After 30 mins, $500 \mu\text{L}$ morin was added to the first bijou bottle. Morin was added to the subsequent samples at 2 mins intervals. $[\text{Mor}]_{\text{sample}} = 1; 2; 3; 4; 5; 6; 7; 8; 9; 10; 11; 12; 12.5 \mu\text{mol.dm}^{-3}$.
- The samples were then allowed to stabilise for 15 mins before scanning.

Each set of experiments was replicated 4 times.

5.2.2.Results

In **Protocol 2**, the change in AIM fluorescence was recorded over time using the TD application in presence or not of $\text{Si}(\text{OH})_4$. The evolution of I_f during time was followed for an excitation wavelength of 420 nm and an emission wavelength of 500 nm. The idea behind the use of such a technique was to obtain information on the change of fluorescence over time after the addition of Al into the cell. The basic concept was to observe in situ the kinetics of the formation of AIM and how $\text{Si}(\text{OH})_4$ might influence the reaction between Al and morin. Another aspect of the experiment was to follow the evolution of pH in situ in order to discuss its importance on the mechanism of formation. Figures 5.2-1 and 5.2-2 show the results obtained by fluorimetry and pH-metry for several replicates in presence or not of 2 mmol.dm^{-3} $\text{Si}(\text{OH})_4$. The first obvious remark about the fluorimetric results was the lack of reproducibility, making impossible any comparison between samples with or without $\text{Si}(\text{OH})_4$. Yet, the analysis of pH indicated that the variations of fluorimetric results

were not due to pH variation. Indeed, even if pH decreased during experiment, this change was too small to induce the dramatic effect observed by fluorimetry. Moreover, it was striking to see the huge difference of intensity between pH 3 and 4. At pH 3, there was no influence of the addition of Al on the slope of the curve, but the intensity was very high. At this pH, morin was completely protonated and was not predicted to react with Al to form AlM. On the other hand, at pH 4 and above, the addition of Al into the cell was noticeable as the intensity and the slope of the curve suddenly varied from a very low, constant intensity to a high, quick reaction. It happened that Al tended to adsorb on the surface of the cell, emphasising the absolute necessity of a good cleaning process. It also occurred to me that the method of preparation of Al stock solution as well as the extremely small volume added into the cell (7 μ L) could lead to a lot of uncertainties which might explain the lack of replication in the results.

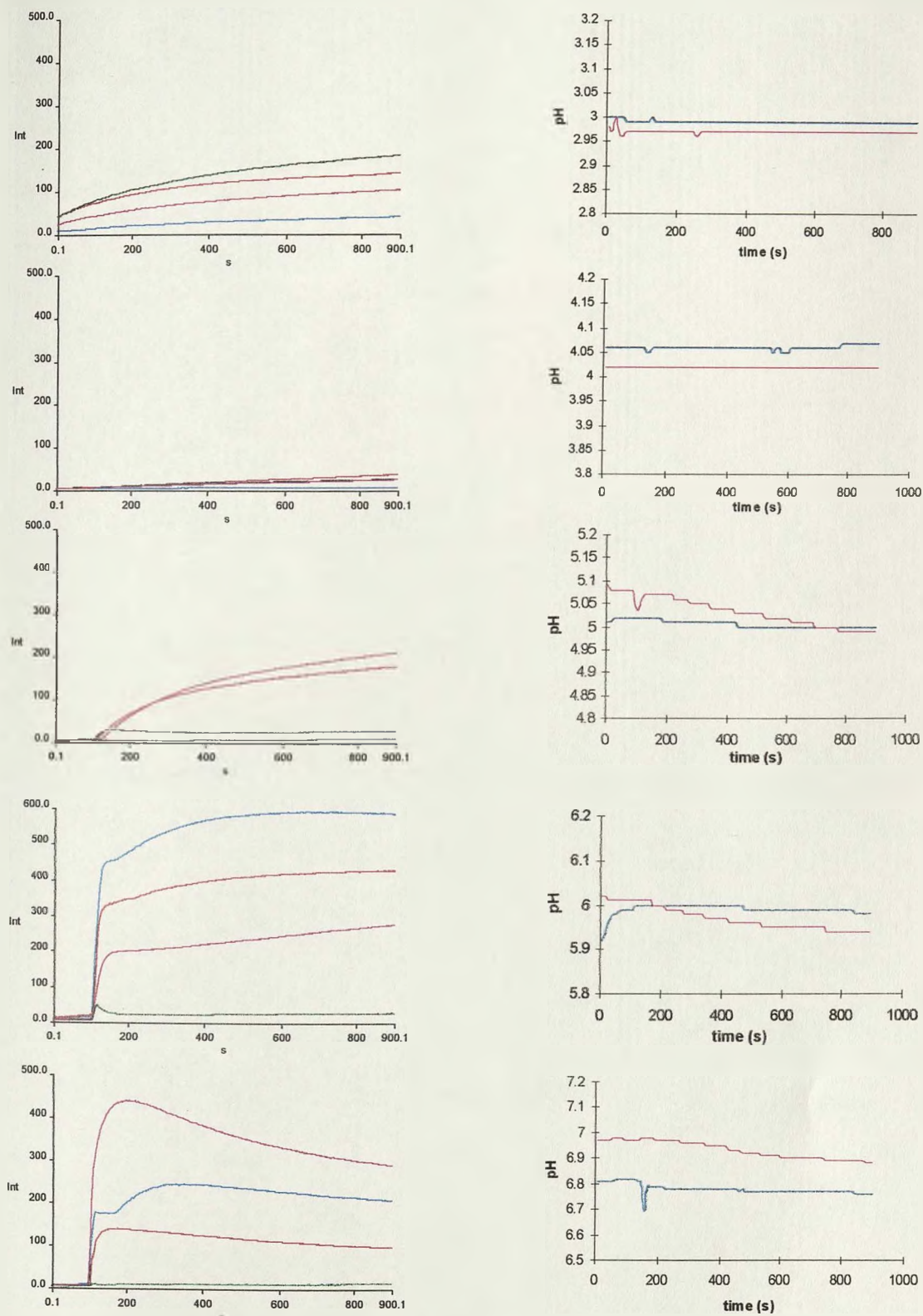


Figure 5.2-1: Fluorimetry time drive ($n = 4$) and pH ($n = 2$) versus time. $[\text{KNO}_3] = 0.1 \text{ mol.dm}^{-3}$,
 $[\text{Morin}] = 1 \text{ } \mu\text{mol.dm}^{-3}$, $[\text{Al}] = 1 \text{ } \mu\text{mol.dm}^{-3}$, $[\text{Si(OH)}_4] = 0 \text{ mmol.dm}^{-3}$.

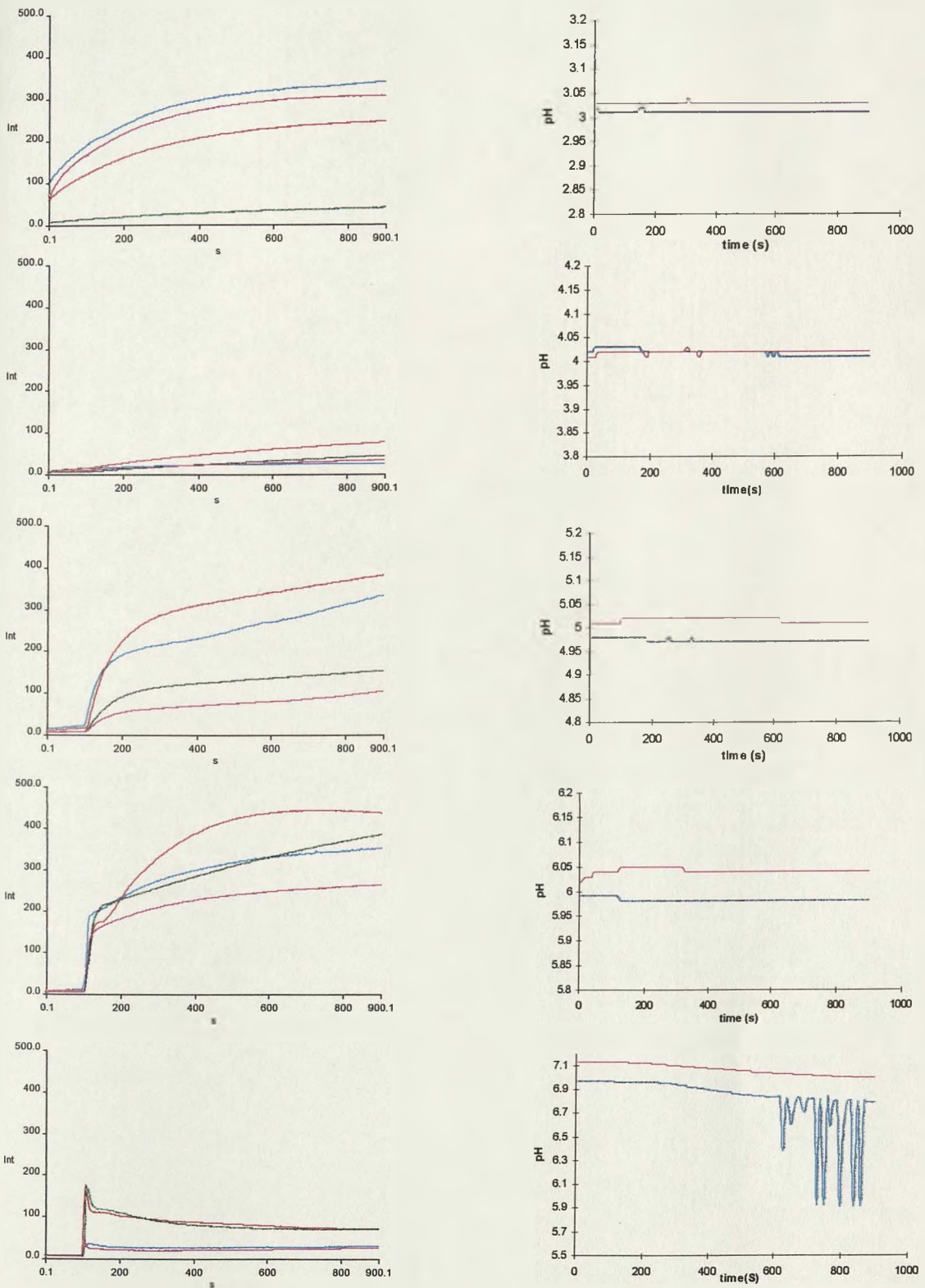


Figure 5.2-2: Fluorimetry time drive ($n=4$) and pH ($n=2$) versus time. $[\text{KNO}_3] = 0.1 \text{ mol.dm}^{-3}$, $[\text{Morin}] = 1 \text{ }\mu\text{mol.dm}^{-3}$, $[\text{Al}] = 1 \text{ }\mu\text{mol.dm}^{-3}$, $[\text{Si}(\text{OH})_4] = 2 \text{ mmol.dm}^{-3}$.

The problems relating to the preparation of the solutions were addressed in **Protocol 4** by using an Al standard solution. UV-visible spectrometry was used to check the formation of Al particulates with increasing pH and after dilution. The spectra were recorded between 900 nm and 250 nm and compared to the reference, i.e. the Al standard solution (pH = 0.4). Figure 5.2-3 presents the UV-visible spectra. A peak was observed at 318 nm, which corresponds to Al. No variation with pH was observed, only a smaller intensity due to dilution effects. Morin and Si(OH)_4 did not influence the absorbance spectra as expected in respect of the low concentrations in use. The other important change in this protocol was that morin was added to the cell containing Al only or Al + Si(OH)_4 . It was another way to look at the competitive reactions between Al + morin and Al + Si(OH)_4 . Figures 5.2-4 and 5.2-5 show the results obtained by fluorimetry for Al only and Al + $2 \text{ mmol}\cdot\text{dm}^{-3} \text{ Si(OH)}_4$ respectively at different pH. If, in general, curves had the same shape for a given pH, it was still impossible to get proper replicates in term of intensity. The variations in intensity as a function of pH were approximately the same in the presence of Si(OH)_4 or not, which may have been an indication of the great influence of pH on the reaction of formation of AlM. But comparison of the results in term of influence of Si(OH)_4 remained impossible. To complete the study, GFAAS experiments were performed on more concentrated Al samples. To enhance any difference in results, samples were prepared with $10 \text{ }\mu\text{mol}\cdot\text{dm}^{-3}$ Al. The effect of age was also checked by measuring the [Al] in solution aged for 24h, in order to control the stability of samples through time. If the results, presented in Table 2.2-3 (Chapter 2), indicated that the samples were quite stable with age (no significant change), they also revealed two substantial effects:

- an apparent loss of total Al, as measured by GFAAS, at certain pH values;
- an influence of Si(OH)_4 on the measurement of Al by GFAAS.

The last point was addressed as described in Chapter 2.2.2, where the importance of a matrix-matched calibration was stressed. It also appeared that a judicious choice of containers, such as Teflon bottles, should reduce the loss of Al by adsorption on the surface.

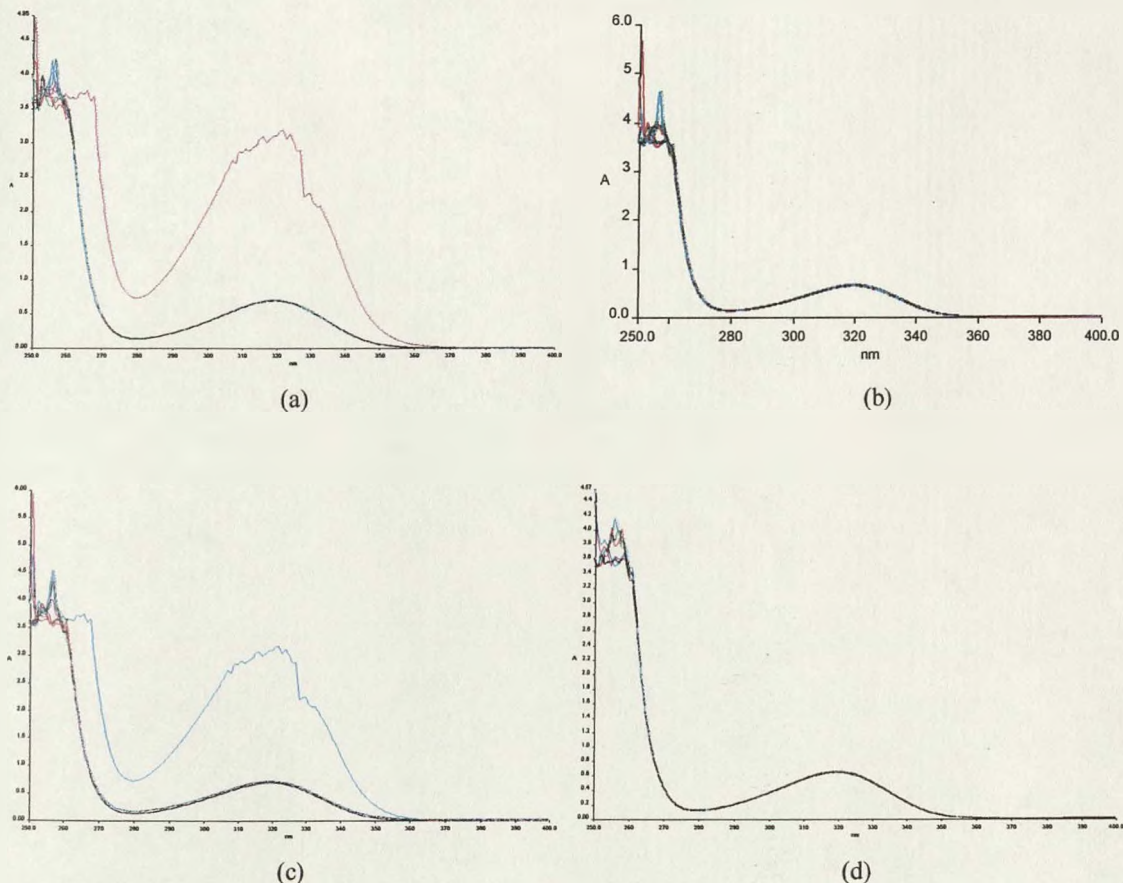


Figure 5.2-3: UV-Visible Absorbance. (a) Reference: $[Al]_{\text{stock solution}} = 37 \text{ mmol.dm}^{-3}$, pH 0.45. $[KNO_3] = 0.1 \text{ mol.dm}^{-3}$, $[Al] = 1 \text{ }\mu\text{mol.dm}^{-3}$. pH range: 3, 4, 4.5, 5, 5.5, 6, 7. (b) $[KNO_3] = 0.1 \text{ mol.dm}^{-3}$, $[Al] = 1 \text{ }\mu\text{mol.dm}^{-3}$ + $[morin] = 1 \text{ }\mu\text{mol.dm}^{-3}$. pH range: 3, 4, 4.5, 5, 5.5, 6, 7. (c) Reference: $[Al]_{\text{stock solution}} = 37 \text{ mmol.dm}^{-3}$, pH 0.45. $[Si(OH)_4] = 2 \text{ mmol.dm}^{-3}$, $[KNO_3] = 0.1 \text{ mol.dm}^{-3}$, $[Al] = 1 \text{ }\mu\text{mol.dm}^{-3}$. pH range: 3, 4, 4.5, 5, 5.5, 6, 7. (d) $[Si(OH)_4] = 2 \text{ mmol.dm}^{-3}$, $[KNO_3] = 0.1 \text{ mol.dm}^{-3}$, $[Al] = 1 \text{ }\mu\text{mol.dm}^{-3}$ + $[morin] = 1 \text{ }\mu\text{mol.dm}^{-3}$. pH range: 3, 4, 4.5, 5, 5.5, 6, 7.

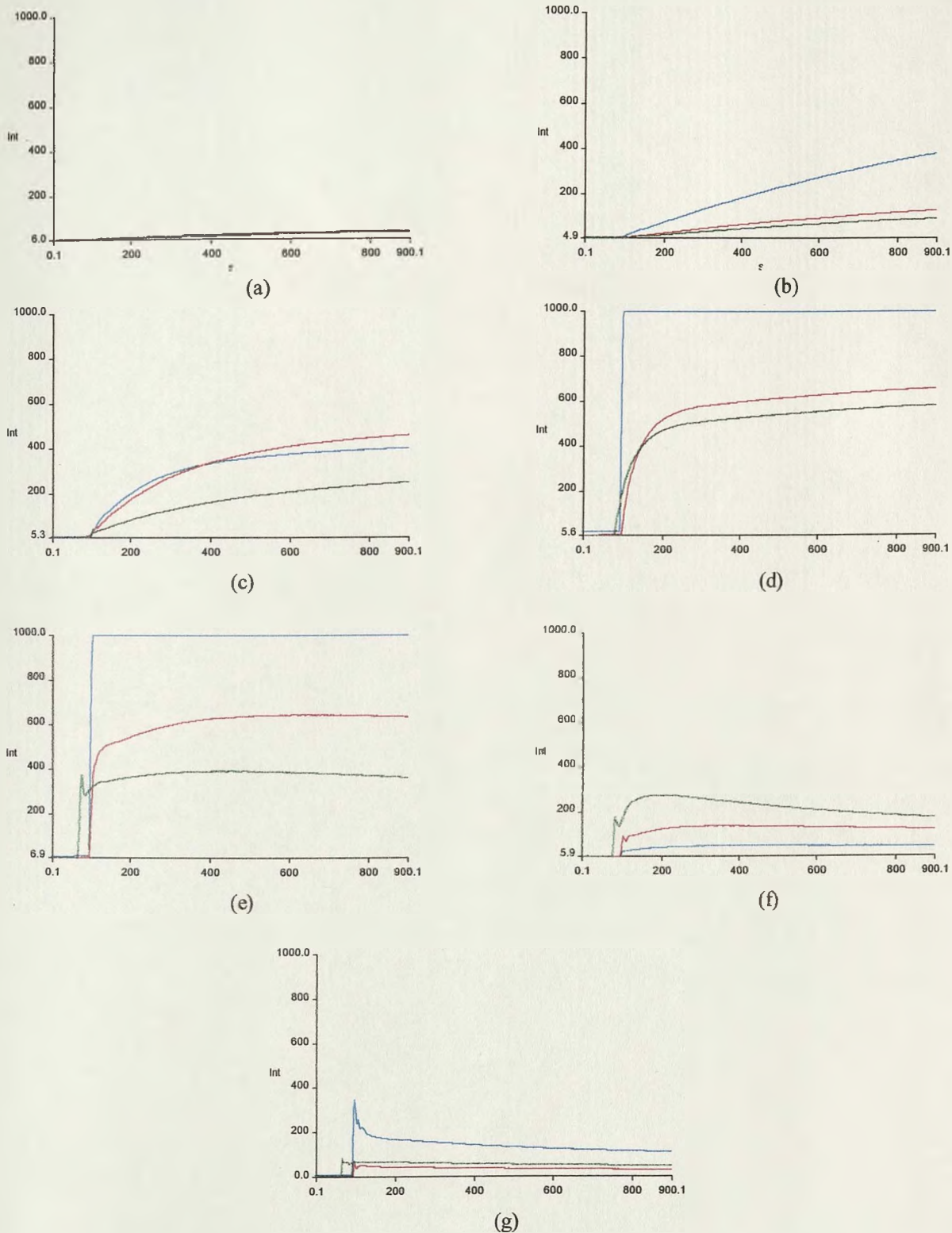


Figure 5.2-4: Fluorimetry time drive at different pH. $[\text{KNO}_3] = 0.1 \text{ mol.dm}^{-3}$, $[\text{Al}] = 1 \mu\text{mol.dm}^{-3}$, $[\text{morin}] = 1 \mu\text{mmol.dm}^{-3}$ after 100s. (a) pH 3. (b) pH 4. (c) pH 4.5. (d) pH 5. (e) pH 5.5. (f) pH 6. (g) pH 7. $N = 3$.

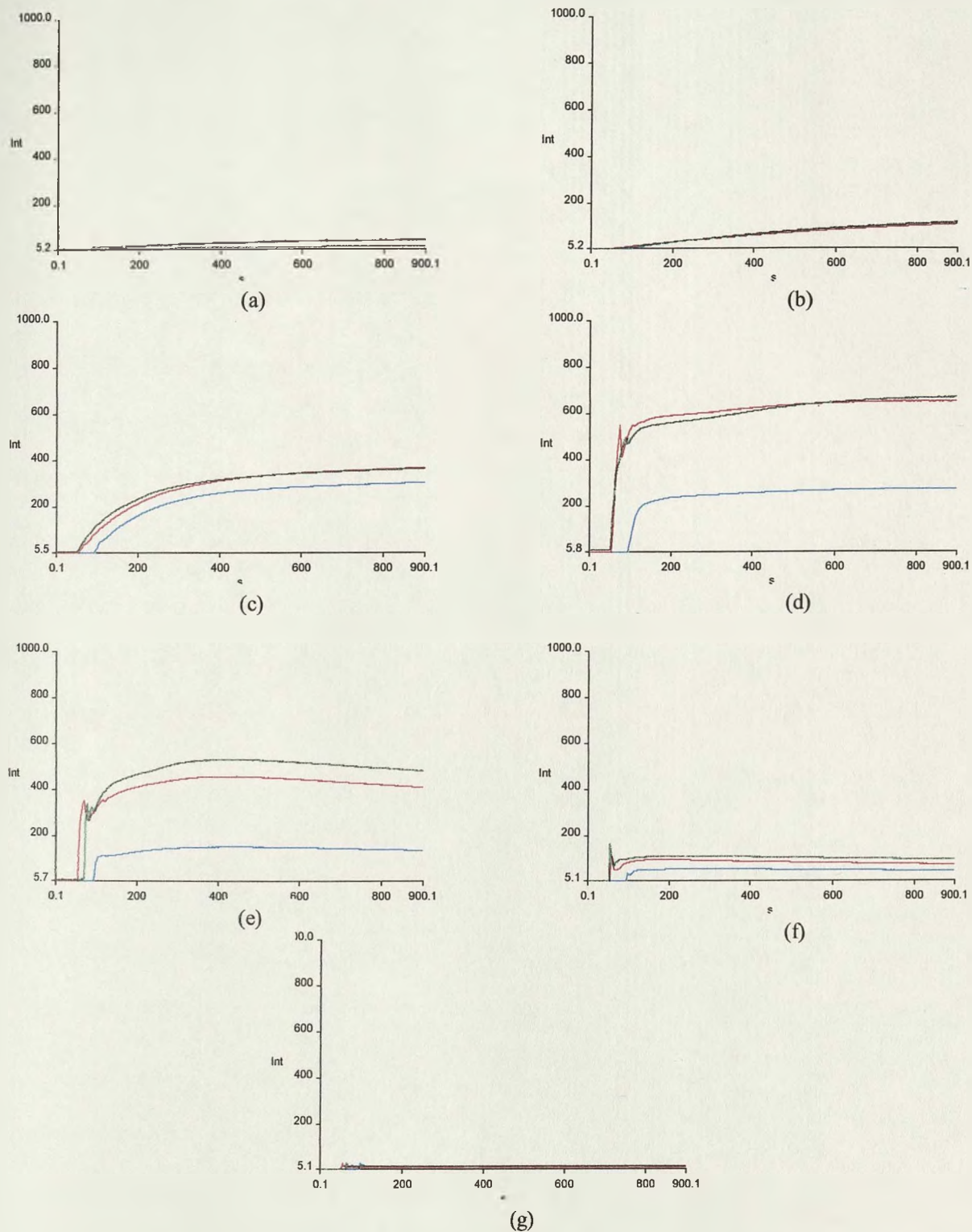


Figure 5.2-5: Fluorimetry time drive at different pH. $[\text{Si}(\text{OH})_4] = 2 \text{ mmol.dm}^{-3}$, $[\text{KNO}_3] = 0.1 \text{ mol.dm}^{-3}$, $[\text{Al}] = 1 \text{ }\mu\text{mol.dm}^{-3}$, $[\text{morin}] = 1 \text{ }\mu\text{mol.dm}^{-3}$ after 100s. (a) pH 3. (b) pH 4. (c) pH 4.5. (d) pH 5. (e) pH 5.5. (f) pH 6. (g) pH 7. $N = 3$.

In view of these results, **Protocol 6** was developed in order to determine under which pH and for which [Al] the identification of HAS formation could be observed by fluorimetry. The spectra recorded by fluorimetry with the TD method to determine the delay time dt are shown in Figure 5.2-6. It appeared that after 900 s, all samples had reached a plateau. It was then assumed that after a delay time $dt = 900$ s, morin had reacted with all the available Al in solution to form AlM. At dt , the final I_f was determined from a scan collecting emission spectra at 500nm. Figure 5.2-7 presents the spectra recorded by fluorimetry using the scan method. In addition, the total [Al] in each solution were measured by GFAAS after fluorimetry to determine the exact amount of Al that was present to react with morin. Table 5.2-6 summarises all the results obtained by pH-metry, fluorimetry and GFAAS. It also includes the estimated concentration of neutral $Al(OH)_3$, as calculated from $[Al]_{nominal}$ and pH:

$$[Al(OH)_3] = \frac{K_{13} [Al^{3+}]}{[H^+]^3}, \quad \log K_{13} = -15.69 \quad \text{at } 25^\circ\text{C} \quad (\text{Baes and Mesmer, 1976})$$

To begin with, the replication was good for all samples and this suggested that the reliability of both sample preparation and the experimental protocol were good. However, the interpretation of these results remained problematic as the variables influencing them (pH, $[Al]_{nominal}$, $[Al]_{GFAAS}$, I_f , $[Si(OH)_4]$) were too numerous and unfortunately interdependent. Moreover, the measurements of [Al] by GFAAS after 7 days, i.e. the [Al] supposedly reacting with morin, were different from the Al amount initially added. A loss of Al was observed especially at high pH, which can be easily explained by the precipitation of $Al(OH)_3$. Yet, the presence of $Si(OH)_4$ appeared to reduce this loss. This last observation was in accordance with the theory of the formation of HAS in which the formation of $Al(OH)_3$ template is pre-requisite to the reaction with $Si(OH)_4$.

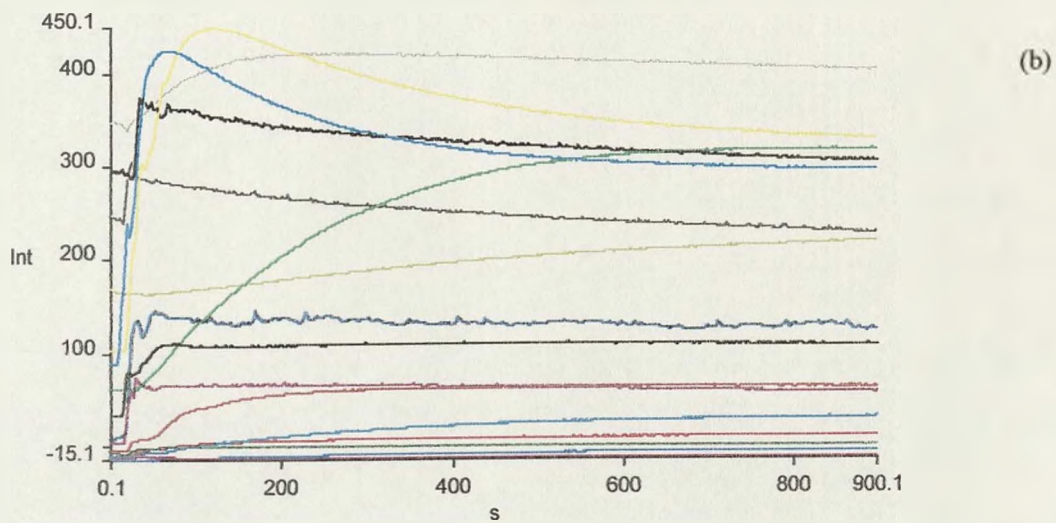
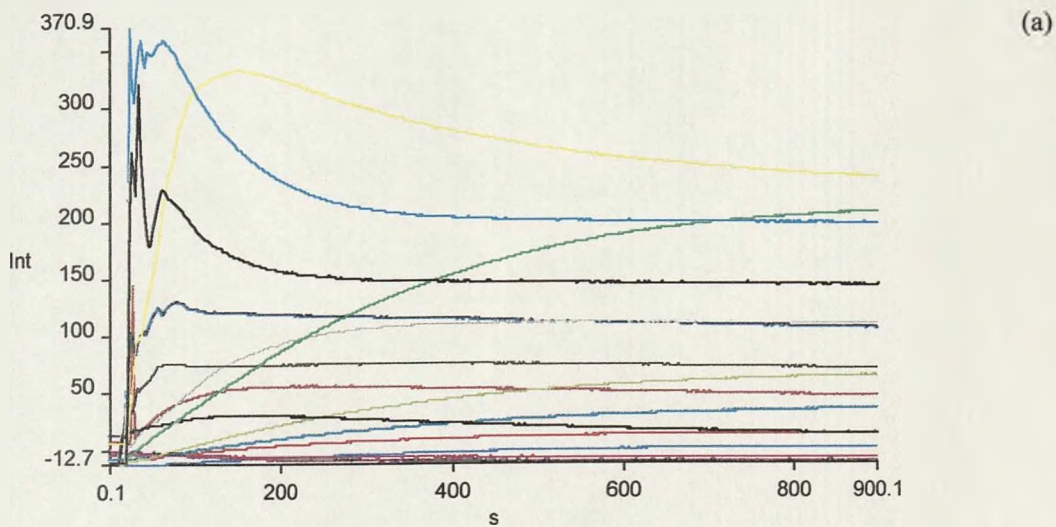


Figure 5.2-6: TD experiments for various [Al]. (a) $[\text{Si}(\text{OH})_4] = 0 \text{ mmol.dm}^{-3}$, $[\text{KNO}_3] = 0.1 \text{ mol.dm}^{-3}$, $[\text{morin}] = 0.1 \text{ }\mu\text{mol.dm}^{-3}$. (b) $[\text{Si}(\text{OH})_4] = 2 \text{ mmol.dm}^{-3}$, $[\text{KNO}_3] = 0.1 \text{ mol.dm}^{-3}$, $[\text{morin}] = 0.1 \text{ }\mu\text{mol.dm}^{-3}$

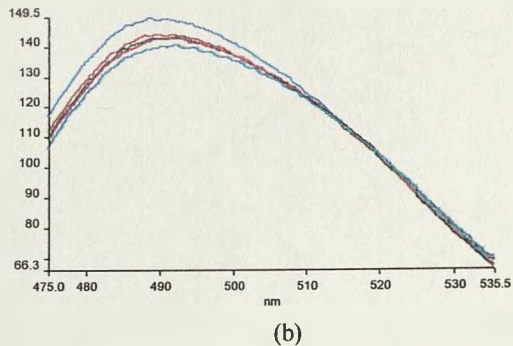
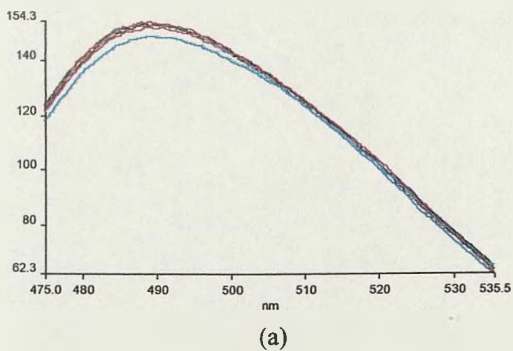


Figure 5.2-7: Examples of replicate scans for a) serie C2, b) serie G2

Table 5.2-6: pH, [Al] measured by GFAAS, [Al] nominal, [Al(OH)₃] nominal calculated, and fluorescence of each sample.

sample	pH	[Al] _{nom} μmol.dm ⁻³	[Al(OH) ₃] _{nom} μmol.dm ⁻³	[Al] _{nom} - [Al(OH) ₃] _{nom}	[Al] _{GFAAS} μmol.dm ⁻³	If	If/[Al] _{GFAAS}
A1	3.95	1	0.0006	0.999	1.7	6.12	3.60
A2	4.13	1	0.0020	0.998	1.4	14.89	10.64
A3	5.03	1	0.1347	0.865	0.8	27.55	34.44
A4	5.49	1	0.3609	0.639	0.6	7.10	11.83
B1	3.91	5	0.0024	4.998	6.7	34.46	5.14
B2	4.46	5	0.0685	4.931	5.4	126.94	23.51
B3	5.04	5	0.6923	4.308	3.8	130.76	34.41
B4	5.35	5	1.4109	3.589	5.2	118.49	22.79
C1	3.96	10	0.0067	9.993	7.41	61.48	8.30
C2	4.47	10	0.1445	9.855	7.22	152.29	21.09
C3	4.91	10	0.9389	9.061	7.59	179.09	23.60
C4	5.53	10	3.8439	6.156	6.5	143.42	22.07
D1	4.01	50	0.0461	49.954	44.4	254.65	5.74
D2	4.41	50	0.5230	49.477	43.3	348.79	8.06
D3	5.09	50	7.9114	42.089	41.7	224.94	5.39
D4	5.64	50	22.5147	27.485	17.6	124.54	7.08
M4	5.5	25	9.1682	15.832	11.1	157.09	14.15
E1	3.93	1	0.0005	0.999	1.1	1.67	1.52
E2	4.41	1	0.0105	0.990	1.8	13.88	7.71
E3	4.97	1	0.1132	0.887	0.96	28.83	30.03
E4	5.72	1	0.4985	0.502	0.4	0.00	0.00
F1	3.84	5	0.0015	4.998	4.8	32.46	6.76
F2	4.25	5	0.0208	4.979	4.4	78.36	17.81
F3	4.96	5	0.5493	4.451	3.5	143.97	41.13
F4	5.1	5	0.8117	4.188	2	101.89	50.94
G1	3.81	10	0.0025	9.998	8.33	50.00	6.00
G2	4.5	10	0.1690	9.831	8.15	143.61	17.62
G3	5.12	10	1.7076	8.292	8.15	150.94	18.52
G4	5.68	10	4.7443	5.256	3.9	6.06	1.55
H1	4.01	50	0.0461	49.954	55.56	302.65	5.45
H2	4.6	50	1.3812	48.619	37.9	289.15	7.63
H3	4.84	50	3.7027	46.297	23.1	199.37	8.63
H4	5.65	50	22.8164	27.184	42.6	17.00	0.40
N1	4.06	25	0.0318	24.968	25.9	269.05	10.39
N2	4.58	25	0.6283	24.372	20.4	245.59	12.04
N3	4.91	25	2.3473	22.653	12.3	170.82	13.89
N4	5.59	25	10.5046	14.495	15.7	19.20	1.22

A first attempt to reduce the number of variables was to express the results obtained as the fluorescence intensity (I_f) per unit of Al present in solution at the time of the experiment, i.e. $[Al]$ measured by GFAAS. Figure 5.2-8 shows the influence of $2 \text{ mmol}\cdot\text{dm}^{-3} \text{ Si(OH)}_4$ on fluorescence per unit of $[Al]_{\text{GFAAS}}$ against pH depending on the initial amount of Al added in the samples. The interpretation of these figures required great caution as the non-stability of some of the parameters such as pH can lead to some misunderstanding of the results. For example, the lack of results on Figure 5.2-8 (a) in presence of Si(OH)_4 for the pH range 5.2-5.8 was a genuine result due to the absence of signal whereas on Figure 5.2-8 (b) the lack of results under the same experimental conditions was due to a drop of pH of the samples, leading to no result for this pH range. Despite the estimation that Si(OH)_4 seemed to be more efficient at high pH (range 5.2-5.8), it was difficult to draw any conclusions from a first view of these figures. The fact that pH influenced both the Al chemistry (i.e. precipitation of Al(OH)_3) and the reaction of formation of AlM precluded an immediate interpretation of the results. As Al(OH)_3 is believed to have a critical role in the formation of HAS, it was appropriate to look at the effect of Si(OH)_4 on the fluorescence in respect of the $[\text{Al(OH)}_3]$ in solution. In Figure 5.2-9, the influence of Si(OH)_4 on the fluorescence per unit of Al measured by GFAAS is plotted against the calculated $[\text{Al(OH)}_3]_{\text{nominal}}$. It revealed a noticeable effect of Si(OH)_4 for high $[\text{Al(OH)}_3]$. But once again, the interdependence of the variables made impossible any objective analysis of the results as underlined at low $[\text{Al(OH)}_3]$ where the plots in both samples, with or without Si(OH)_4 , did not follow an expected decay.

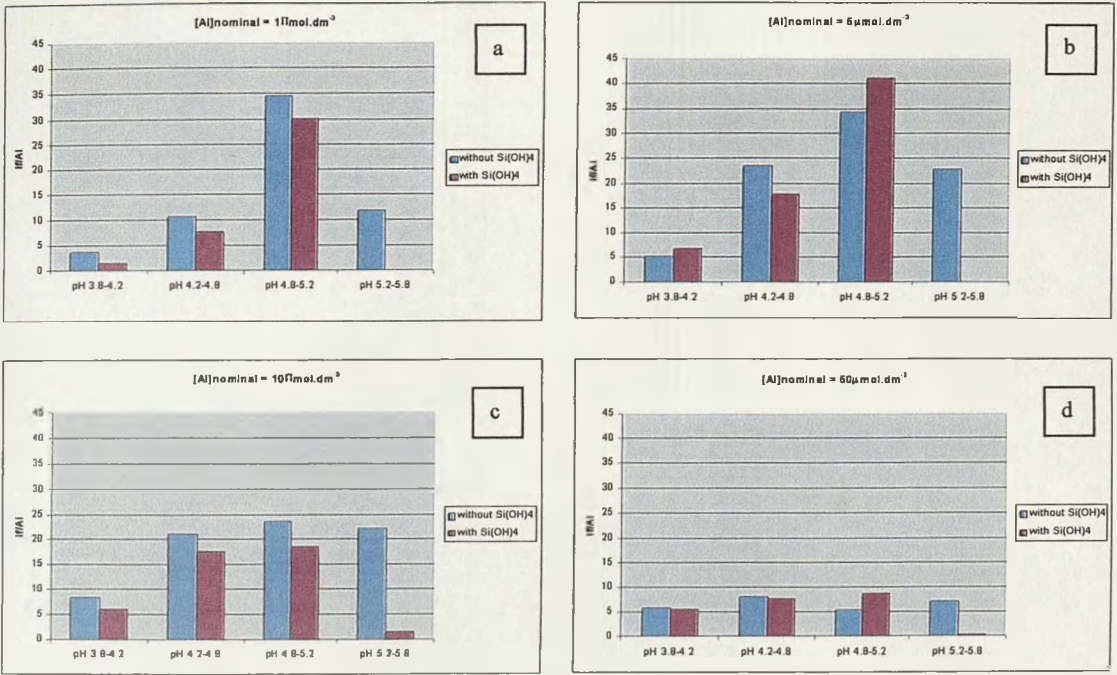


Figure 5.2-8: Influence of 2 mmol.dm⁻³ Si(OH)₄ on the relative fluorescence per unit of Al_{GFAAS} by range of pH.

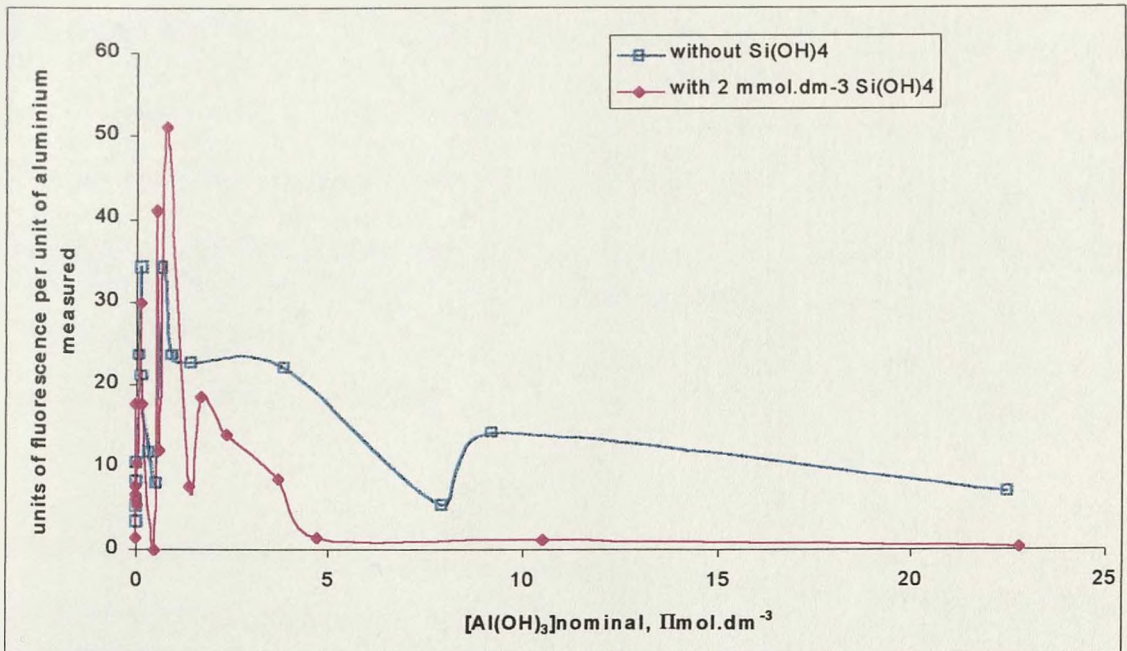


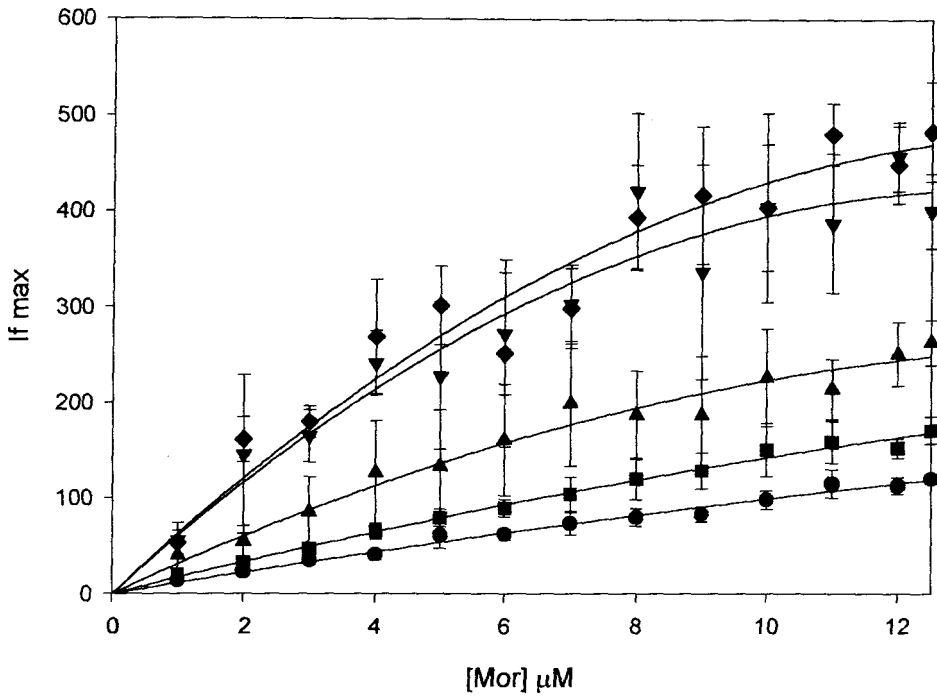
Figure 5.2-9: Influence of 2 mmol.dm⁻³ Si(OH)₄ on the fluorescence per unit of aluminium measured by GFAAS against the calculated [Al(OH)₃] nominal.

As has been underlined in all the previous protocols, one of the major problems in the study of HAS formation was the control of the variables influencing the reaction. The most important of them was pH which influenced the whole chemistry of the species in solution: Al, Si(OH)₄ and morin were all pH-dependant on their interaction with each other. This point was finally been addressed in **Protocols 10 and 11** by using a buffer in the preparation of samples. Fluorimetry was used to determine the influence of Si(OH)₄ on the formation of aluminium-morin complex (AlM) at a fixed pH. In order to find the parameters influencing the reaction, I looked at this effect using two different pH values and five different [Al]. The intensity I_f (directly proportional to the [AlM]) was then measured for a range of [morin] to determine from which concentration the formation of AlM was optimum. A statistical study of the results was performed using the ANOVA calculation. Figures 5.2-10 and 5.2-11 presents the fluorescence intensity measured against [morin] for [Al] range: 0.5, 1, 2, 4, 6 $\mu\text{mol}\cdot\text{dm}^{-3}$ in presence or not of Si(OH)₄, at pH 6.5 and 6 respectively.

The first point to be noticed was the gain of stability in the presence of Si(OH)₄. The results obtained in presence of Si(OH)₄ were more reproducible than those obtained without Si(OH)₄. HAS can be seen as a more stable complex than the different monomeric species in a Al/Mor only system, perhaps implying a stronger formation constant.

Secondly, whilst the results at pH 6.5 were easy to obtain and to interpret, those at pH 6 proved to be more difficult to get, due to the limit of detection of the technique. The intensity of the AlM complex fluorescence was off scale for [Al] as little as 4 $\mu\text{mol}\cdot\text{dm}^{-3}$. That led to the incapacity of measuring quantitatively any effect of Si(OH)₄ on the formation of the complex, even if one could observe it.

a)



b)

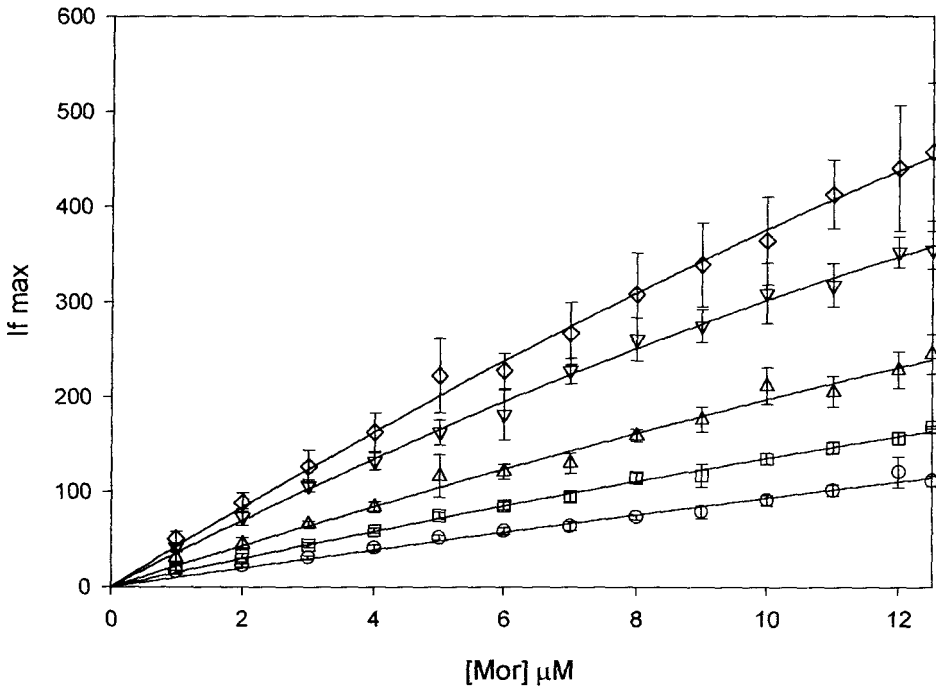
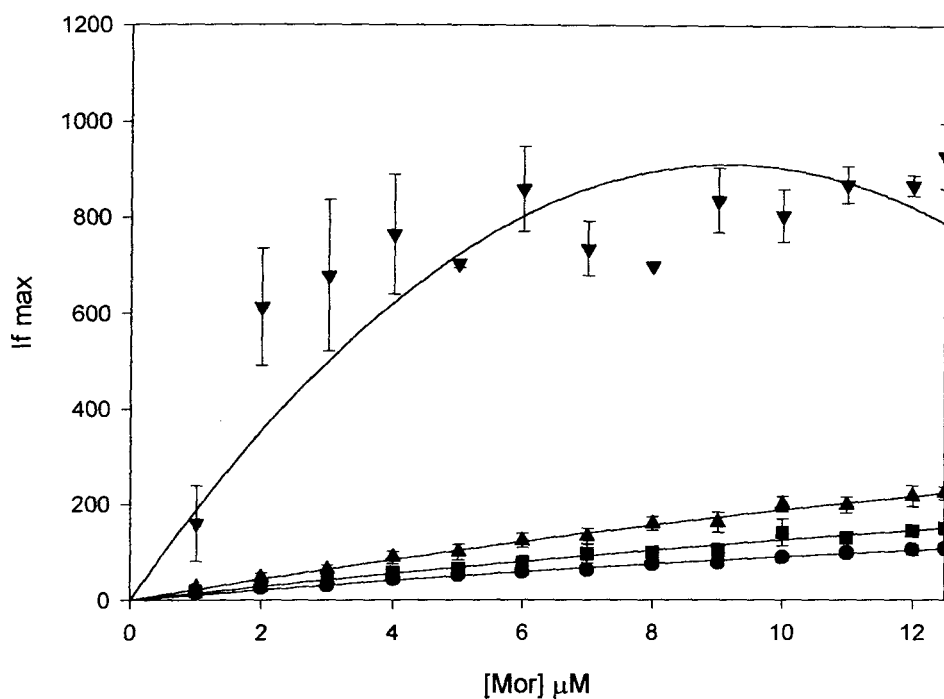


Figure 5.2-10: If measured against [Mor], a: [Al] = 0.5 (circle), 1 (square), 2 (up triangle), 4 (diamond), 6 (down triangle) $\mu\text{mol.dm}^{-3}$, [Si(OH)₄] = 0 mmol.dm^{-3} , 0.1 mol.dm^{-3} KNO₃, 50 mmol.dm^{-3} PIPES. b: [Al] = 0.5 (circle), 1 (square), 2 (up triangle), 4 (diamond), 6 (down triangle) $\mu\text{mol.dm}^{-3}$, [Si(OH)₄] = 2 mmol.dm^{-3} , 0.1 mol.dm^{-3} KNO₃, 50 mmol.dm^{-3} PIPES. N = 4. pH 6.5.

a)



b)

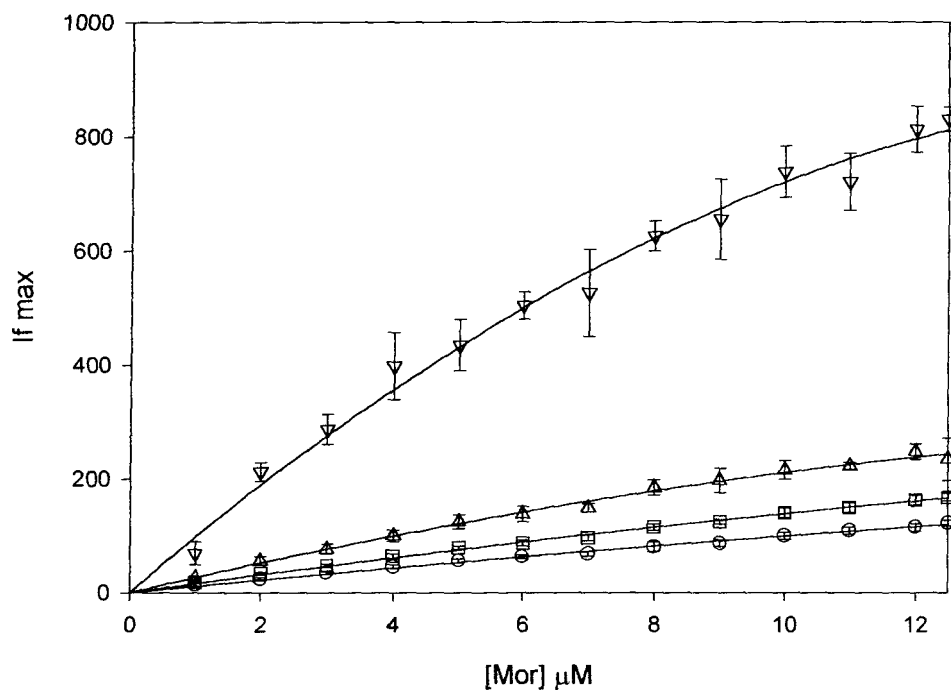


Figure 5.2-11: If measured against [Mor], a: [Al] = 0.5 (circle), 1 (square), 2 (up triangle), 4 (diamond), 6 (down triangle) $\mu\text{mol.dm}^{-3}$, [Si(OH)₄] = 0 mmol.dm^{-3} , 0.1 mol.dm^{-3} KNO₃, 50 mmol.dm^{-3} PIPES. b: [Al] = 0.5 (circle), 1 (square), 2 (up triangle), 4 (diamond), 6 (down triangle) $\mu\text{mol.dm}^{-3}$, [Si(OH)₄] = 2 mmol.dm^{-3} , 0.1 mol.dm^{-3} KNO₃, 50 mmol.dm^{-3} PIPES. N = 4. pH 6.

Another surprising aspect of these results was that a plateau was never reached whatever the [Al] or [Mor]. The formation of AIM has been described as a 1:1 complex, but this experiment showed that the more morin was in solution the more AIM was formed. However, the more important point was the effect of Si(OH)_4 on the formation of the AIM complex. $I_f(+\text{Si})$ was lower than $I_f(-\text{Si})$ for all [Al]. For $[\text{Al}] > 2 \mu\text{mol}\cdot\text{dm}^{-3}$, the results obtained in presence of Si(OH)_4 were statistically ($F_s > F_{0.05}$) different from those obtained without it. This implied that there was less free Al to react with morin. It can be easily deduced that this was due to a part of this Al reacting with Si(OH)_4 to form HAS. Moreover, these results showed that the reaction occurred almost instantly even at a very low [Al]. The effect observed can be expected to be even greater with time.

5.2.3. Discussion

Aside from the results themselves, this section stressed the difficulties that were encountered in the establishment of reliable experimental protocols. The lack of replication in the early protocols illustrated perfectly how external parameters can induce uncertainties.

To begin with, the choice of materials and the importance of the cleaning process were emphasised by the problems resulting from surface adsorption. The sticky nature of morin necessitated a careful cleaning of the fluorimetric cell, using a detergent and not only with ultra-pure water. It was also necessary to use Teflon bottles to reduce the loss of Al by surface adsorption, which was particularly noticeable at higher pH (around 5.5) when the precipitation of Al(OH)_3 was favoured.

The preparation of the samples was also important. It was shown that the use of a certified Al standard solution was preferable to the preparation of a stock solution from $\text{Al(NO}_3)_3 \cdot 9\text{H}_2\text{O}$ as it reduced the uncertainties due to human error. However, it also led to a

change of technique, as the quantities originally added in Protocol 2 and 4 were prone to errors. The TD method required the addition of either Al or morin in situ in order to follow the evolution of the reaction with time. This implied the injection of a very small amount of either solution into the cell in order to limit the variation of the total volume. The complete lack of replication of the results obtained with this technique showed its inadequacy for the purpose of my study and the use of the scan technique was preferred for the following experiments. Notwithstanding, TD proved to be useful to estimate the delay time (dt) necessary for morin to react with all the Al available in solution.

The preparation of the samples was remarkably affected by the change of fluorimetry technique. The scan method gave an instant picture of the chemistry in solution and was therefore independent of the time provided that dt was respected. That allowed the solutions to be mixed before scanning, using larger volume of more dilute stock solutions, hence reducing the number of uncertainties. Consequently, the replication in Protocol 6 and after was good, which sustained the reliability of both the method and the sample preparation.

From the experimental point of view, the results revealed the importance of several factors: (i) pH, (ii) [morin], (iii) [Al], (iv) [Si(OH)₄]. The influence of pH was possibly the most obvious and yet the most difficult to analyse. Despite the lack of replicates in Protocol 4, the effect of pH over If was already noticeable, regardless of the presence or not of Si(OH)₄, with a maximum intensity for pH = 5 and 5.5. In Protocol 6, for [Al] < 25 μmol.dm⁻³, the maximum intensities were found at pH 5. This was easily explained by the 1st proton dissociation constant of morin, pK_{a1} = 5.04 (Browne, 1990). However, if [Al] > 25 μmol.dm⁻³, If was maximum for pH = 4. The problem was that it also affected the total [Al]_{GFAAS} in solution. As the pH increased, [Al(OH)₃] started to precipitate and there was

less Al available in solution to react with morin, this effect being enhanced at high [Al]. As both [morin] and [Al] were highly dependent on pH and the latter was dependent on the stabilisation of the Al species, an interdependence of the variables occurred, making the analysis of the results quasi impossible. By fixing the pH in Protocols 10 and 11 through the use of a buffer, it was possible to discriminate the effect of pH from the effect of concentration of the various species. In these last protocols, a range of [morin] was studied in order to determine the optimum conditions of formation of AlM. A delay time has previously been determined using TD method. It showed that, after 15 minutes, If had reached a plateau for all [Al]. It was then assumed that morin had reacted with all the available Al in solution and that AlM was stable. The reaction between Al and morin was described by Browne (1990b) as a 1:1 reaction. It was then expected that in presence of an excess of morin, the binding between Al and morin would be maximum, leading to the saturation of morin. However, a plateau was never reached for any [morin]. If a delay time was respected to allow the AlM complex to stabilise, the measurement of the complex was done before the aluminium species had the time to reach a equilibrium. This last result stressed the problem of using young Al solutions. The Al system was complex and needed time to equilibrate. The loss of Al, by precipitation of $\text{Al}(\text{OH})_3$ at high pH, measured by GFAAS (Protocols 4 & 6) as well as the not-so-good replication observed for Al/Morin (Protocols 10 & 11) were just further proof of the non-stability of the system. However, the presence of $\text{Si}(\text{OH})_4$ seemed to stabilise the system and to reduce the loss of Al. The replication in Protocols 10 and 11 was better in presence of $\text{Si}(\text{OH})_4$ and a strong effect on If was noticed for $[\text{Al}] > 2 \mu\text{mol}\cdot\text{dm}^{-3}$. All this evidence implied a reaction between $\text{Si}(\text{OH})_4$ and Al when the conditions for $\text{Al}(\text{OH})_3$ to precipitate were fulfilled, i.e. [Al] above the solubility limit.

The last experiments, if failing to provide accurate measurements and definitive conclusions about the system Al/Si(OH)₄/Morin, permitted the optimal conditions under which the reaction between Al and Si(OH)₄ would occur to be defined. pH 6.5 allowed a study on a greater range of [Al] and the higher effect was observed for [morin] = 12.5 μmol.dm⁻³.

5.3.The measurement of the influence of Si(OH)₄ on the AIM formation

5.3.1.Experimental

The preparation of stock solutions was the same as described in the previous section. Table 5.3-1 shows the concentration of compounds in both stock solutions and samples.

Table 5.3-1: Concentrations in stock solutions and samples.

	[KNO ₃] mol.dm ⁻³	[Si(OH) ₄] μmol.dm ⁻³	[Morin] μmol.dm ⁻³	[Al] mode B μmol.dm ⁻³	pH
Stock solutions	0.1	0 / 1 / 10 / 100 / 1000 / 2000	125	250, 500, 1000, 2000, 3000	
samples	0.1	0 / 1 / 10 / 100 / 1000 / 2000	12.5	0.5, 1, 2, 4, 6	6.5

40 samples were prepared at a fixed pH 6.5 with or without Si(OH)₄.

- 2.5 mL of the previously prepared Al stock solution were added to 250 mL of KNO₃ +/- Si(OH)₄, pH < 3, in order to have [Al]_{sample} = 0.5, 1, 2, 4 and 6 μmol.dm⁻³.

- 0.125 g of Na Azide (0.05% w/v) was added to prevent growth of organisms.
- 50 mmol.dm⁻³ PIPES was then added as a buffer.
- pH was then adjusted to 6.5 by addition of NaOH pellets.
- The solutions were stored in the dark.

Every week a scan reading was taken under the following protocol.

- A 5 mL aliquot of each solution was transferred into a bijou bottle.
- 500 μL of morin stock solution was added to the samples at 2 mins intervals. The resulting morin concentration into the sample was 12.5 μmol.dm⁻³.
- After 15 mins, a scan was performed.

After 12 weeks, the remaining solutions were acidified to 1% HNO₃ and the total [Al] was measured by GFAAS, using a matrix-matched calibration.

5.3.2. Results

At the end of the previous section, a protocol was established which showed the influence of Si(OH)₄ on the formation of AIM under defined conditions at an early stage of the reaction but failed to give the necessary results to define the system at equilibrium. In this section, the experiment was set up to provide information on the Al reacting with morin, or free Al, as well as on the Al reacting with Si(OH)₄, by deduction, at equilibrium. The optimal conditions defined in Protocols 10 and 11 were used in this protocol, but on a long term time-scale.

The experiment was carried out for a period of 12 weeks. Figure 5.3-1 shows If recorded over this period for samples a) without and b) with 2 mmol.dm⁻³ Si(OH)₄. The first

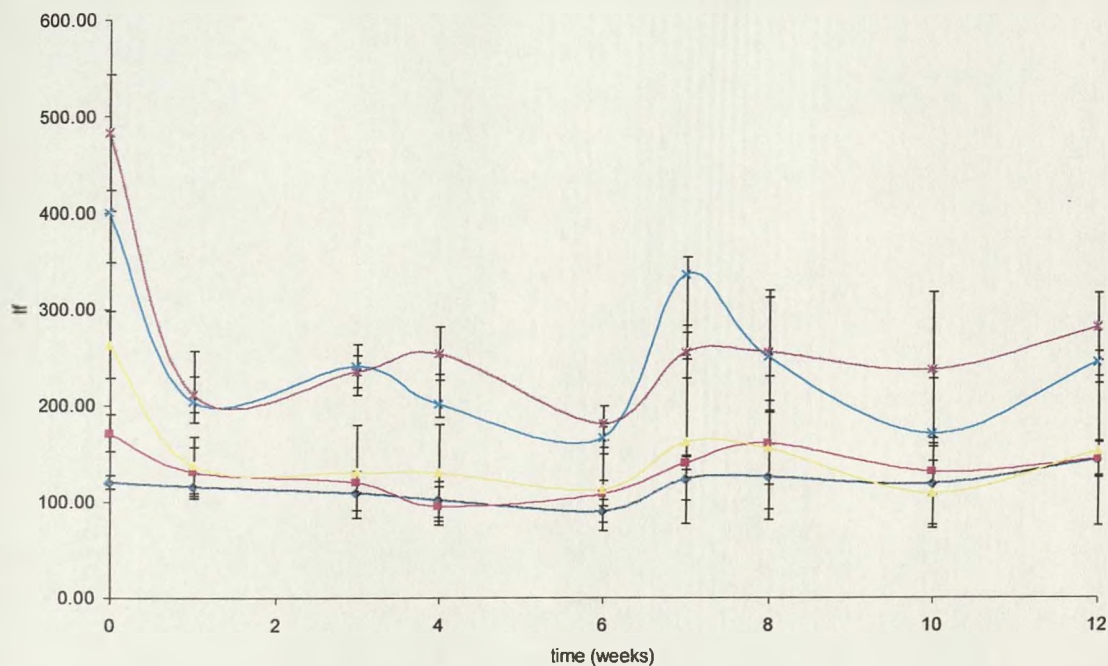
observation to be made was once again the better replication of the measurements in presence of Si(OH)_4 . This confirmed the previous results obtained. After just a week, both systems seemed to settle down and a huge decrease of the intensity could be noticed. However, while Si(OH)_4 samples reached quite quickly an equilibrium state, the same could not be said about the Al only samples. The intensities of the Al only samples first decreased progressively but then showed some difficulty in remaining stable. This was probably due to the phenomenon of the formation/dissolution of Al(OH)_3 preventing the system to stabilise. The presence of a buffer in the samples probably emphasised this effect by hindering any change of pH which under normal conditions was observed when the system reached equilibrium. On the other hand, this phenomenon was not observed on samples containing Si(OH)_4 , meaning that the species formed were a lot more stable in solution. $[\text{Al}]$ played another important role in the equilibrium. The higher the $[\text{Al}]$ in the Al/Mor system, the higher the I_f . But the exact opposite effect was observed in the Al/ Si(OH)_4 /Mor system as I_f decreased when $[\text{Al}]$ was increased.

Considering that the more dramatic effect of $2 \text{ mmol}\cdot\text{dm}^{-3}$ Si(OH)_4 was observed for $[\text{Al}] = 6 \text{ }\mu\text{mol}\cdot\text{dm}^{-3}$, I chose this concentration to study the influence of $[\text{Si(OH)}_4]$ on the reaction. Up to now, Si(OH)_4 was always present in large excess to Al in solution. In order to fully understand the reaction it was, however, necessary to gradually inverse the ratios and to determine the minimum $[\text{Si(OH)}_4]$ required to observe HAS formation by fluorimetry. Figure 5.3-2 presents the I_f measured over 12 weeks for $[\text{Al}] = 6 \text{ }\mu\text{mol}\cdot\text{dm}^{-3}$ and $[\text{Si(OH)}_4] = 0, 1, 10, 100, 1000, 2000 \text{ mmol}\cdot\text{dm}^{-3}$. At first, it seemed that only a large excess of Si(OH)_4 , $[\text{Si(OH)}_4] \geq 100 \text{ }\mu\text{mol}\cdot\text{dm}^{-3}$, had an effect on I_f . The stabilisation of the system also seemed slower, as I_f took more time to reach its lower level. For $[\text{Si(OH)}_4] = 2000 \text{ }\mu\text{mol}\cdot\text{dm}^{-3}$, a plateau was reached after just 1 week, but it took 6 weeks to observe the

same effect for $[\text{Si}(\text{OH})_4] = 1000 \mu\text{mol}\cdot\text{dm}^{-3}$. As $[\text{Si}(\text{OH})_4]$ decreased, it seemed that the kinetics of the reaction slowed down and the system lost stability. A more striking result was that even when $[\text{Si}(\text{OH})_4] = 1000 \mu\text{mol}\cdot\text{dm}^{-3}$, i.e. in large excess, the I_f observed for this concentration was still higher than in presence of $[\text{Si}(\text{OH})_4] = 2000 \mu\text{mol}\cdot\text{dm}^{-3}$. Yet, one could have expected a similar result as there was more than enough $\text{Si}(\text{OH})_4$ in solution to react with the available Al. The same observation could be made for any other $[\text{Si}(\text{OH})_4]$ except $1 \mu\text{mol}\cdot\text{dm}^{-3}$. As I_f depends of the total Al in solution, it was necessary to know the real amount of Al from GFAAS. Table 5.3-2 presents the measurement of the total $[\text{Al}]$ by GFAAS for $[\text{Al}]_{\text{nom}} = 6 \mu\text{mol}\cdot\text{dm}^{-3}$.

The measurement by GFAAS of the total amount of Al in the solutions showed that $[\text{Al}]$ varied even if slightly between samples. However, $[\text{Al}]$ remained accurate and could not explain the large difference of I_f observed for the $[\text{Si}(\text{OH})_4]$ range studied.

a)



b)

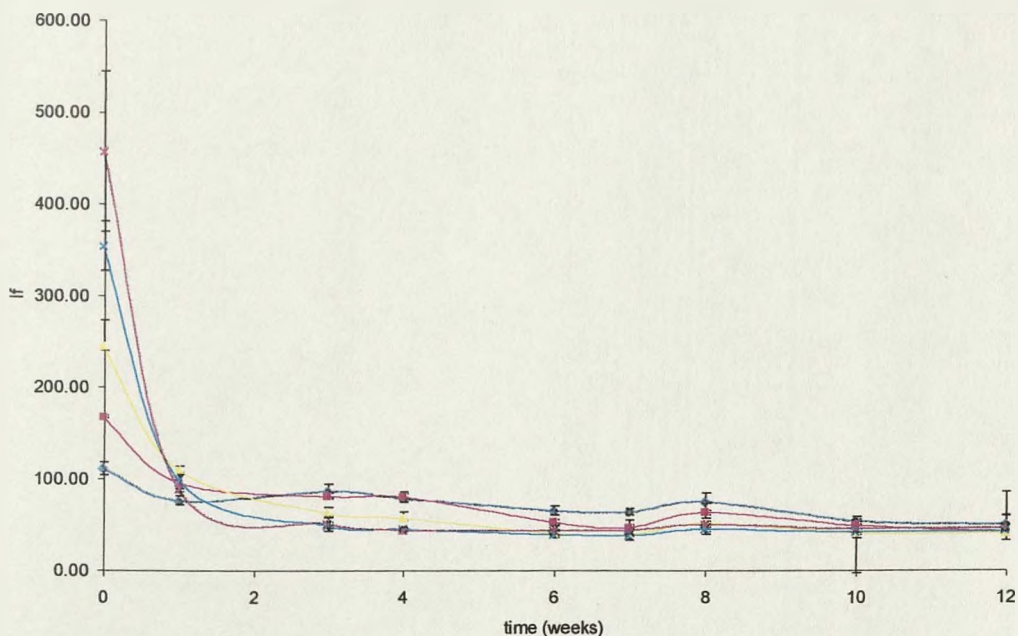


Figure 5.3-1: If measured against time. Blue: $[Al] = 0.5 \mu\text{mol.dm}^{-3}$; Pink: $[Al] = 1 \mu\text{mol.dm}^{-3}$; Yellow: $[Al] = 2 \mu\text{mol.dm}^{-3}$; Turquoise: $[Al] = 4 \mu\text{mol.dm}^{-3}$; Violet: $[Al] = 6 \mu\text{mol.dm}^{-3}$. a) $[Si(OH)_4] = 0 \text{ mmol.dm}^{-3}$, b) $[Si(OH)_4] = 2 \text{ mmol.dm}^{-3}$. $N = 4$.

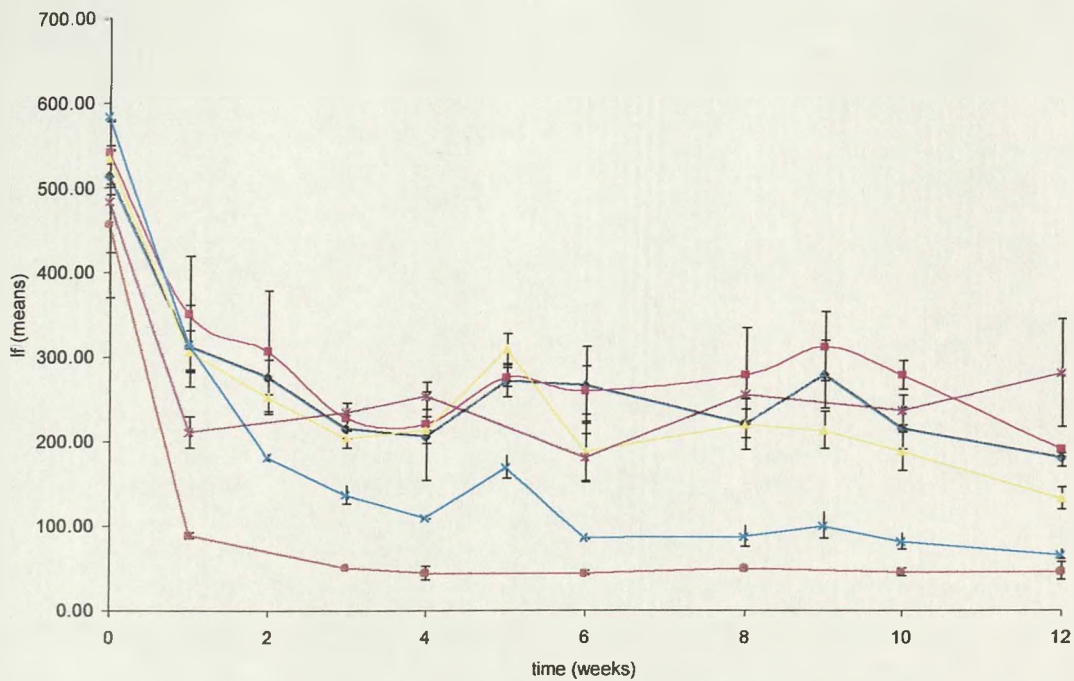


Figure 5.3-2: If measured against time, $[Al] = 6 \mu\text{mol}\cdot\text{dm}^{-3}$. Blue: $[Si(OH)_4] = 1 \mu\text{mol}\cdot\text{dm}^{-3}$; Pink: $[Si(OH)_4] = 10 \mu\text{mol}\cdot\text{dm}^{-3}$; Yellow: $[Si(OH)_4] = 100 \mu\text{mol}\cdot\text{dm}^{-3}$; Turquoise: $[Si(OH)_4] = 1000 \mu\text{mol}\cdot\text{dm}^{-3}$; Violet: $[Si(OH)_4] = 0 \mu\text{mol}\cdot\text{dm}^{-3}$; Brown: $[Si(OH)_4] = 2000 \mu\text{mol}\cdot\text{dm}^{-3}$. $N = 4$.

Table 5.3-2: Measurement of total $[Al]$ by GFAAS, using a matrix-matched calibration. $[Al]_{\text{nominal}} = 6 \mu\text{mol}\cdot\text{dm}^{-3}$. $N = 4$, (standard deviation).

$[Si(OH)_4]$ $\mu\text{mol}\cdot\text{dm}^{-3}$	0	1	10	100	1000	2000
$[Al]$ $\mu\text{mol}\cdot\text{dm}^{-3}$	6.35 (0.53)	6.23 (0.12)	5.86 (0.31)	6.81 (0.55)	6.91 (0.67)	6.76 (0.24)

5.3.3. Discussion

The results obtained with this protocol demonstrated the effect of $[\text{Si}(\text{OH})_4]$ on Al on more than one level. I was not only able to observe this effect at equilibrium but I could also follow its progression with time, getting some information on the stability and the kinetics of the reaction. Ahead of any quantitative determination of the equilibrium constant, the gain of stability observed in presence of $\text{Si}(\text{OH})_4$ gave strong indications of its value. Besides having better replicates, samples with $\text{Si}(\text{OH})_4$ reached an equilibrium state more easily than the samples without, which proved that the species in solution were more prevalent in the system Al/ $\text{Si}(\text{OH})_4$ /Mor than in the system Al/Mor.

However, this effect was also strongly dependant upon $[\text{Si}(\text{OH})_4]$. As $[\text{Si}(\text{OH})_4]$ decreased, the stability of the system weakened and for $[\text{Si}(\text{OH})_4] \leq 10 \mu\text{mol}.\text{dm}^{-3}$, it was difficult to see any improvement from the Al/Mor system. Furthermore, only a large excess of $\text{Si}(\text{OH})_4$ had a significant effect on If. Even then, a noticeable difference was observed between the effect of $[\text{Si}(\text{OH})_4] = 2000 \mu\text{mol}.\text{dm}^{-3}$, $[\text{Si}(\text{OH})_4] = 1000 \mu\text{mol}.\text{dm}^{-3}$ and $[\text{Si}(\text{OH})_4] = 100 \text{mmol}.\text{dm}^{-3}$, as the reaction slowed down and became less and less effective as the concentration decreased. The measurement of the total [Al] by GFAAS showed that the slight variations of [Al] between samples could not be taken as responsible for these results, emphasising the importance of $[\text{Si}(\text{OH})_4]$ on the reactivity.

Despite the overall accuracy of [Al], one should notwithstanding be careful before concluding any pattern in the reactivity between $\text{Si}(\text{OH})_4$ and Al as each result should be quantified and analysed individually. However, the fact that only a large excess of $\text{Si}(\text{OH})_4$ permitted the visualisation of the formation of HAS in a relatively short period of time by fluorimetry remained and stressed the limitation of this method. The study of very low [Al]

solutions was imposed by the high sensitivity of the morin-based speciation technique but it also deserved the intentional design to determine the lowest parameters for which the formation of HAS may occur. It however became a disadvantage in regard to $[\text{Si}(\text{OH})_4]$, as the reaction was less likely to occur in very dilute conditions. One could then argue that due to the excess of $\text{Si}(\text{OH})_4$ the reaction was speeded up and that the same result would have been reached whatever the concentration in due time.

5.4. Conclusions

The first section of this chapter stressed the complexity of the system and as a result the difficulty to establish a reliable protocol for the indirect study of the reaction of formation of HAS using the fluorescent agent morin. The number of variables and parameters to control, i.e. pH, [morin], [Al], $[\text{Si}(\text{OH})_4]$, was the first problem to be addressed. It was even emphasised by their interaction with each other, making the results obtained by fluorimetry impossible to analyse.

It was shown that the control of pH was the key to reduce these variables as it affected the chemistries both of Al and morin and consequently the formation of AlM, directly measured by fluorimetry. Once this point was addressed by using a buffer, fluorimetry proved to be a very useful technique to detect the formation of HAS at [Al] below $6 \mu\text{mol}\cdot\text{dm}^{-3}$. The pH range used for the study indicated that the formation of HAS was favoured when $\text{Al}(\text{OH})_3$ precipitated.

The effect of $\text{Si}(\text{OH})_4$ on the formation of AlM was particularly strong for $[\text{Al}] > 1 \mu\text{mol}\cdot\text{dm}^{-3}$, $[\text{Si}(\text{OH})_4] > 100 \mu\text{mol}\cdot\text{dm}^{-3}$ and pH 6.5. Moreover, it was shown that the kinetics of the reaction was greatly affected by $[\text{Si}(\text{OH})_4]$. The gain of stability of the

results in the presence of Si(OH)_4 gave strong evidence on the equilibrium constant of HAS. The study of this effect over time allowed an observation of the system at pseudo-equilibrium, i.e. when the species present in solution reached a stable state. Finally, the quantification of these results should give us all the information required for the determination of an equilibrium constant of the formation of HAS.

Chapter 6 : The determination of an equilibrium constant for the formation of a hydroxyaluminosilicate.

6.1. Introduction

In the previous chapter, Si(OH)_4 was shown to reduce the expected formation of morin-reactive Al (AlM). The assumption was made that the amount of Al not reacting with morin in the presence of Si(OH)_4 was in fact reacting with Si(OH)_4 to form HAS. However, it was necessary to quantify the results obtained by fluorimetry in order to completely define the system. Moreover, knowledge of the concentration of different species in a defined system could lead to an approximate idea of the equilibrium constant. To get this relevant information, calculations using the software SolGasWater (SGW, Inorganic Chemistry, Umeå University) were performed to describe the known systems: Al and Al/Morin. Deductions from these calculations and from experimental data were then made to quantify the unknown system: Al/Morin/ Si(OH)_4 .

6.2. Description of the different systems

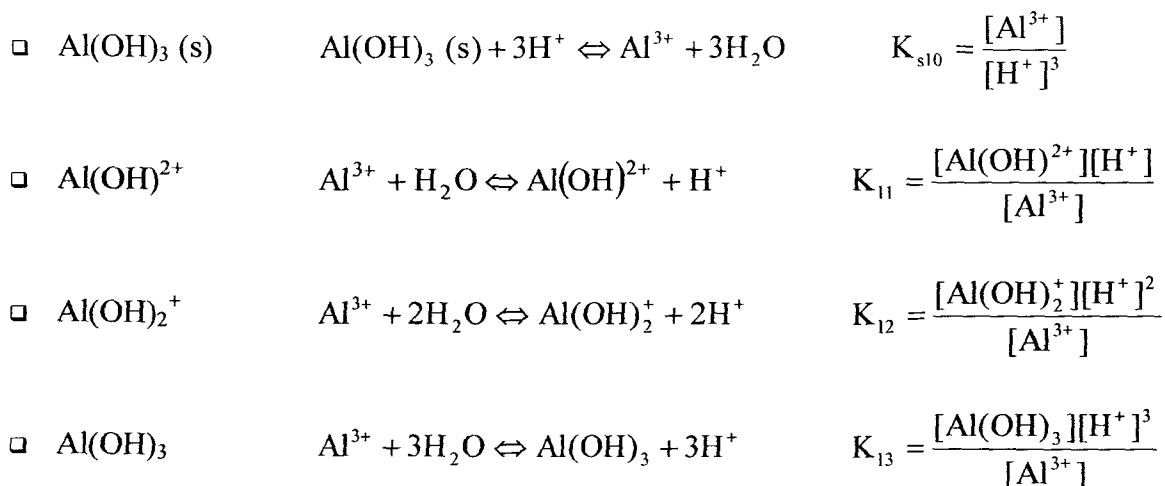
6.2.1. The Al system

- *Species in solution*

Al is the most abundant metal in the earth's crust and many aspects of its speciation in solution has been extensively studied over the years. In nature it exists only in its trivalent state and has a hydration number of 6. Above pH 3, the mononuclear species resulting from the hydrolysis of Al^{3+} are believed to be formed quickly and reversibly. The distribution of the hydrolysed species in solution is dependent upon the precipitation of the

hydroxide, which is generally analogous to gibbsite. However the identification of stable hydrolysis products has been difficult due to the presence of polymeric ions. In recent years, Martin largely reviewed the speciation of Al in solutions (Martin 1991a; Martin 1991b). The first and only form of hydrolysed Al in dilute solution above pH 3 is $\text{Al}(\text{H}_2\text{O})_6^{3+}$, provided that no complex-forming counter-ions are present. When the pH increases to 4-5, the product of the first deprotonation $\text{Al}(\text{H}_2\text{O})_5\text{OH}^{2+}$ becomes predominant. As the pH reaches the range 5-7, the second, third and fourth deprotonation occur, forming $\text{Al}(\text{H}_2\text{O})_4(\text{OH})_2^+$, $\text{Al}(\text{OH})_3(\text{aq})$ and $\text{Al}(\text{OH})_4^-$ respectively. All the ions coexist in varying proportions depending on the pH. Polymeric cations can also form around pH 5, such as $\text{Al}_{13}\text{O}_4(\text{OH})_{24}(\text{OH}_2)_{12}^{7+}$. Above pH 7, $\text{Al}(\text{OH})_4^-$ is the predominant species over the entire pH range (Akitt 1989). It is important to notice that the coordination number of Al shifts from 6 to 4 with the increase of the deprotonation, and incidentally with increasing pH, as Al is octahedral in $\text{Al}(\text{H}_2\text{O})_6^{3+}$, both octahedral and tetrahedral in Al_{13} and finally tetrahedral in $\text{Al}(\text{OH})_4^-$. In this study, only the monomeric species were taken into account. The distribution of the hydrolysis products at 25°C in the Al system is shown in Figure 6.2-1

• *Equilibrium reactions*





• *Mass balance relationship*

$$[\text{Al}] = [\text{Al}^{3+}] + [\text{Al(OH)}^{2+}] + [\text{Al(OH)}_2^+] + [\text{Al(OH)}_3] + [\text{Al(OH)}_4^-] + [\text{Al(OH)}_3(\text{s})]$$

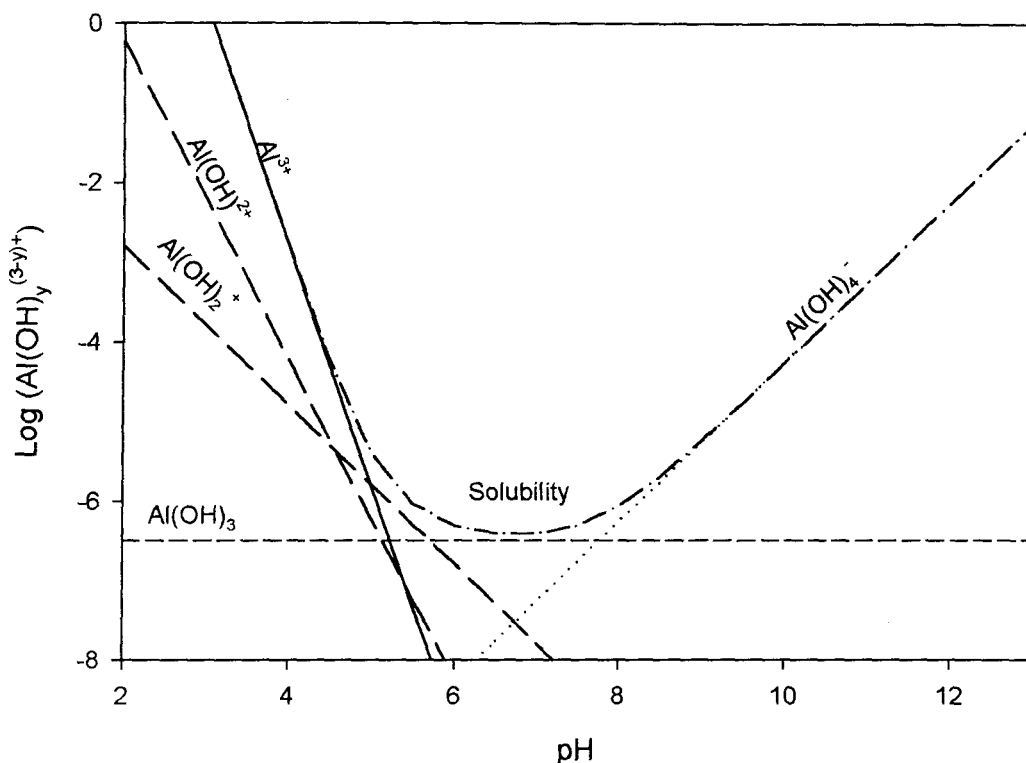


Figure 6.2-1: Distribution of hydrolysis products in Al only system, 0.1 mmol.dm⁻³ KNO₃, 25°C.

6.2.2. The Al/Morin system

• *Species in solution*

Although morin is a pentaprotic acid, it is described with a monoprotic model in the acidic pH range (Browne et al. 1990a; Browne et al. 1990b). The first deprotonation is more likely to occur on the 3-hydroxy group due to the proximity of the 4-keto oxygen. The

deprotonated morin ($L = H_4Mor^-$) can then react with Al to form a 1:1 complex. Higher order complexes are unlikely to form in the acidic pH range as further deprotonation would not occur below pH 7. The chemistry of the 1:1 complex can be described as the formation of 3 complexes: (i) AlL , (ii) $AlL(OH)$, (iii) $AlL(OH)_2$. Before going any further in the quantification of any data, it was necessary to discriminate which species of morin were actually fluorescing. In order to address this point, AlM (i.e. the fluorescing complex) was measured by fluorimetry over the acidic pH range for $[Al] = 0.5 \mu mol.dm^{-3}$ and $[morin] = 12.5 \mu mol.dm^{-3}$. The evolution of I_f was then compared to the calculated hydrolysis profiles of (i) AlL , (ii) $AlL(OH)$, (iii) $AlL(OH)_2$ and (iv) $AlL + AlL(OH) + AlL(OH)_2$. The results are shown in Figure 6.2-2. In view of these results, the assumption that $[AlM] = [AlL] + [AlL(OH)] + [AlL(OH)_2]$ was made and sustained for the rest of the calculation process. A distribution of the Al hydrolysis products in presence of $[morin] = 12.5 \mu mol.dm^{-3}$ at $25^\circ C$ is depicted in Figure 6.2-3. Consequently, a general equilibrium constant for AlM formation could be described as:

$$[AlM] = [AlL] + [AlL(OH)] + [AlL(OH)_2]$$

$$[AlM] = \beta_{1,0} [M^-] [Al^{3+}] + \beta_{1,1} \frac{[M^-] [Al^{3+}]}{[H^+]} + \beta_{1,2} \frac{[M^-] [Al^{3+}]}{[H^+]^2}$$

$$[AlM] = \left(\beta_{1,0} + \frac{\beta_{1,1}}{[H^+]} + \frac{\beta_{1,2}}{[H^+]^2} \right) [M^-] [Al^{3+}]$$

$$K_{AlM} = \frac{[AlM]}{[M^-][Al^{3+}]} = \beta_{1,0} + \frac{\beta_{1,1}}{[H^+]} + \frac{\beta_{1,2}}{[H^+]^2}$$

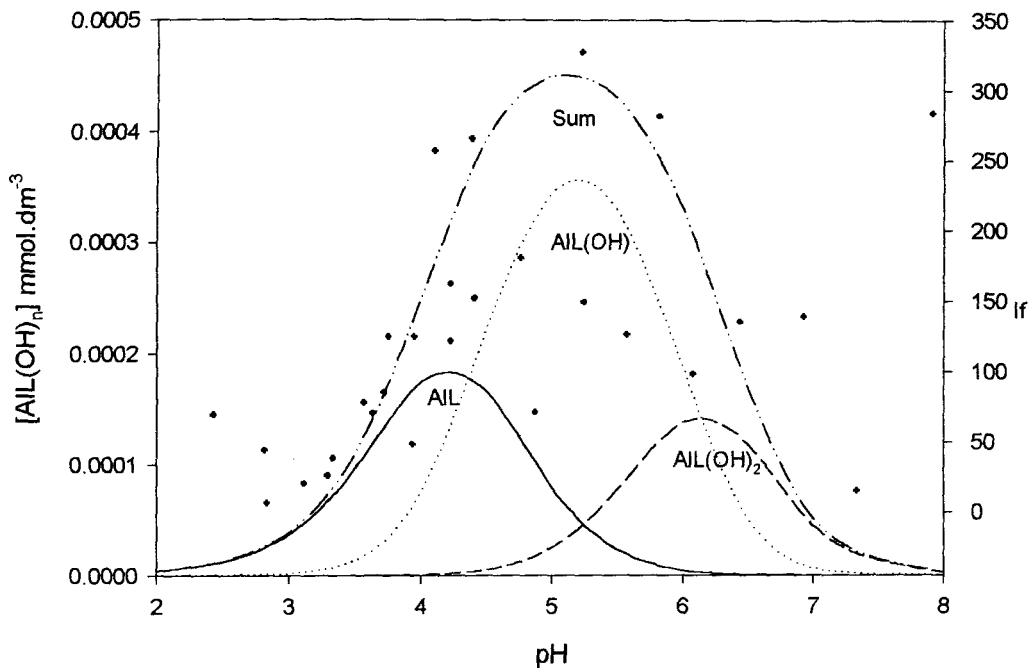
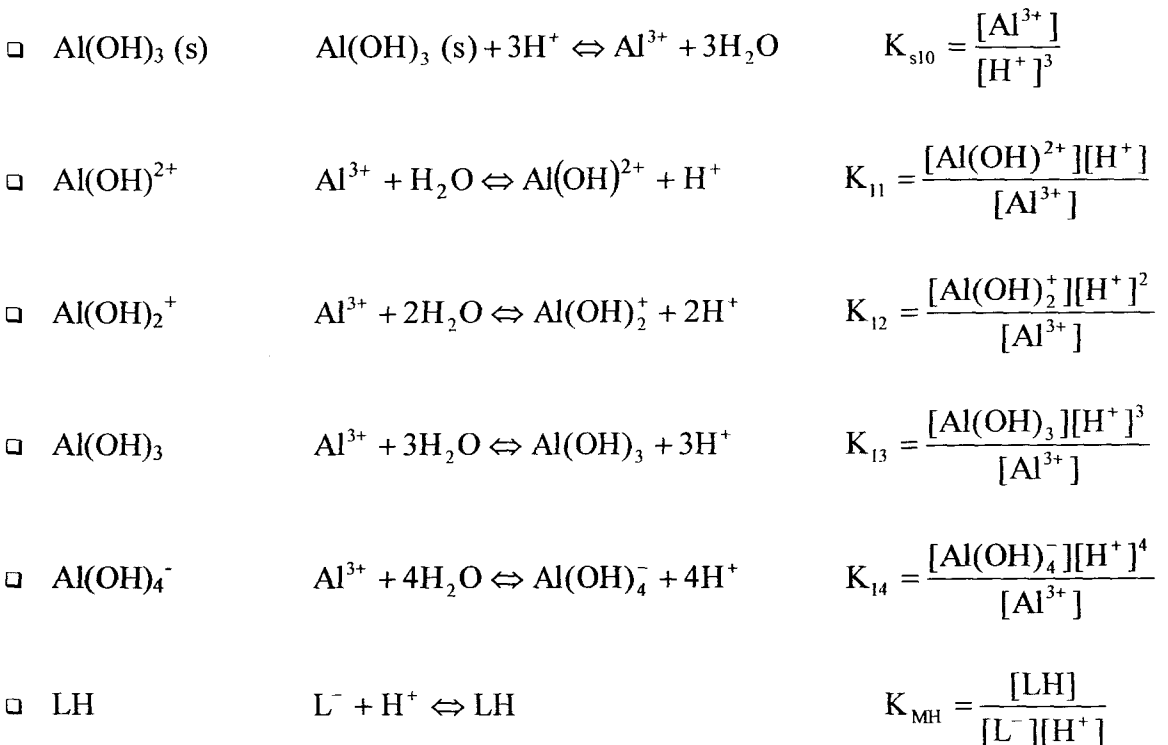
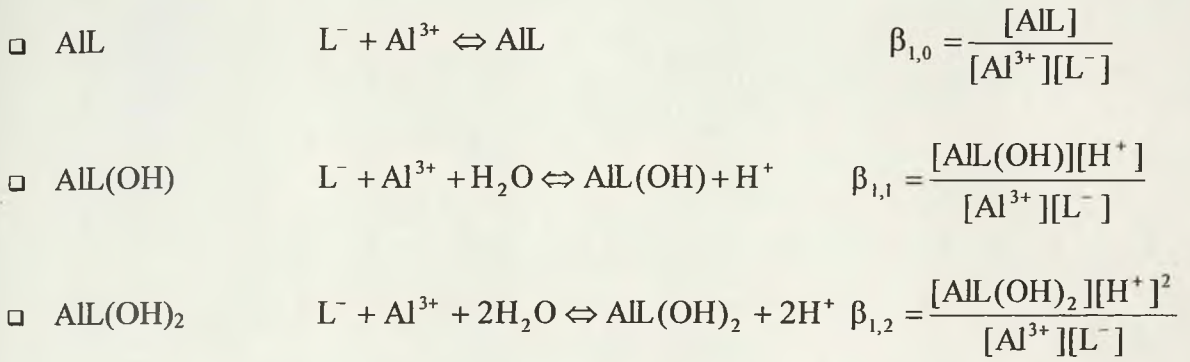


Figure 6.2-2: $[Al] = 0.5 \mu\text{mol.dm}^{-3}$, $[\text{morin}] = 12.5 \mu\text{mol.dm}^{-3}$. Lines: $Al(OH)_n$ hydrolysis profiles calculated using SGW. Dot: experimental I_f measured by fluorimetry.

• *Equilibrium reactions*





• Mass balance relationships

$$[\text{AlM}] = [\text{AIL}] + [\text{AIL(OH)}] + [\text{AIL(OH)}_2]$$

$$[\text{morin}] = [\text{L}^-] + [\text{LH}] + [\text{AlM}]$$

$$[\text{Al}] = \underbrace{[\text{Al}^{3+}] + [\text{Al(OH)}^{2+}] + [\text{Al(OH)}_2^+] + [\text{Al(OH)}_3] + [\text{Al(OH)}_4^-]}_{\text{Monomeric species}} + \underbrace{[\text{AlM}] + [\text{Al(OH)}_3(\text{s})]}_{\text{Fluorescent aluminium}}$$

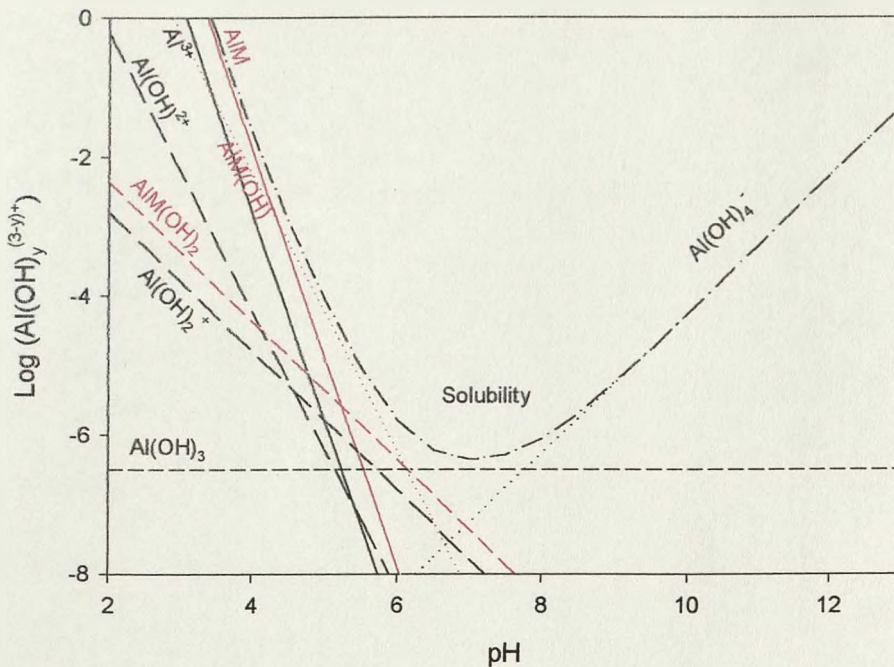


Figure 6.2-3: Distribution of hydrolysis products in Al/Mor system, 0.1 mmol.dm⁻³ KNO₃, 25°C.

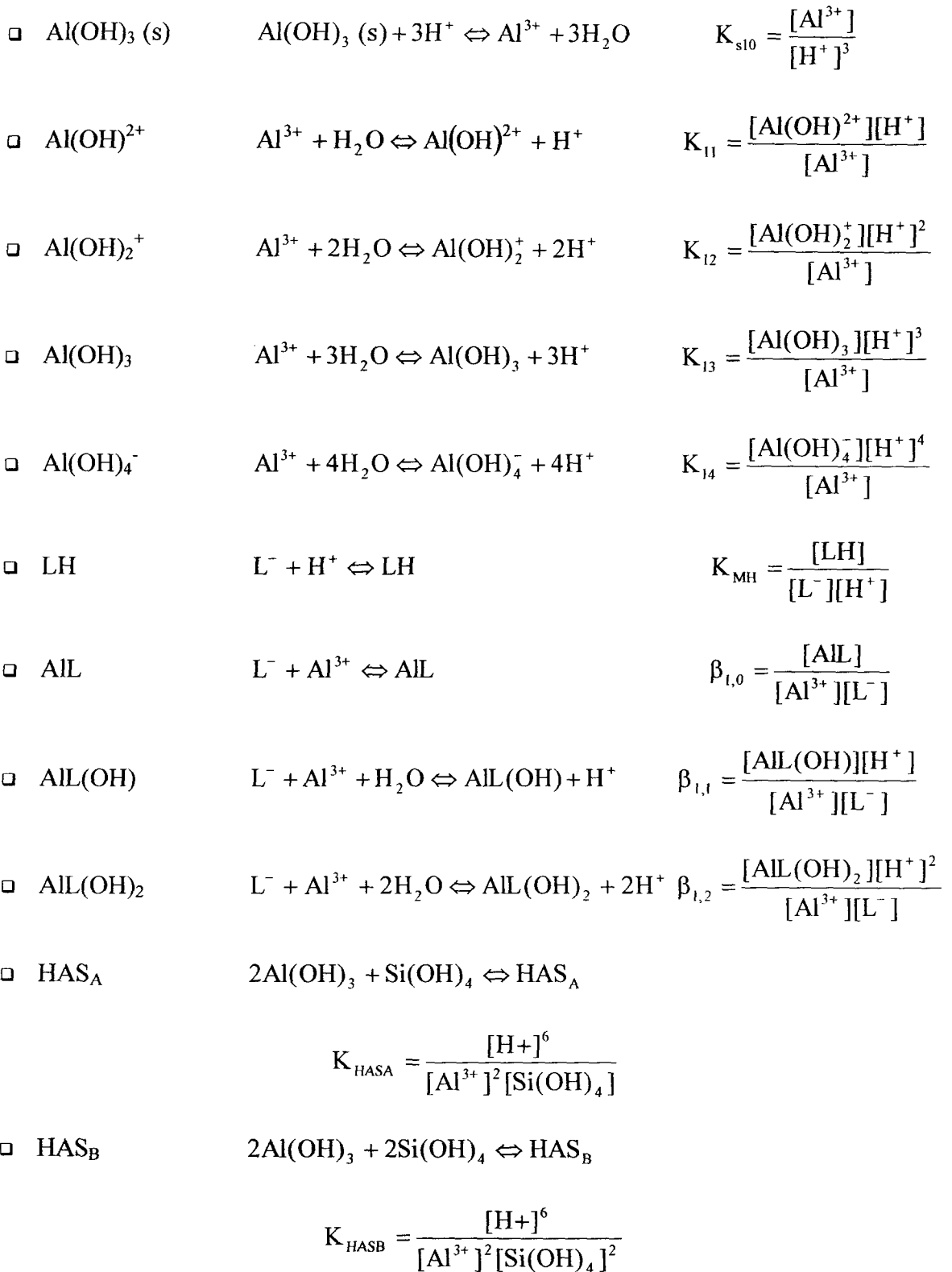
$$[\text{morin}] = 12.5 \mu\text{mol.dm}^{-3}$$

6.2.3. The Al/Si(OH)₄/Morin system

• *Species in solution*

Several studies have been carried out on the interaction between Al and Si(OH)₄ leading to the identification of soluble aluminosilicates of proposed formula AlH₃SiO₄²⁺ (Browne and Driscoll 1992; Farmer and Lumsdon 1994; Gout et al. 1999; Pokrovski et al. 1996). However the stability of this species at solution pH > 4 has been disputed (Exley and Birchall 1995) and no direct characterisation of AlH₃SiO₄²⁺ has, as yet, been possible. On the other hand, HAS have been identified and precipitated from acidic solutions of Si(OH)₄ and Al (Exley et al. 2002; Lou and Huang 1988; Lumsdon and Farmer 1995; Wada and Kubo 1975). It was also suggested that the mechanism of formation of HAS involved the competitive condensation of Si(OH)₄ with hydroxyaluminium templates (Exley and Birchall 1992b; Exley and Birchall 1993). Characterisation of the precipitated materials by ²⁹Si and ²⁷Al solid-state NMR coupled with SEM-EDX showed that depending on the Al:Si ratio in the parent solution two forms of HAS can precipitate (Doucet et al. 2001b). When Al is in excess in solution, HAS are made up of octahedral Al and Q³(3Al) Si with a Si:Al ratio in the material around 0.5; these HAS are referred to as HAS_A. When Si(OH)₄ is present in excess in the parent solution, the material collected is found to be a mixture of a small percentage of HAS_A and a majority of Al and Si tetrahedra referred to as HAS_B and the Si:Al ratio in the material is around 1. These results led to a proposed unit structure of (i) HAS_A: 2 Al for 1 Si(OH)₄ and (ii) HAS_B: 2 Al for 2 Si(OH)₄.

•Equilibrium reactions



• *Mass balance relationships*

$$[AlM]=[AlL]+[AlL(OH)]+[AlL(OH)_2]$$

$$[morin]=[L^-]+[LH]+[AlM]$$

$$[Al] = [Al^{3+}] + [Al(OH)^{2+}] + [Al(OH)_2^+] + [Al(OH)_3] + [Al(OH)_4^-] + [AlM] +$$

Monomeric species

Fluorescent aluminium

$$[Al(OH)_3](s) + 2[HAS]$$

6.2.4. Equilibrium constants

Equilibrium constants are strongly dependant upon the medium in which the solutions are prepared. It was therefore necessary to correct the values obtained in the literature in order to take into account the influence of the ionic strength of the salt present in solution. Throughout all of my study, I prepared samples in a 0.1 mol.dm⁻³ KNO₃ medium.

The corrected constant Q_{xy} can be expressed as:

$$\log Q_{xy} = \log K_{xy} + \frac{aI^{1/2}}{(1+I^{1/2})} + bm_x \quad (\text{Baes and Mesmer 1976})$$

where K_{xy} is the equilibrium constant, I the ionic strength, m the molality of the medium (moles/kg of water) and a and b are temperature dependent constants.

The ionic strength is expressed as :

$$I = \frac{1}{2} \sum c_i \times z_i^2$$

For 0.1 mol.dm⁻³ KNO₃, $m/c = 1.0046$ and $I = 0.1$.

The modified constants are given in Table 6.2-1.

Table 6.2-1: Corrected equilibrium constants for 0.1 mol.dm⁻³ KNO₃ medium at 25°C. (1) Baes and Mesmer, 1976 (2) Browne et al, 1990.

	Log K _{xy}	a ⁽¹⁾	b ⁽¹⁾	Log Q _{xy}
K _{s10}	8.5 ⁽¹⁾	3.066	-0.45	9.19
K ₁₁	-4.97 ⁽¹⁾	-2.044	0.52	-5.41
K ₁₂	-9.3 ⁽¹⁾	-3.066	0.55	-9.98
K ₁₃	-15 ⁽¹⁾	-3.066	0.45	-15.69
K ₁₄	-23 ⁽¹⁾	-2.044	0.36	-23.45
K _{MH}	5.04 ⁽²⁾	-	-	-
β _{1,0}	5.86 ⁽²⁾	-	-	-
β _{1,1}	1.50 ⁽²⁾	-	-	-
β _{1,2}	-4.63 ⁽²⁾	-	-	-

6.3. Calculations using the fluorimetry data and SGW

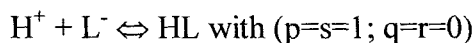
The matrix used for the purpose of calculations with the software SGW is presented in Table 6.3-1. The system is defined by its compounds (C) and a reaction can be then generally written as:



and its equilibrium is ruled by the constant:

$$\beta_{pqrs} = \frac{[(\text{H}^+)_p (\text{Al}^{3+})_q (\text{Si}(\text{OH})_4)_r (\text{L}^-)_s]}{[\text{H}^+]^p [\text{Al}^{3+}]^q [\text{Si}(\text{OH})_4]^r [\text{L}^-]^s}$$

For example, the first protonation of morin (L⁻) is:



In order to define fully a system, it is then necessary (i) to identify all the present reactions, (ii) to find the right value for $\log\beta$ in accordance with the initial system (iii) to specify the phase of the product of the reaction (soluble/solid). The matrix summarises all the possible reactions considered in the system.

Table 6.3-1: Matrix used for the calculations by SGW.

<i>Species</i>	<i>Log β_{pqrs}</i>		<i>p</i>	<i>q</i>	<i>r</i>	<i>s</i>	<i>Phase</i>	
H^+	0	C	1	0	0	0	Soluble	Use
Al^{3+}	0	C	0	1	0	0	Soluble	Use
$Si(OH)_4$	0	C	0	0	1	0	Soluble	Use
L^-	0	C	0	0	0	1	Soluble	Use
HL	5.04		1	0	0	1	Soluble	Use
$Al(OH)^{2+}$	-5.41		-1	1	0	0	Soluble	Use
$Al(OH)_2^+$	-9.98		-2	1	0	0	Soluble	Use
$Al(OH)_3$	-15.69		-3	1	0	0	Soluble	Use
$Al(OH)_4^-$	-23.45		-4	1	0	0	Soluble	Use
Al_{13}	-98.73		-32	13	0	0	Soluble	Not use
AIL	5.86		0	1	0	1	Soluble	Use
AILOH	1.5		-1	1	0	1	Soluble	Use
$AIL(OH)_2$	-4.63		-2	1	0	1	Soluble	Use
$Al(OH)_3(s)$	-9.19		-3	1	0	0	Solid	Use
HAS_A	?		-6	2	1	0	Solid	Use
HAS_B	?		-6	2	2	0	Solid	Use

6.3.1. Calibration

The first step towards the determination of the equilibrium constant of formation of HAS was the quantification of the fluorimetric data obtained as described in Chapter 5. For this purpose it was first necessary to establish a relationship between the results obtained by fluorimetry for the Al/Mor system at equilibrium (If after 12 weeks) and the species concentrations calculated using the software SGW from $[Al]_{GFAAS}$ ($[AlM]$) such as :

$$[AlM] = f(If)$$

In order to ensure that the measurement of AlM species in the calibration was not affected by the precipitation of $Al(OH)_3$, the measurements of AlM by fluorimetry and the related

calculations by SGW were performed for undersaturated solutions of [Al], i.e. [Al] = 0.1, 0.2, 0.3, 0.4, 0.5 $\mu\text{mol}\cdot\text{dm}^{-3}$ and [Mor]= 12.5 $\mu\text{mol}\cdot\text{dm}^{-3}$ at pH 6.5.

Figure 6.3-1 plots I_f against [AlM] and the regression showing the relationship between [AlM] and I_f . The above equation could then be expressed as:

$$[\text{AlM}] = 3.062 \times 10^{-10} I_f + 2.289 \times 10^{-12} I_f^2$$

This calibration was then used to quantify the results obtained by fluorimetry for the Al/Morin and Al/Si(OH)₄/Morin systems. The total [Al] in samples was measured by GFAAS, using a matrix-matched calibration (Schneider and Exley 2001). Figure 6.3-2 shows the calculated [AlM] by SGW in the Al/Mor system at equilibrium, compared to the experimentally measured [AlM] in Al/Mor and Al/Si(OH)₄/Mor systems. A relatively good agreement of the experimental results with the calculated concentrations was observed for the Al/Mor system. The theoretical curve reached a plateau when [Al] increased due to the precipitation of Al(OH)₃ which limited the amount of Al available to react with morin. Even if the equilibrium state was not fully reached, the experimental data follows the same trend as those obtained with SGW. A possible explanation for the small discrepancy between calculation and experiment may be the formation of a complex of higher coordination between Al and morin. The assumption that only the first deprotonation of morin takes part in the reaction with Al has always been made in the calculation of equilibrium constant for the AlM species. However, a higher proton dissociation could be responsible for the approximation made during the calibration. The presence of Si(OH)₄ reduced [AlM] in solution at equilibrium. This was noticeable for [Si(OH)₄] as low as 1 $\mu\text{mol}\cdot\text{dm}^{-3}$ but it was highly dependant upon [Si(OH)₄]. [AlM] reached a minimum only in the presence of a huge excess of Si(OH)₄, i.e. for [Si(OH)₄] above 1000 $\mu\text{mol}\cdot\text{dm}^{-3}$.

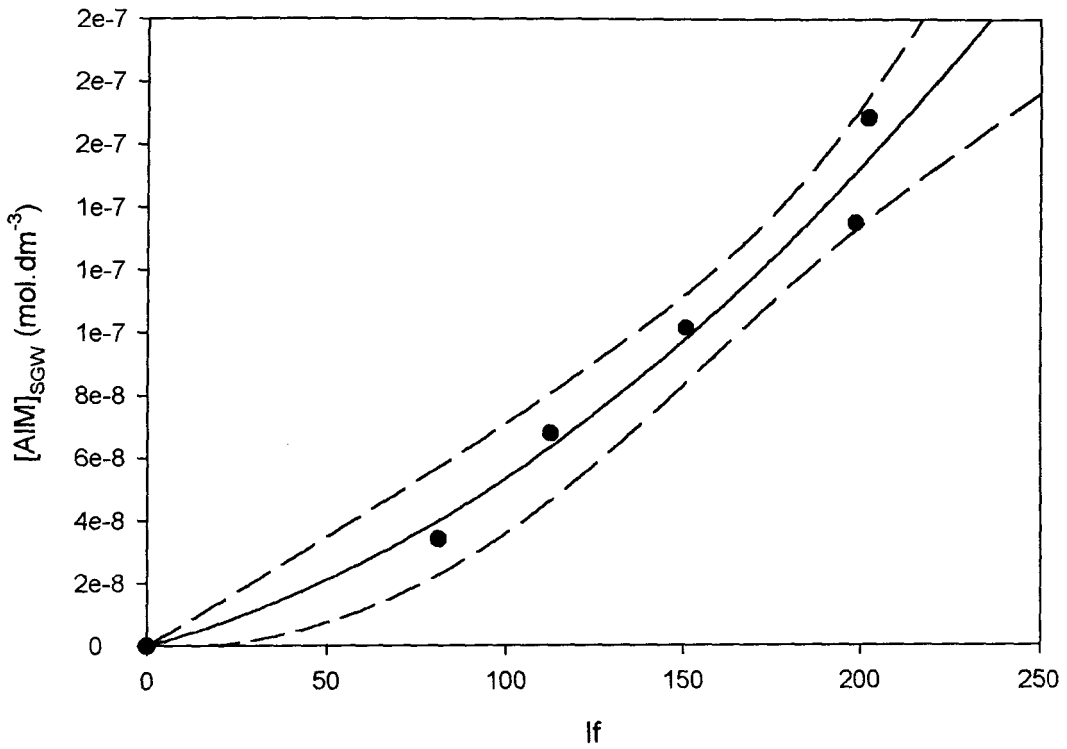


Figure 6.3-1: calibration curve pH = 6.5, $[Al]_{tot} = 0.1, 0.2, 0.3, 0.4, 0.5 \mu\text{mol.dm}^{-3}$, $[Mor] = 12.5 \mu\text{mol.dm}^{-3}$. Dots: experimental data. Solid line: linear regression, $a = 3.0619 \times 10^{-10}$ and $b = 2.289 \times 10^{-12}$. Long dash: confidence intervals (95%).

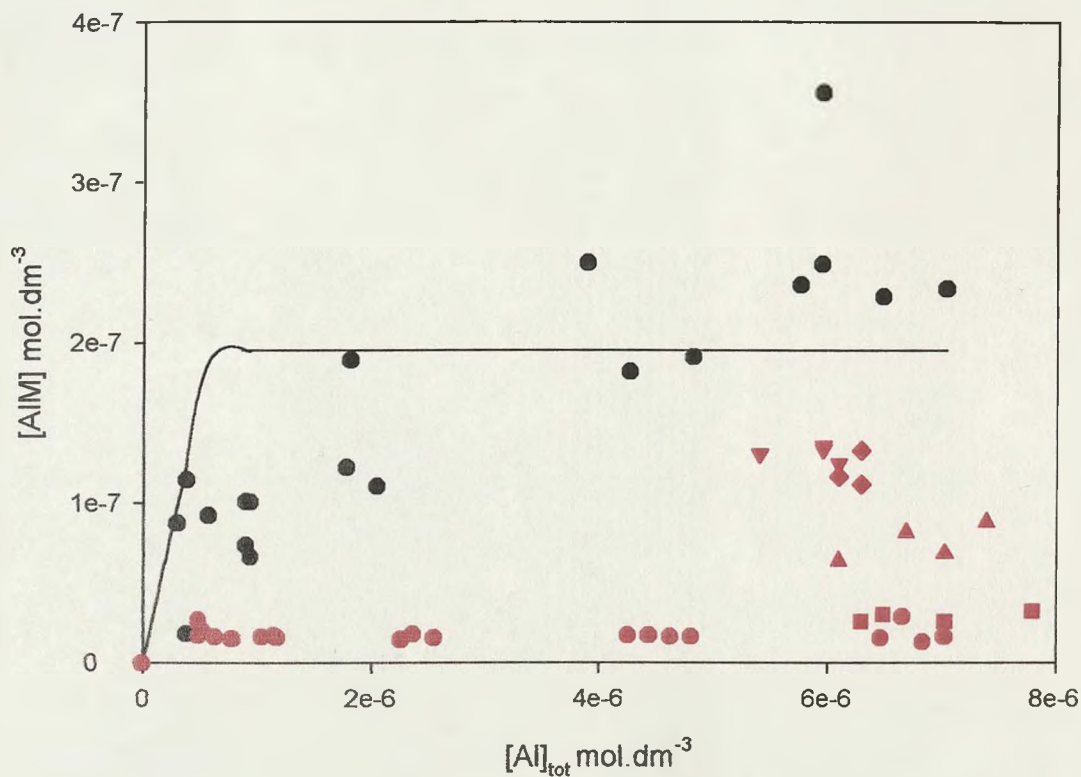


Figure 6.3-2: Effect of $[\text{Si}(\text{OH})_4]$ and $[\text{Al}]_{\text{GFAAS}}$ on $[\text{AlM}]$. Line: $[\text{AlM}]$ as determined by calculations with SGW. Black circle: $[\text{Si}(\text{OH})_4] = 0 \mu\text{mol}\cdot\text{dm}^{-3}$. Red diamond: $[\text{Si}(\text{OH})_4] = 1 \mu\text{mol}\cdot\text{dm}^{-3}$. Red triangle down: $[\text{Si}(\text{OH})_4] = 10 \mu\text{mol}\cdot\text{dm}^{-3}$. Red triangle up: $[\text{Si}(\text{OH})_4] = 100 \mu\text{mol}\cdot\text{dm}^{-3}$. Red square: $[\text{Si}(\text{OH})_4] = 1000 \mu\text{mol}\cdot\text{dm}^{-3}$. Red circle: $[\text{Si}(\text{OH})_4] = 2000 \mu\text{mol}\cdot\text{dm}^{-3}$. $\text{pH} = 6.5$, $[\text{Mor}] = 12.5 \mu\text{mol}\cdot\text{dm}^{-3}$.

6.3.2. Calculation of K_{HAS}

Knowing $[AlM]$ in the presence of $Si(OH)_4$ at equilibrium, it was then possible to determine $[Al^{3+}]$ at equilibrium using the appropriate equation:

$$[Al^{3+}] = \frac{[AlM]}{[M^-]K_{AlM}}$$

The equilibrium concentrations of all the other Al monomeric species were then deduced from $[Al^{3+}]$ using the equilibrium reactions described in the previous section of this chapter. The only unknown is the HAS equilibrium constant. The concentration of solid species, taking in account that there are 2 Al per HAS, can be deduced from the mass balance relationship as:

$$[\text{Solid species}] = [Al]_{\text{tot}} - \Sigma[\text{monomeric species}] = [Al(OH)_3] + 2 [HAS]$$

Table 6.3-1 presents the results of these calculations. Unfortunately, it was then impossible to distinguish between the precipitation of $Al(OH)_3$ and the formation of HAS. In order to get a first estimation of the constant of formation of HAS, it was necessary to consider $Si(OH)_4$ in large excess, i.e. $[Si(OH)_4] = 2 \text{ mmol.dm}^{-3}$. The predominant form of HAS when $Si \gg Al$ was then HAS_B . The highest amount of Al present in the samples being $6 \mu\text{mol.dm}^{-3}$, $[HAS_B] \leq 6 \mu\text{mol.dm}^{-3}$. For that concentration, the formation of HAS_B would affect only slightly the amount of $Si(OH)_4$ present at equilibrium, as the amount of $Si(OH)_4$ involved in the formation of HAS would be negligible ($\leq 12 \mu\text{mol.dm}^{-3}$). I could then calculate an estimated value for K_{HASB} as all the parameters are known:

$$\boxed{\text{Log}K_{HASB} = \text{Log}\left(\frac{[H^+]^6}{[Al^{3+}]^2 [Si(OH)_4]^2}\right) = -10.94 \pm 0.10} \text{ at } 20^\circ\text{C}$$

I used this constant in the SGW software to test its reliability over the total range of the experimental data obtained by fluorimetry. The results obtained with SGW for this

constant are presented into Table 6.3-2 together with the correlation coefficient between experimental and SGW data.

Table 6.3-1: Quantification of the fluorimetry data in presence of $\text{Si}(\text{OH})_4$ and calculations of the different Al species concentrations.

$[\text{Si}(\text{OH})_4]$ μM	[Al] M GFAAS	[AlM] M fluo	[M] M SGW	$[\text{Al}^{3+}]$ M	$[\text{Al}(\text{OH})^{2+}]$ M	$[\text{Al}(\text{OH})_2^+]$ M	$[\text{Al}(\text{OH})_3]$ M	$[\text{Al}(\text{OH})_4^-]$ M	[solid] M
10	5.40E-06	1.41E-07	1.05E-05	4.05E-11	4.99E-10	4.25E-08	2.62E-07	1.44E-08	4.94E-06
10	5.96E-06	1.45E-07	1.03E-05	4.22E-11	5.19E-10	4.42E-08	2.72E-07	1.50E-08	5.48E-06
10	5.96E-06	1.47E-07	1.03E-05	4.26E-11	5.24E-10	4.46E-08	2.75E-07	1.51E-08	5.48E-06
10	6.10E-06	1.34E-07	1.03E-05	3.92E-11	4.83E-10	4.11E-08	2.53E-07	1.39E-08	5.66E-06
100	6.10E-06	6.82E-08	1.03E-05	1.99E-11	2.45E-10	2.08E-08	1.28E-07	7.06E-09	5.88E-06
100	6.70E-06	8.75E-08	1.01E-05	2.59E-11	3.19E-10	2.72E-08	1.68E-07	9.21E-09	6.41E-06
100	7.04E-06	7.33E-08	1.00E-05	2.19E-11	2.70E-10	2.30E-08	1.42E-07	7.78E-09	6.79E-06
100	7.40E-06	9.46E-08	9.95E-06	2.85E-11	3.51E-10	2.99E-08	1.84E-07	1.01E-08	7.08E-06
1000	6.30E-06	2.73E-08	1.02E-05	8.00E-12	9.84E-11	8.37E-09	5.16E-08	2.84E-09	6.21E-06
1000	6.50E-06	3.19E-08	1.02E-05	9.41E-12	1.16E-10	9.85E-09	6.07E-08	3.34E-09	6.39E-06
1000	7.04E-06	2.74E-08	1.00E-05	8.18E-12	1.01E-10	8.57E-09	5.28E-08	2.90E-09	6.95E-06
1000	7.80E-06	3.41E-08	9.85E-06	1.04E-11	1.28E-10	1.09E-08	6.71E-08	3.69E-09	7.68E-06
2000	4.80E-07	2.30E-08	1.19E-05	7.04E-12	8.66E-11	7.37E-09	4.55E-08	2.50E-09	3.97E-07
2000	4.80E-07	1.82E-08	1.19E-05	4.57E-12	5.63E-11	4.79E-09	2.95E-08	1.62E-09	4.26E-07
2000	5.20E-07	2.10E-08	1.19E-05	5.29E-12	6.51E-11	5.54E-09	3.41E-08	1.88E-09	4.57E-07
2000	6.30E-07	1.73E-08	1.19E-05	4.39E-12	5.40E-11	4.59E-09	2.83E-08	1.56E-09	5.78E-07
2000	7.80E-07	1.57E-08	1.18E-05	3.99E-12	4.91E-11	4.18E-09	2.58E-08	1.42E-09	7.33E-07
2000	1.04E-06	1.69E-08	1.17E-05	4.32E-12	5.31E-11	4.52E-09	2.79E-08	1.53E-09	9.89E-07
2000	1.15E-06	1.82E-08	1.17E-05	4.66E-12	5.73E-11	4.88E-09	3.01E-08	1.65E-09	1.10E-06
2000	1.18E-06	1.66E-08	1.17E-05	4.26E-12	5.24E-11	4.46E-09	2.75E-08	1.51E-09	1.13E-06
2000	2.26E-06	1.51E-08	1.14E-05	4.00E-12	4.92E-11	4.19E-09	2.58E-08	1.42E-09	2.21E-06
2000	2.26E-06	1.53E-08	1.14E-05	4.04E-12	4.96E-11	4.23E-09	2.61E-08	1.43E-09	2.21E-06
2000	2.37E-06	1.88E-08	1.13E-05	4.99E-12	6.14E-11	5.22E-09	3.22E-08	1.77E-09	2.31E-06
2000	2.55E-06	1.63E-08	1.13E-05	4.33E-12	5.32E-11	4.53E-09	2.79E-08	1.53E-09	2.50E-06
2000	4.26E-06	1.78E-08	1.08E-05	4.96E-12	6.10E-11	5.19E-09	3.20E-08	1.76E-09	4.20E-06
2000	4.44E-06	1.82E-08	1.07E-05	5.08E-12	6.25E-11	5.32E-09	3.28E-08	1.80E-09	4.38E-06
2000	4.63E-06	1.70E-08	1.07E-05	4.78E-12	5.88E-11	5.00E-09	3.08E-08	1.70E-09	4.58E-06
2000	4.81E-06	1.73E-08	1.06E-05	4.90E-12	6.03E-11	5.13E-09	3.16E-08	1.74E-09	4.75E-06
2000	6.48E-06	1.63E-08	1.02E-05	4.79E-12	5.89E-11	5.02E-09	3.09E-08	1.70E-09	6.43E-06
2000	6.67E-06	3.04E-08	1.01E-05	8.99E-12	1.11E-10	9.42E-09	5.81E-08	3.19E-09	6.57E-06
2000	6.85E-06	1.39E-08	1.01E-05	4.15E-12	5.10E-11	4.34E-09	2.68E-08	1.47E-09	6.80E-06
2000	7.04E-06	1.70E-08	1.00E-05	5.08E-12	6.25E-11	5.32E-09	3.28E-08	1.80E-09	6.98E-06

Table 6.3-2: Concentrations of the main species obtained by SGW using the constant of formation Log

$K_{HASB} = -10.94$. The correlation factor indicates the degree of similarity between the data obtained experimentally by fluorimetry (Table 6.3-1) and those obtained by SGW with 1=identical, 0=different.

[Si(OH) ₄] μM	[Al] M GFAAS	[Si(OH) ₄] M	[AlM] M	[Al ³⁺] M	[Al(OH) ₃](s) M	[HAS] M	[solid] M
10	5.40E-06	1.00E-05	1.95E-07	4.90E-11	4.82E-06	0.00E+00	4.82E-06
10	5.96E-06	1.00E-05	1.95E-07	4.90E-11	5.38E-06	0.00E+00	5.38E-06
10	5.96E-06	1.00E-05	1.95E-07	4.90E-11	5.38E-06	0.00E+00	5.38E-06
10	6.10E-06	1.00E-05	1.95E-07	4.90E-11	5.52E-06	0.00E+00	5.52E-06
100	6.10E-06	1.00E-04	1.95E-07	4.90E-11	5.52E-06	0.00E+00	5.52E-06
100	6.70E-06	1.00E-04	1.95E-07	4.90E-11	6.12E-06	0.00E+00	6.12E-06
100	7.04E-06	1.00E-04	1.95E-07	4.90E-11	6.46E-06	0.00E+00	6.46E-06
100	7.40E-06	1.00E-04	1.95E-07	4.90E-11	6.82E-06	0.00E+00	6.82E-06
1000	6.30E-06	9.94E-04	3.79E-08	9.39E-12	0.00E+00	3.09E-06	6.19E-06
1000	6.50E-06	9.94E-04	3.79E-08	9.39E-12	0.00E+00	3.19E-06	6.39E-06
1000	7.04E-06	9.93E-04	3.79E-08	9.40E-12	0.00E+00	3.46E-06	6.93E-06
1000	7.80E-06	9.92E-04	3.80E-08	9.40E-12	0.00E+00	3.84E-06	7.69E-06
2000	4.80E-07	2.00E-03	1.89E-08	4.67E-12	0.00E+00	2.12E-07	4.24E-07
2000	4.80E-07	2.00E-03	1.89E-08	4.67E-12	0.00E+00	2.12E-07	4.24E-07
2000	5.20E-07	2.00E-03	1.89E-08	4.67E-12	0.00E+00	2.32E-07	4.64E-07
2000	6.30E-07	2.00E-03	1.89E-08	4.67E-12	0.00E+00	2.87E-07	5.74E-07
2000	7.80E-07	2.00E-03	1.89E-08	4.67E-12	0.00E+00	3.62E-07	7.24E-07
2000	1.04E-06	2.00E-03	1.89E-08	4.67E-12	0.00E+00	4.92E-07	9.84E-07
2000	1.15E-06	2.00E-03	1.89E-08	4.67E-12	0.00E+00	5.47E-07	1.09E-06
2000	1.18E-06	2.00E-03	1.89E-08	4.67E-12	0.00E+00	5.62E-07	1.12E-06
2000	2.26E-06	2.00E-03	1.89E-08	4.67E-12	0.00E+00	1.10E-06	2.20E-06
2000	2.37E-06	2.00E-03	1.89E-08	4.67E-12	0.00E+00	1.16E-06	2.31E-06
2000	2.55E-06	2.00E-03	1.89E-08	4.67E-12	0.00E+00	1.25E-06	2.49E-06
2000	4.26E-06	2.00E-03	1.89E-08	4.68E-12	0.00E+00	2.10E-06	4.20E-06
2000	4.44E-06	2.00E-03	1.89E-08	4.68E-12	0.00E+00	2.19E-06	4.38E-06
2000	4.63E-06	2.00E-03	1.89E-08	4.68E-12	0.00E+00	2.29E-06	4.57E-06
2000	4.81E-06	2.00E-03	1.89E-08	4.68E-12	0.00E+00	2.38E-06	4.75E-06
2000	6.48E-06	1.99E-03	1.89E-08	4.68E-12	0.00E+00	3.21E-06	6.42E-06
2000	6.67E-06	1.99E-03	1.89E-08	4.68E-12	0.00E+00	3.31E-06	6.61E-06
2000	6.85E-06	1.99E-03	1.89E-08	4.68E-12	0.00E+00	3.40E-06	6.79E-06
2000	7.04E-06	1.99E-03	1.89E-08	4.68E-12	0.00E+00	3.49E-06	6.98E-06
Correlation coefficient			0.93	0.93			0.99

Figure 6.3-3 presents $[Al^{3+}]$ obtained both by fluorimetry and by SGW using K_{HASB} for the different $[Al]$ and $[Si(OH)_4]$. The calculations made with SGW fitted almost perfectly the experimental data (correlation > 0.9) indicating the validity of the constant K_{HASB} . For $[Al] > 2 \mu\text{mol}\cdot\text{dm}^{-3}$, the calculated $[Al^{3+}]$ was very similar to the fluorimetric $[Al^{3+}]$ for all $[Si(OH)_4]$. One can notice that for $[Al] < 2 \mu\text{mol}\cdot\text{dm}^{-3}$, the $[Al^{3+}]$ obtained by fluorimetry at $[Si(OH)_4]$ was underestimated. The fluorimetric measurements indicated a lower $[Al^{3+}]$ than predicted by the calculations using SGW. This could be the result of working under saturation. Indeed, at pH 6.5 and $[Al] = 0.5 \mu\text{mol}\cdot\text{dm}^{-3}$, no $Al(OH)_{3(s)}$ is expected to precipitate. In my approach, the formation of $Al(OH)_3$ was a prerequisite to the formation of HAS and this condition was implied in the constant itself. Therefore, when $Al(OH)_{3(s)}$ is not formed, i.e. below saturation, HAS could not be formed and consequently, the formation of AIM should not be affected by the presence of $Si(OH)_4$. This could also be the result of the approximation inherent to the calibration.

The use of SGW also gave access to very important information on the respective amounts of $Al(OH)_{3(s)}$ and HAS formed whereas fluorimetry could only give the total amount of solid species formed. Figure 6.3-4 presents the effect of $[Si(OH)_4]$ on the formation of HAS_B and $Al(OH)_{3(s)}$ for the different $[Al]$ used experimentally. For $[Si(OH)_4] = 2000$ and $1000 \text{ mmol}\cdot\text{dm}^{-3}$, HAS was the only solid species formed in preference to $Al(OH)_{3(s)}$ for each $[Al]$ tested. Furthermore, the molar fraction of HAS to the total amount of Al was higher than the molar fraction of $Al(OH)_{3(s)}$ expected in absence of $Si(OH)_4$. This observation indicated that HAS is more stable than $Al(OH)_{3(s)}$. However, for smaller amounts of $Si(OH)_4$ ($[Si(OH)_4] = 100$ and $10 \mu\text{mol}\cdot\text{dm}^{-3}$), $Al(OH)_{3(s)}$ precipitated in preference to HAS_B despite $[Si(OH)_4]$ being in excess to $[Al]$. This could be explained by the fact that the $[Al]$ studied were very small ($[Al]_{\text{max}} = 7.04 \mu\text{mol}\cdot\text{dm}^{-3}$). Under these conditions, $Al(OH)_{3(s)}$ is easily formed. A great excess of $Si(OH)_4$ was therefore necessary

to shift the equilibrium towards a more stable state by forming HAS_B . This also indicated the limit of formation of HAS_B . For $[\text{Al}]$ below $10 \mu\text{mol}\cdot\text{dm}^{-3}$, it seems that a huge excess of $\text{Si}(\text{OH})_4$ (at least 100 fold) is necessary at pH 6.5 to form HAS_B .

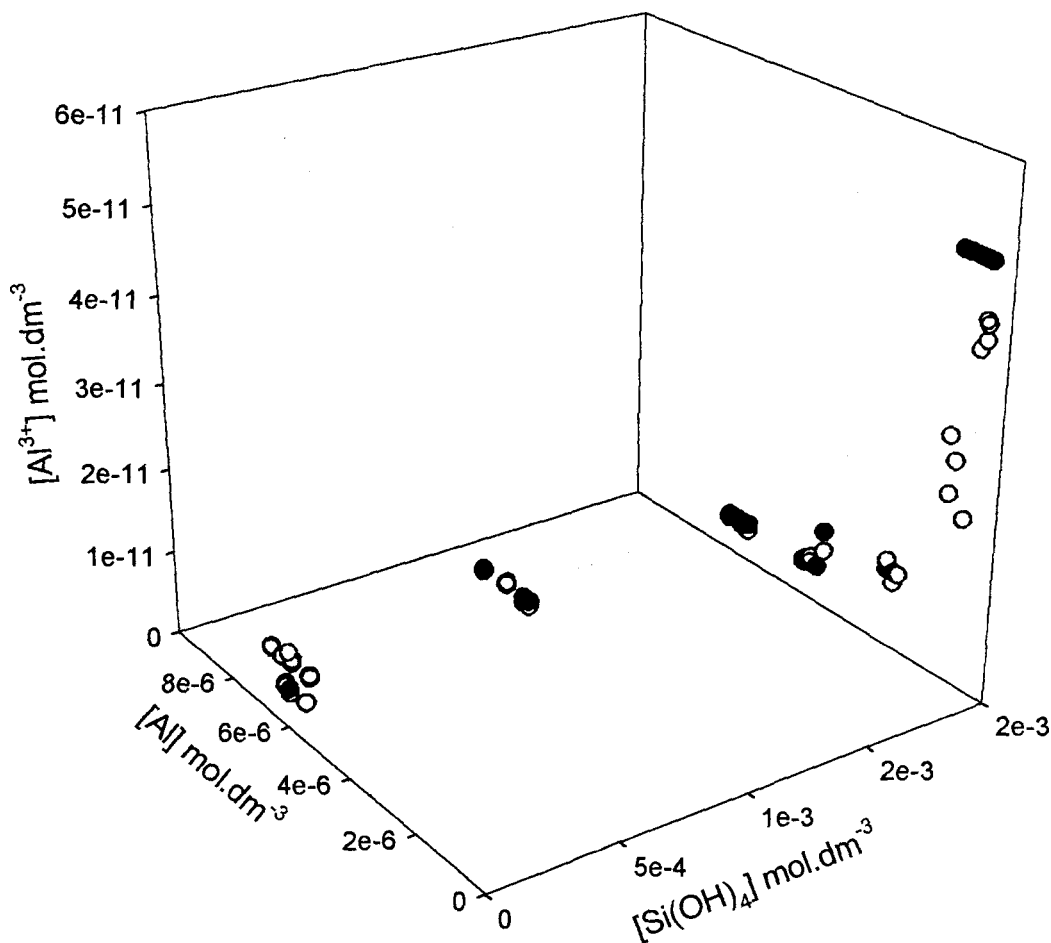


Figure 6.3-3: Comparison of $[\text{Al}^{3+}]$ obtained either from fluorimetric data (open circles) or from SGW using $\text{Log } K_{\text{HASB}} = -10.94$ (closed circled).

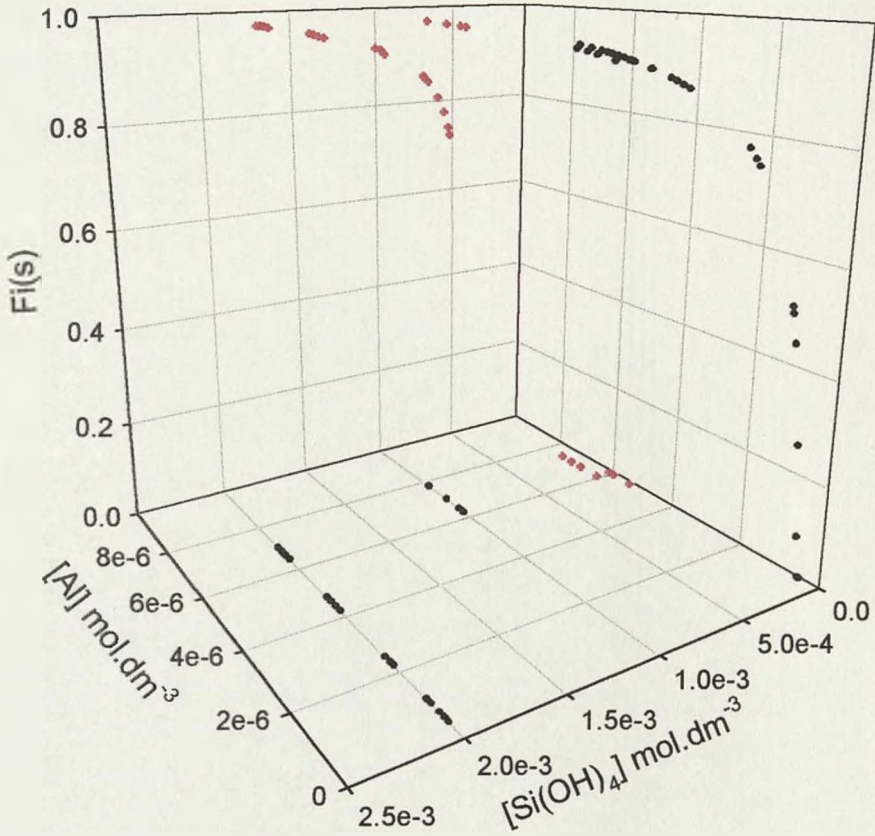


Figure 6.3-4: Influence of $[\text{Si}(\text{OH})_4]$ and $[\text{Al}]$ at pH 6.5 on the formation of $\text{Al}(\text{OH})_3$ (black dot) and HAS_B (red dot) as determined by SGW using $\text{Log } K_{\text{HAS}_B} = -10.94$. $F_i(s)$ is the molar fraction of solid = $[\text{solid species}]/[\text{Al}]$.

6.4. The use of K_{HASB} to describe Al/Si(OH)₄ systems

The value determined in the previous section of this chapter for $\text{Log } K_{HASB} = -10.94$, at 20°C, was proved to be in accordance with the experimental results measured by fluorimetry. It was now necessary (i) to determine the limiting parameters for which HAS_B will form, (ii) to compare the results predicted by calculations to experimentally known $[HAS]$ and (iii) to compare K_{HASB} to other constants of formation.

6.4.1. The limits of formation of HAS_B

In order to determine the limiting parameters (pH, $[Al]$, $[Si(OH)_4]$) for which HAS_B will form, SGW was used to study several Al/Si(OH)₄ systems. By definition, HAS_B can form only if $Al(OH)_3$ templates are present. This predicates that the minimum $[Al]$ required for the formation of HAS_B is above the minimum solubility. In the previous section, it was shown that, at pH 6.5, $[Al]$ as little as $0.5 \mu\text{mol}\cdot\text{dm}^{-3}$ could form HAS_B if $[Si(OH)_4] = 2000 \mu\text{mol}\cdot\text{dm}^{-3}$. This would be the starting point of this study. Figure 6.4-1 presents the distribution of species for $[Al] = 0.5 \text{ mmol}\cdot\text{dm}^{-3}$ and $[Si(OH)_4] = 2000 \mu\text{mol}\cdot\text{dm}^{-3}$ with pH. There was no $Al(OH)_3(s)$ formed under these conditions. HAS_B formed in the pH range: 5-8.75 and reached a maximum for pH = 6.75. Figure 6.4-2 shows the influence of $[Si(OH)_4]$ and pH on the formation of HAS_B for $[Al] = 0.5 \mu\text{mol}\cdot\text{dm}^{-3}$. For $[Si(OH)_4]$ below $200 \mu\text{mol}\cdot\text{dm}^{-3}$, $Al(OH)_3(s)$ precipitates in preference of HAS_B . When $[Si(OH)_4]$ decreased from $2000 \mu\text{mol}\cdot\text{dm}^{-3}$ to $200 \mu\text{mol}\cdot\text{dm}^{-3}$, $[HAS_B]$ decreased but the pH of maximum formation stayed the same. The width of the pH range for which HAS_B is formed decreased as well around the pH of maximum formation, i.e. pH 6.75. The minimum amount of $Si(OH)_4$ required for the formation of HAS_B is $200 \mu\text{mol}\cdot\text{dm}^{-3}$ in the pH range 6-7.25 with a maximum at pH 6.75.

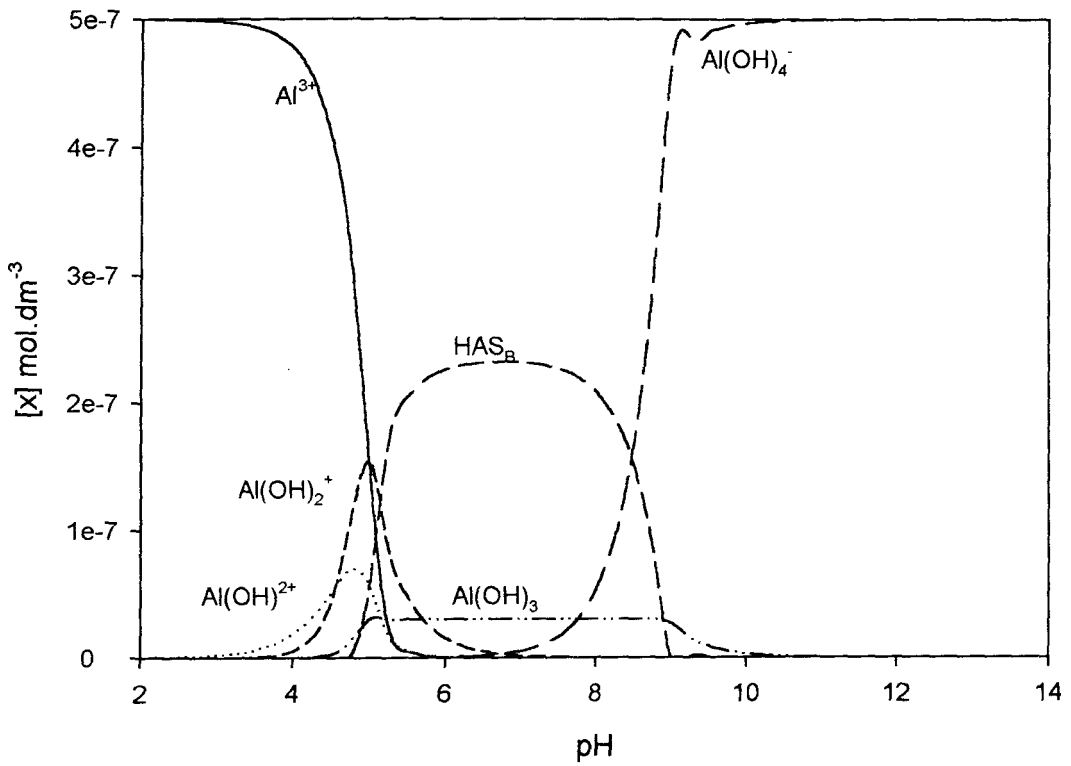


Figure 6.4-1: Distribution of species for $[Al] = 0.5 \mu\text{mol.dm}^{-3}$ and $[Si(OH)_4] = 2000 \mu\text{mol.dm}^{-3}$ at 20°C .

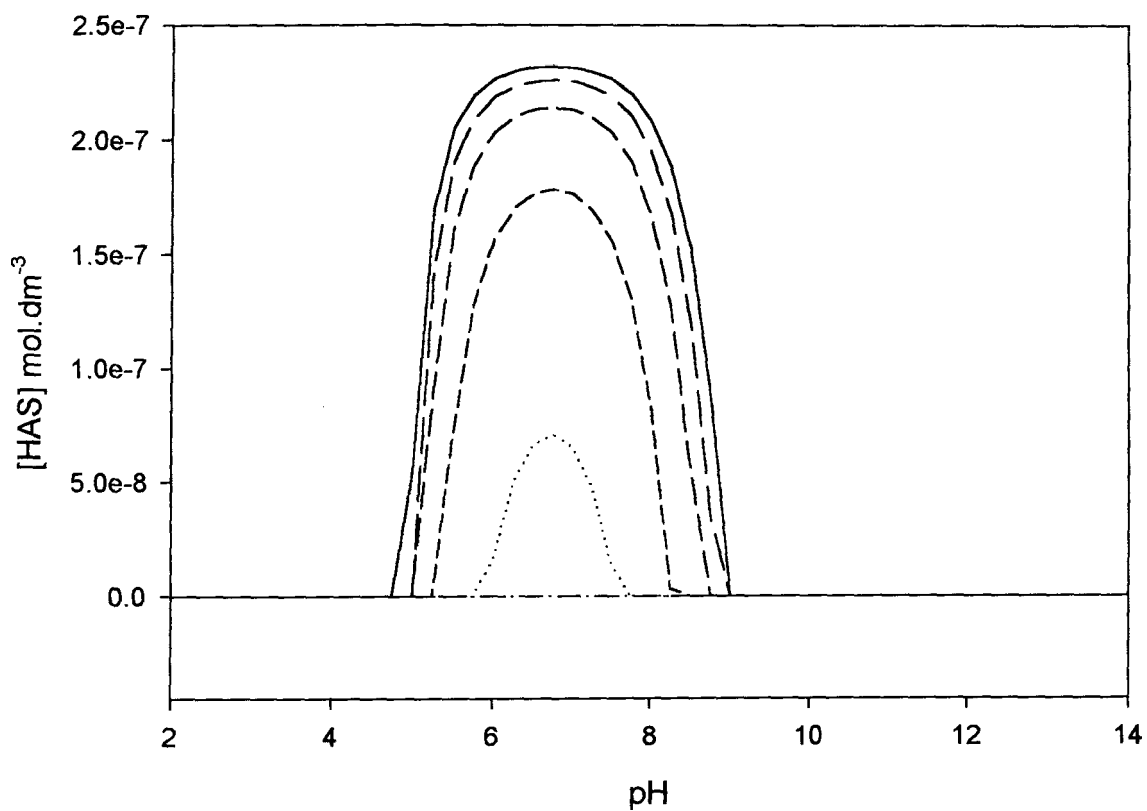


Figure 6.4-2: Effect of $[\text{Si(OH)}_4]$ and pH on the formation of HAS_B for $[\text{Al}] = 0.5 \mu\text{mol.dm}^{-3}$. Solid: $[\text{Si(OH)}_4] = 2000 \mu\text{mol.dm}^{-3}$; long dash: $[\text{Si(OH)}_4] = 1500 \mu\text{mol.dm}^{-3}$; medium dash: $[\text{Si(OH)}_4] = 1000 \mu\text{mol.dm}^{-3}$; short dash: $[\text{Si(OH)}_4] = 500 \mu\text{mol.dm}^{-3}$; dotted: $[\text{Si(OH)}_4] = 200 \mu\text{mol.dm}^{-3}$; dash-dot: $[\text{Si(OH)}_4] = 190 \mu\text{mol.dm}^{-3}$.

6.4.2. Comparison between calculations and previous experimental results

Doucet used membrane filtration to identify the formation of HAS at different pH and parent solution Al:Si ratios (Doucet et al. 2001a). He used GFAAS to measure [Al] before and after filtration, to give an indirect measurement of [Al] present in the solid material collected on the membrane (pore size: 0.1 μm). The solutions he studied were 6 months old. I used SGW on the same set of data to compare the experimental results with the calculated predictions. Table 7.4-1 presents the measurements before and after filtration and the results of the calculations by SGW. In micro-filtration, the estimated amount of species in solid, $[\text{Al}]_{\text{solid}}$ and $[\text{Si}]_{\text{solid}}$, were calculated as the difference between the total amount present in the parent solution and the amount left in solution after filtration, i.e. $[\text{Al}]_{<0.1\mu\text{m}}$ and $[\text{Si}]_{<0.1\mu\text{m}}$. In SGW, $[\text{Al}]_{\text{solid}}$ is calculated from $[\text{HAS}_B]$ as $[\text{Al}]_{\text{solid}}=2[\text{HAS}_B]$ and $[\text{Si}]_{\text{solid}}$ was the difference between the total amount of Si in the parent solution and $[\text{Si}(\text{OH})_4]$ at equilibrium.

Table 6.4-1: Comparison of experimental measurement of [Al] and [Si] by micro-filtration and calculations with SGW under the same conditions. The parent solution Al:Si ratio is given in $\mu\text{mol.dm}^{-3}$. ³ $[\text{Al}]_{<0.1\mu\text{m}}$ and $[\text{Si}]_{<0.1\mu\text{m}}$ are the concentrations measured in the filtrate (Doucet et al. 2001a). $[\text{Al}]_{\text{solid}}$ and $[\text{Si}]_{\text{solid}}$ are the concentration of species in the material collected. All concentrations are given in $\mu\text{mol.dm}^{-3}$.

Al/Si solution	pH	Micro-filtration				SGW		
		$[\text{Al}]_{<0.1\mu\text{m}}$	$[\text{Si}]_{<0.1\mu\text{m}}$	$[\text{Al}]_{\text{solid}}$	$[\text{Si}]_{\text{solid}}$	$[\text{HAS}_B]$	$[\text{Al}]_{\text{solid}}$	$[\text{Si}]_{\text{solid}}$
25/50	3.98	22.1	44.9	2.9	5.1	0	0	0
50/100	3.97	41.6	79.0	8.4	21.0	0	0	0
250/500	3.98	211.7	361.2	38.3	138.8	0	0	0
1000/2000	3.97	782.7	1408.3	217.3	591.7	353	706	707
25/50	4.88	18.2	45.5	6.8	4.5	0	0	0
50/100	4.79	34.0	93.5	16.0	6.5	0	0	0
250/500	4.53	71.3	412.8	178.7	87.2	108	216	216
1000/2000	4.54	52.6	1194.4	947.4	805.6	496	992	991
25/50	5.49	1.0	41.4	24.0	8.6	0	0	0
50/100	5.51	12.4	66.4	37.6	33.6	0	0	0
250/500	5.53	23.8	252.1	226.2	247.9	125	250	249
1000/2000	5.51	346.3	809.2	653.7	1190.8	500	1000	1000

The distribution of Al species with pH for several parent solutions Al:Si ratios (expressed in $\text{mmol}\cdot\text{dm}^{-3}$) = 0.025/0.050, 0.05/0.1, 0.25/0.5, 1/2 are presented in Figures 6.4-3 (a) (b) (c) and (d) respectively. The results found by SGW were in correlation with the observations made using filtration especially at higher pH and for Al:Si > 250/500. The presence of Si and Al in some of the material collected by filtration when not predicted by SGW could however account for the formation of HAS_A. Doucet showed that HAS formed at low pH and in parent solution containing low [Al] and [Si(OH)₄] had a Si:Al ratio close to 0.5, indicating the formation of HAS_A. SGW used the constant KHAS_B and cannot therefore predict the formation of HAS_A as no constant describing this reaction is known.

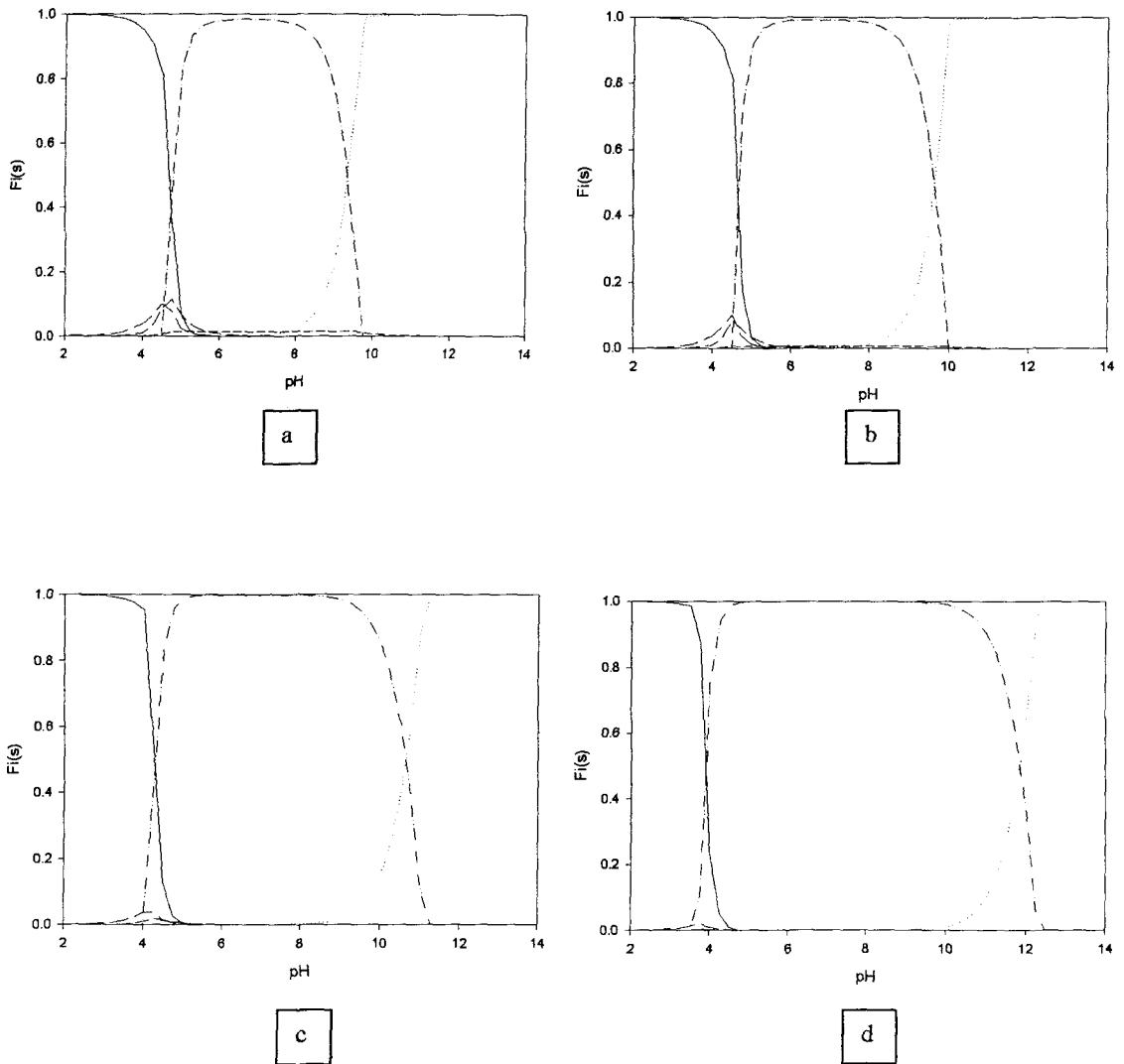


Figure 6.4-3: Distribution of Al species with pH. (a) Al:Si = 0.025/0.05; (b) Al:Si = 0.05/0.1; (c) Al:Si = 0.25/0.5; (d) Al:Si = 1/2. Solid: Al^{3+} ; long dash: $Al(OH)^{2+}$; medium dash: $Al(OH)_2^+$; short dash: $Al(OH)_3$; dotted: $Al(OH)_4^-$; dash-dot: $Al(OH)_3(s)$; dash-dot-dot: HAS_B . Species are expressed as molar fraction to the total amount of Al.

6.5. Conclusions

The combination of fluorimetry measurements and calculations using SGW for the quantification of those measurements led to the determination of an equilibrium constant of the formation of HAS_B, with an estimated value of:

$$\text{Log } K_{\text{HASB}} = -10.94 \pm 0.1, \text{ at } 20^\circ\text{C}$$

This constant, when used in the speciation software, fitted the experimental results obtained by fluorimetry. It was then possible to set the limits of formation for HAS_B. The minimum [Al] required was dependant on the solubility, as the formation of Al(OH)₃ templates is prerequisite to the formation of HAS. In this condition, at least 200 μmol.dm⁻³ Si(OH)₄ was necessary in a pH range 6-7.25. The more [Si(OH)₄] increased, the wider the pH range of formation of HAS_B. It was also shown that, for any [Si(OH)₄] and [Al], the pH of maximum formation was 6.75. When [Si(OH)₄] was maximum, i.e. 2 mmol.dm⁻³, the minimum pH of formation was 4.

However, there was a downside to this approach to the problem due to the limits of the fluorimetry technique. Fluorimetry is a very sensitive technique, implying the measurement only of very low amount of Al. Therefore, it was impossible to measure the influence of Si(OH)₄ on the formation of AlM for [Al]>[Si(OH)₄] and, consequently, to access to relevant information on the formation of HAS_A. This could be noticed especially when compared to experimental measurements of [Al] and [Si] in material collected by filtration. When HAS_B was the only form expected, the calculations matched the experiment, but if HAS_A or a mixture of HAS_A and HAS_B was formed, the lack of information on K_{HASA} was reflected on the calculated results. Further studies of the reaction between Al and Si(OH)₄ when [Al]>[Si(OH)₄] could lead to the determination of K_{HASA}. In the meantime, the use of K_{HASB} should be restricted to the description of systems where [Si(OH)₄]>[Al].

Chapter 7 : General discussion. Hydroxyaluminosilicates as a control of the toxicity of aluminium.

Silicic acid ($\text{Si}(\text{OH})_4$) has been proved to be of crucial importance in the control of the toxicity of Al through the formation of HAS. Hence, understanding the chemistry of HAS in terms of their structural characterisation and mechanism and kinetics of formation is essential in order to comprehend not only the reaction between Al and $\text{Si}(\text{OH})_4$ but also in regard to the reaction of Al with other species in the natural environment. More specifically, in a number of studies on the control of Al toxicity by $\text{Si}(\text{OH})_4$, the lack of a constant of formation for HAS has prevented a quantitative chemical explanation of fish survival in acidic waters containing both a toxic level of Al and $\text{Si}(\text{OH})_4$. The constants presently available to describe the formation of Al-Si complexes such as $\text{AlH}_3\text{SiO}_4^{2+}$ or AlSiO_4^- have not provided a relevant explanation for such a phenomenon, possibly because they describe soluble species whereas HAS are solid species. It is therefore of interest to apply the constant determined in this work ($\log K_{\text{HASB}} = -10.94$) to these earlier fish studies to see if it is more successful in bringing together the chemistry of HAS formation and Al toxicity in fish.. Calculations of Al:Si chemistry in different systems described elsewhere (Birchall et al. 1989; Camilleri et al. 2003; Exley et al. 1997) were performed using the software SolGasWater for the species presented in Table 7.1-1. The percentage of fish survival as well as the percentage of calculated species of Al (only for species > 1%) were plotted against the Si:Al molar ratio in the experimental waters to which fish were exposed. The biologically available Al represents the more reactive, hence toxic, species and was estimated following the extended free ion activity model (Brown and Markish 2000):

$$\text{Bioavailable Al} = \text{Al}^{3+} + 0.67 \times \text{AlOH}^{2+} + 0.33 \times \text{Al}(\text{OH})_2^+$$

Table 7.1-1: Selected stability constants for key Al species used in SGW

Al Species	Log K	Reference
AlOH^{2+}	-5.41	Baes et Mesmer (1976)
Al(OH)_2^+	-9.98	
Al(OH)_3	-15.69	
Al(OH)_4^-	-23.45	
$\text{AlH}_3\text{SiO}_4^{2+}$	-2.44	Pokrovski (1996)
AlSiO_4^-	-19.10	Pokrovski (1998)
HAS_B	-10.94	Chapter 6
Al(OH)_3 (gibbsite)	9.19	Baes et Mesmer (1976)

In their 1989 paper, Birchall *et al.* produced the first evidence of a reduction in the toxicity of Al in fish in the presence of Si(OH)_4 . Their study showed that an excess of Si(OH)_4 over Al eliminated the acute toxicity of Al at pH 5 and they suggested that the formation of HAS could explain this phenomenon by controlling the biological availability of Al. Table 7.1-2 summarises their experimental conditions and compares their toxicological results with the calculated speciation of Al using the stability constants described in Table 7.1-1. Figure 7.1-1 presents the influence of the Si:Al molar ratio on the percentage of survival of Atlantic salmon fry, together with the distribution of predominant Al species ($> 1\%$). From these speciation results, neither the formation of $\text{AlH}_3\text{SiO}_4^{2+}$ ($< 1\%$) nor AlSiO_4^- ($< 0.01\%$) can explain the reduction of toxicity observed in fish. There is no HAS_B predicted to form under these experimental conditions, as the maximum amount of Si(OH)_4 was below the cut-off $[\text{Si(OH)}_4]$ of $200 \mu\text{mol}\cdot\text{dm}^{-3}$ imposed by the use of K_{HAS_B} . As pointed out in Chapter 6, the evaluation of the constant is restricted by the limits of detection of the fluorimetric method. K_{HAS_B} is an experimental constant, i.e. it is based on experimental measurement of the stability of HAS_B in respect of its ability to keep Al out of morin. Moreover, the formation of HAS_B is highly dependent upon 3 linked factors: $[\text{Al}]$, $[\text{Si(OH)}_4]$, and pH. The distribution curve is centred on the pH of maximum formation (pH = 6.75) and its width depends on both $[\text{Al}]$ and $[\text{Si(OH)}_4]$. A minimum $[\text{Si(OH)}_4]$ was estimated at $200 \mu\text{mol}\cdot\text{dm}^{-3}$ for $[\text{Al}] = 0.5 \mu\text{mol}\cdot\text{dm}^{-3}$.

The inadequacy I observed to explain the reduction of Al toxicity observed in fish by Birchall *et al.* by the formation of HAS_B using $\text{Log } K_{\text{HAS}_B} = -10.94$ seems to support the observations of Lumsdon and Farmer (1995), when they affirmed that the formation of proto-imogolite (or HAS_A) would not reduce Al toxicity under the experimental conditions described by Birchall *et al.* (1989). Using the solubility constant they determined for proto-imogolite ($\text{Log } K_{s_0} = 7.604$ at 15°C), they showed that the amount of HAS_A predicted to

form for $[\text{Si}(\text{OH})_4] = 100 \mu\text{mol}\cdot\text{dm}^{-3}$ at pH 4.96, will be in equilibrium with about $11 \mu\text{mol}\cdot\text{dm}^{-3}$ of monomeric Al species, i.e. more than the total Al present in the toxicity experiments of Birchall et al. (1989). They concluded from these calculations that Al toxicity could not be reduced through the interaction of Al with $\text{Si}(\text{OH})_4$ (the formation of HAS_A) but that $\text{Si}(\text{OH})_4$ would however prevent the precipitation of $\text{Al}(\text{OH})_3$. They disregarded the fact that their constant describes the solubility and not the formation of HAS_A , i.e. how kinetically stable HAS_A is towards dissolution. Moreover, their constant describes a system where $[\text{Al}] > [\text{Si}(\text{OH})_4]$ (HAS_A) and cannot therefore be suitably applied to a system where $[\text{Si}(\text{OH})_4] > [\text{Al}]$ (HAS_B), a situation where Birchall et al. noticed a complete eradication of Al toxicity.

In the present work, there is no HAS_B formed for Si:Al = 0.09 and 0.89 as HAS_A would be the expected form of HAS. For Si:Al = 3.71 and 13.01, HAS_B , despite being the predominant form of HAS for these ratio, is not predicted to form according to the calculations. Far from denying the validity of the constant, this observation highlights the limits of K_{HASB} linked to the method of its determination. For $[\text{Si}(\text{OH})_4]$ below $200 \mu\text{mol}\cdot\text{dm}^{-3}$, HAS_B is still very likely to form even if its capacity to grow and to aggregate in order to reach a more stable size is highly affected by the kinetics of the reaction. This suggests that K_{HASB} describes the constant of formation of HAS_B at equilibrium, i.e. when HAS_B had reached a stable state towards dissolution.

Table 7.1-2: Experimental conditions and results from Birchall et al (1989) with calculated speciation.

Tot [Al]	Tot [Si]		Survival	Al _{bio}	Al(OH) _{3(s)}	AlH ₃ SiO ₄ ²⁺	AlSiO ₄ ⁻	HAS _B	
$\mu\text{mol.dm}^{-3}$	Si:Al ratio	pH			%				
7.15	93.06	13.01	4.9	100	43.55	31.11	0.87	0.01	0
6.70	24.89	3.71	4.9	< 10	55.19	16.63	0.28	3.88e-3	0
6.22	5.46	0.87	4.9	< 20	56.12	14.44	0.06	9.39e-4	0
6.26	0.60	0.09	4.9	0	55.76	15.05	7.09e-3	1.02e-4	0

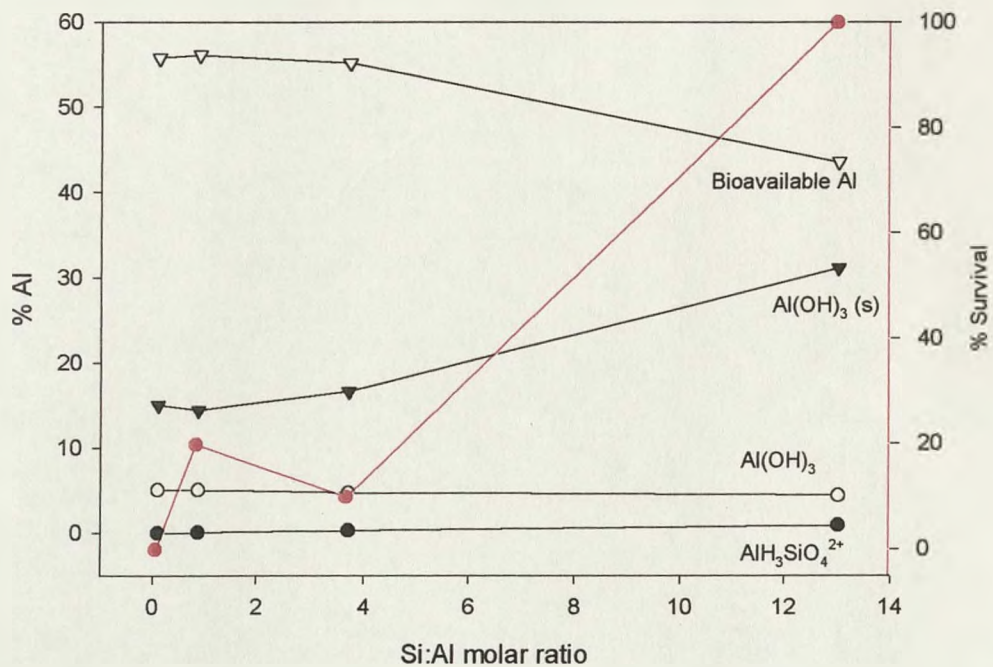


Figure 7.1-1: Distribution of Al species together with percentage of survival of Atlantic salmon fry at pH 5 with increasing Si:Al ratio.

When Exley et al (1997) investigated the relationship between the formation of HAS and the reduction of toxicity in fish, they observed that HAS were formed and identified for a Si(OH)_4 level of $100 \mu\text{mol.dm}^{-3}$, but that they were not stable enough to eliminate Al toxicity (Exley et al. 1997). They used two sets of data: (i) Al and Si(OH)_4 were directly diluted to the required concentration into the fish tanks and (ii) stock solutions of more concentrated Si:Al solutions were prepared and aged before being diluted into the fish tanks to similar concentrations to those used in treatment (i). A summary of their experimental conditions with the fish survival for each treatment is presented in Tables 7.1-3 and 7.1-4 together with the distribution of Al species as calculated using SGW. Figures 7.1-2 and 7.1-3 show the influence of the Si:Al molar ratios on the percentage of fish survival and the distribution of Al species ($> 1\%$) for treatments (i) and (ii) respectively. In treatment (i), when $[\text{Al}]$ varies from 9 to $20 \mu\text{mol.dm}^{-3}$ and $[\text{Si(OH)}_4]$ from 0.5 to $210 \mu\text{mol.dm}^{-3}$ at pH 5-5.2, there is no predicted formation of HAS_B for $[\text{Si(OH)}_4] < 100 \mu\text{mol.dm}^{-3}$. When $[\text{Si(OH)}_4]$ increased together with the Si:Al molar ratio, the predicted $[\text{HAS}_B]$ becomes higher to finally be the predominant Al species in solution, reducing the amount of bioavailable Al, and, concomitantly, the percentage of survival slightly increased. However, the toxicity of Al was still high as the highest percentage of survival was only 14%. This inadequacy between formation of HAS_B and toxicity could be explained by the stability of the material formed. The maximum survival was obtained for a solution aged for 168 h whereas all the other tank solutions were only aged for 24 h. For such low $[\text{Al}]$ and $[\text{Si(OH)}_4]$, and despite the Si:Al ratio, the size of HAS_B particles may not have reached a stable state as was demonstrated by AFM in Chapter 4. This means that, despite the formation of HAS_B , the particles did not have the time to aggregate to a suitable size in order to successfully retain Al^{3+} . In Chapter 4, it was shown that although particles were observable by AFM after just one day, the phenomenon of aggregation, and hence the

stability of the material toward solubility, is a much longer process. The modelling of the formation of HAS_B using K_{HASB} describes the system at equilibrium, i.e. when HAS_B has reached a stable size in regards of solubility. Whilst it helps to describe the system thermodynamically, i.e. in terms of species concentration and pH, K_{HASB} does not take into account the kinetic factor which describes the agglomeration of particles. Therefore, for solutions with low concentrations of Al and Si(OH)₄, the formation of HAS_B will occur but the phenomenon of aggregation towards the equilibrium system will be very slow. In the meantime, the availability of Al³⁺ will only be marginally affected by HAS formation, that is until its size prevents its rapid dissolution to give up Al³⁺ to any adjacent biological ligands.

This is supported by the results shown in treatment (ii). When stock solutions of high [Al] and [Si(OH)₄] were prepared and aged before being diluted into the fish tanks, there is no doubt that stable HAS_B would be formed as [Al] = 1000 μmol.dm⁻³ and [Si(OH)₄] varies from 0 to 2000 μmol.dm⁻³ (Doucet et al. 2001a). Consequently, upon dilution of these preformed HAS into the fish tanks there was a perfect correlation between the increase in fish survival and the formation of HAS_B in the Al/Si(OH)₄ stock solutions. By using stock solution of high [Al] and [Si(OH)₄], stable HAS were formed and they were not affected by the subsequent dilution. However, the limit of detection of the fluorimeter prevented any advances towards the determination of the constant of formation for HAS_A. Fluorimetry was used to study competition between Si(OH)₄ and morin towards Al. The use of freshly prepared solutions limited the maximum concentration of Al to 6 μmol.dm⁻³ for the fluorimetric measurements to be in scale. In order to observe a significant effect of Si(OH)₄ on the reaction of formation of the Al-morin complex, it was also necessary to use a large excess of Si(OH)₄. It was therefore impossible to access to any information on systems compatible with the formation of HAS_A, as it would have required the use of an

amount of Al higher than $[\text{Si}(\text{OH})_4]$. The absence of such a constant in the speciation of Al species by SGW may be problematic at some Si:Al ratio. At Si:Al = 0.5, HAS_A is the expected form of HAS.

Table 7.1-3: Experimental conditions and results from Exley et al (1997) with calculated speciation.

Treatments (i)									
Tot [Al]	Tot [Si]	Survival		Al_{bio}	$\text{Al}(\text{OH})_{3(s)}$	$\text{AlH}_3\text{SiO}_4^{2+}$	AlSiO_4^-	HAS_B	
$\mu\text{mol.dm}^{-3}$	Si:Al ratio	pH				%			
19.80	0.50	0.025	4.99	4	13.28	78.44	1.48e-3	3.03e-5	0.00
9.00	2.70	0.30	5.20	0	9.86	78.11	6.71e-3	5.84e-4	0.00
16.20	96.60	5.96	4.99	3	16.23	73.30	0.35	7.16e-3	0.00
18.40	191.70	10.42	4.99	0	14.29	70.53	0.60	0.01	5.64
11.40	210.00	18.42	5.24	14	6.15	0.00	0.31	0.03	85.08
11.30	208.70	18.47	5.20	6	7.50	0.00	0.37	0.03	82.92

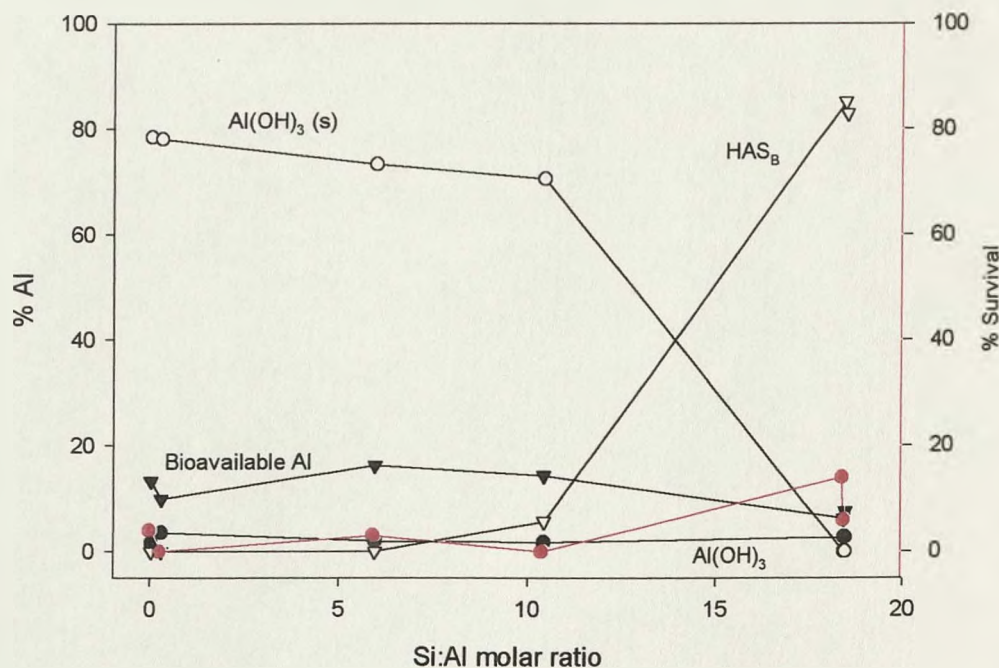


Figure 7.1-2: Distribution of Al species together with percentage of survival of rainbow trout fry with increasing Si:Al ratio for treatment (i).

Table 7.1-4: Experimental conditions and results from Exley et al (1997) with calculated speciation.

Treatments (ii)

Tot [Al]	Tot [Si]		Survival	Al _{bio}	Al(OH) _{3(s)}	AlH ₃ SiO ₄ ²⁺	AlSiO ₄ ⁻	HAS _B
μmol.dm ⁻³	Si:Al ratio	pH				%		
1000	0	0	5.43	0	0.03	99.89	0.00	0.00
1000	500	0.5	5.44	47	0.03	68.94	1.41e-3	6.45e-4
1000	1000	1	5.45	64	0.03	18.95	1.34e-3	6.60e-4
1000	2000	2	5.49	100	5.1e-3	0.00	1.12e-3	7.24e-4

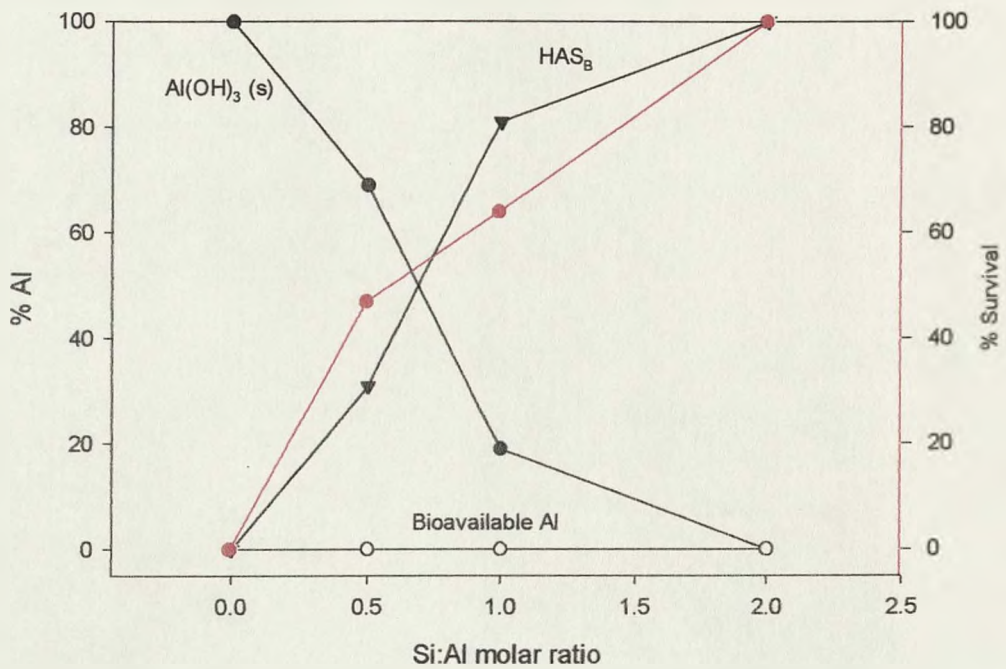


Figure 7.1-3: Distribution of Al species together with percentage of survival of rainbow trout fry with increasing Si:Al ratio for treatment (ii).

At Si:Al = 1, one should expect a mixture of HAS_A and HAS_B. This could explain why despite the prediction of 80% of HAS_B, the percentage of survival in fish does not exceed 64%. AFM experiments suggested that HAS_A was less stable and slower to aggregate due to its positive charge. It also seems that the structure of HAS_B provides a better surrounding of Al than HAS_A. This could affect the way of controlling the toxicity of Al and suggests that HAS_B is favoured in this respect. The structure of HAS_A (Figure 7.1-5a) offers the possibility of an attack through the Al-OH bonds whereas these bonds are not present anymore in HAS_B (Figure 7.1-5b). The approach to the Al groups in HAS_B is protected by the presence of two Si groups, involving an attack through the Si-OH bounds. HAS_B is therefore less likely to release Al than HAS_A and should be structurally more stable. This could explain why, at Si:Al = 2, when more than 99 % of the total Al is HAS_B, 100% of the fish survived the Al toxicity.

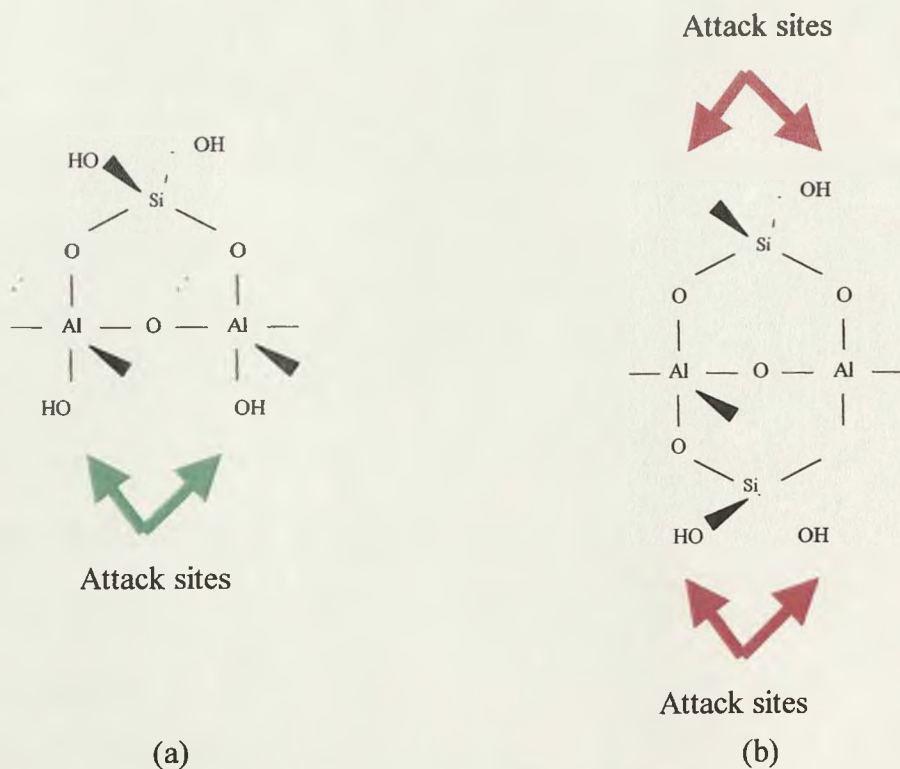


Figure 7.1-4: Attack sites on (a) HAS_A structure and (b) HAS_B structure.

More recently, Camilleri et al observed that, despite a high level of Al, the acidic waters (pH 4.9-5.6) of Gadji Creek (Australia) were non-toxic to the fish population (Camilleri et al. 2003). They revealed that these waters also contain an elevated level of Si but they failed to associate this phenomenon with the formation of HAS in the absence of a constant of formation such as K_{HASB} to model the Al speciation in this environment. They relied on the constants available to them to describe the formation of Al-Si complexes, i.e. $AlH_3SiO_4^{2+}$ and $AlSiO_4^-$, and showed that less than 1% of the total Al was complexed with Al and could not therefore account for the reduction of Al toxicity. The determination of K_{HASB} in this present research should therefore shed new light on their experimental results. Table 7.1-5 summarises their experimental conditions and survival results as well as the speciation modelling using the constants reported in Table 7.1-1. Figure 7.1-5 presents the influence of Si:Al molar ratio on the percentage of fish survival and on the distribution of Al species (> 1%). When $[Si] \leq [Al]$, the calculations did not predict the formation of HAS_B . Although their results reports an increase of the survival to 67% and 40% for Si:Al = 0.5 and 1 respectively, this cannot be explained by the formation of HAS_B . At these ratios, HAS_A is the predominant form of HAS and as pointed out before, the growth and the shape of HAS_A is less effective in reducing the Al toxicity. For Si:Al molar ratio above 2, HAS_B is formed and the survival is strongly improved. This reinforced the concept of HAS_B being the most adequate form to control the biological availability of Al. The advances made in the present work in regard of both the determination of K_{HASB} and the importance of the phenomenon of aggregation for the stability of HAS_A and HAS_B toward dissolution allows a quantitative chemical explanation of the experimental results reported by Camilleri et al. The calculations clearly demonstrated that the formation of HAS is responsible for the decrease of the acute Al toxicity to fish.

Table 7.1-5: Experimental conditions and results from Camilleri et al (2003) with calculated speciation.

Tot [Al]	Tot [Si]		Survival	Al _{bio}	Al(OH) _{3(s)}	AlH ₃ SiO ₄ ²⁺	AlSiO ₄ ⁻	HAS _B
μmol.dm ⁻³	Si:Al ratio	pH				%		
74.07	0.00	0.00	4.90	0	5.94	91.35	0.00	0.00
55.55	0.00	0.00	5.00	0	4.47	92.63	0.00	0.00
74.07	37.03	0.50	5.00	67	3.35	94.44	0.02	6.14e-4
55.55	55.55	1.00	5.00	40	4.47	92.58	0.05	1.22e-3
74.07	192.59	2.60	5.30	100	0.76	95.24	0.03	6.31e-3
55.55	261.11	4.70	5.00	77	4.07	0.00	0.19	4.21e-3
74.07	370.37	5.00	5.50	100	0.22	0.00	0.01	0.01
74.07	681.48	9.20	5.90	93	0.03	0.00	2.29e-3	0.02
55.55	516.66	9.30	4.80	87	5.91	0.00	0.48	2.66e-3
55.55	1027.77	18.50	4.80	100	2.82	0.00	0.48	2.66e-3

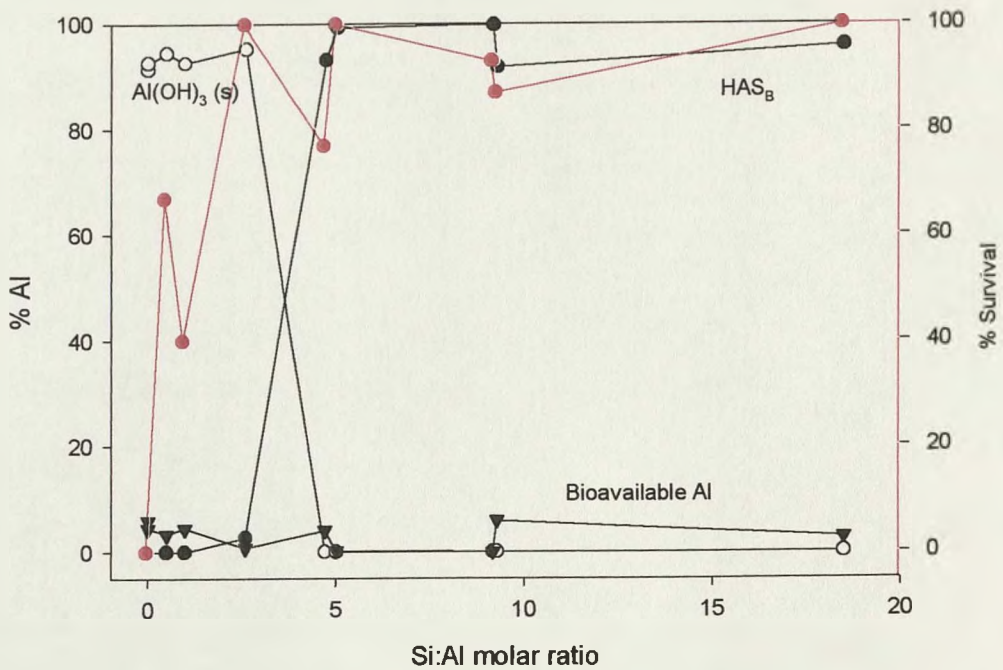


Figure 7.1-5: Distribution of Al species together with percentage of survival of *M. morgurnda* with increasing Si:Al ratio.

The difference in structure between HAS_A and HAS_B may explain that the percentage of survival was dependent upon the Si:Al ratios present in water. When $[Al]$ was in excess to $[Si(OH)_4]$, HAS_A is formed. The presence of two Al-OH bounds in its structure makes it more likely to release Al to a competitive binding site, such as the fish gill surface. On the other hand, when $[Si(OH)_4]$ is in excess to $[Al]$, the surrounding of Al by Si-OH bounds in the HAS_B structure should prevent any further attack to the Al site. Moreover, as Si-OH is weaker than Al-OH in regards of acidity, HAS_B should be more stable towards dissociation in an acidic environment. Consequently, the formation of stable HAS_B is more effective than HAS_A to control Al toxicity by reducing the possible binding of Al with any other complex.

The use of K_{HASB} to model the speciation of Al species in these different systems presents strong evidence to support the hypothesis that the formation of HAS reduces the acute toxicity of Al in fish. It also highlights the importance of the stability of HAS towards dissolution in the process. In accordance with the AFM results, it seems that HAS_B is not only quicker to aggregate and therefore to stabilise but its shape in itself seems to contribute towards its ability to control the biological availability of Al. The presence of Si-OH bonds prevents any approach of other complexing molecule on the Al sites and the dissociation of HAS_B to release Al. However, the AFM technique is somehow disadvantageous to study the agglomeration of HAS as it focuses more particularly on the observation of the interaction of the particles with a surface.

Finally, by determining a constant of formation for HAS_B , this present work provides a new insight in the understanding of the Al speciation and should help to better comprehend the geochemical impact of $Si(OH)_4$ on Al in natural water. However, this constant is highly

dependent upon its method of determination as it results from an indirect method of measurement. Thus, this definition of K_{HASB} represents the competitive reaction of Si(OH)_4 with Al in respect of morin. It is also important to point out the limiting factors in connection with the formation of HAS_B . It was shown that the minimum $[\text{Al}]$ was $0.5 \mu\text{mol}\cdot\text{dm}^{-3}$, i.e. above saturation. This strongly supports the hypothesis that the formation of Al(OH)_3 is prerequisite to the formation of HAS. The reaction is also highly dependent upon pH, with a pH of maximum formation at 6.5, and $[\text{Si(OH)}_4]$. These three factors being interdependent, it is possible to compensate a low pH by a higher amount of Si(OH)_4 and Al.

It is also important to note that the value found in this work for K_{HASB} is in the range of the values determined in a previous study on the interaction of Al with Si(OH)_4 (Hem et al. 1973). Hem et al used microfiltration to determine the concentrations of Al and Si(OH)_4 in solution in equilibrium with a solid phase they associated with clay. They estimated a solubility constant of $10^{11.28}$ for the following reaction:



The development made in the chemistry of HAS since their study indicates that the material collected under their experimental conditions is likely to be HAS_B . The technical approach made in the present work to determine K_{HASB} combines the aqueous chemistry of the HAS, as the formation of HAS was measured indirectly in solution without any precipitation occurring, with the definition of HAS as a solid phase. Such a definition relies on the ability to collect HAS by filtration. Previous studies showed that HAS_B can be removed using a $2 \mu\text{m}$ membrane filter whereas HAS_A required the use of a $0.2 \mu\text{m}$ membrane (Doucet et al. 2001b). This emphasised the difference of nature of the two forms of HAS. Moreover, the cut-off value normally used in the field studies to separate solid from soluble phases is $0.45 \mu\text{m}$. One could then argue that HAS_B fulfilled the

definition of a solid phase whilst HAS_A , using the arbitrary definition of solubility applied in field studies ($< 0.45 \mu\text{m}$), should be considered as a soluble phase. The fact that both for their formation require the formation of $\text{Al}(\text{OH})_3$ (a solid phase) suggests that both HAS_A and HAS_B should be considered as solid phases. However, because of the limitations inherent in the fluorimetry technique, a constant of formation for HAS_A remains uncertain and more studies, using other methods of determination, would be necessary to define completely the kinetics related to HAS.

The determination of an equilibrium constant of formation of HAS_B is only the first step toward a fuller definition of the kinetics underlying the chemistry of HAS. The effect of temperature, medium as well as the possible interaction with other ions, such as fluoride, should now be studied. The control of the solubility of Al by gibbsite, and its inadequacy to describe the Al speciation in natural water, should also be challenged using K_{HASB} . A better characterisation of both HAS_A and HAS_B using advanced solid state NMR techniques should also give a better insight of the structure and consequently to the mechanism of formation of HAS.

Appendix A: "Silicic acid (Si(OH)₄) is a significant influence upon the atomic absorption signal of aluminium measured by graphite furnace atomic absorption spectrometry (GFAAS)."

Schneider, C. and C. Exley (2001). Journal of Inorganic Biochemistry 87(1-2): 45-50.

Silicic acid ($\text{Si}(\text{OH})_4$) is a significant influence upon the atomic absorption signal of aluminium measured by graphite furnace atomic absorption spectrometry (GFAAS)

Celine Schneider, Christopher Exley*

Birchall Centre for Inorganic Chemistry and Materials Science, School of Chemistry and Physics, Keele University, Staffordshire ST5 5BG, UK

Received 31 March 2001; accepted 10 May 2001

Abstract

We have identified silicic acid ($\text{Si}(\text{OH})_4$) as an important modifier of the absorbance signal of aluminium measured by graphite furnace atomic absorption spectrometry (GFAAS). The presence of $\text{Si}(\text{OH})_4$ enhanced the signal by as much as 50%. The extent of the enhancement was dependent upon both $[\text{Al}]$ and $[\text{Si}(\text{OH})_4]$ and was maximal when $[\text{Al}] \leq 4.44 \mu\text{mol dm}^{-3}$ and $[\text{Si}(\text{OH})_4] \geq 0.50 \text{ mmol dm}^{-3}$. The enhancement of the Al absorbance signal was not linearly related to $[\text{Si}(\text{OH})_4]$ and the effect was, generally, saturated, for all $[\text{Al}]$ tested, at $[\text{Si}(\text{OH})_4] \geq 0.50 \text{ mmol dm}^{-3}$. $\text{Si}(\text{OH})_4$ was significantly more effective in enhancing the Al absorbance signal than $\text{Mg}(\text{NO}_3)_2$. However, the co-occurrence of $10 \text{ mmol dm}^{-3} \text{ Mg}(\text{NO}_3)_2$ and $2 \text{ mmol dm}^{-3} \text{ Si}(\text{OH})_4$ in samples abolished the enhancement due to $\text{Si}(\text{OH})_4$. The presence of $\text{Si}(\text{OH})_4$ in samples could result in an overestimation of the Al content of those samples by as much as 50%. Errors in the measurement of Al in samples containing $\text{Si}(\text{OH})_4$ could be prevented using matrix-matched calibration standards. Our observation could have serious implications for the determination of Al in aqueous samples of both geochemical and biological interest. It may also point towards the application of $\text{Si}(\text{OH})_4$ as a novel and effective matrix modifier in the determination of Al by GFAAS since the inclusion of $\text{Si}(\text{OH})_4$ in standards and samples improved the limit of detection of Al from ca 8 nmol dm^{-3} to 3 nmol dm^{-3} . © 2001 Elsevier Science B.V. All rights reserved.

Keywords: Graphite furnace atomic absorption spectrometry; Aluminium determination in aqueous samples; Silicic acid; Matrix modifier

1. Introduction

Graphite furnace atomic absorption spectrometry (GFAAS) is probably the technique of choice for the determination of low concentrations of aluminium (Al) in aqueous samples of geochemical and biological interest [1–7]. Al measurement by GFAAS has a long history and a significant research effort has been concentrated upon the improvement of this technique [1,3,8–10]. A great deal of research carried out in our laboratory concerns the bioinorganic chemistry of Al and Si [11–18] and has involved the measurement of Al, and occasionally Si, by GFAAS. It has only now come to our attention that the presence of silicic acid ($\text{Si}(\text{OH})_4$) in aqueous samples containing relatively low concentrations of Al ($< 5.0 \mu\text{mol dm}^{-3}$) will influence the atomic absorption signal of Al measured by GFAAS.

Herein we report upon the nature and extent of the influence of $\text{Si}(\text{OH})_4$ and make a suggestion as to how the effect can be compensated for and used to advantage in the determination of Al by GFAAS.

2. Materials and methods

2.1. Instrumentation and reagents

All analyses were carried out using a model 3300 spectrometer incorporating an HGA600 furnace and an AS60 autosampler (PerkinElmer Instruments, Beaconsfield, UK). Samples were atomised directly on the wall of pyrolytically coated graphite tubes (PerkinElmer Instruments, Beaconsfield, UK). The instrumental conditions are given in Table 1. Al standards were prepared from a certified Al stock (37 mmol dm^{-3} in 2% HNO_3 ; PerkinElmer Instruments, Beaconsfield, UK) in ultrapure water (conductivity below $0.5 \mu\text{S cm}^{-1}$) or ultrapure water

*Corresponding author. Tel.: +44-1782-584-080; fax: +44-1782-712-378.

E-mail address: cha38@keele.ac.uk (C. Exley).

Table 1
Instrument conditions and furnace programme for the measurement of aluminium by GFAAS

Instrumental conditions			
Wavelength	309.3 nm		
Lamp current	25 mA		
Slit width	0.7 nm (low)		
Inert gas/flow-rate	Argon/300 ml min ⁻¹ *		
Background correction	On (Deuterium)		
Signal measurement	Peak area (integrated absorbance)		
Read time/BOC time	2 s/5 s		
Furnace programme			
Step	Temperature/°C	Ramp/s	Hold/s
1	80	5	5
2	120	10	30
3	500	10	10
4	1450	10	15
5	2650	0	5
6	2700	1	5

* Stop flow in the atomisation step (step 5 of the furnace programme).

containing a known concentration of Si(OH)₄. Si(OH)₄ was prepared by cation-exchange of a 2 mmol dm⁻³ Na₄SiO₄ solution [12] and used at an appropriate dilution. Magnesium was added as Mg(NO₃)₂·6H₂O (Aldrich, Lewes, UK).

2.2. Influence of Si(OH)₄ on Al absorption signal

Al standard solutions of 1.11, 2.22, 3.33, 4.44, 4.82, 5.56, 6.67, 7.78 and 8.89 μmol dm⁻³ were manually prepared in PTFE bottles in either 1% HNO₃ or 1% HNO₃+2 mmol dm⁻³ Si(OH)₄. In addition Al standards of 2.22, 4.82 and 7.78 μmol dm⁻³ were prepared in 1% HNO₃+0.1, 0.5 and 1.0 mmol dm⁻³ Si(OH)₄. Five replicates of each standard were prepared and each standard was analysed 5 times. To account for the proportionality of quantitative absorption analysis, as is described by the Beer-Lambert law, the injection volumes were adjusted (10–40 μl) such that equivalent standards ±Si(OH)₄ were measured within a similar range of absorbances. The results were expressed as:

$$\text{Absorbance (Al + Si(OH)}_4\text{) / Absorbance (Al only)}$$

Raw data were normally distributed and statistical significance ($P < 0.01$) was determined using Student's *t*-test.

2.3. Preparation of Al calibration curves in the presence of different [Si(OH)₄]

Al standard solutions of concentration 2.22 μmol dm⁻³ were prepared in 1% HNO₃ containing 0, 0.1, 0.2, 0.4, 0.8

and 1.0 mmol dm⁻³ Si(OH)₄. Each of these standards was then used by the autosampler to prepare calibration curves incorporating standards of 0.37, 0.74, 1.48 and 2.22 μmol dm⁻³ Al. Five replicates of each standard were prepared and each standard was analysed 3 times. Injection volume was 30 μl in each case. The results were expressed as absolute absorbances. Data were normally distributed and statistical significance ($P < 0.01$) was determined using Student's *t*-test.

2.4. Influence of 10 mmol dm⁻³ Mg(NO₃)₂ on the enhancement of the Al absorption signal by Si(OH)₄

Al standard solutions of concentration 2.22, 4.81 and 7.78 μmol dm⁻³ were prepared in 1% HNO₃ containing either (i) no further addition; (ii) 10 mmol dm⁻³ Mg(NO₃)₂; (iii) 2 mmol dm⁻³ Si(OH)₄ or (iv) 10 mmol dm⁻³ Mg(NO₃)₂+2 mmol dm⁻³ Si(OH)₄. Five replicates of each standard were prepared and each standard was analysed 3 times. Injection volumes were adjusted (10–20 μl) to account for the proportionality of absorption analyses as is described by the Beer-Lambert law. The results were expressed as absorbance ratios. Raw data were normally distributed and statistical significance ($P < 0.01$) was determined using Student's *t*-test.

2.5. Application of the enhancement of the absorption signal of Al by Si(OH)₄ to real samples containing different concentrations of Al and Si(OH)₄

Thirty-three samples, from a previous study [18], which contained known amounts of Si(OH)₄ (range 0.05–2.00 mmol dm⁻³) and unknown amounts of Al (range 0.5–2.0 μmol dm⁻³) were analysed for Al by GFAAS using either: (i) Al standards with no added Si(OH)₄ or (ii) Al standards which contained the Si(OH)₄ concentration known to be present in the unknown sample. In addition, 2 further unknown samples taken from hot springs in southern Iceland [19] were analysed for Si(OH)₄ using the molybdenum-blue assay [20] and then for Al by GFAAS using standards prepared with or without the requisite [Si(OH)₄]. The results were expressed as a plot of [Al]_{-Si} against [Al]_{+Si}. If the presence of Si(OH)₄ in the Al standard was without influence upon the computed [Al] the points would describe a straight line with a gradient of 1.0. To demonstrate unequivocally which of the computed [Al], i.e. using Al standards + or -Si(OH)₄, was representative of the actual [Al] in each sample Al standard solutions of certified concentration 1.0, 1.5 and 2.0 μmol dm⁻³ were prepared in 1% HNO₃ in the presence of either 0, 0.05, 0.10, 0.50 or 2.00 mmol dm⁻³ Si(OH)₄ and their [Al] were determined using Al calibration curves prepared in either the absence or presence (0, 0.05, 0.10, 0.50 and 2.00 mmol dm⁻³) of Si(OH)₄.

3. Results

3.1. Influence of $\text{Si}(\text{OH})_4$ on Al absorption signal

The limit of detection, defined as the concentration of Al which resulted in an absorbance signal which was equal to 3 times the standard deviation on the blank, was 8 and 3 nmol dm^{-3} for Al measured in the absence and presence of 2 mmol dm^{-3} $\text{Si}(\text{OH})_4$ respectively. These gave highly acceptable levels of quantitation of 0.08 and 0.03 $\mu\text{mol dm}^{-3}$. The much improved level of quantitation in the presence of $\text{Si}(\text{OH})_4$ was reflected in the enhancement of the Al absorption signal, $(\text{Al})_{\text{abs}}$, by $\text{Si}(\text{OH})_4$ by as much as 50%. The enhancement was dependent upon both $[\text{Al}]$ and $[\text{Si}(\text{OH})_4]$ (Fig. 1) and was found to be maximal when $[\text{Al}] \leq 4.44 \mu\text{mol dm}^{-3}$ and $[\text{Si}(\text{OH})_4] \geq 0.50 \text{mmol dm}^{-3}$. All $[\text{Si}(\text{OH})_4]$ tested significantly increased ($P < 0.01$) $(\text{Al})_{\text{abs}}$ at $[\text{Al}] \leq 4.44 \mu\text{mol dm}^{-3}$ whereas the lowest $[\text{Si}(\text{OH})_4]$ tested (0.10 mmol dm^{-3}) did not increase $(\text{Al})_{\text{abs}}$ significantly at higher $[\text{Al}]$. The enhancement of $(\text{Al})_{\text{abs}}$ was not linearly related to $[\text{Si}(\text{OH})_4]$ although at 2.22 $\mu\text{mol dm}^{-3}$ Al the enhancement by 2.0 mmol dm^{-3} $\text{Si}(\text{OH})_4$ was significantly ($P < 0.01$) higher than either 1.0 or 0.5 mmol dm^{-3} .

3.2. Influence of $[\text{Si}(\text{OH})_4]$ on an Al calibration curve

Al calibration curves prepared in the presence of a range of $[\text{Si}(\text{OH})_4]$ confirmed the enhancement of $(\text{Al})_{\text{abs}}$ by $\text{Si}(\text{OH})_4$ (Fig. 2) and emphasised the lack of dose-response with increasing $[\text{Si}(\text{OH})_4]$. For $[\text{Al}]$ in the range 0.37–2.22 $\mu\text{mol dm}^{-3}$ all $[\text{Si}(\text{OH})_4]$ enhanced $(\text{Al})_{\text{abs}}$ although the absorbances were only significantly ($P < 0.01$) increased at $[\text{Si}(\text{OH})_4] \geq 0.40 \text{mmol dm}^{-3}$. For example at

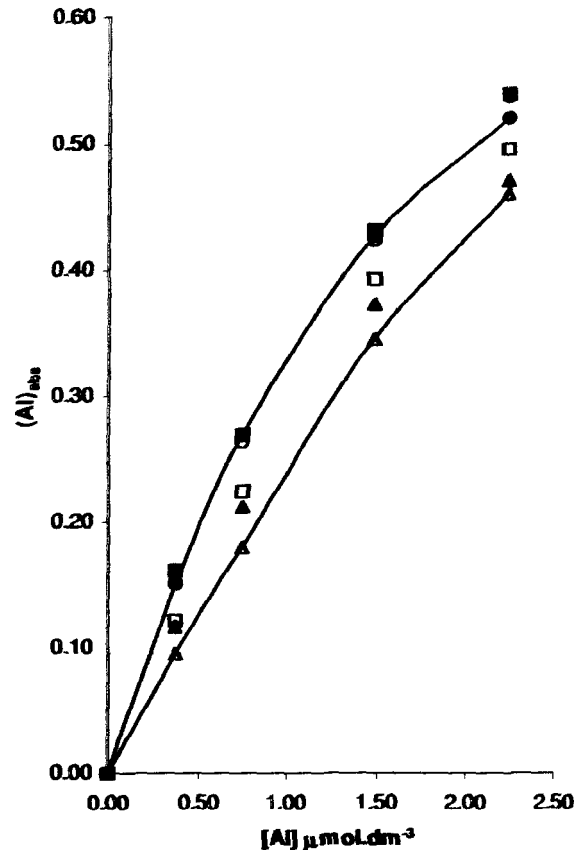


Fig. 2. The influence of the presence of different $[\text{Si}(\text{OH})_4]$ in Al standards on the calibration curves prepared from the same standards. Key: (Δ) — 0 $\text{Si}(\text{OH})_4$; (\blacktriangle) — 0.1 mmol dm^{-3} $\text{Si}(\text{OH})_4$; (\square) — 0.2 mmol dm^{-3} $\text{Si}(\text{OH})_4$; (\blacksquare) — 0.4 mmol dm^{-3} $\text{Si}(\text{OH})_4$; (\circ) — 0.8 mmol dm^{-3} $\text{Si}(\text{OH})_4$; (\bullet) — 1.0 mmol dm^{-3} $\text{Si}(\text{OH})_4$. Lines of 'best fit' are drawn for 0 and 1.0 mmol dm^{-3} $\text{Si}(\text{OH})_4$. Mean and S.D. are plotted, $n=5$.

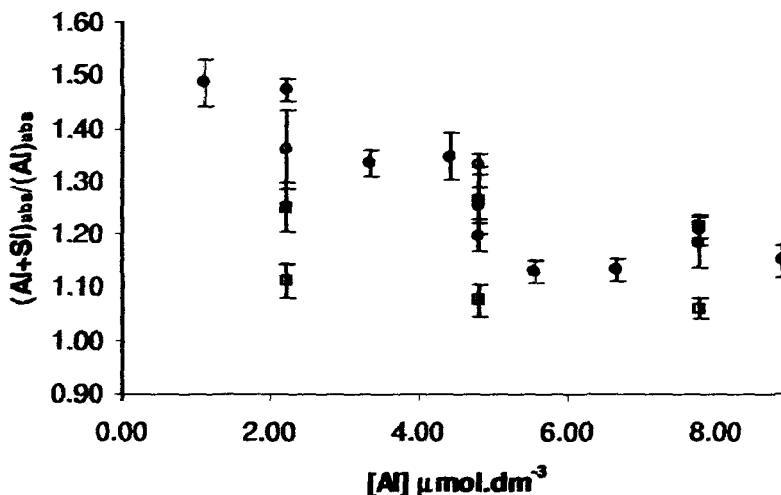


Fig. 1. The influence of $[\text{Al}]$ on its enhancement by $\text{Si}(\text{OH})_4$. Each symbol represents a different $[\text{Si}(\text{OH})_4]$ and is expressed as a proportion of $(\text{Al})_{\text{abs}}$ in the absence of added $\text{Si}(\text{OH})_4$. Key: The $[\text{Si}(\text{OH})_4]$ in each Al standard is represented by: (\bullet) — 2.0 mmol dm^{-3} $\text{Si}(\text{OH})_4$; (\circ) — 1.0 mmol dm^{-3} $\text{Si}(\text{OH})_4$; (\blacksquare) — 0.5 mmol dm^{-3} $\text{Si}(\text{OH})_4$; (\square) — 0.1 mmol dm^{-3} $\text{Si}(\text{OH})_4$. Mean and S.D. are plotted, $n=5$.

0.74 $\mu\text{mol dm}^{-3}$ Al, the mean (+S.D.) absorbance signals were: 0.180 (0.038); 0.213 (0.034); 0.225 (0.039); 0.270 (0.041); 0.264 (0.028) and 0.269 (0.057) for standards containing 0; 0.1; 0.2; 0.4; 0.8 and 1.0 mmol dm^{-3} Si(OH)_4 respectively.

3.3. Influence of 10 mmol dm^{-3} $\text{Mg(NO}_3)_2$ on the enhancement of the Al absorption signal by Si(OH)_4

$\text{Mg(NO}_3)_2$ enhanced $(\text{Al})_{\text{abs}}$ at each of the $[\text{Al}]$ tested (Fig. 3). However, its effect upon $(\text{Al})_{\text{abs}}$ was not as great as Si(OH)_4 . The increase in $(\text{Al})_{\text{abs}}$ induced by Mg was significantly ($P < 0.01$) below that of Si(OH)_4 at 2.22 $\mu\text{mol dm}^{-3}$ Al. When $\text{Mg(NO}_3)_2$ was used in combination with Si(OH)_4 , the increase in $(\text{Al})_{\text{abs}}$ due to Si(OH)_4 was abolished whereas that due to Mg remained. This influence of Mg was particularly apparent at 2.22 $\mu\text{mol dm}^{-3}$ Al.

3.4. Application of the enhancement of the absorption signal of Al by Si(OH)_4 to real samples containing different concentrations of Al and Si(OH)_4

There were significant differences between the $[\text{Al}]$ of unknown samples when they were determined using Al calibration curves prepared in either the absence ($[\text{Al}]_{-\text{Si}}$) or presence ($[\text{Al}]_{+\text{Si}}$) of $[\text{Si(OH)}_4] \geq 0.5 \text{ mmol dm}^{-3}$ (Fig. 4). The use of matrix-matched calibration standards resulted in lower $[\text{Al}]$ in all of the unknown samples except in those which contained 0.05 mmol dm^{-3} Si(OH)_4 .

To determine which set of Al measurements were representative of the true $[\text{Al}]$ in the unknown samples Al standards were prepared $\pm \text{Si(OH)}_4$ using a certified Al

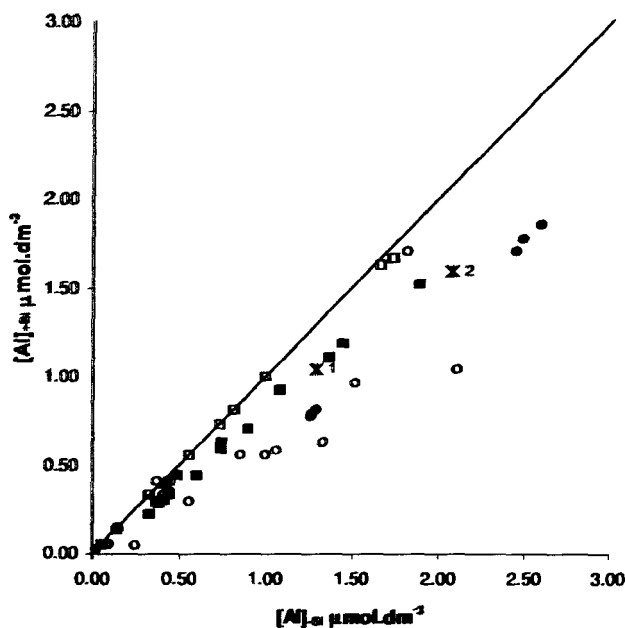


Fig. 4. Plot of the $[\text{Al}]$ of 33 unknown Al samples measured in either the presence ($[\text{Al}]_{+\text{Si}}$) or absence ($[\text{Al}]_{-\text{Si}}$) of the sample concentration of Si(OH)_4 in the Al standards. The straight line indicates when the measurement of Al in the samples was unaffected by the presence of Si(OH)_4 in the samples. Key: The concentrations of Si(OH)_4 in the samples are given by: (●) — 2.0 mmol dm^{-3} Si(OH)_4 ; (○) — 0.5 mmol dm^{-3} Si(OH)_4 ; (■) — 0.1 mmol dm^{-3} Si(OH)_4 ; (□) — 0.05 mmol dm^{-3} Si(OH)_4 ; (*) — denotes the 2 Icelandic hot spring samples.

stock solution. A plot of $[\text{Al}]_{\text{nominal}}$ against $[\text{Al}]_{\text{absolute}}$ for each $[\text{Si(OH)}_4]$ showed that the application of matrix-matched standards (i.e. containing the requisite $[\text{Si(OH)}_4]$)

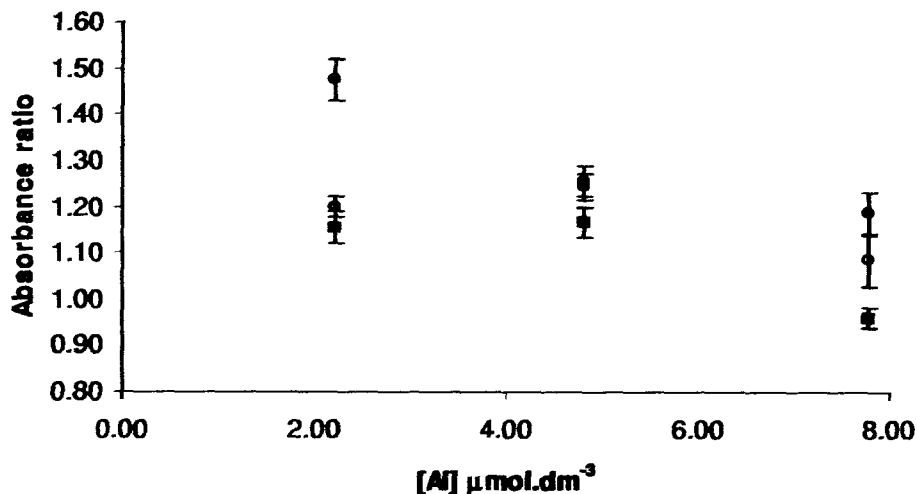


Fig. 3. The influence of 10 mmol dm^{-3} $\text{Mg(NO}_3)_2$ on the enhancement of the Al absorbance signal in the presence and absence of 2.0 mmol dm^{-3} Si(OH)_4 . Key: The different absorbance ratio's are indicated by: (●) — $(\text{Al} + \text{Si})_{\text{abs}} / (\text{Al})_{\text{abs}}$; (○) — $(\text{Al} + \text{Mg})_{\text{abs}} / (\text{Al})_{\text{abs}}$; (■) — $(\text{Al} + \text{Si} + \text{Mg})_{\text{abs}} / (\text{Al})_{\text{abs}}$. Mean and S.D. are plotted, $n=5$.

resulted in the most accurate determination of the actual [Al] (Fig. 5a–e).

3.5. Optimisation of the furnace conditions for samples/standards containing $\text{Si}(\text{OH})_4$

The presence of up to 2 mmol dm^{-3} $\text{Si}(\text{OH})_4$ had no influence upon the optimal pre-treatment or atomisation temperatures. Therefore, samples which contained $\text{Si}(\text{OH})_4$

should be analysed for Al using the instrument and furnace conditions outlined in Table 1.

4. Discussion

We have demonstrated that the measurement of Al in aqueous samples by GFAAS was significantly influenced by the presence of $\text{Si}(\text{OH})_4$. We have shown that $\text{Si}(\text{OH})_4$

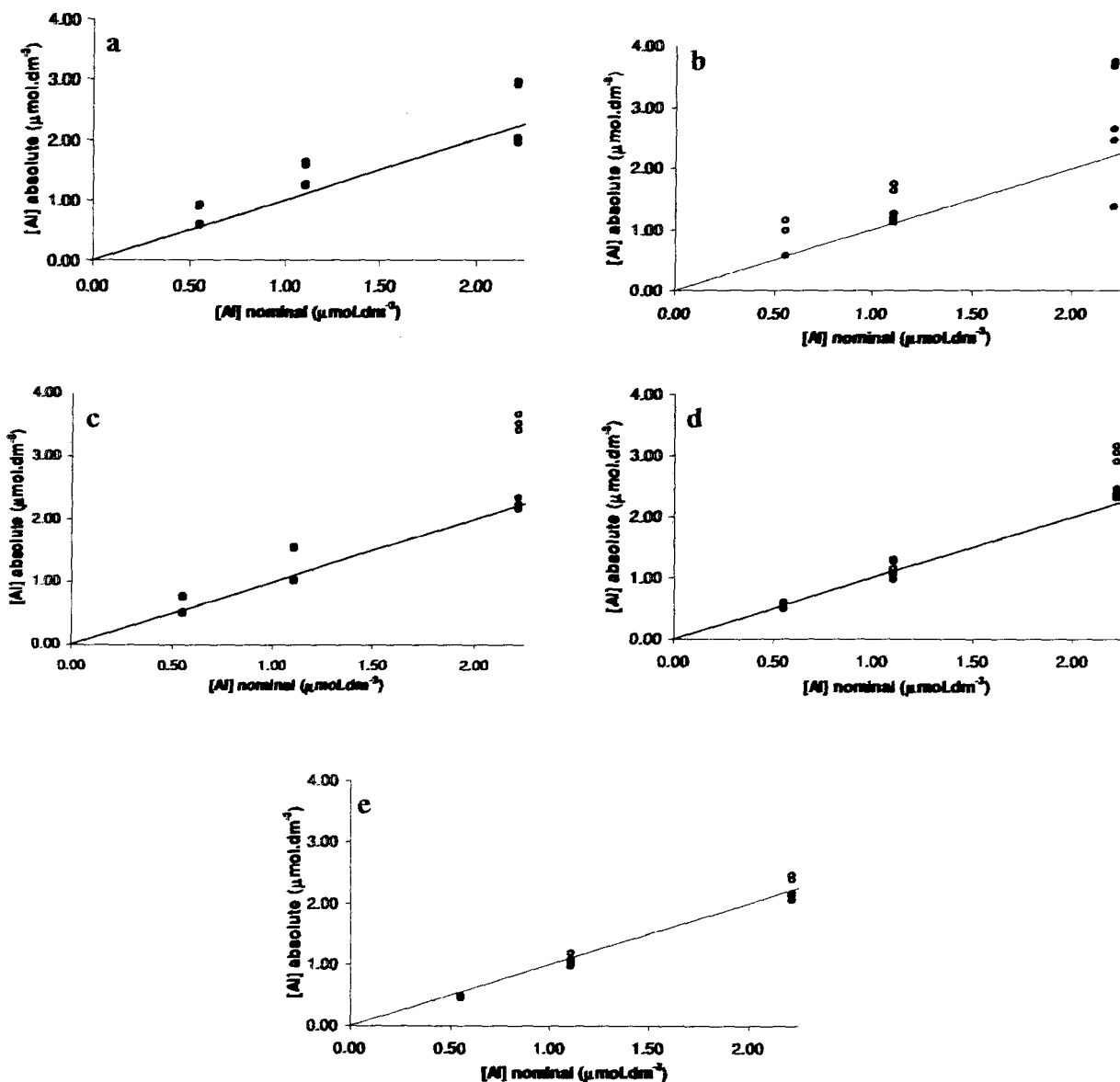


Fig. 5. Plot of the measured [Al] of 3 Al samples of known concentration using either matrix-matched (●) or non-matrix matched (○) calibration standards. The solid line is used to show what the measured [Al] should be and, therefore, the proximity of the points to this line is an indication of the precision of the measurement. Key: The concentrations of $\text{Si}(\text{OH})_4$ in the aluminium samples (and the matrix-matched calibration standards) are given by: (a) 2.0 mmol dm^{-3} ; (b) 1.0 mmol dm^{-3} ; (c) 0.5 mmol dm^{-3} ; (d) 0.1 mmol dm^{-3} ; (e) $0.05 \text{ mmol dm}^{-3}$. Three replicates of each Al sample were measured for each of the $\text{Si}(\text{OH})_4$ concentrations.

increased $(Al)_{abs}$ and that this effect was most pronounced in samples containing $[Al] \leq 4.44 \mu\text{mol dm}^{-3}$ and $[Si(OH)_4] \geq 0.40 \text{ mmol dm}^{-3}$. The presence of $Si(OH)_4$ was found to result in an over-estimation (by up to 50%) of the true $[Al]$ unless $Si(OH)_4$ was included as a constituent of Al standards used to prepare calibration curves. The application of matrix-matched standards (i.e. the inclusion in each standard of an appropriate $[Si(OH)_4]$) both ensured an accurate Al determination and a higher level of quantitation than was achieved using non-matrix-matched standards. The enhancement of $(Al)_{abs}$ by $Si(OH)_4$ was significantly more pronounced than that due to an excess of $Mg(NO_3)_2$ though the co-inclusion of both of these modifiers resulted in the abolition of the $Si(OH)_4$ effect.

The use of Si as a modifier in GFAAS has been studied previously and an effect upon $(Al)_{abs}$ was noted [21]. Our independent observation of this effect of Si has confirmed the previous research and identified the solution conditions under which Si will act as an efficient modifier. It is worthy of note that $2 \text{ mmol dm}^{-3} Si(OH)_4$ resulted in a significantly greater enhancement of $(Al)_{abs}$ than $10 \text{ mmol dm}^{-3} Mg(NO_3)_2$. The mechanism of action of Si in enhancing $(Al)_{abs}$ was not investigated in this study although we were able to show that its presence had no influence on either the optimum pre-treatment temperature or the optimum atomisation temperature (results not shown). We can only speculate that the presence of Si reduced aluminium carbide formation during atomisation [22].

The significance of our findings may be two-fold. First, they might act as a warning against not using matrix-matched standards in the preparation of calibration curves for Al determination. There are a number of instances where the co-occurrence in samples of Al and Si would be expected, for example, in biological fluids such as serum and in soil and surface waters. In either of these examples the over-estimations of $[Al]$ that would result could have significant bearings upon any conclusions that were drawn from the results. For example, in the hot spring samples analysed in this study (Fig. 4) the failure to use matrix-matched standards resulted in over-estimates of $[Al]$ of 25–30%. However, we have also shown that over-estimates of $[Al]$ may not occur if an excess of $Mg(NO_3)_2$ was already being used as a matrix modifier. Secondly, our results have suggested that Si may be a more efficient modifier than Mg and particularly at lower $[Al]$. The possibility of using a Si modifier in GFAAS to measure

lower $[Al]$ more accurately may well be a useful advance in the field.

Acknowledgements

This research was supported by EPSRC, The Royal Society and Dow Corning Ltd.

References

- [1] F.F. Lopez, C. Cabrera, M.L. Lorenzo, M.C. Lopez, J. Food Sci. 65 (2000) 206.
- [2] K. Popinska, J. Kierkus, M. Lyszkowska, J. Socha, E. Pietraszek, W. Kmiotek, J. Ksiazyk, Nutrition 15 (1999) 683.
- [3] Y. Ezo, A. Takatsu, T. Kuroiwa, S. Eyama, A. Uchiyumi, Bunseki Kagaku 48 (1999) 1013.
- [4] N. Campillo, P. Vinas, I. Lopez-Garcia, M. Hernandez-Cordoba, Talanta 48 (1999) 905.
- [5] I. Kristjansson, T. Faresjö, C. Lionis, A.R. Nosratabadi, K. Gudmundsson, A. Halling, C. Tagesson, Eur. J. Epidemiol. 16 (2000) 231.
- [6] E.B. Dawson, D.R. Evans, W.A. Harris, L.C. Powell, Biol. Trace Elem. Res. 74 (2000) 97.
- [7] V. Riihimäki, H. Hänninen, R. Akila, T. Kovala, E. Kuosma, H. Paakkulainen, S. Valkonen, B. Engström, Scand. J. Work Environ. Health 26 (2000) 118.
- [8] D.C. Manning, W. Slavín, G.R. Carrick, Spectrochim. Acta 37B (1982) 331.
- [9] C.L. Craney, K. Swartout, F.W. Smith III, C.D. West, Anal. Chem. 58 (1986) 656.
- [10] S.P. Ericson, Atom. Spect. 13 (1992) 208.
- [11] J.D. Birchall, C. Exley, J.S. Chappell, M.J. Phillips, Nature 338 (1989) 146.
- [12] C. Exley, J.D. Birchall, Polyhedron 11 (1992) 1901.
- [13] C. Exley, J.D. Birchall, Polyhedron 12 (1993) 1007.
- [14] C. Exley, A. Tollervey, G. Gray, S. Roberts, J.D. Birchall, Proc. Roy. Soc. London B 253 (1993) 93.
- [15] C. Exley, N.C. Price, J.D. Birchall, J. Inorg. Biochem. 54 (1994) 297.
- [16] C. Exley, J.K. Pinnegar, H. Taylor, J. Theor. Biol. 189 (1997) 133.
- [17] C. Exley, J. Inorg. Biochem. 69 (1998) 139.
- [18] F.J. Doucet, C. Schneider, S.J. Bones, A. Kretchmer, I. Moss, P. Tekely, C. Exley, Geochim. Cosmochim. Acta 65 (2001) 2461.
- [19] I.J. Fairchild, A.F. Tooth, A.J. Russell, Geochemistry of the earth's surface, in: H. Armansson (Ed.), Proceedings of the 5th International Symposium on Geochemistry of the Earth's Surface, Reykavik, Iceland, Balkema, Rotterdam, 1999, pp. 91–94.
- [20] J.P. Mullen, J.P. Riley, Anal. Chim. Acta 12 (1955) 162.
- [21] I. Nukatsuka, K. Anezaki, S. Kubota, K. Ohzeki, Anal. Chim. Acta 415 (2000) 221.
- [22] B.V. L'vov, N.P. Romanova, L.K. Polzik, Spectrochim. Acta 46B (1991) 1001.

Appendix B: "The reaction of aluminium with silicic acid in acidic solution: an important mechanism in controlling the biological availability of aluminium?"

Exley, C., C. Schneider and F. Doucet. (2002). Coordination Chemistry Reviews **228**(2): 127-135.

The reaction of aluminium with silicic acid in acidic solution: an important mechanism in controlling the biological availability of aluminium?

Christopher Exley^{a,*}, Celine Schneider^a, Frédéric J. Doucet^b

^a *Birchall Centre for Inorganic Chemistry and Materials Science, School of Chemistry and Physics, Keele University, Staffordshire ST5 5BG, UK*

^b *Department of Chemistry, The Radiochemical Centre of Excellence, The University of Manchester, Oxford Road, Manchester M13 9PL, UK*

Received 30 November 2001; accepted 4 March 2002

Contents

Abstract	127
1. Preface	127
2. Historical perspective	128
3. The mechanism of formation of HAS	130
4. HAS and the biological availability of Al	134
Acknowledgements	135
References	135

Abstract

The reaction of aluminium (Al) with monomeric silicic acid ($\text{Si}(\text{OH})_4$) to form an hydroxyaluminosilicate (HAS) has been well documented over the past 40 or so years. The formation of an aluminium hydroxide template, upon which $\text{Si}(\text{OH})_4$ will condense in competition with Al, was demonstrated to be a prerequisite to HAS formation. This initial reaction results in the formation of a slowly aggregating HAS, with a Si:Al ratio of 0.5, in which silicon tetrahedra are bonded to Al octahedra through three Si–O–Al linkages. We have called this HAS_A . In solutions in which the concentration of $\text{Si}(\text{OH})_4 \geq \text{Al}$ HAS_A acts as a template for the incorporation of further silicon tetrahedra to give a rapidly precipitating HAS (that we have called HAS_B), with a Si:Al ratio of 1.0, in which up to 50% of the constituent Al has adopted tetrahedral geometry. There are, at present, no reliable constants to describe either the formation or the solubility of these HAS. They are extremely insoluble and are likely to play an important role in the control of the release of Al from the edaphic to the aquatic environment. They may also have an important role in Al homeostasis in biota though the evidence to support this is more tentative. © 2002 Elsevier Science B.V. All rights reserved.

Keywords: Aluminium; Silicic acid; Hydroxyaluminosilicate

1. Preface

The primary objective of this review was to critically evaluate scientific literature that has reported the interaction of aluminium (Al) with monomeric silicic acid ($\text{Si}(\text{OH})_4$) in acidic solution. (A comprehensive and authoritative review of all silicate complexes of Al has recently been published [1].) A secondary objective was

to update the significance of this chemistry to the biological availability of Al. A particular bone of contention in this field is the definition of what constitutes $\text{Si}(\text{OH})_4$. We have attempted to reduce the ambiguity that surrounds this definition by only reviewing research in which every attempt had been made to ensure that the only reactive form of silicon in experimental solutions was the neutral monomer and was not charged or polymeric forms of this weak acid. Our interpretation of ‘every attempt’ has excluded any research in which: (i) the concentration of $\text{Si}(\text{OH})_4$ in either stock or experimental solutions exceeded 2.00 mmol l^{-1} ($\text{Si}(\text{OH})_4$ will autocondense at concentrations

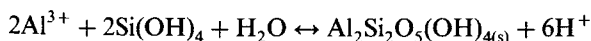
* Corresponding author. Tel.: +44-1782-584080; fax: +44-1782-712378.

E-mail address: cha38@keele.ac.uk (C. Exley).

greater than 2.00 mmol l^{-1} [2]); (ii) Si(OH)_4 was derived from the slow dissolution of inorganic silica (polysilicates are found in equilibrium with slowly dissolving silica [3,4]); (iii) Si(OH)_4 was derived from the hydrolysis of an organosilane and the success of the hydrolysis was not confirmed using the rapid formation of the molybdosilicic acid complex; (iv) the literature contained insufficient detail of the provenance of the Si(OH)_4 used in experiments. We have also limited the scope of this review to acidic solutions ($\text{pH} < 7.00$) to reduce the possibility of significant contributions from deprotonated Si(OH)_4 . Our interpretation of Si(OH)_4 will not be accepted universally. It has resulted in many more exclusions than inclusions. However, until we have definitive data concerning the forms of silicon in undersaturated solutions of Si(OH)_4 , perhaps using ^{29}Si -enriched solutions and NMR, we shall continue to define solutions by using these criteria.

2. Historical perspective

It is our opinion that the most appropriate technique for the preparation of solutions of Si(OH)_4 is the cation exchange of undersaturated solutions of sodium silicate. When, in the mid-60s, Polzer et al., used this method to prepare acidic (pH ca. 5.00) solutions of constant ionic strength containing Si(OH)_4 ($0\text{--}1.63 \text{ mmol l}^{-1}$) and Al (ca. 0.30 mmol l^{-1}) they were able to demonstrate the formation of amorphous precipitates of hydroxyaluminosilicate (HAS) with Si:Al molar ratios of between 0.5 and 1.0 [5]. The precipitates were separated by filtration ($0.10 \mu\text{m}$ membrane filters) and their compositions were obtained from the differences in concentration of Al and Si(OH)_4 before and after filtration. The Si:Al molar ratio of one precipitate was measured directly by an unspecified wet chemical method. A later study by the same group using the same methods showed that all precipitates that were isolated from solutions in which Si(OH)_4 was present to considerable excess had Si:Al molar ratios of about 1.0 [6]. Using data for the concentrations of Al and Si(OH)_4 that had passed through the $0.10 \mu\text{m}$ filter as estimates of Al^{3+} and Si(OH)_4 in equilibrium with the solid phase and the postulated synthesis reaction shown below (assumption that HAS was kaolinite or halloysite);



an equilibrium constant of $10^{11.3}$ was estimated.

One of the most complete studies of the interaction of Al with Si(OH)_4 was carried out in the mid-70s by Luciuk and Huang [7]. They investigated the influence of solution age and OH/Al ratio on the precipitation of HAS from solutions containing Si(OH)_4 and Al (0.15 and 1.52 mmol l^{-1}) at a ratio of either 0.5 or 1.0. They

made a number of important observations which included; (i) the reaction between Al and Si(OH)_4 at the OH/Al ratio of 3 did not result in the significant release of H^+ or H_3O^+ ; (ii) at the same OH/Al ratio and at the higher initial concentration of Al, the reaction of Si(OH)_4 with Al was preceded by further reactions between Si(OH)_4 and the preformed HAS; (iii) at OH/Al ratios of 1 and 2 the presence of Si(OH)_4 both reduced the amount of precipitate that could be removed by filtration ($0.025 \mu\text{m}$ filter) and increased the proportion of Al that had been experimentally classified as non-extractable; (iv) all precipitated HAS were amorphous to X-ray diffraction; (v) analyses of precipitates by IR showed that the formation of HAS at OH/Al of 3 resulted in the disappearance of peaks attributable to Al–OH vibrations and the appearance of peaks attributable to Si–OH vibrations; (vi) HAS precipitates formed after 100 days aging in solutions in which the Si:Al molar ratio was either 0.5 or 1.0 were composed of Si and Al in molar ratios of 0.45 and 0.67, respectively. These observations helped Luciuk and Huang to conclude that the HAS precipitates identified in their experiments had been formed by the condensation of Si(OH)_4 at hydroxyl bridges and/or Al–OH on aluminium hydroxide lattices.

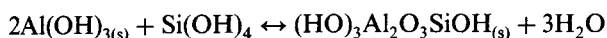
The early work from the groups of JD Hem and PM Huang was supported and extended in its scope by Wada [8,9]. In particular, cation exchange was used to retain HAS and to identify their composition in solutions of fixed concentration of Al and different pH, concentrations of Si(OH)_4 and age. It was demonstrated that for solutions of OH/Al ≥ 1 the primary determinant of the Si:Al molar ratio of the HAS was the ratio of Si(OH)_4 to Al in the parent solution. In solutions that had been aged for 100 days the Si:Al ratio of HAS ranged from ca. 0.40 (for parent solutions with an excess of Al) to ca. 1.0 (for solutions with an excess of Si(OH)_4). An increasing excess of Si(OH)_4 did not result in a higher content of Si in the retained HAS. Because of their composition, the HAS were likened to the soil aluminosilicates allophane and imogolite. However, unlike these structures they were amorphous to X-ray diffraction and had no distinct structure when viewed under the electron microscope [9].

Prominent in the field of the reaction of Si(OH)_4 with Al is Farmer's group in Aberdeen, Scotland, pioneers in the identification and structural characterisation of imogolite [10]; they also demonstrated the formation of HAS of Si:Al molar ratio of 0.50 in acidic solutions (pH 4.50–5.50) in which the concentration of Si(OH)_4 exceeded 0.10 mmol l^{-1} [11]. When these solutions were heated, they generated imogolite and this prompted Farmer to call the precursors to this phase, the aforementioned HAS, protoimogolite. It is unusual that Farmer's group did not observe the formation of HAS of Si:Al molar ratio of 1.0 when Si(OH)_4 was present to

excess in their solutions. This group have continued their investigations into 'proto-imogolite' and they have used potentiometry [12] to determine a formation constant of $pK_{110} = 2.50 \pm 0.05$ for the putative species;



and equilibrium dialysis and the above formation constant to obtain a solubility expression, $\log K_{\text{so}} = 7.02$, for a protoimogolite sol [13];



The inability of this solubility expression to explain the formation of HAS in both synthetic and natural waters has raised some discussion in the scientific literature [14–16].

We have been investigating the reaction of Al with $\text{Si}(\text{OH})_4$ for the last 15 years with particular emphasis on the influence of this reaction on the biological availability of Al [17–19]. Initial research served, in the main, to confirm the aforementioned earlier studies and used both membrane filtration and cation exchange to demonstrate the formation in acidic solutions of HAS of Si:Al molar ratios 0.3–0.6 [19,20]. A lack of reliable quantitative data describing both the formation and solubility of HAS in acid solution prompted an investigation into HAS formation at an environmentally (physiologically) significant concentration of Al [21,22]. Equilibrium dialysis, using tubing with a nominal pore size of ca. 1 nm, was used to confirm the formation of HAS in acidic solutions containing 0.10 mmol l^{-1} $\text{Si}(\text{OH})_4$ and only $4.0 \mu\text{mol l}^{-1}$ Al. The dialysis experiment showed that HAS colloids were significantly smaller than hydroxyaluminium (HA) colloids formed and aged under the same solution conditions. It was proposed that the formation of HAS involved the poisoning of HA polymerisation by $\text{Si}(\text{OH})_4$ [22]. Subsequent experiments using the same low concentration of Al used membrane filtration (40 nm nominal filter rating) to describe how $\text{Si}(\text{OH})_4$ influenced the formation and precipitation of HAS in acidic solution [21]. In solutions in which $\text{Si}(\text{OH})_4$ was present to considerable excess, the formation of HAS was instantaneous. The aggregation of colloidal HAS to a filterable size was significantly slower than the corresponding HA colloids. The latter showed an unchanged particle size distribution after about 3 weeks whereas HAS were still aggregating towards a filterable size after 12 weeks. In addition the pH of minimum solubility had shifted from ca. pH 6.50 for HA colloids to ca. pH 5.50 for HAS. It was interesting to note that this shift in the pH of minimum solubility corresponded closely to the base-neutralising capacity of the solutions. Solutions in which HAS were the predominant form of Al were unable to buffer base additions at pH greater than ca. 5.20 whereas in solutions of HA colloids, this buffering capacity was evident up to ca. pH 5.90. This research

confirmed the formation of HAS in acidic solutions containing only $4.0 \mu\text{mol l}^{-1}$ total Al and it provided a great deal of support for the proposed mechanism of their formation. However, it was only recently that the next significant step forward towards the confirmation of this mechanism was made.

We began by using a combination of membrane filtration (0.1 μm membrane filter) and morin-Al fluorescence (estimate of the fast-reactive Al fraction) to demonstrate that HAS were only formed in solutions which were saturated with respect to amorphous aluminium hydroxide [23,24]. The next challenge was to understand the structure and stoichiometry of HAS that were formed under various solution conditions. This was achieved by collecting HAS formed in synthetic solutions in sufficient quantities to enable their structures to be probed by solid state NMR [24]. After 3 months aging at ca. pH 6.20 HAS were collected by filtration from solutions in which the $\text{Si}(\text{OH})_4$ to Al ratio varied from 8:1 (2.0 mmol l^{-1} $\text{Si}(\text{OH})_4$) to 1:4 (0.5 mmol l^{-1} $\text{Si}(\text{OH})_4$). HAS that were formed in parent solutions in which the concentration of $\text{Si}(\text{OH})_4 \geq \text{Al}$ had aggregated sufficiently to be removed using a 2.0 μm membrane filter whereas those HAS that were formed in parent solutions in which Al was present to excess were collected using a 0.2 μm membrane filter. This was our first indication that we should expect to find more than one form of HAS in the parent solutions. Solid state ^{29}Si - and ^{27}Al -NMR combined with elemental composition by SEM-EDX revealed two distinct forms of HAS (Fig. 1). HAS_A had an ideal Si:Al ratio of 0.5 and its structure was dominated by Si coordinated through three Si–O–Al linkages ($\text{Q}^3(3\text{Al})$) to Al in an octahedral geometry. HAS_B had an ideal Si:Al ratio of 1.0 and whilst it retained some of the structure of HAS_A its structure now included a significant framework of Si ($\text{Q}^4(1-2\text{Al})$ and $\text{Q}^3(1-2\text{Al})$) and Al tetrahedra. HAS_B had no Al-associated protons and a maximum of one silanol group per Si. HAS_A was the predominant HAS formed in parent solutions in which Al was present to excess whereas HAS_B predominated in parent solutions in which $\text{Si}(\text{OH})_4$ was present to excess. We used atomic force microscopy (AFM) to confirm that the precipitates that we had isolated using filtration and analysed by NMR were representative of the colloidal HAS in the parent solutions (Fig. 2). We identified two distinct forms of colloidal HAS, rectangular (up to 170 nm in length) and discoid (up to 43 nm in diameter), and the occurrence of these forms in the parent solutions matched the occurrence of HAS_A (rectangular) and HAS_B (discoid) in the precipitates that had been filtered from the same solutions. It was of note that HAS_B was not found in those solutions in which Al was present to excess whereas HAS_A was found in solutions in which Si was present to excess [23]. We have proposed structures for HAS_A and HAS_B and have suggested how HAS_B

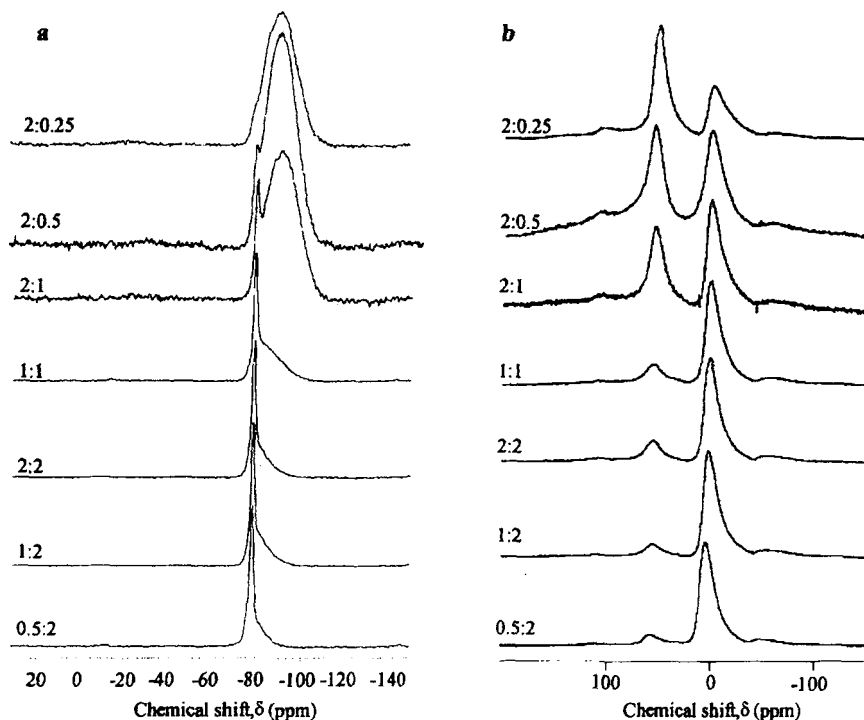


Fig. 1. The influence of different combinations of Si(OH)_4 and Al (units are mmol dm^{-3}) in treatment solutions on the structure of precipitated HAS. Representative spectra of two to three replicate samples are shown. (a) ^{29}Si -CP-MAS NMR. Field strength: 9.4 Tesla. Contact time: 5 ms. Sample spinning speed close to 5 kHz. Acquisition time: 129 ms. Pulse delay: 5 s. Chemical shifts referenced to Q8M8. Each spectrum was collected from 3500 to 5000 scans. (b) ^{27}Al -HD-MAS NMR. Field strength: 9.4 Tesla. Sample spinning speed close to 4 kHz. Acquisition time: 30 ms. Pulse delay: 1 s. Chemical shifts referenced to 1 M $\text{Al(H}_2\text{O)}_6^{3+}$ solution. Each spectrum was collected from 5000 scans. (Reproduced with permission from [24].)

was formed from the interaction of HAS_A with excess Si(OH)_4 [24].

3. The mechanism of formation of HAS

It has proven to be an easier task to identify the formation of HAS than to elucidate their mechanism of formation. In the early 1990s we proposed that the formation of HAS involved the inhibition of the growth of aluminium hydroxide by the substitution of hydroxylated Al by Si(OH)_4 [22]. Luciuik and Huang had come to the same conclusion almost 20 years earlier [7]! Both groups, and others [5,6,8,9], had observed that the presence of Si(OH)_4 in a saturated solution of Al acted to both increase the proportion of Al that passed through a membrane filter and reduce the fraction of Al that was experimentally defined as being in a monomeric form. The consensus of opinion was that Si(OH)_4 had reacted with a HA template to form HAS which had subsequently grown at a very much reduced rate to that of aluminium hydroxide in equivalent solutions in which Si(OH)_4 was absent. Other consistent observations have been the reduced base-neutralising capacities of Al solutions containing Si(OH)_4 [7,21] and

the dependence of the Si:Al ratio of HAS precipitates on the ratio of Si(OH)_4 to Al in parent solutions [9,24].

The recent elucidation of the structures and stoichiometries of two distinct HAS, HAS_A and HAS_B [24], which are probably identical to the HAS that have been identified by other means in earlier work will now help in elucidating their mechanisms of formation. For example, it would now seem very likely that the HAS of Si:Al molar ratio of 1.0 identified by Hem and coworkers [5,6] were neither kaolinite nor halloysite but rather an HAS (HAS_B) in which Al was present as a 50:50 mixture of octahedral and tetrahedral geometries. We also know that this HAS was formed as the result of the continued incorporation of Si(OH)_4 into another HAS (HAS_A) [24], a reaction that had been alluded to in an earlier publication [7]. A summary of proposed reaction schemes for the formation of the simplest precursors to HAS_A colloids is presented in Fig. 3. It is interesting that Schemes 1–3 show Si(OH)_4 condensing with hydroxyl or water groups on an aluminium hydroxide framework in which the adjacent Al atoms are joined by two hydroxy bridges. These double-hydroxy bridges are the main repetitive units in the hydrated structures of the crystalline forms of both aluminium hydroxide, such as gibbsite, bayerite and nordstrandite, and a number of aluminosilicates, includ-

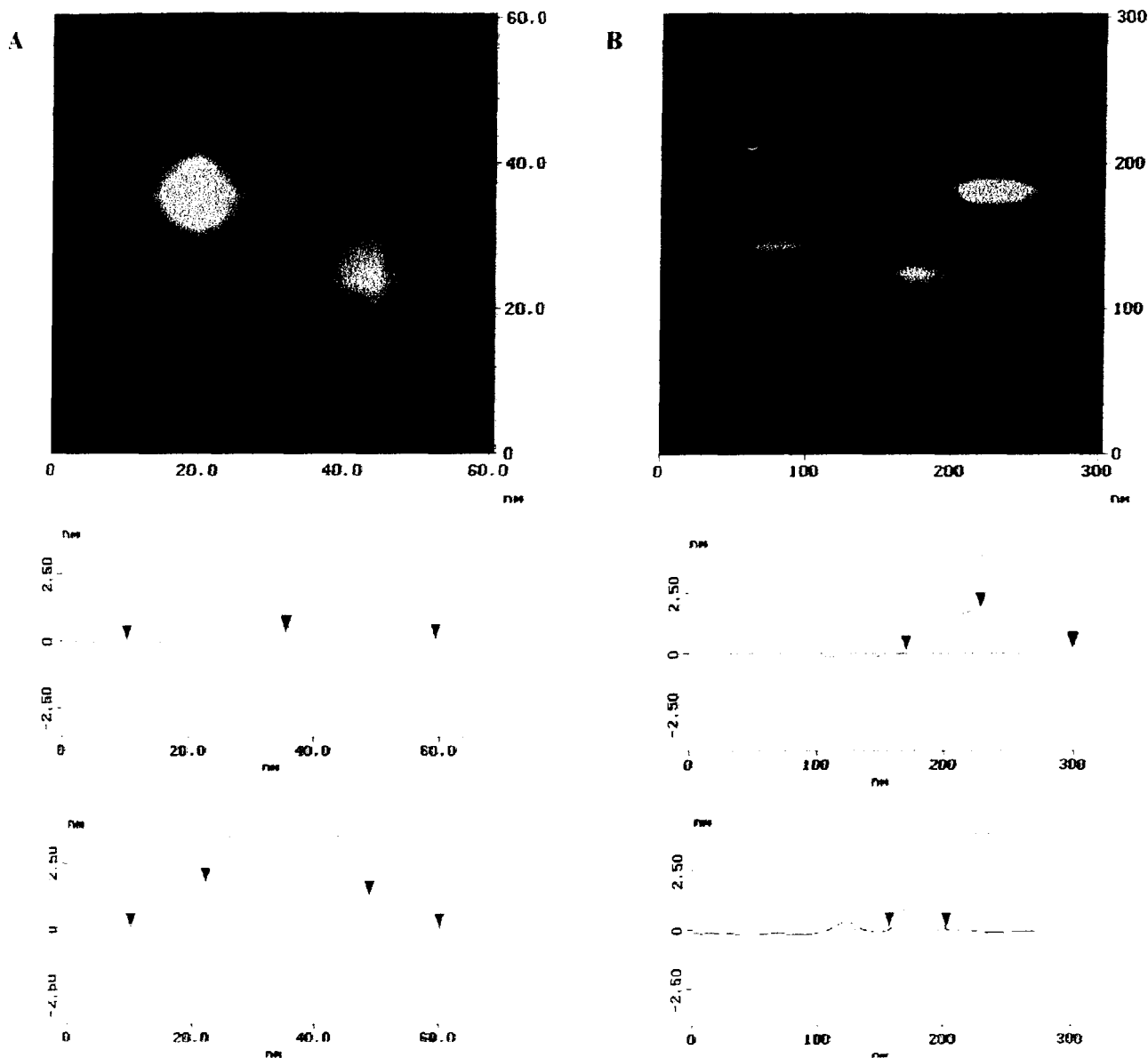


Fig. 2. Close up AFM images of representative individual HAS structures and line profiles representing the section analysis of these two structures: (A) discoid HAS, depth 1–2 nm, diameter 23–25 nm; (B) rectangular HAS, depth 1–2 nm, width 40–45 nm, length 87–170 nm. (Reproduced with permission from [23].)

ing imogolite, kaolinite and halloysite. The HAS that are formed from the interaction of $\text{Si}(\text{OH})_4$ with Al are amorphous to both wide angle and small angle X-ray diffraction spectrometry [5–7,24] and do not show any distinct structural features under the electron microscope [24]. The amorphous nature of HAS has been one of the most consistent observations made by researchers in the field over the years and this must bring into question the appropriateness of reaction schemes which suggest that $\text{Si}(\text{OH})_4$ will condense at or across groups which are supported by a double-hydroxy bridge structure? For example, whilst the crystalline alumin-

silicate imogolite will apparently satisfy much of the structural and stoichiometric data available for HAS_A , ($\text{Si}:\text{Al}$ ratio = 0.50; Si coordinated through three Si–O–Al linkages to octahedral Al), HAS_A is an amorphous mineral with no gross structural similarity to imogolite. It is also easy to imagine how $\text{Si}(\text{OH})_4$ could be trapped within the hexagonal framework of individual gibbsite units through condensation across alternate hydroxy bridges, these units then coalescing to build a structure with a Si:Al ratio of 0.5 (Fig. 4). However, it is difficult to see how the incorporation of $\text{Si}(\text{OH})_4$ in such a structure would lead to a significant reduction in the

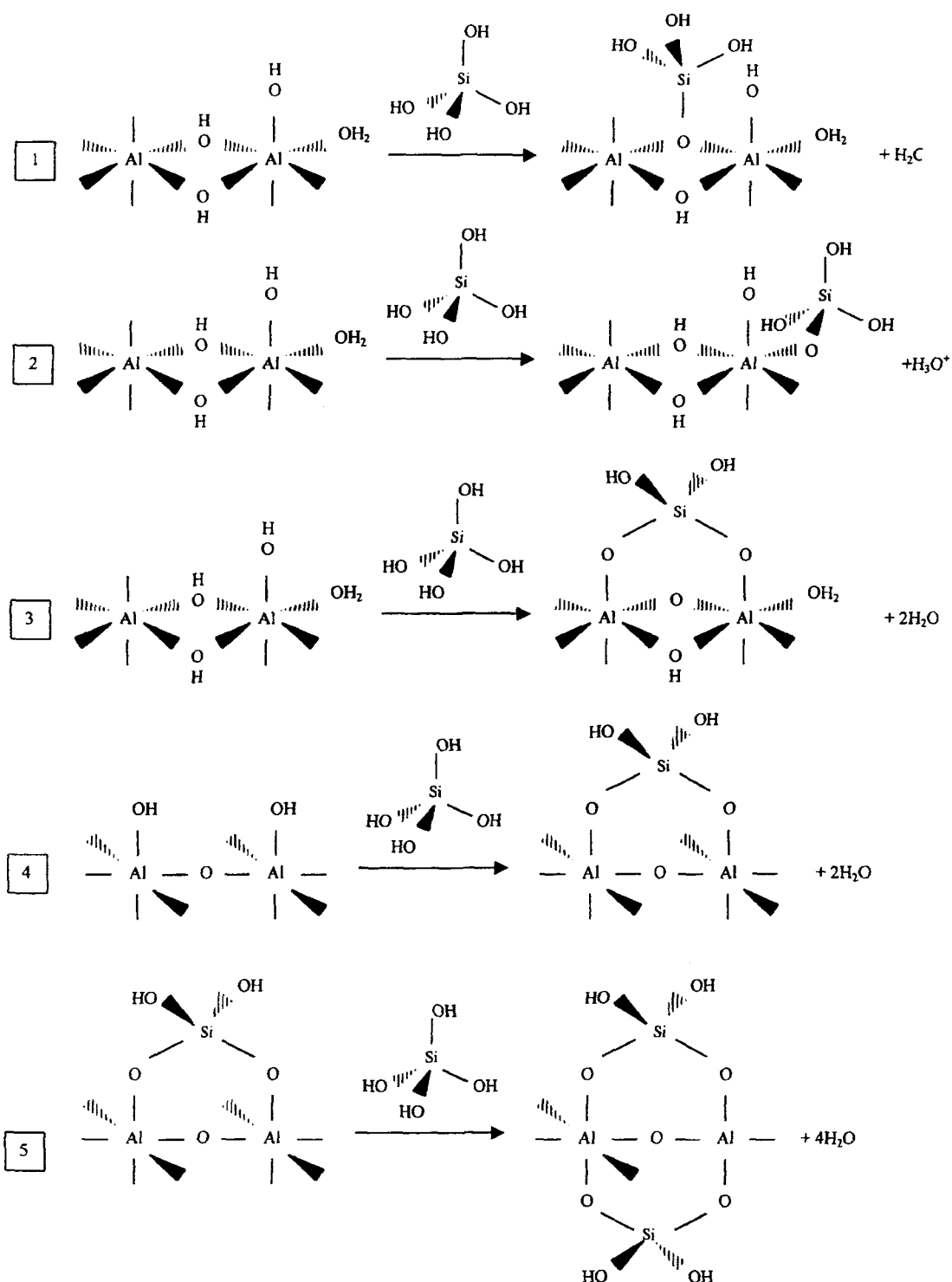


Fig. 3. Schematic showing possible reaction schemes for the formation of the precursors to HAS_A (Scheme 1–4) and HAS_B (Scheme 5).

growth of the gibbsite (aluminium hydroxide) sheet since the growth sites have not been blocked by the inclusion of Si(OH)₄. The growth sites would be blocked if the imogolite sheet curled to form tubes. However,

these structures or even fragments of these structures are not formed in HAS prepared at room temperature. Whilst it has been shown that boiling a solution of an HAS prepared in a similar manner to HAS_A will result

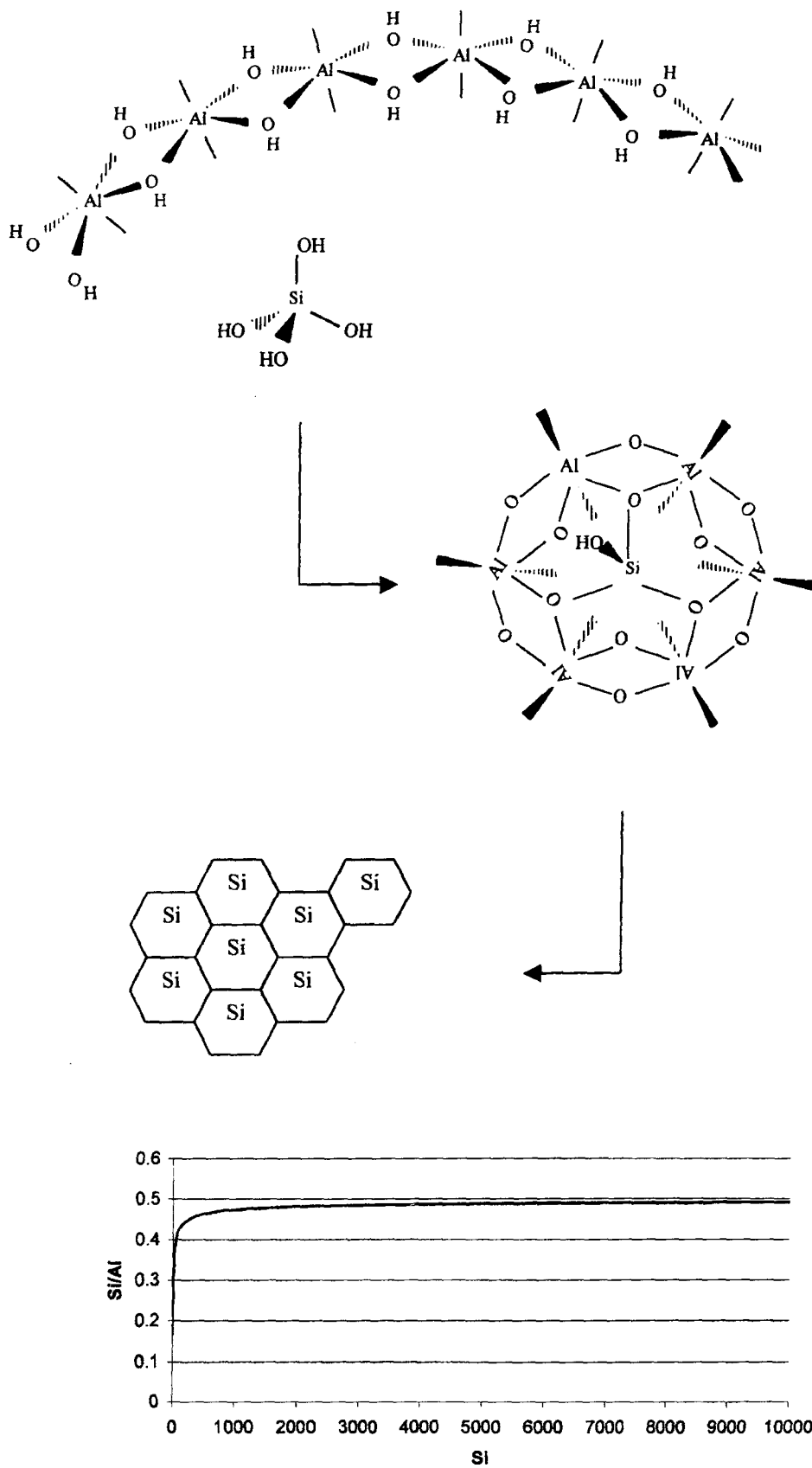


Fig. 4. Schematic showing a possible chain of events leading to the formation of protoimogolite.

in the formation of imogolite [25] this is not direct evidence that HAS_A has either the structure of imogolite or that it would, in time, form imogolite in the natural environment. It is very likely that the act of boiling will bring with it its own influences on the arrangement and rearrangement of the Si tetrahedra and Al octahedra in producing the extremely stable crystalline phase of imogolite.

It is clear from experiments that the condensation of Si(OH)₄ at growth sites on aluminium hydroxide is competitive with further condensation reactions with HA units. To be competitive the reaction with Si(OH)₄ must be kinetically and thermodynamically preferable. Single replacements of Al–OH or Al–OH₂ with Al–OSi(OH)₃ are unlikely to be competitive. The instability of the putative AlSiO(OH)₃²⁺ species in competition with OH[−] is testimony to the unfavoured nature of this reaction in solutions which are saturated with respect to an amorphous aluminium hydroxide phase [12,26]. We have speculated that the initial condensation reaction will involve Si(OH)₄ bridging Al–OH on adjacent Al atoms (Fig. 3; Scheme 4) and that the interaction with Si(OH)₄ will be stabilised further by a third Si–O–Al linkage upon the aggregation of these HAS units [24]. This interaction would favour growth in one particular direction and this is in fact what we have observed for HAS_A using AFM (Fig. 2). Such a reaction scheme is also supported by titration data which together suggest that the interaction with Si(OH)₄ does not involve any proton release [7,21].

In much of the earlier research on the formation of HAS Si(OH)₄ was present in solutions to excess and we now know that under these conditions the predominant form of HAS would be HAS_B [24]. The structure of HAS_B was a surprise and not least because of the high proportion of tetrahedrally coordinated Al but also because of the room temperature dehydroxylation reactions which allowed the further incorporation of Si(OH)₄ into the HAS_A structure. HAS_B must have a smaller unit structure than HAS_A since its growth sites are severely limited by the inclusion of further Si(OH)₄ and the switch in geometry of up to 50% of the coordinated Al. The smaller unit size of HAS_B was supported by AFM (Fig. 2). However, HAS_B is likely to be uncharged, at least in acidic solution, and will aggregate much more rapidly than HAS_A. This explains the ease with which it can be filtered from solution in comparison to both HAS_A and aluminium hydroxide [24].

There has been up until now only one valid attempt to determine the solubility of HAS formed from the interaction of Si(OH)₄ with Al and this was only applied to HAS equivalent to what has now been identified as HAS_A [13]. It is likely that this has significantly underestimated the solubility of this HAS and it may turn out that HAS_B is an even more insoluble HAS. We have

been following the dissolution of both of these HAS for over 18 months now and we have yet to record any measurable release of Al. We are in the process of quantifying the formation and solubility of HAS_A and HAS_B and we hope to be able to report on the progress of this research in the near future.

4. HAS and the biological availability of Al

It is not yet clear at which level Si(OH)₄ will have a significant impact upon the biological availability, and hence toxicity of Al. There has been much speculation about the amelioration of Al toxicity by Si(OH)₄ though we have found very few experiments which have investigated, indirectly or directly, the toxicity of HAS in biota. We found that this was particularly the case when we applied our criteria for excluding studies in which there was some ambiguity about the reactive form of silicon. Even our own ‘seminal’ study [27] has failed these criteria as we were unable to guarantee that Si(OH)₄ was the only form of reactive silicon in the stock solutions used in these experiments!

The research which has shown a protective effect of Si(OH)₄ in Alzheimer’s disease [28–30] and Al-related renal disease [31] was circumstantial in that it did not demonstrate a direct involvement of HAS. However, it was interesting that each of these studies demonstrated that Si(OH)₄ was only protective at concentrations in excess of 150–200 μmol l^{−1}. The question as to the mechanism of these protective effects has not been answered though it may have involved both non-systemic (e.g. reduced absorption of Al [32]) and systemic (e.g. accelerated excretion of Al [33]) formation of HAS.

Al toxicity in plants was ameliorated by Si(OH)₄ acting, apparently, both ex planta [34] and in planta [35]. In the former study the authors demonstrated a reduced concentration of monomeric Al (total [Al] of 60 and 120 μmol l^{−1}) in the presence of 4.0 μmol l^{−1} Si(OH)₄ at pH 4.0. However, the low pH of the solution would make it difficult to ascribe the protective effect of Si(OH)₄ to the ex planta formation of HAS. In another study Si(OH)₄ both increased and decreased the toxicity of Al in barley. Again, the low solution pH used in this study (pH 4.2) would probably have prevented any ex planta formation of HAS. The ability of Si(OH)₄ to increase the biological availability of inorganic phosphate in algae in the presence of Al was attributed to the formation of HAS [36]. Al limited the biological availability of phosphate in both a diatom, *Navicula pelliculosa*, and a green alga, *Chlorella vulgaris*, and this effect was abolished in the presence of Si(OH)₄ in excess of 100 μmol l^{−1}. This prompted the suggestion that a mechanism of silicon essentiality in biology was to

maintain the biological availability of phosphate in the presence of Al.

The only experiment to have prepared HAS, identified their presence in solution and, thereafter, tested their toxicity was carried out in fish in acidic water [37]. HAS prepared from stock solutions which included 2.0 mmol l⁻¹ Si(OH)₄ and 1.0 mmol l⁻¹ Al (most probably a mixture of what we now know as HAS_A and HAS_B) were, upon being diluted into a fish assay at pH 5.5 to give a total concentration of Al of ca. 13.0 μmol l⁻¹, completely non-toxic. The same concentration of Al added from a stock solution in which there was not any Si(OH)₄ resulted in 100% death of fish within 48 h exposure. Clearly preformed HAS which have been allowed to aggregate to a filterable size (ca. > 100 nm) were stable when they were diluted into the fish assay system. What is not yet known is the degree of aggregation that would be required to result in biologically inert HAS.

The formation of HAS is an important control of the biological availability of Al. However, it would seem that this control is mainly geochemical in nature with HAS contributing to Al solubility control in the natural environment [21]. There is some in vitro evidence that the formation of HAS might act directly in limiting the biological availability of Al (for example, in preventing Al being bound by biomolecules [38,39]) though we do not yet have a mechanism to explain how stable HAS might be formed in vivo. The ubiquity of Al in the earth's crust is slowly being matched by the ubiquitous number of applications of Al in modern life. If we are to sustain this 'Al Age' we must ensure that Al will be used safely and its unique inorganic chemistry with Si(OH)₄ may be important in achieving this aim.

Acknowledgements

The authors acknowledge the support of The Royal Society, EPSRC and Dow Corning Limited in the preparation of this review. We would also like to acknowledge the helpful comments of two anonymous reviewers.

References

- [1] T.W. Swaddle, *Coord. Chem. Rev.* 219 (2001) 665.
- [2] R.K. Iler, *The Chemistry of Silica*, Wiley-Interscience, New York, 1979.
- [3] M. Dietzel, *Geochim. Cosmochim. Acta* 64 (2000) 3275.
- [4] S.D. Kinrade, A.S. Schach, R.J. Hamilton, C.T.G. Knight, *Chem. Commun.* (2001) 1564.
- [5] W.L. Polzer, J.D. Hem, H.J. Gabe, US Geological Survey Professional Paper 575-B, 1967, B128.
- [6] J.D. Hem, C. Roberson, C. Lind, W.L. Polzer, US Geological Survey Water-Supply Paper 1827-E, 1973, E1.
- [7] G.M. Luciuk, P.M. Huang, *Soil Sci. Soc. Am. J.* 38 (1974) 235.
- [8] K. Wada, H. Kubo, *J. Soil Sci.* 26 (1975) 100.
- [9] S.-I. Wada, K. Wada, *J. Soil Sci.* 31 (1980) 457.
- [10] P. Cradwick, V. Farmer, J. Russell, C. Masson, K. Wada, N. Yoshinaga, *Nat. Phys. Sci.* 240 (1972) 187.
- [11] V.C. Farmer, A.R. Fraser, *J. Soil Sci.* 33 (1982) 737.
- [12] V.C. Farmer, D.G. Lumsdon, *Geochim. Cosmochim. Acta* 58 (1994) 3331.
- [13] D.G. Lumsdon, V.C. Farmer, *Eur. J. Soil Sci.* 46 (1995) 179.
- [14] C. Exley, J.D. Birchall, *Eur. J. Soil Sci.* 47 (1996) 137.
- [15] F. Gerard, J.P. Boudot, J. Ranger, *Appl. Geochem.* 16 (2001) 513.
- [16] M. Simonsson, D. Berggren, *Eur. J. Soil Sci.* 49 (1998) 317.
- [17] C. Exley, *J. Inorg. Biochem.* 69 (1998) 139.
- [18] J.D. Birchall, J.S. Chappell, *Lancet* 2 (1988) 1008.
- [19] J.S. Chappell, J.D. Birchall, *Inorg. Chim. Acta-Bioinorg. Chem.* 153 (1988) 1.
- [20] J.D. Birchall, J.S. Chappell, *Clin. Chem.* 34 (1988) 265.
- [21] C. Exley, J.D. Birchall, *Polyhedron* 12 (1993) 1007.
- [22] C. Exley, J.D. Birchall, *Polyhedron* 11 (1992) 1901.
- [23] F. Doucet, M. Rotov, C. Exley, *J. Inorg. Biochem.* 87 (2001) 71.
- [24] F.J. Doucet, C. Schneider, S.J. Bones, A. Kretschmer, I. Moss, P. Tekely, C. Exley, *Geochim. Cosmochim. Acta* 65 (2001) 2461.
- [25] V.C. Farmer, M.J. Adams, A.R. Fraser, F. Palmieri, *Clay Miner.* 18 (1983) 459.
- [26] C. Exley, J.D. Birchall, *Geochim. Cosmochim. Acta* 59 (1995) 1017.
- [27] J.D. Birchall, C. Exley, J.S. Chappell, M.J. Phillips, *Nature* 338 (1989) 146.
- [28] H. Jacqmin-Gadda, D. Commenges, L. Letenneur, J.F. Dartigues, *Epidemiology* 7 (1996) 281.
- [29] V. Rondeau, D. Commenges, H. Jacqmin-Gadda, J.F. Dartigues, *Am. J. Epidemiol.* 152 (2000) 59.
- [30] V. Rondeau, H. Jacqmin-Gadda, D. Commenges, J.F. Dartigues, *Am. J. Epidemiol.* 154 (2001) 288.
- [31] R. Parry, D. Plowman, H.T. Delves, N.B. Roberts, J.D. Birchall, J.P. Bellia, A. Davenport, R. Ahmad, I. Fahal, P. Altmann, *Nephrol. Dial. Transplant.* 13 (1998) 1759.
- [32] J.A. Edwardson, P.B. Moore, I.N. Ferrier, J.S. Lilley, G.W.A. Newton, J. Barker, J. Templar, J.P. Day, *Lancet* 342 (1993) 211.
- [33] J.P. Bellia, J.D. Birchall, N.B. Roberts, *Ann. Clin. Lab. Sci.* 26 (1996) 227.
- [34] J. Barcelo, P. Guevara, C. Poschenrieder, *Plant Soil* 154 (1993) 249.
- [35] I. Corrales, C. Poschenrieder, J. Barcelo, *Plant Soil* 190 (1997) 203.
- [36] C. Exley, A. Tollervey, G. Gray, S. Roberts, J.D. Birchall, *Proc. R. Soc. London Ser. B-Biol. Sci.* 253 (1993) 93.
- [37] C. Exley, J.K. Pinnegar, H. Taylor, *J. Theor. Biol.* 189 (1997) 133.
- [38] E. Rowatt, R.J.P. Williams, *Coord. Chem. Rev.* 149 (1996) 167.
- [39] C. Exley, N.C. Price, J.D. Birchall, *J. Inorg. Biochem.* 54 (1994) 297.

References

- (1996). Research issues in Aluminium toxicity, R. A. Yokel and M. S. Golub, Taylor & Francis.
- Abreo, K. (2001). Aluminium-induced bone disease: Implications for Alzheimer's disease. Aluminium and Alzheimer's disease. The science that describes the link. C. Exley, Elsevier Science: 37-58.
- Akitt, J. W. (1989). "Multinuclear Studies of Aluminum Compounds." Progress in Nuclear Magnetic Resonance Spectroscopy **21**: 1-149.
- Altmann, P. (2001). Aluminium induced disease in subject with and without renal failure - does it help us to understand the role of aluminium in Alzheimer's disease? Aluminium and Alzheimer's disease. The science that describes the link. C. Exley, Elsevier Science: 1-36.
- Andrew, E. R., A. Bradbury and R. G. Eades (1958). "Nuclear magnetic resonance spectra from a crystal rotated at high speed." Nature **182**: 1659.
- Aston, S. (1983). Natural water and atmospheric chemistry of silicon., S. R. Aston, Silicon geochemistry and biochemistry, London, Academic Press.
- Bache, B. W. (1986a). Journal of the Geological Society **143**: 699.
- Bache, B. W. (1986b). "Aluminum Mobilization in Soils and Waters." Journal of the Geological Society **143**: 699-706.
- Baes, C. J. and R. E. Mesmer (1976). The hydrolysis of cations, W.-I. publication, New York, John Wiley & Sons.

- Barr, T. L. (1983). "An Xps Study of Si as It Occurs in Adsorbents, Catalysts, and Thin-Films." Applied Surface Science **15**(1-4): 1-35.
- Barr, T. L. (1990). "The Nature of the Relative Bonding Chemistry in Zeolites - an Xps Study." Zeolites **10**(8): 760-765.
- Barr, T. L. (1995). "Comparative Electron-Spectroscopy for Chemical-Analysis and Nuclear-Magnetic-Resonance Analysis of High-Surface-Area Materials - Zeolites." Microporous Materials **3**(4-5): 557-564.
- Barr, T. L. and M. A. Lishka (1986). "Esca Studies of the Surface-Chemistry of Zeolites." Journal of the American Chemical Society **108**(12): 3178-3186.
- Barr, T. L., S. Seal, L. M. Chen and C. C. Kao (1994). "A New Interpretation of the Binding-Energies in X-Ray Photoelectron Studies of Oxides." Thin Solid Films **253**(1-2): 277-284.
- Barr, T. L., S. Seal, H. He and J. Klinowski (1995). "X-Ray Photoelectron Spectroscopic Studies of Kaolinite and Montmorillonite." Vacuum **46**(12): 1391-1395.
- Barr, T. L., S. Seal, K. Wozniak and J. Klinowski (1997). "ESCA studies of the coordination state of aluminium in oxide environments." Journal of the Chemical Society-Faraday Transactions **93**(1): 181-186.
- Belia, J. P., J. D. Birchall and N. B. Roberts (1996). Annals of Clinical and Laboratory Science **26**: 227-233.
- Berube, D. and D. G. Brule (1999). "A field aluminium speciation method to study aluminium hazard in water." Fresenius Journal of Analytical Chemistry **363**(5-6): 566-570.

- Birchall, J. D., C. Exley, J. S. Chappell and M. J. Phillips (1989). "Acute Toxicity of Aluminum to Fish Eliminated in Silicon-Rich Acid Waters." Nature **338**(6211): 146-148.
- Blinka, T. A. (1983). "NMR for ^{29}Si : INEPT and DEPT techniques." Review for Advances in Organometallic Chemistry **23**: 193-217.
- Brezonik, P. L., C. E. Mach and C. J. Sampson (2003). "Geochemical controls for Al, Fe, Mn, Cd, Cu, Pb, and Zn during experimental acidification and recovery of Little Rock Lake, WI, USA." Biogeochemistry **62**(2): 119-143.
- Briggs, D. and M. P. Seah Practical surface analysis, 2nd edition, Wiley.
- Brown, P. L. and S. J. Markish (2000). "Evaluation of the free ion activity model of metal-organism interaction. 2. Extension of the conceptual model." Aquatic Toxicology **54**: 177-194.
- Browne, B. A. and C. T. Driscoll (1992). "Soluble Aluminum Silicates - Stoichiometry, Stability, and Implications for Environmental Geochemistry." Science **256**(5064): 1667-1670.
- Browne, B. A., C. T. Driscoll and J. G. McColl (1990a). "Aluminum Speciation Using Morin .2. Principles and Procedures." Journal of Environmental Quality **19**(1): 73-82.
- Browne, B. A., J. G. McColl and C. T. Driscoll (1990b). "Aluminum Speciation Using Morin .1. Morin and Its Complexes with Aluminum." Journal of Environmental Quality **19**(1): 65-72.

- Camilleri, C., S. J. Markish, B. N. Noller, C. J. Turley, G. Parker and R. A. van Dam (2003). "Silica reduces the toxicity of aluminium to a tropical freshwater fish (*Morgurnda morgurnda*)." Chemosphere **50**: 355-364.
- Campbell, P. G. C., M. Bisson, R. Bougie, A. Tessier and J. P. Villeneuve (1983). "Speciation of Aluminum in Acidic Fresh-Waters." Analytical Chemistry **55**(14): 2246-2252.
- Carlisle, E. (1972). "Silicon: an essential element for the chick." Science **178**: 619-621.
- Carlisle, E. (1974). "Silicon as an essential element." Federation Proceedings **33**(6): 1758-1766.
- Carpenter, J. C., J. A. Cella and S. B. Dorn (1995). "Study of the degradation of polydimethylsiloxanes in soil." Environmental Science and Technology **29**: 864-868.
- Chadwick, D. J. and J. Whelan (1992). *Aluminium in biology and medicine*. New-York, Wiley. **169**.
- Childs, C. W., K. Inoue, H. Seyama, M. Soma, B. K. G. Theng and G. Yuan (1997). "X-ray photoelectron spectroscopic characterisation of silica springs allophane." Clay Minerals **32**: 565-572.
- Craney, C. L., K. Swartout, F. W. Smith and C. D. West (1986). "Improvement of Trace Aluminum Determination by Electrothermal Atomic-Absorption Spectrophotometry Using Phosphoric-Acid." Analytical Chemistry **58**(3): 656-658.

- Doucet, F. J., M. E. Rotov and C. Exley (2001a). "Direct and indirect identification of the formation of hydroxyaluminosilicates in acidic solutions." Journal of Inorganic Biochemistry **87**(1-2): 71-79.
- Doucet, F. J., C. Schneider, S. J. Bones, A. Kretchmer, I. Moss, P. Tekely and C. Exley (2001b). "The formation of hydroxyaluminosilicates of geochemical and biological significance." Geochimica Et Cosmochimica Acta **65**(15): 2461-2467.
- Edwardson, J. A., P. B. Moore, I. N. Ferrier, J. S. Lilley, G. W. A. Newton, J. Barker, J. Templar and J. P. Day (1993). Lancet(211-212).
- Epstein, E. (1994). "The anomaly of silicon in plant biology." Proceedings of the National Academy of Sciences of the United States of America **91**(1): 11-17.
- Epstein, E. (1999). "Silicon." Annual Review Plant Physiology and Plant Molecular Biology **50**: 641-664.
- Exley, C. (1996). "Aluminium in the brain and heart of the rainbow trout." Journal of Fish Biology **48**(4): 706-713.
- Exley, C. (1998). "Silicon in life: A bioinorganic solution to bioorganic essentiality." Journal of Inorganic Biochemistry **69**(3): 139-144.
- Exley, C. (2001). Aluminium and Alzheimer's disease. The science that describes the link., Elsevier.
- Exley, C. and J. D. Birchall (1992a). "The Cellular Toxicity of Aluminum." Journal of Theoretical Biology **159**(1): 83-98.

- Exley, C. and J. D. Birchall (1992b). "Hydroxyaluminosilicate Formation in Solutions of Low Total Aluminum Concentration." Polyhedron **11**(15): 1901-1907.
- Exley, C. and J. D. Birchall (1993). "A Mechanism of Hydroxyaluminosilicate Formation." Polyhedron **12**(9): 1007-1017.
- Exley, C. and J. D. Birchall (1995). "An Assessment of Complex-Formation between Aluminum and Silicic-Acid in Acidic Solutions - Comment." Geochimica Et Cosmochimica Acta **59**(5): 1017-1017.
- Exley, C., J. S. Chappell and J. D. Birchall (1991). "A Mechanism for Acute Aluminum Toxicity in Fish." Journal of Theoretical Biology **151**(3): 417-428.
- Exley, C., J. K. Pinnegar and H. Taylor (1997). "Hydroxyaluminosilicates and acute aluminium toxicity in fish." Journal of Theoretical Biology **189**(2): 133-139.
- Exley, C., C. Schneider and F. J. Doucet (2002). "The reaction of aluminium with silicic acid in acidic solution: an important mechanism in controlling the biological availability of aluminium?" Coordination Chemistry Reviews **228**(2): 127-135.
- Exley, C. and W. Struthers (1992). "The Localization of Aluminum in the Tissues of the Rainbow- Trout." Aquaculture **100**(1-3): 323-324.
- Exley, C., A. J. Wicks, R. B. Hubert and J. D. Birchall (1994). "Polynuclear Aluminum and Acute Aluminum Toxicity in the Fish." Journal of Theoretical Biology **167**(4): 415-416.
- Exley, C., A. J. Wicks, R. B. Hubert and J. D. Birchall (1996). "Kinetic constraints in acute aluminium toxicity in the rainbow trout (*Oncorhynchus mykiss*)." Journal of Theoretical Biology **179**(1): 25-31.

Fairchild, I. J., J. A. Killawee, M. J. Sharp, B. Spiro, B. Hubbard, R. D. Lorrain and J. L. Tison (1999). "Solute generation and transfer from a chemically reactive alpine glacial-proglacial system." Earth Surface Processes and Landforms **24**(13): 1189-1211.

Farmer, V. C. and D. G. Lumsdon (1994). "An assessment of complex formation between aluminium and silicic acid in acidic solutions." Geochimica Et Cosmochimica Acta **58**: 3331-3334.

Fifield, F. W. and D. Kealey (2000). Principles and practice of analytical chemistry, 5th edition, B. S. Ltd.

Frech, W., E. Lundberg and A. Cedergren (1985). "Investigations of Some Methods Used to Reduce Interference Effects in Graphite-Furnace Atomic-Absorption Spectrometry." Progress in Analytical Atomic Spectroscopy **8**(3-4): 257-370.

Furrer, G., B. L. Phillips, K. U. Ulrich, R. Pothig and W. H. Casey (2002). "The origin of aluminium flocs in polluted streams." Science **297**: 2245-2247.

Ganrot, P. O. (1986). "Metabolism and possible health effects of aluminium."

Gardiner, P. E., J. M. Ottaway, G. S. Fell and D. J. Halls (1981). "Determination of Aluminum in Blood-Plasma or Serum by Electrothermal Atomic-Absorption Spectrometry." Analytica Chimica Acta **128**(JUL): 57-66.

Gout, R., G. S. Pokrovski, J. Schott and A. Zwick (1999). "Raman spectroscopy study of aluminium silicate complexation in acidic solutions from 25 to 150C." Journal of Solution Chemistry **28**(1): 73-82.

- Griessbach, E. F. C. and R. G. Lehmann (1999). "Degradation of polydimethylsiloxane fluids in the environment-A review." Chemosphere **56(6)**: 1461-1466.
- He, H., T. L. Barr and J. Klinowski (1995). "Esca and Solid-State Nmr-Studies of Allophane." Clay Minerals **30(3)**: 201-209.
- Hem, J. D., C. Roberson, C. Lind and W. L. Polzer (1973). "Chemical interactions of aluminium with aqueous silica at 25C." US Geological Survey Water-Supply paper **1827-E**: E1.
- Hodson, M. J. and A. G. Sangster (1999). "Aluminium/silicon interaction in conifers." Journal of Inorganic Biochemistry **76**: 89-98.
- Hyde, J. F. (1953). "Silanol Derivatives of the dimethyl substituted organosilicon compounds." Journal of the American Chemical Society **75**: 2166-2167.
- Industries, U. C. (1980). Silicon in waters and effluents, London, Her Majesty's Stationary Office.
- Katskov, D. A., G. Daminelli and P. Tittarelli (1999). "Effect of magnesium nitrate vaporization on gas temperature in the graphite furnace." Spectrochimica Acta Part B-Atomic Spectroscopy **54(7)**: 1045-1062.
- Kessemeier, H. and R. E. Norberg (1967). "Pulsed nuclear magnetic resonance in rotating solids." Physical Review **155**: 321-337.
- King, S. J., J. P. Day, C. Oldham, J. F. Popplewell, P. Ackrill, P. B. Moore, G. A. Taylor, J. A. Edwardson, L. K. Fifield, K. Liu and R. G. Cresswell (1997). Nuclear Instruments and Methods in Physics Research B **123**: 254-258.

- Klinowski, J. and T. L. Barr (1999). "NMR and ESCA chemical shifts in aluminosilicates: A critical discussion." Accounts of Chemical Research **32**(8): 633-640.
- Lajunen, L. H. J., P. Kokkonen, J. Karijoki, V. Porkka and E. Saari (1990). "Determination of Aluminum, Arsenic, and Phosphorus in Silicon by Graphite-Furnace Atomic-Absorption Spectrometry and Direct- Current Plasma-Atomic Emission-Spectrometry." Atomic Spectroscopy **11**(5): 193-197.
- Lehmann, R. G. and J. R. Miller (1996). "Volatilization and sorption of dimethylsilanediol in soil." Environmental Toxicology and Chemistry **15**(9): 1455-1460.
- Lehmann, R. G., J. R. Miller and H. P. Collins (1998). "Microbial degradation of dimethylsilanediol in soil." Water Air and Soil Pollution **106**(1-2): 111-122.
- Lehmann, R. G., J. R. Miller and G. E. Kozerski (2000). "Degradation of silicone polymer in a field soil under natural conditions." Chemosphere **41**(5): 743-749.
- Lehmann, R. G., J. R. Miller and G. E. Kozerski (2002). "Fate of dimethylsilanediol in a grass and soil system." Applied Soil Ecology **19**(2): 103-111.
- Lehmann, R. G., S. Varaprath, R. B. Annelin and J. L. Arndt (1995). "Degradation of Silicone Polymer in a Variety of Soils." Environmental Toxicology and Chemistry **14**(8): 1299-1305.
- Lou, G. and P. M. Huang (1988). "Hydroxy-aluminosilicate interlayers in montmorillonite: implications for acidic environments." Nature **335**: 625-627.
- Lowe, I. J. (1959). "Free induction decays of rotating solids." Physical Review Letters **2**(7): 285-287.

- Luciuk, G. M. and P. M. Huang (1974). "Effect of monosilicic acid on hydrolytic reactions of aluminium." Soil Science Society American Proceeding **38**: 235-244.
- Lumsdon, D. G. and V. C. Farmer (1995). "Solubility Characteristics of Proto-Imogolite Sols - How Silicic-Acid Can De-Toxify Aluminum Solutions." European Journal of Soil Science **46**(2): 179-186.
- Lvov, B. V. (1978). "Electrothermal atomisation-the way toward absolute methods of atomic absorption analysis." Spectrochimica Acta Part B **33B**: 153-193.
- Lvov, B. V., N. P. Romanova and L. K. Polzik (1991). "Formation of Soot During the Decomposition of Gaseous Carbides in Graphite-Furnace Atomic-Absorption Spectrometry." Spectrochimica Acta Part B-Atomic Spectroscopy **46**(6-7): 1001-1008.
- Manning, D. C. and W. Slavin (1983). "The Determination of Trace-Elements in Natural-Waters Using the Stabilized Temperature Platform Furnace." Applied Spectroscopy **37**(1): 1-11.
- Manning, D. C., W. Slavin and G. R. Carrick (1982). "Investigation of Aluminum Interferences Using the Stabilized Temperature Platform Furnace." Spectrochimica Acta Part B-Atomic Spectroscopy **37**(4): 331-341.
- Martin, R. B. (1991a). Aluminium in Biology and Medecine, M. Nicolini, P. F. Zatta and B. Corain, New York, Raven Press.
- Martin, R. B. (1991b). "Fe³⁺ and Al³⁺ Hydrolysis Equilibria - Cooperativity in Al³⁺ Hydrolysis Reactions." Journal of Inorganic Biochemistry **44**(2): 141-147.

- Martin, R. B. (1994). "Aluminium: a neurotoxic product of acid rain." Accounts of Chemical Research **27**: 204-210.
- McKeague, J. and M. Cline (1963). "Silica in solid solutions. II. The adsorption of monosilicic acid by soil and by other substances." Canadian Journal of Soil Science **43**: 83-96.
- Mehring, M. (1983). High resolution NMR spectroscopy in solids, 2nd ed., Springer-Verlag, Berlin.
- Neal, C. (1995). "Aluminium speciation variations in an acidic upland stream draining the Hafren spruce forest, Plynlimon, Mid-Wales." Journal of Hydrology **164**: 39-51.
- Neal, C., R. A. Skeffington, R. J. Williams and D. J. Roberts (1987). "Aluminium solubility controls in acidic wates: the need of a reappraisal." Earth and Planetary Science Letters **86**: 105-112.
- Neal, C., J. Wilkinson, M. Neal, M. Harrow, H. Wickham, L. Hill and C. Morfitt (1997). "The hydrochemistry of the headwaters of the river Severn Plynlimon." Hydrology and Earth System Sciences **1**(3): 583-617.
- Neal, C. and R. J. Williams (1988). "Towards Establishing Aluminum Hydroxy Silicate Solubility Relationships for Natural-Waters." Journal of Hydrology **97**(3-4): 347-352.
- Nukatsuka, I., K. Anezaki, S. Kubota and K. Ohzeki (2000). "Enhancement of the atomic absorption signal by silicate at electrothermal atomic absorption spectrometry." Analytica Chimica Acta **415**(1-2): 221-227.

- Ohlsson, K. E. A., A. Cedergren and W. Frech (1992a). "Alh Spike Formation in a Graphite Atomizer." Spectrochimica Acta Part B-Atomic Spectroscopy **47**(14): 1525-1533.
- Ohlsson, K. E. A., E. Iwamoto, W. Frech and A. Cedergren (1992b). "Transfer of Aluminum Compounds and Spike Atomization in a Spatially Isothermal Graphite Atomizer." Spectrochimica Acta Part B-Atomic Spectroscopy **47**(12): 1341-1352.
- Paces, T. (1978). "Reversible control of aqueous aluminum and silica during the irreversible evolution of natural waters." Geochimica Et Cosmochimica Acta **42**: 1487-1493.
- Pines, A., M. G. Gibby and J. S. Waugh (1973). "Proton-enhanced NMR of dilute spins in solids." journal of Chemical Physics **59**: 569-590.
- Plochmann, R. (1984). "Air-Pollution and the Dying Forests of Europe." American Forests **90**(6): 17-&.
- Pokrovski, G. S., J. Schott, J. C. Harrichoury and A. S. Sergeyeve (1996). "The stability of aluminium silicate complexes in acidic solutions from 25 to 150C." Geochimica Et Cosmochimica Acta **60**(14): 2495-2501.
- Pokrovski, G. S., J. Schott, S. Salvi, R. Gout and J. D. Kubicki (1998). "Structure and stability of aluminium-silica complexes in neutral to basic solutions: experimental study and molecular orbital calculations." Mineralogical Magazine **62A**: 1194-1195.
- Poplewell, J. F., S. J. King, J. P. Day, P. Ackrill, L. K. Fifield, R. G. Cresswell, M. L. di Tada and K. Liu (1998). "Kinetics of uptake and elimination of silicic acid by a

human subject: a novel application of ^{32}Si and accelerator mass spectrometry."

Journal of Inorganic Biochemistry **69**: 177-180.

Postel, S. (1984). "Air-Pollution, Acid-Rain, and the Future of Forests .2." American Forests **90**(8): 12-16.

Rafi, M., E. Epstein and R. Falk (1997). "Silicon deprivation causes physical abnormalities in wheat (*triticum aestivum*)." Journal of Plant Physiology **151**(497-501).

Ranau, R., J. Ochleschlaegen and H. Steinhart (1999). "Determination of aluminium in the edible part of fish by GFAAS after sample pretreatment with microwave activated oxygen plasma." Fresenius Journal of Analytical Chemistry **364**: 599-604.

Schecher, W. D. and C. T. Driscoll (1988). "An evaluation of equilibrium calculations within acidification models: The effect of uncertainty in measured chemical components." Water Resources Research **24**: 533-542.

Schneider, C. and C. Exley (2001). "Silicic acid ($\text{Si}(\text{OH})_4$) is a significant influence upon the atomic absorption signal of aluminium measured by graphite furnace atomic absorption spectrometry (GFAAS)." Journal of Inorganic Biochemistry **87**(1-2): 45-50.

Seyama, H. and M. Soma (1988). Application of X-ray photoelectron spectroscopy to the study of silicate minerals. Research report 111. Tsukuba, National Institute for environmental Studies: 121p.

Sharpe, M. R. (1984). "Stray Light in Uv-Vis Spectrophotometers." Analytical Chemistry **56**(2): A339-&.

- Shwartz, K. and D. Milne (1972). "Growth-promoting effects of silicon in rats." Nature **239**(5371): 333-334.
- Sjoberg, S. (1996). "Silica in aqueous environments." Journal of Non-Crystalline Solids **196**: 51-57.
- Skog, Hooler and Nieman (1998). Principles of instrumental analysis.
- Slavin, W., D. C. Manning and G. R. Carrick (1981). "The stabilized temperature platform furnace." Atomic Spectroscopy **2**(5): 137-145.
- Spivack, J. L., E. R. Pohl and P. Kochs (1997). Organoalkoxysilanes, Organosilanols, and Organosiloxanols. The Handbook of Environmental Chemistry. G. Chandra. Berlin Heidelberg, Springer-Verlag. **3, part H**: 105-135.
- Sturgeon, R. E., C. L. Chakrabarti and C. H. Langford (1976). "Study on the mechanism of atom formation in graphite furnace atomic absorption spectrometry." Analytical Chemistry **48**: 1792-1807.
- Styris, D. L. and D. A. Redfield (1987). "Mechanisms of Graphite-Furnace Atomization of Aluminum by Molecular-Beam Sampling Mass-Spectrometry." Analytical Chemistry **59**(24): 2891-2897.
- Swaddle, T. W. (2001). "Silicate complexes of aluminium (III) in aqueous systems." Coordination Chemistry Reviews **219-221**: 665-686.
- Tomanek, A. (1991). Silicones and Industries, W.-C. GmbH, Munich, Germany.
- Varapath, S. and R. G. Lehmann (1997). "Speciation and quantitation of degradation products of silicones (silanes/siloxane diols) by gas chromatography-mass

spectrometry and stability of dimethylsilandiol." Journal of Environmental Polymer Degradation **5**(1): 17-31.

Wada, K. and H. Kubo (1975). "Precipitation of amorphous aluminosilicates from solutions containing monomeric silica and aluminium ions." Journal of Soil Science **26**: 100-111.

Wood, M. and J. E. Cooper (1984). "Aluminum Toxicity and Multiplication of Rhizobium-Trifolii in a Defined Growth-Medium." Soil Biology & Biochemistry **16**(6): 571-576.

Wood, M., J. E. Cooper and A. J. Holding (1984). "Aluminum Toxicity and Nodulation of Trifolium-Repens." Plant and Soil **78**(3): 381-391.

Woolfson, A. D. and G. M. Gracey (1987). "Matrix Effects in the Determination of Aluminum in Dialysis Fluids by Graphite-Furnace Atomic-Absorption Spectrometry." Analyst **112**(10): 1387-1389.

Xu, N., V. Majidi, W. R. Markesbery and W. D. Ehmann (1992). "Brain Aluminum in Alzheimers-Disease Using an Improved Gfaas Method." Neurotoxicology **13**(4): 735-743.